CRANFIELD UNIVERSITY

Mathias Usman Bonet

Techno-Environmental Assessment of Marine gas turbines for the Propulsion of Merchant ships

School of Engineering
Power and Propulsion Department

PhD
Academic Year: 2010 - 2011

Supervisor: Prof Pericles Pilidis
Dr Georgios Doulgeris

July 2011

CRANFIELD UNIVERSITY

School of Engineering

Power and Propulsion Department

PhD

Academic Year 2010 - 2011

Mathias Usman Bonet

Techno-Environmental Assessment of Marine gas turbines for the Propulsion of Merchant ships

Supervisor: Prof Pericles Pilidis
Dr Georgios Doulgeris

July 2011

ABSTRACT

This research study seeks to evaluate the techno-economic and environmental implications of a variety of aero-derivative marine gas turbine cycles that have been modelled for the propulsion of different types of merchant ships. It involves the installation and operation of gas turbine propulsion systems in different marine environmental conditions and aims to evaluate the effect of the aerodynamic and hydrodynamic variations expected to be encountered by these ships when they navigate across different climates and oceans along selected fixed trade routes.

A combination of simulation tools developed in Cranfield University at the Department of Power and Propulsion including the validated gas turbine modelling and simulation code called “Turbomatch” and the “APPEM” simulation code for the analysis and Prediction of exhaust pollutants have been used along with the ongoing development of an integrated marine gas turbine propulsion system simulation platform known as “Poseidon”. It is the main objective of this research to upgrade the competence level of “Poseidon” so as to facilitate the conduct of a variety of longer and more complex oceangoing voyage scenarios through the introduction of an ambient temperature variation numerical module. Expanding the existing code has facilitated the prediction of the effect of varying aerodynamic and hydrodynamic conditions that may be encountered by gas turbine propulsion systems when such ships navigate through unstable ocean environments along their fixed trade routes at sea.

The consequences of operating the marine gas turbines under ideal weather conditions has been investigated and compared with a wide range of severe operating scenarios under unstable weather and sea conditions in combination with hull fouling has been assessed. The techno-economic and environmental benefits of intercooling/exhaust waste heat recuperation of the ICR model have been predicted through the evaluation of different ship propulsion performance parameters in a variety of voyage analysis leading to the prediction of fuel consumption quantities, emission of NOx, CO2, CO and UHCs and the

estimation of the HPT blade life as well. The different gas turbine cycle configurations of the research were found to respond differently when operated under various environmental profiles of the ship's trade route and the number of units for each model required to meet the power plant capacity in each scenario and for each ship was assessed. The study therefore adds to the understanding of the operating costs and asset management of marine gas turbine propulsion systems of any ocean carrier and in addition it reveals the economic potentials of using BOG as the main fuel for firing gas turbine propulsion plants of LNG Carriers.

Keywords:

Performance, Emissions, Weather, Sea states, Voyage, Hull Fouling, Transit time, BOG

ACKNOWLEDGEMENTS

My supervisors, Professor Pericles Pilidis and Dr Georgios Doulgeris - for their guidance, support, encouragement and patience throughout the program

The Petroleum Technology Development Fund (PTDF) of Nigeria, for the lavish funding of the research and generous opportunity to be one of their PhD scholars

The Nigerian Defence Academy, for their understanding and prolonged study leave with pay in spite of unforeseen circumstances

Dr Luca Marinai, who took me through the preliminary stages and encouraged me to continue struggling against the initial challenges,

Dr Tsoudis Evangelos, my former colleague whose experience and friendship made me to be part of “Poseidon”.

Dr Bhavik Mody also a colleague in the marine gas turbine research team

Mr Michael Corsar, a dependable friend that was there to help when I needed assistance.

My wife, Mrs Asabe Bonet, without whose support and encouragement, the program stood the chance of being aborted midway.

My Daughter, Evelyn and my two sons, Charles and Sheyin who never ceased to pray for Daddy’s success while struggling to stand on their feet at the same time.

My friends and brothers in Lord Engr Odalas Maijama’a Labi and Engr Musa Useni Yakubu,

Dr O. F. Agboola and Engr Akindapo, whose friendship and support cannot be expressed through ink and paper.

My colleagues at the Mechanical Engineering Department of NDA Kaduna, Nigeria

TABLE OF CONTENTS

LIST OF FIGURES

LIST OF TABLES

LIST OF EQUATIONS

NOMENCLATURE

AWC	Adverse Weather Conditions
A_M	Area of Midship Section
B	Breadth
BOG	Boil Off Gas
B_{WL}	Breadth on Waterline
C	Dimensionless Coefficient
C_B	Block Coefficient
C_F	Frictional Resistance Coefficient
CL	Cruise Liner
C_M	Mid ship Coefficient
CO	Carbon Monoxide
CO_2	Carbon Dioxide
CODAG	Combined Diesel and Gas turbine
CODLAG	Combined Diesel, Electric and Gas turbine
CODOG	Combined Diesel or Gas turbine
COGAG	Combined Gas Turbine and Gas turbine
COGES	Combined Gas turbine and Steam drive Electric System
COGOG	Combined Gas Turbine or Gas turbine
COT	Compressor Outlet Temperature
C_P	Specific Heat Coefficient at Constant Pressure
C_V	Specific Heat Coefficient at Constant Volume
C_{WP}	Water plane Coefficient
D	Ship Hull Depth
DFDE	Dual Fuel Diesel Electric Propulsion
DFDM	Dual Fuel Diesel Mechanical Propulsion
DFGE	Dual Fuel Gas turbine Electric Propulsion
Dwt	Deadweight
F	Reference Force
FAR	Fuel Air Ratio
FB	Fuel Burned
FB_{MDO}	Volume of Diesel Fuel Burned [m^3]

F_{BOG}	Volume of BOG Fuel Burned [m^3]
FF	Fuel Flow
F_n	Froude Number
GE	General Electric
GT	Gas Turbine
h_b	Blade Height
HFO	Heavy Fuel Oil
HPC	High Pressure Compressor
HPT	High Pressure Turbine
HR1	Hull Fouling Roughness of 120µm
HR2	Hull Fouling Roughness of 240µm
HR3	Hull Fouling Roughness of 360µm
HSF	High Speed Ferry
IFEP	Integrated Full Electric Propulsion
ISA	International Standard Atmosphere
IWC	Ideal Weather Conditions
KRISO	Korean Research Institute of Ships and Ocean engineering
K_s	Shroud Parameter
L	Ship's Length
LCC	Life Cycle Cost
LNG	Liquefied Natural Gas
LNGC	Liquefied Natural Gas Carrier
L_{OA}	Length Overall of a Ship
LPC	Low Pressure Compressor
L_{PP}	Length Between Perpendicular
LPT	Low Pressure Turbine
L_{WL}	Length on Waterline
MCR	Maximum Continuous Running
MDO	Marine Diesel Oil
MF	Mass Flow
MGO	Marine Gas Oil
MN	Mega Newtons
MT	Marine Trent
MW	Megawatts
NBOG	Natural Boil Off Gas
nm	Nautical Mile
N_{od}	Turbine Shaft Off Design Rotational Speed

NO_x	Nitrogen Oxide
N_{RT}	Ship's Annual Sailing Time (75% of the year)
OD	Off Design
P_{amb}	Ambient Pressure
P_B	Brake Power
P_D	Delivered Power
P_E	Effective Power
PR	Pressure Ratio
P_S	Shaft Power
P_T	Thrust Power
Q_{AL}	Annual Loaded LNG Cargo
Q_{BOG}	Total Quantity of BOG Released
Q_C	Installed Cargo Capacity of LNGC
Q_{Del}	Quantity of LNG Cargo Delivered per year
Q_{Load}	Loaded LNG Cargo from Production Terminal
Q_{MDO}	Quantity of Diesel Fuel
R_A	Air Resistance
R_F	Frictional Resistance
r_{mb}	Distance from Mid shaft to Mid blade
R_R	Residual Resistance
R_T	Total Resistance
S	Range of Voyage [nm]
SAC	Single ANNULAR Combustor
SFC	Specific Fuel Consumption
SFDM+R	Single Fuel Diesel Mechanical and Reliquefaction
SO_X	Sulphur Dioxides
SSD	Slow Speed Diesel
T	Draught
t	Thrust Deduction Factor
T_{amb}	Ambient Temperature
T_b	Blade Temperature
T_c	Blade Cooling Temperature

TET	Turbine Entry Temperature
t_f	Blade Creep Life Fraction
T_g	Gas Temperature
T_{RT}	Duration of LNGC Round Trip
T_V	Duration of a Single Voyage
UHC	Unburned Hydrocarbons
UKHO	UK Hydrological Office
UKMO	UK Meteorological Office
V_A	Speed of Advance
V_S	Ship's Service Speed
w	Wake Fraction
GREEK	
Δ	Displacement [tons]
Δ_t	Voyage Duration [Days]
µm	Surface Roughness [Microns]
γ	Ratio of Specific Heats
ε	Blade Cooling Effectiveness
η_h	Hull Efficiency
η_o	Open Water Efficiency
η_P	Propeller Efficiency
η_r	Relative Rotative Efficiency
η_{th}	Thermal Efficiency
ρ	Water Density
ρ_b	Material Density
σ_{cfd}	Blade Centrifugal Stress at Design Point
σ_{cfo}	Blade off-design Centrifugal Stress

1 GENERAL INTRODUCTION

1.1 Research Rationale

The development of the aero-derivative gas turbine has acquired a dominant role in the powering of most modern naval vessels due to its benefits of compactness, simplicity, ease of installation and maintenance, environmental friendliness and the capability to achieve higher sustained sea speeds. Its application in the propulsion of merchant ships is still being weighed down by high operating costs due to lower fuel efficiency and fuel quality restrictions. Other traditional prime movers such as diesels and steam turbines have demonstrated a greater advantage mainly due to their capability in burning low grade fuels. Of recent however, its patronage has been boosted by more applications in the area of passenger ship (Fast ferries and Cruise ships) propulsion by exploiting its potential for higher speeds that lead to faster transportation of goods and services when used as the main propulsion prime mover. The poor fuel economy can be overcome by combining it with either a diesel engine or a small size gas turbine capable satisfying the vessels part load performance at low power demands and having the main engine to come online only at higher power requirements.

In the case of the LNG cargo ship (LNG Carrier), the steam turbine has dominated as the traditional propulsion engine due mainly to its effective use of boil off gas (BOG) as the main fuel. Therefore one of the objectives of this research is the evaluation the economic potential of the aero-derivative gas turbine when using the LNG BOG as its main fuel but with a dual fuel arrangement that has liquid fuel only as a backup.

1.2 Problem Statement

A prototype integrated marine propulsion simulation platform ‘Poseidon’ [1], consisting of a numerical model in which a ship is coupled to a gas turbine propulsion system has been developed. It is capable of assessing the techno-economic and environmental interactions of the marine gas turbine propulsion

system by predicting the effect of the environment on gas turbine performance on the one hand while predicting the impact of the gas turbine on the environment through the exhaust pollutants emissions on the other hand. It has been tried for the programming of a variety of voyage scenarios with assumptions of diverse sea climate and hydrodynamic conditions with arbitrary data. Its development and initial implementation saw it through voyage scenarios that could not go beyond twenty four hours and as a result, could not be applied in cases of long hauled oceangoing voyages in which the ship was expected to experience a complex variation of weather and sea conditions as it travels from one ocean through another before getting to its final destination. The current research is seeking to build on the gains of this prototype simulation platform for the conduct of a comparative analysis of a variety of marine aero-derivative gas turbine propulsion systems involving different ship types.

1.3 Aim and Objectives of the Thesis

This research aims to investigate the performance of several aero-derivative marine gas turbine models with regards to their application as propulsion prime movers of a variety of merchant vessels by evaluating the effect of varying environmental conditions of their voyages.

1.3.1 Objectives

The main objectives include the following:

- To further develop “Poseidon” and implement the program in the simulation of long hauled voyages for the prediction of the marine gas turbine propulsion performance and exhaust pollutant emissions so as to be able to evaluate the operating costs of any oceangoing merchant vessel
- To assess how the marine environment affects the performance of the gas turbine as well as assessing the gas turbine exhaust pollution of the marine environment.

- To evaluate the expected benefits to be derived from the use of BOG in a dual fuel configuration of a gas turbine power plant for the propulsion of a LNG Carrier.

1.3.2 Milestones

In order to achieve the aforementioned aim and objectives, the following were considered as major milestones necessary for facilitating the successful completion of the research:

- Modelling and simulation of a variety of gas turbine cycles and conducting design and off design performance analysis by assuming changes in the ambient conditions of their operation.
- Development of a variety of merchant ship models based on different geometry, cargo capacity, propulsion power requirement and type of cargo.
- Selection of loading and discharge ports for each of the vessels and estimating the environmental conditions (weather and sea states) existing along the fixed transit routes selected for each vessel according to seasons.
- Developing the existing ‘Poseidon’ simulation code [1] in order to facilitate the simulation of the various propulsion power plants according to the variety of voyages and investigated scenarios in each case
- Evaluation of the main output parameters which determine the quantities of fuel burn, emission pollutants and engine life consumption of the gas turbine models according to the variety of selected investigation scenarios.
- Conduct a comparative analysis of the performance of each of the gas turbines in relation to the various vessels and configuration of the power plants

- Conduct an evaluation of the various gas turbine models in relation to the utilization of the boil off gas (BOG) for the LNG Carrier.

Though the steam turbine has continuously dominated as the conventional propulsion prime mover for liquefied natural gas vessels (LNGCs) mainly due to its ability to utilize the natural boil off gas (NBOG) on board the vessel, the search for alternative propulsion systems with higher economic and environmental benefits have been intensified and this work contributes to the several proposals from manufacturers as found in literature.

The type of cargo and the cargo carrying capacity are the fundamental defining characteristics that determine the type, configuration and physical dimensions of any marine vessel. Therefore, the quantity of cargo delivered per unit time is a function of the ship speed but fuel efficiency and annual fuel costs are the governing influence in determining the type of propulsion plant for merchant ships and so the choice of a sustained sea speed is an important parameter for minimizing the overall cost of marine transportation and the annual cost of operating a ship [2].

1.3.3 "Installed" Performance Investigation Scenarios

Under the "installed" performance investigation, voyage analysis for each of the vessels was conducted in respect of each of the four gas turbines and the following scenarios were assumed for the three seasons under consideration:

- Ideal Weather Conditions (IWC)
- Adverse Weather Conditions (AWC)
- Adverse Weather Conditions with combined with increased ship hull roughness of 120μm
- Adverse Weather Conditions with combined with increased ship hull roughness of 240μm
- Adverse Weather Conditions with combined with increased ship hull roughness of 360μm

The daily weather forecast for the month of January was selected to represent the winter season while August was selected as the month in which the summer season may be considered to be at its peak. For the input weather data representing a mid season, the month of May and or October were used to represent the conditions that exist in spring time. For each of the selected seasons, the simulation platform was deployed to conduct five different voyages for every gas turbine model.

For every one of the vessels under investigation therefore, a total of 60 voyages were conducted in order to undertake a comparative analysis for the variety of gas turbine under investigation.

1.4 The Simulation Platform

'Poseidon' is being successfully developed and implemented by adopting the Holtrop regression analysis method [3]. It has proved to be a viable tool for marine gas turbine propulsion systems investigations by predicting the effects of the hostile marine environment.[1]. It has been developed further to enable the input of forecasted daily ambient temperature values for the respective fixed trade routes by obtaining data from the United Kingdom Meteorological Office [4].

1.4.1 Selected Aero-Derivative Models

The marine gas turbine, like most other prime movers used for marine propulsion, is usually an adaptation of a machine that was originally developed for some other purpose and the aero-derivative version has been found to be the most favourable option when compared with its heavy duty counterpart. Therefore, four different configurations of the aero-derivative marine gas turbine have been selected and adopted for the purpose of this research and among them is the

- Simple Cycle, Single Spool model
- Inter-cooled Recuperated model

- Simple Cycle, Two Spool model

Although a great deal of research has been successfully conducted in the area of ‘uninstalled’ performance investigation of gas turbine engines operating in the marine environment through digital simulation, The development and application of “Poseidon” for TERA and the assessment of the gas turbine operation in a marine environment is part of the continuous effort to further compliment the success of other existing gas turbine simulation platforms at the Cranfield University. The “TURBOMATCH” scheme is a key component and forms the basis for any investigation of both aircraft and land based applications. The simulation package has been combined together with “APPEM” (Analysis and Prediction of Pollutant Emissions) to enable the prediction of gas turbine exhaust pollutant emissions in the marine environment. By predicting the emission quantities of Carbon monoxide (CO), Unburned Hydrocarbons (UHC), Nitrogen Oxides (NOx) and Carbon Dioxide (CO_2), the impact of the gas turbine operation in a marine environment can be evaluated as part of the operating cost of the marine gas turbine propulsion machinery.

1.5 Author’s Contribution

The main objective of the present thesis is to bring “Poseidon” to a more superior level of competence for the improved assessment of the effect the marine environment on the performance and pollutant emissions of marine gas turbines. It introduces an additional numerical module for predicting the hourly variation of long range voyages for ocean carriers transiting between complex climatic weather variations in different oceans.

This has further contributed to the existing proposals for adopting the aero-derivative gas turbine as the main propulsion engine of merchant ships currently dominated by the diesel propulsion systems. It differs from the initial version through the introduction of a numerical module by which longer trade routes can be well profiled to accommodate the environmental variations to be encountered when the vessel moves from one climate to another. Accordingly, four trade routes covering long distances and duration of transit times have

been developed and assigned to four models of merchant vessels. By including daily ambient temperature and sea state from official weather and ocean tide forecasting organizations, an integrated assessment of the aerodynamic and hydrodynamic effects on the ship performance and the gas turbine pollutant emissions potentials of each gas turbine model could be monitored and predicted through the voyage. was predicted for every vessel when operated along their fixed trade routes. The marine gas turbine propulsion simulation platform for the investigation and prediction of the environmental impact on each gas turbine cycle by conducting series of long range ocean carrier voyages under a variety of operating scenarios.

The handling of the boil-off gas during LNG vessel operation is a key issue in the technical and economic assessment of the complete energy system [5]. Accordingly, the benefits of using the boil off gas of a LNG LNGC as fuel for its gas turbine propulsion machinery have also been investigated and appropriate economic and environmental benefits have been predicted for each of the gas turbines.

Altogether, the research has contributed in further proposing the marine gas turbine as a viable propulsion alternative for oceangoing merchant vessels.

1.6 Thesis Structure

The thesis is a component of the ongoing efforts in proposing the aero-derivative gas turbine as a viable alternative to traditional reciprocating prime movers in the merchant ship propulsion industry. It consists of seven chapters as follows:

Chapter 1 represents the introduction of the subject by defining the problem, the rationale and main objectives of the research by restating the possible contributions of the author. It also tries to describe the expected milestones that would motivate the author to score the expected goals of the research.

Chapter 2 constitutes a summary of the literature supporting the theory behind every stage of the investigation. Apart from giving an overview of the aero-

derivative gas turbine technology, the literature review also represents a definition of the technical and economic considerations that are appropriate for the selection of any marine gas turbine as a merchant ship propulsion prime mover. It briefly refers to the previous and current experience of the marine gas turbine, citing various examples of the application especially in cruise ship and fast speed ferries. A description of hull forms and design factors has also been highlighted in this chapter.

Chapter 3 defines the methodology and the tools employed in the conduct of all the investigations involved in the research. It explains the different aspects and the stages that are required to be followed in order to generate and analyse expected results. It also gives an insight to the stages for implementing the series of simulation tools for the investigation of engine performance, pollutant emissions and engine life consumption. Also discussed is the composition of the entire simulation platform and the inputs required in each case scenario.

Chapter 4 attempts to set the stage for the determining the right combination of the various models of the research by ascertaining the particular number of gas turbine engines that may be required in the composition of all the power plants involved in the research. It summarizes the power requirement not only for sustaining the service speed of every of the ships but it compares the different gas turbines to determine how they will respond in the face of varying weather and sea conditions. The management of propulsion with a view to ensuring enough redundancy were predicted in each case scenario.

Chapter 5 is dedicated to the discussion of the results of the simulated investigations of all the vessels except the LNG carrier. The performance of each of the gas turbines as applied to the propulsion of each of the vessels was discussed and analysed. Major areas of interest included the quantities of fuel burned per voyage

Chapter 6 is dedicated to discussions on the results of the simulated investigations and predictions generated by the voyage analysis of the LNG

Carrier in which the management of the BOG as a component of the proposed duel fuel arrangement was a major subject that was critically analysed.

Chapter 7 is a summary of the conclusions derived from the research defining current impact of the marine gas turbine as well as the limitations the constraints of the current research by recommending the aspects of the work that may require further investigation with a view to obtaining better results.

2 LITERATURE REVIEW

This chapter summarizes the relevant information that has been published in the literature related to aero-derivative marine gas turbines and their application as propulsion machinery for various types of merchant seagoing vessels and with particular interest in the LNG Carrier. Divided into six main segments, it first seeks to present a general background of the aero-derivative gas turbine by concentrating on the main technical and economic considerations that affect the selection of the gas turbine propulsion plant as a viable alternative. It goes further to identify the aero-derived models (according to cycle configurations) relevant to the application and the merchant ships on which the technology has been successfully implemented. The various methods of the coupling the gas turbine to the ship's propulsion machinery has also been presented while viewing the operating requirements in relation to the hostile marine environment is a necessary component of the research and some of the factors affecting performance have been documented. Furthermore, with regards to the expected variations in weather conditions at sea, the chapter specifically emphasises the effect of changing the ambient temperatures, pressures and site location as important parameters for consideration in relation to gas turbine engine performance as may be experienced by any vessel while transiting between terminals. The chapter concludes by reviewing the alternative propulsion options for the LNG Carrier with a special focus on the gas turbine as the main subject.

2.1 Technical and Economic Considerations for Selecting GT Propulsion plant

The increasing demand for economical and rapid movement of both passengers and freight has brought renewed momentum to the marine propulsion systems [6] and some of the technical and economic considerations for selecting a gas turbine as the propulsion prime mover for any vessel may include the engine's initial cost, the operating cost, reliability and environmental friendliness [7]. Its high power output and very compact dimensions and low weight are some of

the major attributes that make it a very suitable alternative in competition with traditional propulsion systems. The gas turbine is equally low in noise and vibration as well as possessing the added advantages of high torque, low lube oil consumption and rapid on-sight engine module change out leading to easy maintenance. Although the initial cost of this alternative may appear to be higher, the cost of installation is made insignificant by its simplicity and moderate physical dimensions. The ship's operating cost depends on its overall physical dimensions and the power required for its propulsion in line with the operating profile necessary for sustaining the service speed and the trade distance. Flexibility to different market requirements and the propulsion plant efficiency of the gas turbine is an important component for evaluating the overall operating cost

2.2 The Aero-derivative Technology

Aircraft gas turbine design can be adapted for use in land-based and sea applications which turns the engine into what is termed an aero-derivative gas turbine. Ref [8] in a background statement revealed that lightweight aero-derived gas turbines lend themselves particularly to naval applications where weight and space are of primary importance. He highlighted how Rolls-Royce had introduced a number of gas turbines into the marine market over the last 40 years, starting with the commercially successful marine version of the 3MW industrial Proteus engine. Other engines listed among the simple cycle collection from Roll-Royce are the Tyne (4MW), the Spey (12.5, 18 or 19MW) [9] and the Olympus models [10]. However, various manufacturers in the industry have successfully implemented this technology of which the simple cycle, single spool LM2500 series from GE [11], the Rolls-Royce simple cycle, dual spool MT30 (Marine Trent) [12] and the intercooled recuperated WR21[13] [14] models can be cited as clear examples among many others as reflected in the SFC curves illustrated in Figure 2:7.

A summary of the aero-derivative gas turbine application in merchant ship propulsion [15] is presented and formatted in Table 2:1. In addition, Table 2:2

illustrates the adaptation of the aero-derivative gas turbine as an alternative to diesel propulsion power plants in high speed ferries (HSF) and the Cruise liner segments of the industry from the 1990s to date.

Table 2:1 A Summary of some existing aero-derivative marine gas turbines

Manufacturer	Model	Aero-derived from	Rated Power [KW	Mass flow [kg/s]	Length [mm]	Total height [mm]	Ratio [kg/KW]
ABB	GT35	-	17,00 18,300	93.50	11,300	3,000.0	1.53 1.42
GE	LM500	TF34/CF34	4,470	16.00	2,960	910.0	0.2
GE	LM1600	F404	14,920	47.00	4,240	2,030	0.24
GE	LM2500	TF39/CF6	25,050	70.00	6,520	2,040	0.18
GE	LM2500+	TF39/CF6	30,200	83.92	6,700	2,040	0.18
GE	LM6000	CF6-80-C2	44,700	127.00	7,300	2,500	0.18
RR	MT30	Trent 800	36,000	113.00	8,600	3,540	0.61
RR	WR21	RB211	25,200	73,50	8,000	4,830	1.81

The cycle configuration of the gas turbine models involved in this research are closely linked to those highlighted in the above table including the intercooled-recuperated WR21. The other three models equally replicate the simple cycle, single spool and dual spool arrangements adopted by the two major manufacturers, Rolls-Royce and GE.

In 1960 marine gas turbines had an efficiency of around 25% at their rated power, while second generation aero-derivatives were introduced in the 1970s with efficiencies of around 35% but subsequent advances in design refinements, new materials and cooling techniques, and the appropriate matching of higher compressor pressure ratios have resulted in some large simple cycle turbines achieving efficiencies of over 40% [9].

Table 2:2 A Selected ship reference list with marine GT application

Ship Type	Ship Name	GT model	No. of engines	Country	Build year
Cat ferry	Stena Carisma	GT35	2	Sweden	1997
Cat ferry	Luciano Frederico L	GT35	2	Spain	1997
HSF	Foilcat	LM500	3	H. Kong	1995
HSF	Foilcat Prototype	LM500	2	Norway	1991
HSF	Seajet 250	LM1600	2	Denmark	1996
HSF	Katana	LM1600	1	Germany	1991
HSF	Destriero	LM1600	3	Italy	1991
RP ferry	#1500	LM2500	2	Japan	2005
CL	Noordam	LM2500	1	USA	2006
CL	Westerdam	LM2500	1	USA	2004
HSF	Auto Express 86	LM2500	2	Denmark	2000
HSF	HSS1500	LM2500	2	Sweden	1995
HSF	Aquastrada	LM2500	1	Italy	1993
CL	Jewel of the seas	LM2500+	2	USA	2004
CL	Island Princess	LM2500+	1	USA	2003
CL	Queen Mary 2	LM2500+	2	USA	2003
HSF	SNCM-Corsaire 13000	LM2500+	2	France	2000
HSF	NEL-Corsaire 14000	LM2500+	2	Greece	2000

2.2.1 Simple Cycle Options

2.2.1.1 The GE LM2500

GE is the world's largest aero-derivative service provider [16] and the LM2500 has been designed in a simple cycle configuration to provide quality and durability with valuable benefits aboard floating or fixed offshore facilities. Table 2:2 shows how it has been found to be very suitable for application in HSF and Cruise Liners in different regions of the world. Its many years of service have seen it being upgraded from the baseline LM2500 with an output of 25MW to the LM2500+G4 version up to a power output of 36.3MW.

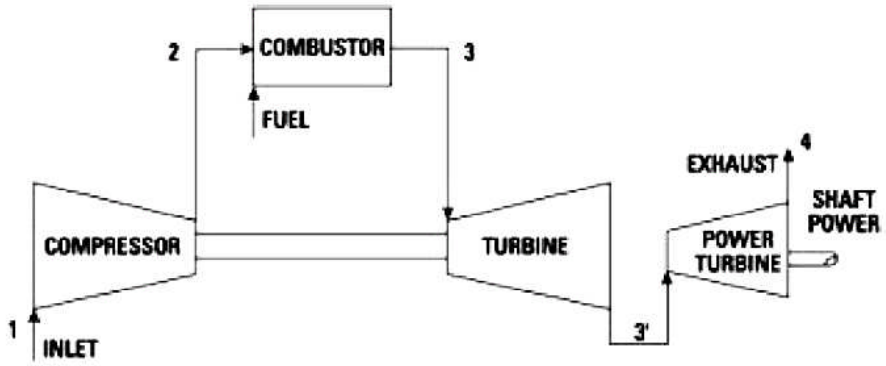

Figure 2:1 Component illustration of the simple cycle gas turbine

A typical installation of this engine is on the Queen Mary 2 Cruise Liner, where two LM2500 engines combine with four diesel engines [17] to provide flexibility that allows the vessel to run at lower speeds while cruising or crossing the Atlantic at higher speeds. Its design is such that the gas turbines provide 50MW of the power requirement, while the balance is supplied by the diesel engines. Depending on the sea state and wind, the daily consumption at a speed of 29 knots, is approximately 261 tons of HFO for the diesel engines and 237 tons of MGO for the gas turbines. Furthermore, the Fuel tank capacities are quoted to be approximately 5,500 m^3 for the HFO and 3,700 m^3 for the gas turbines [18]. The Rolls-Royce marine Trent MT30 illustrated in Figure 2:2 (a) is a typical example.

2.2.1.2 The Rolls Royce MT30

Compact and lightweight, the MT30 marine gas turbine illustrated in Figure 2:2 [19] is a member of the Rolls-Royce engine family that has accumulated more than 30 million flying hours since entry into service in 1996. It features an eight-stage variable geometry low pressure compressor (LPC) and a six-stage high pressure compressor (HPC) with the core derived from the aero Trent 800 while its four-stage power turbine was derived from the industrial Trent. Designed to provide cost efficient propulsion for both commercial and naval application, it is ideal for vessels requiring high power density. Its design incorporates the latest blade cooling technologies and key components are protectively coated for service in the marine environment so as to reduce maintenance and deliver a

long service life. It is also designed to facilitate dual fuel capability to enable it burn boil off gas (BOG) when installed on LNG Carriers.

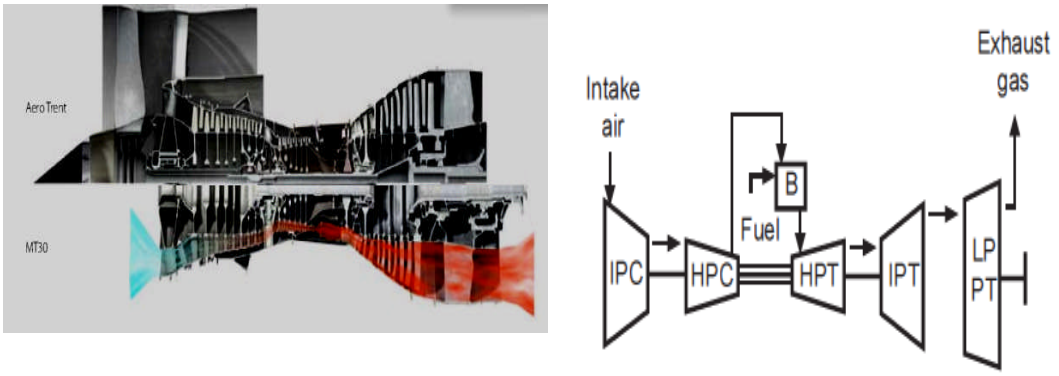

(a) (b)

Figure 2:2 (a) Derivation of the MT30 from the RR aero Trent gas turbine and [20] **(b) its cycle configuration**

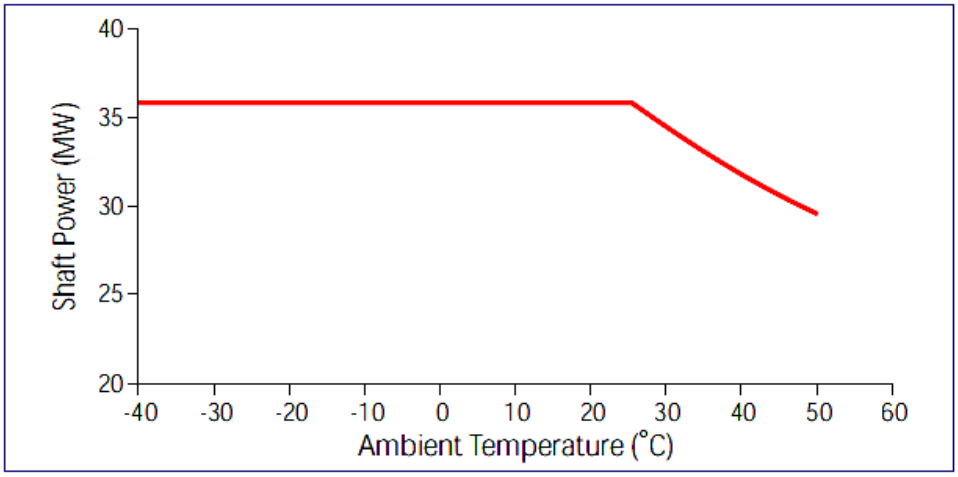

Figure 2:3 Variation of power output with changes in ambient temperature for the MT30 [19]

2.2.2 The Advanced Cycle Options

The slow pace of the successful application of the marine gas turbine in merchant ship propulsion has been largely due to the inability of the basic simple cycle to perform efficiently at lower power settings at its initial stages of development. However, the development of advanced cycles such as the WR21

which incorporates intercooling and heat exchange so as to increase the part load efficiency resulted in improved efficiency at lower power levels.

An intercooler however, is an air-to-liquid heat exchanger used during the compression process to enhance the specific power of the engine by cooling the airflow midway through the compression process [21]. The reduction in the energy required during compression is then reflected in an increase in the power output. A recuperator on the other hand is used to transfer heat from the exhaust gas to the engine airflow in order to reduce the fuel required during combustion.

Figure 2:7 compares the performance of some existing marine gas turbines by analysing their performance by drawing up the variation of SFC with increase in power. With an efficiency of between 40% and 46%, it is considerably higher than the 36% for the simple cycle and only slightly less than the 48% for the combined cycle efficiency. With an estimated lifetime of up to 100,000 hrs, the heat exchanger is of a compact plate and fin design [22].

In contrast to the combined cycle, the design does not require hours to warm up and it is inherently simpler, smaller and cheaper. It also has considerable waste heat left in the exhaust for possible onboard utilization and it has a facility generate more when the recuperator and intercooler are bypassed. Being the most advanced marine gas turbine currently available, the WR21 exemplifies the next generation of ship propulsion prime movers aimed at offering a combination of high power density, low fuel consumption and environmentally sound solutions.

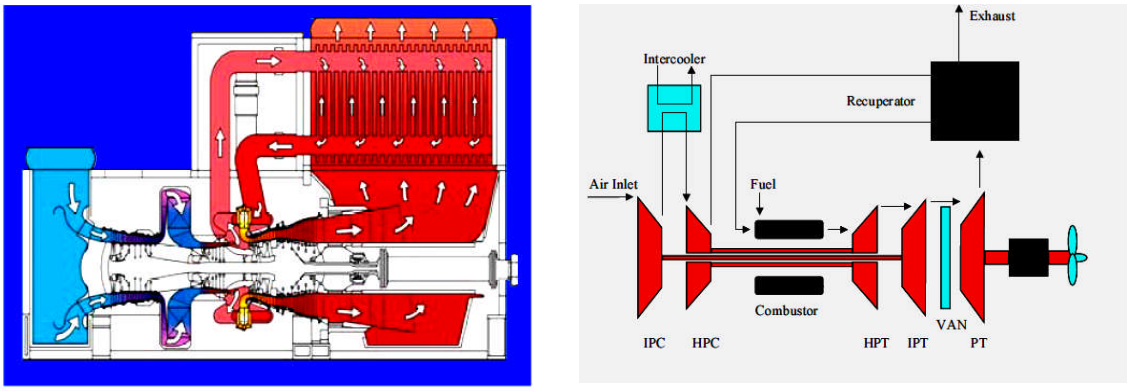

Figure 2:4 (a) Principle of operation and cycle configuration of the WR21 intercooled-recuperated gas turbine [13]

Another option with considerable interest is in the use of other complex cycles in Cruise applications as illustrated by the selection of a combined Gas turbine and Steam Electric drive system (COGES) for Celebrity Cruises' Millennium class ships, in which a steam turbine cycle rather than intercooling and recuperation are chosen as an alternative solution to reduce fuel consumption through the recovery of exhaust heat [6].

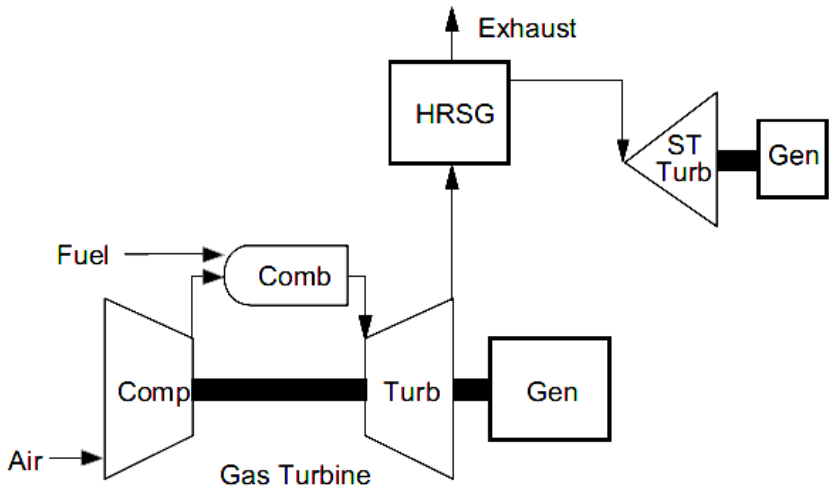

Figure 2:5 Schematic Illustration of the combined cycle option

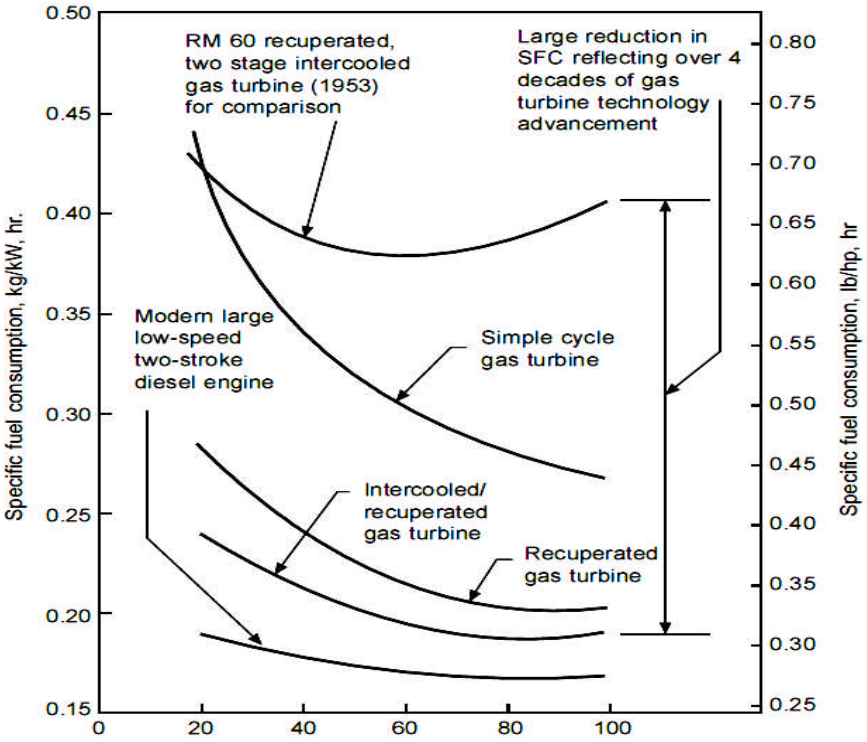

Figure 2:6 A comparison of SFC curves against load for various gas turbine cycles and a low speed two-stroke diesel engine [9]

2.3 Merchant ships Operated by Marine Gas Turbines

Gas turbines have dominated warship propulsion for many years but their potential remains to be fully realised in the commercial sector [9].

In an attempt to investigate a wide variety of gas turbine cycles, the models involved in this research were selected based on the simple cycle and the intercooled cycle layout. The simple cycles include one single-spool and two dual-spool configurations

In 1960 marine gas turbines had an efficiency of around 25% at their rated power, while second generation aero-derivatives were introduced in the 1970s with efficiencies of around 35% but subsequent advances in design refinements, new materials and cooling techniques, and the appropriate matching of higher compressor pressure ratios have resulted in some large simple cycle turbines achieving efficiencies of over 40% [11]

A record of the application of aero-derivative gas turbines as propulsion prime movers for Cruise Liners (CL) and large high speed passenger ferries (HSF) is tabulated in Table 2:2. The advantage of the gas turbine in these types of ships has to do with the extreme high power requirement which is difficult to be satisfied with diesel machinery alone and particularly in the case of the Cruise liners, the compactness associated with the gas turbine engine can be exploited for creating extra accommodation or public spaces. The summary of current application of the gas turbine in the industry also highlights the high power-to-weight ratio leading to compactness and weight saving which further releases machinery space for extra revenue earning activities [9]. The choice of the gas turbine as an alternative to the diesel engine can bring about substantial reductions in total ship cost. In addition to that, the intensive manpower and heavy maintenance requirements alongside the larger crews and increase harbour down time can be avoided [13].

Fundamental to the design of a main propulsion plant is the coordination of the prime mover with a transmission system and a propulsor and the basic choices when selecting a prime mover are diesel engine, gas turbine or steam turbine [23].

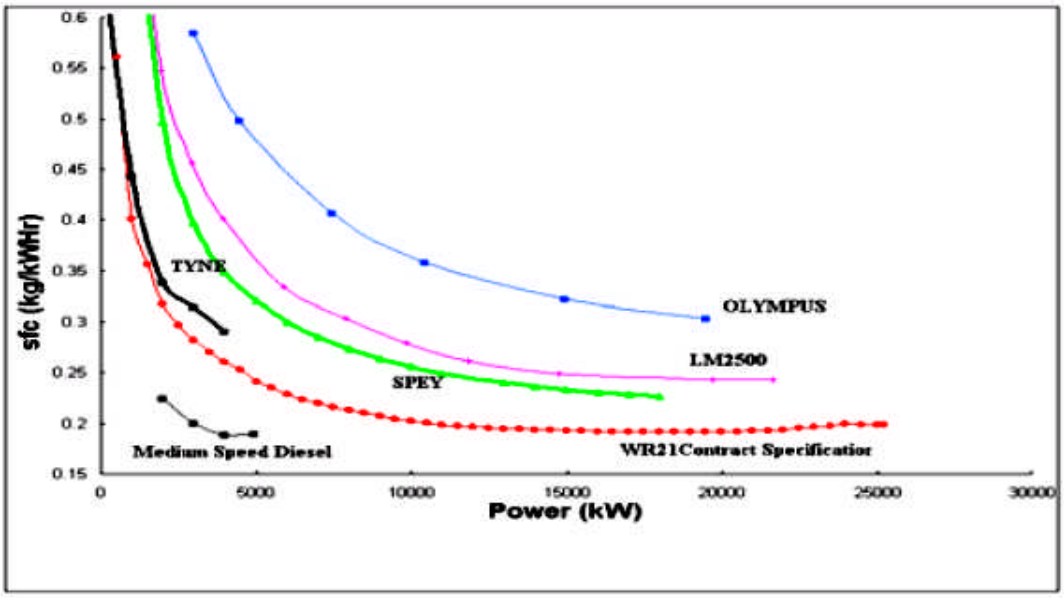

Figure 2:7 WR21 fuel consumption compared to simple cycle [13]

2.4 Propulsion Machinery Configuration

The gas turbine is a flexible prime mover that can be applied not only alone but in combination with others and conventional gas turbine propulsion systems utilize cruise engines (either diesel or gas turbine) to provide low speed fuel economy together with a boost gas turbine to provide the high power for top speed operations [14] . Such a combination can either operate as a (CODAG) Combined Diesel and Gas turbine or (CODOG) Combined Diesel or Gas turbine configuration in a direct mechanical drive system. This combination along with the Combined Diesel Electric and Gas turbine (CODLAG) are frequently adopted by high speed naval vessels. Usually, a controllable pitch propeller is fitted with such combinations in order to match the different operating conditions for each prime mover [2]. Other combinations that have been implemented in the industry include the, Combined Gas turbine and/or Gas turbine (COGAG/COGOG) configured to operate in a Father and son relationship. The Rolls-Royce 18MW Spey and the 4MW Tyne have been observed as a convenient COGOG combination [10]. In explaining the Canadian experience with aero-derivative gas turbines, Saravanmuttoo [24] cited the example of a 4000 ton ship designed for a maximum speed of 32 knots and requiring 50,000shp (37.3MW) but at a typical cruise speed of 16 knots, the power requirement was only about 4.5MW.and that the problem was overcome by the use of combinations such as COGOG or CODOG.

Both the COGES and CODLAG configurations can be categorised as the conventional electric combinations, while the Integrated Full Electric Propulsion (IFEP) and its Podded counterpart are innovative electric propulsion systems.

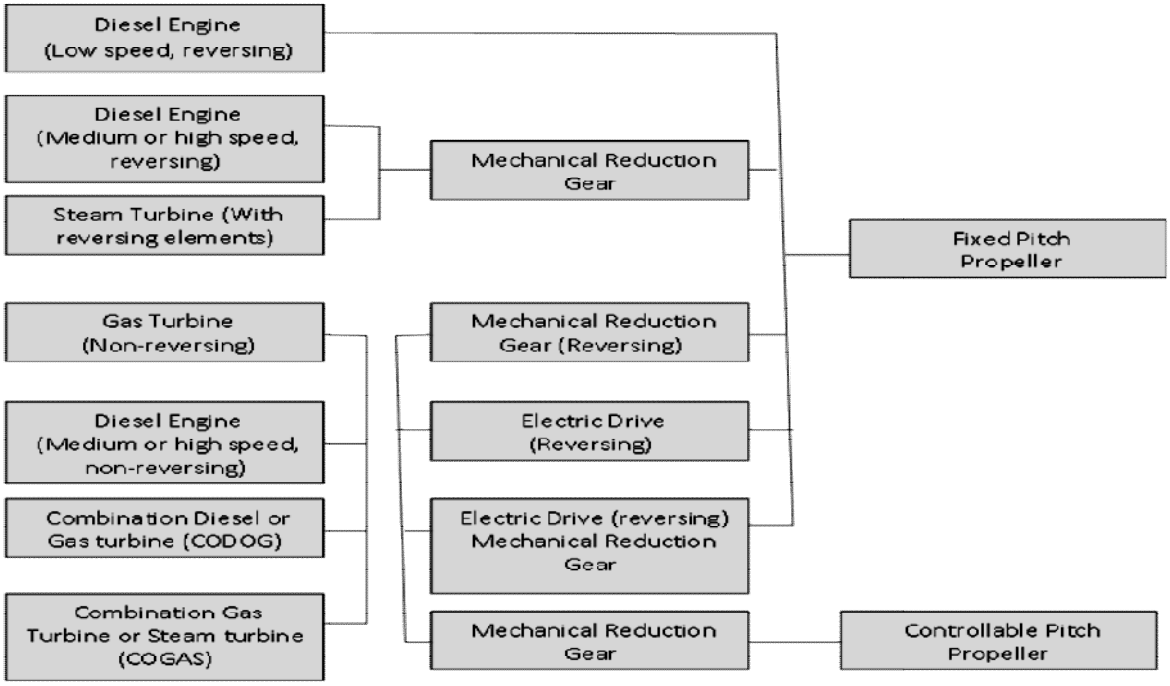

Figure 2:8 Principal alternatives in the selection of propulsion arrangements [23]

2.4.1 Electric Propulsion Drives

When compared with other conventional types of propulsion drive alternatives, the electrical connection between the generator and the propulsion motor provides a freedom of arrangement that is not offered in a mechanical drive system. The advantages of this configuration have the potential of outweighing the inherently higher first cost, increased weight and space and the higher transmission losses associated with it. Among its attractive features is the ease and convenience with which the propeller speed and its direction of rotation can be controlled. In a multiple prime mover arrangement, this alternative provides a convenient means of coupling several units to the propeller without the use of mechanical clutches or couplings which makes It contribute to more efficient vessel operation thereby, making it possible for enough down time for scheduled maintenance on units not required for propulsion.

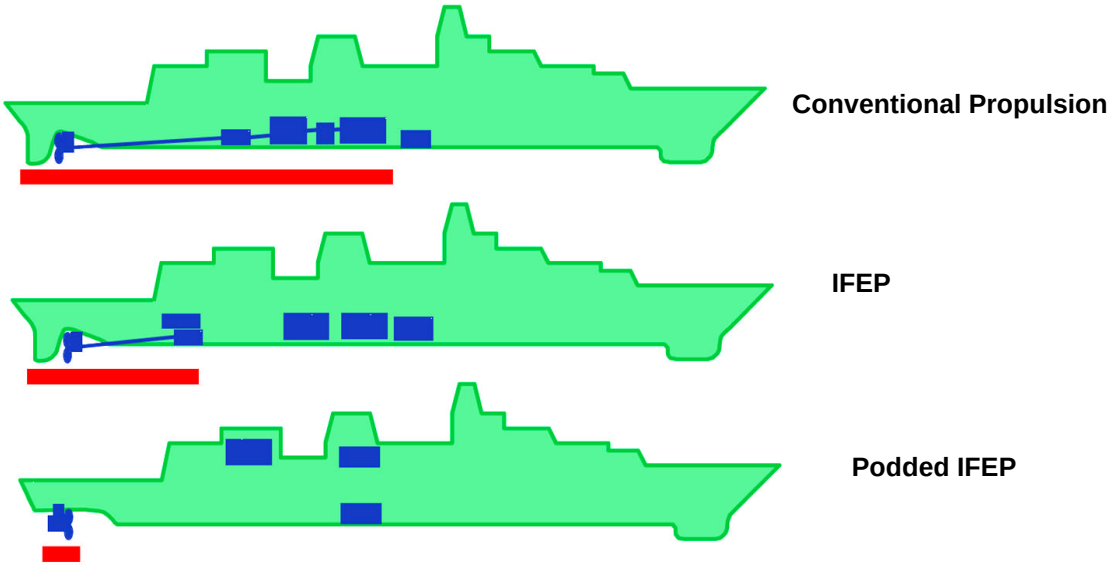

Figure 2:9 Layouts of mechanical and electric propulsion systems [6]

Main propulsion generator power may be used for other functions when their full output power is not required for its primary function [25]. In general, these drives are used in the following types of applications:

- Vessels requiring a high degree of manoeuvrability, such as ferries
- Vessels with large hotel loads, such as Cruise ships
- Vessels using non-reversing prime movers, high speed and multiple prime movers (gas turbines and many high speed diesels)
- Deep water submergence vehicles which employ relatively small amounts of propulsion power and move at low speed by using energy obtained from batteries.

Nearly all the power generated on ships is accomplished using AC generators and when the term of DC propulsion is used, it only implies that the system incorporates a means of converting the AC to DC such that a DC motor can be coupled to the propeller.

2.5 Operating Requirements

The initial issues that need to be addressed in the technical requirements setting process to form the basic definition of the commercial ship may include the cargo type and capacity, principal characteristics, additional port requirements, rules and regulations, service speed, endurance, design environmental conditions and the vessel design life [26]. In line with this, good practice dictates that a ship's propulsion plant be rated such that the desired ship speed can be attained with additional power capabilities held in reserve to allow for a degradation of performance with time [23]. Furthermore, the continuing internationalisation of trade and production combined with the increasing congestion on land and in the air is generating interest in novel concepts for fast cargo and passenger vessels [6]. These requirements apply to all the diverse configurations.

2.5.1 Operating Environment

The Operating environment of the marine gas turbine provides some unique challenges [27] in which a considerable amount of moisture, laden with salt and other marine elements can be sucked through the intake, into the engine along with the large amounts of air associated with gas turbine. Although salty air has never really been a problem, the engine needs to be adapted in order to prevent corrosion and the possible blocking of passages. In addition to this, the gas turbine is exposed to hostility due to pitching, rolling, yawing, propeller vibration etc and as such, proper care must be exercised in the design and maintenance of dampening structures.

The thermodynamic cycle analysis of the gas turbine models conducted in this research using performance parameters such as pressure, temperature, specific heat, efficiency factors and adiabatic compression exponent has shown that the higher the firing temperature of the gas turbine the more power to be derived and the more economic the fuel flow. It also shows that any increase in pressure ratio results in maximum power and maximum thermal efficiency, and the higher the PR, the greater the benefits from the increased firing

temperature. Greater efficiency can be achieved in simple cycles by adopting high pressure ratios while the combined cycle obtains it with more modest pressure ratios and greater firing temperatures. A typical simple cycle engine can convert 30% to 40% of its fuel input into shaft power and only but 1% to 2% of the remainder is in the form of exhaust heat.

2.5.2 Factors Affecting Gas Turbine Performance

The performance of the gas turbine can be altered by anything that affects the density and/or mass flow of the air intake to the compressor and the following are the most obvious factors:

- Ambient weather conditions from the reference sea level conditions of 15^{o}C and 1.0325 bar – This has a pronounced effect on the gas turbine overall performance so much that a change of 10^{o}C can affect the power output by as much as 5% for a constant TET [28]

- Increase in site elevation – Air density reduces as the site elevation increases

- Increase in humidity, but it is less than the loss due to temperature.

- Inlet and exhaust losses –air filters, silencers and evaporative coolers at the inlet or heat recovery devices at the outlet all cause pressure losses in the system

- Fuels – Natural gas (methane) produces nearly 2% more power than does distillate oil and this is due to the higher specific heat in the combustion products resulting from the higher water vapour content produced by the higher hydrogen/carbon ratio of methane [29]

- Water or steam injection – Used for NO_x control to meet applicable emissions regulations while increasing power output due to the additional mass flow resulting from it

- Air extraction – Most gas turbines are capable of providing up to 10% which can be used for a variety of purposes including starting other gas turbines, as anti-icing air for the intake duct during cold weather operation or for attenuating machinery and propeller noise.[21]

Table 2:3 Effects of Pressure drop of 10 mbar (4 inches H_2O) for a typical gas turbine - GEMS7001EA [29]

GT Performance Losses	Inlet Ducting	Outlet Ducting
Power output [%]	1.4	0.42
Heat Rate increase [%]	0.45	0.42
Exhaust Temperature Increase [^{o} C]	1.1	1.1

Even though the evaluation of these research gas turbine models has included the effect of site elevation by assuming between -400m to +400m, the correction of altitude or barometric pressure is considered as straight forward.

2.6 Elementary Terms for Defining Ship Hull Forms

The parameter values of any ship design impact on one another and once the hull is broadly defined, an estimate can be made of the brake power required to drive it through the water at the required speed. The brake power required dictates the physical size of the propulsion plant and this influences the size of the engine room and the overall size of the ship [30]

The quality of any marine vessel as being fit to accomplish its intended mission is known as seaworthiness and it is on this basis that Marine Engineers must seek to determine the nature of the environment under which the intended vessel is expected to operate and to ensure that the following parameters are well defined:

- The vessel's structure
- Stability and motions
- Resistance and powering

2.6.1 Displacement and Deadweight

This is generally defined as the weight of the water displaced by the immersed part of the ship. On the other hand, since the specific weight of sea water is 10,053N.m^3, displacement can then be considered as a force and be expressed in Newtons (N) or Mega-Newtons (MN) whereby, 1 MN of displacement will be equal to 99.47 m^3. It is to be determined by the length and breadth of the ship hull depending on the shape chosen for the design. Propulsion, electrical and auxiliary machinery, together with fuel, occupies a good percentage of the displacement in most ships but improved technologies when collectively applied have the potential to reduce this while simultaneously improving other ship performance characteristics [31]

Table 2:4 Examples of the relationship between Displacement, Deadweight Tonnage and Lightweight [31]

Ship Type	Dwt/Light Weight ratio	Displacement/Dwt ratio
Tanker/ Bulk Carrier	6	1.17
Container ship	2.5-3.0	1.33-1.40

Also, of significant importance to the design and operation of any merchant ship and its earning capacity are the measurements of ‘tonnage’ and ‘deadweight. The deadweight can be defined as the cargo, stores, fuels, lube oils, water, personnel and other effects that the ship can carry when loaded to specific load draft. It differs from the ship’s lightweight which comprises of the hull weight and machinery only. On the other hand, the volume of a ship is expressed in tons of 2.83 m^3 each and is referred to as the ship’s tonnage which represents the parameter used for determining charges for berthing, docking, passage through canals and locks and many other facilities required for the ship’s smooth operation.

2.6.2 Description of Hull Forms and Design Factors

The design of a new vessel typically begins with a careful analysis of the existing fleet in order to obtain general information on the type of vessel of

interest and the recommended approach to obtain an initial estimate of vessel length, beam, depth and design draft is to use a data set of similar vessels through inspection of the use of regression equations using primary functional requirements such as cargo deadweight and speed as independent variables [32]. Some of the most important parameters necessary for describing the seaworthiness of any marine vessel in line with the aforementioned requirements may include the physical dimensions of the hull and the cargo carrying capacity among others. Therefore, in order to properly establish the seaworthiness of the selected designs of the ship model dedicated for this research, some of the most important parameters were defined.

Of great significance for the ship propulsion is that of its hull that is under the water line in which the choice of the design draught depends on the degree of load. The ship's overall length, L_{OA} is normally of no consequence when calculating the hull's water resistance but the length of the water line, L_{WL} and the so called length between perpendiculars, L_{PP}

Other important factors are the draught; T is defined as the vertical distance from the water line to that point of the hull which is deepest in the water and the breadth on water line, B_{WL}. These dimensions are further converted into form coefficients in order to ease the task of designing a ship from start to finish.

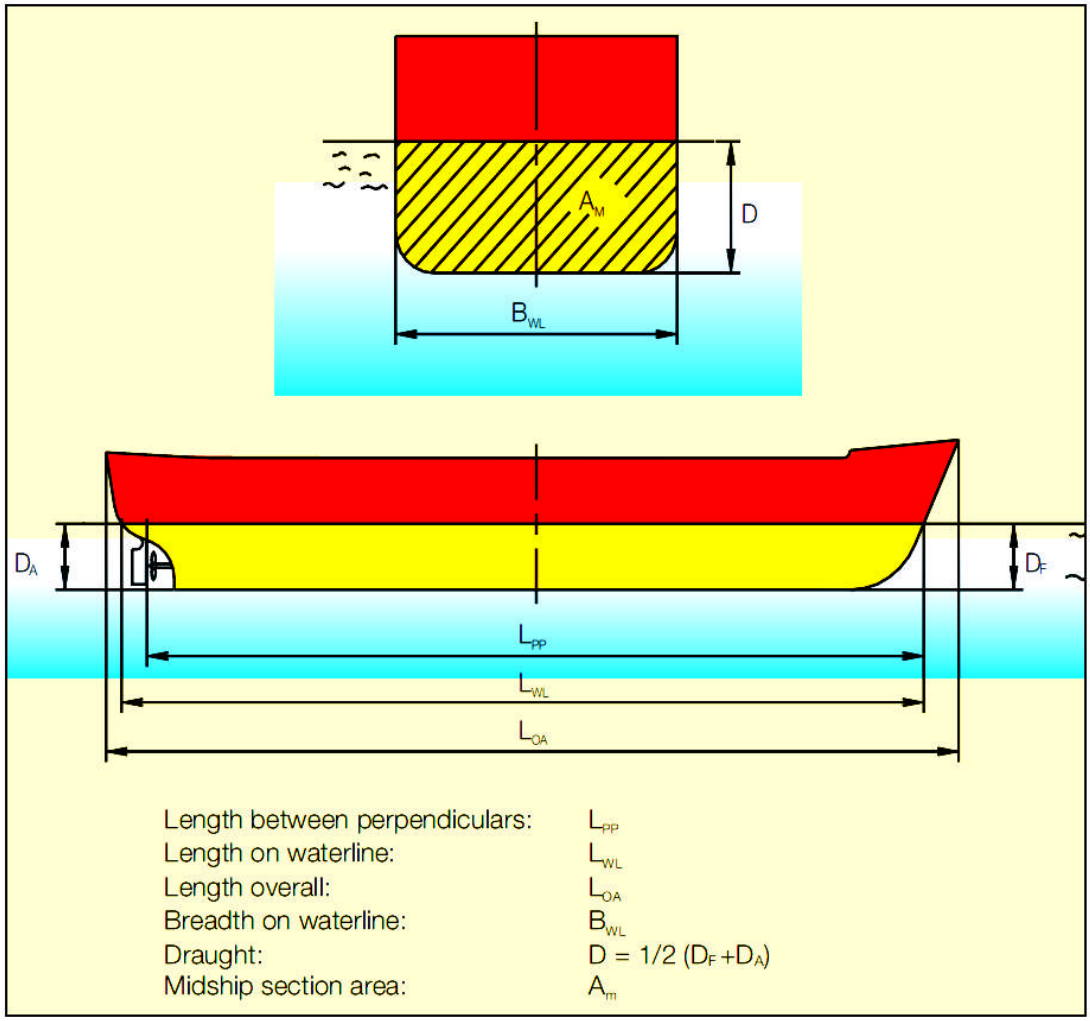

Figure 2:10 Some Important Dimensions of a Ship Hull [33]

$$L_{PP} = 0.97 \times L_{WL}$$ **Equation (2-1)**

Various form coefficients are used to express the shape of the hull and its moulded body. The most important of these coefficients is the block coefficient, C_B which is defined as the ratio between the displacement volume, ∇ [34] and the volume of a box with dimensions (L_{WL} x B_{WL} x T) as represented in Equation (2-2) .

$$C_B = \frac{\nabla}{LBT}$$ **Equation (2-2)**

The midship coefficient is a measure of the fullness of the maximum section represented by Equation (2-3). Where A_M is the area of the midship section

$$C_M = \frac{\mathrm{A_M}}{\mathrm{B_{WL}\ x\ T}} \qquad \textbf{Equation (2-3)}$$

As an important parameter in powering estimates, the Prismatic coefficient is a measure of the fullness of the ends of the hull. It expresses the ratio between the displacement volume and the product of the midship frame section area A_M and the length of the water line L_{WL} represented by Equation (2-4)

$$C_P = \frac{\nabla}{\mathrm{L_{WL}\ x\ A_M}} = \frac{\nabla}{\mathrm{C_M \times B_{WL} \times D \times L_{WL}}} = \frac{\mathrm{C_B}}{\mathrm{C_M}} \qquad \textbf{Equation (2-4)}$$

The water plane area coefficient is a measure of the fullness of the water plane and expresses the ratio between the vessel's water line area, A_{WL} and the product of the length, L_{WL} and the breath, B_{WL} of the ship on the water line as represented in Equation (2-5)

$$C_{WP} = \frac{\mathrm{A_{WL}}}{\mathrm{L_{WL}\ x\ B_{WL}}} \equiv \mathrm{C_B} + 0.10 \qquad \textbf{Equation (2-5)}$$

2.6.3 Hull Resistance

To facilitate the development of an acceptable method for predicting the preliminary propulsion power requirement, the problem is broken down into the following components which either directly attribute to, or influence its value:

- Hull resistance
- Appendage resistance
- Effect of hull roughness
- Effect of hull fouling
- propulsion factors

- transmission of power (propeller)
- wind resistance
- influence of sea state (wave height)

A ship's resistance is particularly influenced by its speed, displacement and hull form and the total resistance, R_T consists of many source resistances, R which can be divided into three main groups of Frictional, Residual and Air resistances. The influence of the frictional and the residual depends on how much of the hull is below the water line while that of the air depends on how much of the ship is above the water line. All of these have been considered in the models that have been designed in this text.

Details of some of the most important parameters that have been calculated for designing the ship models are summarised in Table 2:5.

The dynamic force that results when the sea water is hit by the ship's hull creates a relationship between the speed of the water, V and its density, ρ resulting in a dynamic pressure, $(\frac{1}{2} \times \rho \times V^2)$ .which is also known as the Bernoulli equation and by utilizing a dimensionless coefficient, C, it is used as the basis for calculating the source resistances. The general data for resistance calculations uses the dynamic pressure which exerts a reference force F, on the hull's wetted surface area A_S, (including the rudder's surface) in relationship to C in the following equations:

$$F = \frac{1}{2} \times \rho \times V^2 \times A_S \qquad \textbf{Equation (2-6)}$$

$$R = C \times F \qquad \textbf{Equation (2-7)}$$

The frictional resistance R_F of the hull depends on the size of the hull's surface area A_S and on the specific frictional resistance coefficient C_F. It increases with fouling of the hull which may arise as a result of the growth of marine biological organisms in the form of sea grass, algae or barnacles. It represents a considerable part of the ship's total resistance in the region of between 70-90%

for low speed ships and sometimes less than 40% for high speed ships. The frictional resistance increases at a rate that is virtually equal to the square of the vessel's speed.

On its own part, residual resistance R_R comprises wave resistance and eddy resistance. Wave resistance refers to the energy loss due to the waves created during the vessel's propulsion through the water, while the eddy refers to the energy loss caused by flow separation which creates eddies particularly at the aft end of the ship. The wave resistance affects the speed of the ship such that a barrier could be imposed at such a point when the propulsion can no longer cause the desired increase in speed and converts it into wave energy.

Although anti fouling paints are normally employed as anti-fouling agents, the effect of ship hull surface corrosion and fouling along with its counterpart effect from sea waves on the performance of the marine gas turbine are a major subject in the current research.

The ship's total towing resistance therefore is the sum of the friction, residual and air resistance:

$$R_T = R_F + R_R + R_A \qquad \textbf{Equation (2-8)}$$

The corresponding towing power necessary for moving the ship through the water at a speed, V is known as the effective power, P_E as described in Equation (2-9).

2.6.4 Determination of ship Hull Resistance

Tremendous reference to the statistical regression analysis conducted by J. Holtrop [3] was used to form the main structure of the marine gas turbine simulation "Poseidon" code developed by Tsoudis, [1]. The present work seeks to build on that foundation in order to accomplish a comparative analysis of a combination of different GT and ship configurations that have been identified in the research.

Hull resistance can be predicted with various degrees of accuracy using either theoretical, statistical, experimental or empirical methods or a combination of either of them and although series of test data is the most reliable means of estimating the resistance of a ship through the construction of a scale model of its underwater portions, the process is lengthy and requires estimates to be made for the major hull characteristics.

Table 2:5 Main Characteristics of the Ship Types under Investigation

Ship types	LNGC	Cargo ship	Cruise ship	Passenger Ferry
Length at water level, L_{WL} [m]	266.0	287	283.5	188.54
Maximum Beam, B [m]	42.6	40.0	39.0	25.0
Average design draft, T [m]	11.3	14.0	9.0	6.40
Block coefficient, C_B	0.7493	0.65	0.65	0.55
Midship coefficient, C_M	0.9857	0.975	0.98	0.93
Water plane coefficient, C_{WP}	0.7848	0.75	0.78	0.69
Service speed, V_s [knots]	19.5	25.0	22.0	30
Froude Number, F_n	0.1964	0.4746	0.4172	0.34687
Displacement, Δ [tons]	965604.88	2215031.21	1636347.992	166978.368
Wetted surface, S_w[m^2]	13831.0	24592.051	20662.695	4916.588
Lambda, λ	0.93	0.84	0.91	0.63
Prime mover Brake power [KW]	29801.96	87242.59	64428.72	46576.05
Effective power [KW]	16126.95	38786.30	26803.82	24481.29
Total resistance [N]	1.607743e+006	3.427321e+006	2.605348e+006	1.641101e+006

In order to establish the machinery and engine room size and weight which will directly influence the overall size of the vessel, an early estimate of the resistance is required.

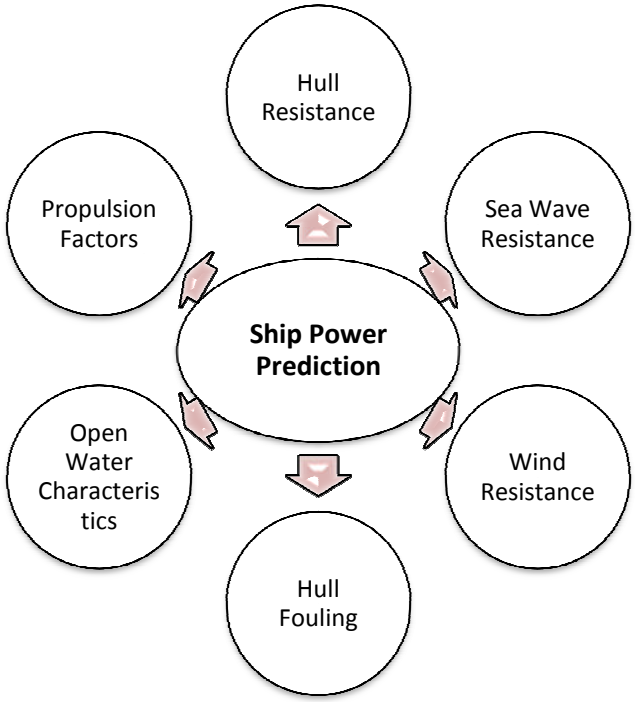

Figure 2:11 Composition of the Ship Power Prediction Model

2.6.5 The Propeller

In practice, one or other propulsive devices are required for the conversion of the power produced by the ship's main engines into thrust. Devices available range from a water paddle to a water jet but none however are 100% efficient. For the purpose of this study only the screw type propeller will be considered i.e. no consideration given to highly skewed, surface piercing and super cavitating versions.

2.6.6 Propulsion Performance estimation

The determination of the required propulsion power and engine sizing requires working from a hull total tow rope resistance prediction to the required installed prime mover brake power. The current approach has evolved from the tradition of initially testing a hull or a series of hulls without a propeller and on the other hand, testing a propeller or a series of propellers without a hull before linking the two together through the definition of hull-propeller interaction factors.

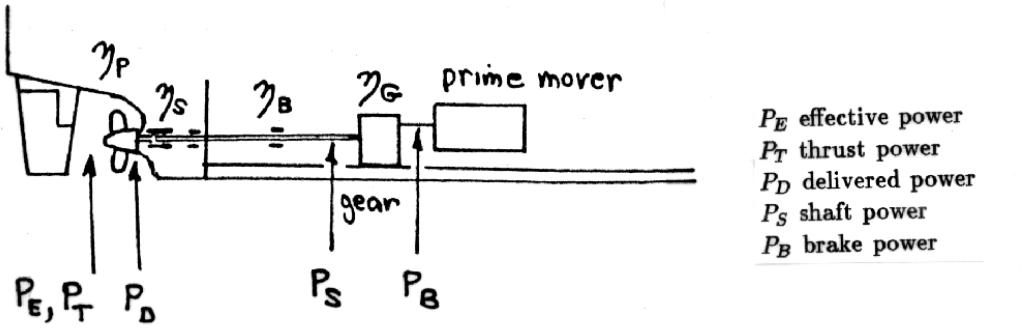

Figure 2:12 Variation of ship power along its path of transmission [32]

The flow of the ship's propulsion power from its prime mover (source) through the shaft and bearings to the propeller, (sink) is illustrated schematically in Figure 2:12.

When the ship hull is without a propeller behind it, the total resistance to be encountered, R_T (N) at a speed, V (m/s) can be expressed as the effective power

$$P_E = \frac{\mathrm{R_T}}{1000} \times \mathrm{V\ (KW)} \qquad \textbf{Equation (2-9)}$$

The open water test of a propeller without a hull in front of it will generate a thrust, T at a speed V_A and with an open water propeller efficiency η_o which can be expressed as the thrust power.

$$P_T = \frac{\mathrm{T} \times \mathrm{V_A}}{1000} \times \mathrm{V\ (KW)} \qquad \textbf{Equation (2-10)}$$

The results for the hull without the propeller and for the propeller without the hull can be linked together by the definition of the hull-propeller interaction factors defined as follows: The shape of the hull, the viscosity of the water and

$$V_A = \mathrm{V}(1 - \mathrm{w}) \qquad \textbf{Equation (2-11)}$$

$$T = \mathrm{R_T}/(1 - \mathrm{t}) \qquad \textbf{Equation (2-12)}$$

$$\eta_P = \eta_o \times \eta_r$$ **Equation (2-13)**

The wake fraction (w) is the factor that accounts for the difference between the ship speed (V_s) and the speed of advance of the propeller (V_a). On the other hand, the thrust deduction factor (t) accounts for the increase in resistance due to the propeller suction and is defined as the difference in thrust and the ship resistance.

η_P = behind the hull condition propeller efficiency

η_r = relative rotative efficiency that adjusts the propeller's open water efficiency to its efficiency behind the hull

By substituting Equation (2-11) and Equation (2-12) into Equation (2-10) and using Equation (2-9) will yield the relationship between the thrust power and the effective power

$$P_T = \mathrm{P_E}\frac{(1-\mathrm{w})}{(1-\mathrm{t})}$$ **Equation (2-14)**

We can then conveniently define the group of terms called the hull efficiency

$$\eta_h = \frac{(1-\mathrm{t})}{(1-\mathrm{w})} = \frac{\mathrm{P_E}}{\mathrm{P_T}}$$ **Equation (2-15)**

The hull efficiency therefore can be viewed as the ratio of the work done on the hull P_E to the work done by the propeller P_T

Furthermore, the input power delivered to the propeller P_D is related to the input thrust power from the propeller P_T by the behind the hull efficiency Equation (2-13) and when we use Equation (2-14), it yields

$$P_D = \frac{\mathrm{P_T}}{\eta_\mathrm{P}} = \frac{\mathrm{P_T}}{(\eta_\mathrm{o} \times \eta_\mathrm{r})} = \frac{\mathrm{P_E}}{(\eta_\mathrm{h} \times \eta_\mathrm{o} \times \eta_\mathrm{r})}$$ **Equation (2-16)**

2.7 LNGC Gas Turbine Propulsion Systems

The basic choices when selecting a LNGC's prime mover are a diesel engine, a gas turbine or steam turbine [23] but the simplicity and reliability in consuming the natural boil off gas has established the steam turbine as the traditional propulsion system despite its relatively low efficiency. The possibility of increasing the size of future LNG Carriers is one of the factors that have initiated the search for alternative systems and diesel alternatives of either the high efficiency, two stroke slow speed (SSD) option or the dual fuel diesel electric (DFDE) were observed by Moon [35] as being very popular propulsion system alternatives with advantages of high fuel efficiency and freedom of fuel choice between fuel oil and natural/forced BOG. On the other hand, a study by Haglind [36] has suggested that the diesel engine would have to be adapted for a gaseous fuel; otherwise expensive re-liquefaction plants would be required onboard, making it a less attractive option, because of the inherent economic (considering both first costs and operating costs) and redundancy disadvantages. In order to show the true revenue making potential of the gas turbine driven LNGC, Gupta et al [37] compared it with the current state of the art conventional LNGC and the gas turbine electric podded drive was found to have the best revenue making capacity due to its combined benefits of high cargo capacity and Highly efficient propulsion system. Next to it was its mechanical drive counterpart offering unsurpassed thermal efficiency and high cargo capacity as well.

Haglind [36] in his review of gas turbine and steam turbine combined cycles, has reasoned that the space requirement for a gas turbine-based plant is very low and for a given power level, the weight of such a plant is lower than that consisting of diesel engines and makes the ship to benefit from a reduced engine weight by lowering its displacement, thereby reducing the power required for propulsion. Alternatively, unless the ship is volume-constrained, the cargo/passenger capacity may be increased while retaining the displacement.

To check the economic viability of the gas turbine LNGC propulsion system, the comparative life cycle cost (LCC) approach presented by Chang [38] will be adopted in this thesis.

2.8 LNGC Propulsion System Alternatives

Recently, the LNG shipping industry has observed a dramatic change in propulsion system beyond the old denominator of the steam turbine and the strong competitors are as follows:

- Single-fuel (low speed) diesel mechanical propulsion and re-liquefaction (SFDM+R)
- Dual fuel gas turbine electric (DFGE)
- Dual-fuel (low speed) diesel mechanical propulsion (DFDM)
- Dual-fuel steam turbine mechanical propulsion with Reheating (DFSMR)
- Dual-fuel (medium speed) diesel electric propulsion (DFDE)

The optimal choice of either of these alternatives depends on the capital investment as well as the operating cost. Mention has already been made that this thesis is mainly concerned with the operating cost component of the gas turbine option which depends largely on the operating conditions to be determined by the chosen path designed for the sail of the LNG Carrier. The cargo capacity, voyage duration, main engine idling time, sea water temperature, atmospheric temperature are different from ship to ship. Other factors include the system availability which also depends on the configuration of the propulsion system (especially the existence of redundant back-up systems), system failure rate and repair time about which the situation is entangled by specific advocates who mostly choose to magnify the benefits while shrinking the shortcomings of their products.

There is a surge in new projects for the construction of LNG carriers which has generated interest in the development of alternative propulsion systems to the traditional gas fired steam plants. Since 2004, many LNG Carrier projects with

propulsion systems other than the steam turbine have been under construction and it is claimed that the preferred solutions include those already listed above. There were 155 LNG Carriers with a total capacity of about 18 million m^3 in operation. Among them, 125 were with capacities from 120 km^3 and above, 15 of them had capacities between 50 km^3 and 120 km^3 and the other 15 had less than 50 km^3. Within the same period, there were about 55 new projects under construction, from which 46 of them were with a capacity of 138 km^3 or greater and 9 had less than 138 km^3 while 5 were to be delivered in 2004 while placing for 6 new orders within the same period of time [39].

The quest for more efficient systems with better capability for burning the BOG as an alternative makes the environmental friendly characteristics of the gas turbine along with its added merits of compactness and ease of maintenance as well as its available manpower and ease of automation is the main driver of this research to evaluate the gas turbine as a viable alternative propulsion system to the steam turbine without shrinking the relative shortcomings associated with it.

Having defined the characteristic parameters that are capable of affecting engine performance as the oceangoing LNG Carrier sails along its trade route, the possible scenarios were simulated with each of the gas turbine engines installed, one after the other and case after case.

2.9 Use of LNG as Fuel on Other Ship Types

LNG (Liquefied Natural Gas) is natural gas that has been cooled in order to be converted to liquid form, requiring a temperature near -162^oC for the purpose of transporting it in specially designed tanker ships for transportation across long distances from producing locations to consuming regions. It has now been proposed as an alternative solution to the challenge of cleaner shipping fuels, particularly for relatively short and scheduled trades in northern Europe [40] [41]. Usually, it has to be re-heated to convert to gaseous form before combustion in an engine or before insertion into the gas pipeline grid, if imported as part of a general gas supply. It is the cleanest of all fossil fuels and

it is mainly a mixture of hydrocarbon gases, odourless and colourless in its pure form.

The proposal for using LNG as fuel for other ship types other than the LNG Carrier [41] may be limited by the fact that the commodity today is not a common fuel source and one of the downsides of its application in other ship types is that the tanks will take up a lot of space inside the ship due to their cylindrical shape. However, there very many reasons why it stands out as the marine fuel for shipping in the future which may include:

- LNG reduces considerably air pollution in port cities, on fairways and on the "Highways of the Sea"
- By only one measure LNG fullfills all MARPOL Annex VI and European Fuel Directive requirements
- LNG reduces particulate matter emissions by 100%
- LNG reduces SOx emissions by 100%
- LNG reduces NOx emissions by 70%
- LNG reduces CO2 emissions by 25%
- No particle filters required
- No Selective Catalytic Reduction or other NOx minimising technology required

3 RESEARCH METHODOLOGY

The major focus of this investigation is to conduct a comparative analysis involving all the possible configurations of the marine gas turbine propulsion systems by undertaking a variety of voyages. The work was conceived with a view to assess the Techno-economic and Environmental factors involved in adopting the gas turbine engine as a preferred alternative propulsion prime mover for some category of merchant ships and the LNG Carrier in particular. A variety of simulations have been conducted for the off design performance investigation and the analysis of pollutant emissions as well as the HPT blade creep life prediction.

3.1 The Research models

Different gas turbine cycle designs were modelled and simulated in accordance with anticipated off design conditions that were expected to be encountered when these models were finally installed and operated in the marine environments where the vessels ship would be travelling.

A model of an LNG Carrier was necessary but three other types of seagoing merchant vessels were also modelled among which are a cargo ship, a cruise liner and a fast speed ferry. The simulation would only be possible having established a fixed voyage route for each of these ships while taking into account all the environmental and hydrodynamic factors likely to affect the behaviour of the gas turbine. To this end, a transit route was adopted for each ship only by establishing their loading and offloading terminals. The weather and sea state profiles along these routes were also established. For the purpose of an effective analysis, several scenarios of the case study were made possible by to establishing the weather profiles for three different seasons of the year and data for temperature and sea states for all the locations along the routes were obtained for winter, spring and summer weather. In addition to this, the effect of hull fouling was added in three different dimensions under three levels of hull roughness in steps of 120μm up to 360μm.

3.1.1 TURBOMATCH Conception of the Gas Turbine Models

The ‘TURBOMATCH’ scheme, which is a simulation code and a product of the ongoing research efforts in gas turbines at the Power and Propulsion Department of Cranfield University, was deployed for developing the four aero-derivative marine gas turbine models. This simulation code is a research tool for the conduct of design and off design performance calculations for existing and conceivable gas turbine thermodynamic cycles. It is a scheme that utilizes pre-programmed routines called “bricks” in a FORTRAN environment and with the use of interfaced “code words”, it provides the user with the ability to simulate the operational state of the gas turbine as the working fluid flows from one component to another throughout the cycle. The outcome of the simulation generates values of engine power output or thrust, fuel consumption and the mass flow of the air among many other performance parameters as output. The general basic fuel type accepted in the process is kerosene with a calorific value of 43.165 MJ/kg [42] [43].

The simulation provides valuable detailed information about the performance of every component and determines the properties of the gas at each station within the gas flow path. The output is presented both in “txt” files and excel spread sheet thereby affording us the flexibility to break the results into tables for the sake of interpolating the data at a later stage.

3.1.1.1 Uninstalled” Performance Simulation

The sizes and power rating of the gas turbine engines conceived for the purpose of the investigation were first considered and the guessed values of mass flow, pressure ratio and Combustor Outlet Temperature (COT) or Turbine Entry Temperature (TET) were decided upon to form the basic inputs required for building the models. Apart from assessing their design point performance, it was also necessary for the simulation to be conducted at off-design so as to obtain their overall performance throughout the entire operating range of speed and power output.

3.1.1.2 Off-Design Operational Range

The values considered for the range of ambient temperature variation were pegged between 0^{o}C and 40^{o}C while the ambient pressure was assumed to be varying with changes in altitude between -400m and +400m. The results obtained were plotted and will be further discussed in the next Chapter. Two samples of the tabulated results representing the power output variation of the 25MW Inter-cooled Recuperated model both at lower and higher power setting are illustrated in Table 3:1 and Table 3:2.

3.1.2 Exhaust Pollutant Emissions Model

For many years, there was little concern about gas turbine emissions except for the need to eliminate smoke from the exhaust. Gas turbine combustion is a clean and efficient steady flow process that burns the hydrocarbon fuel using a large amount of air so as to keep the turbine entry temperature at an appropriate value. As the population of gas turbines increase, the situation changed and the issue of emissions control has become one of the most important factors in the design and operation of land-based and marine gas turbines. The environmental impact cost due to emissions from regular operation of ships involves damages done to the air, water, soil and climate [44] Although the combustion efficiency of the gas turbine is typically between 98.5% and 99.5%, the percentage loss still results in the promotion of two toxic pollutants in the form of unburned hydrocarbons (UHCs) along with its colourless and odourless counterpart known as carbon monoxide (CO). UHCs on the other hand, have the characteristic smell usually found in airport environments. Another pollutant formed during the process of combustion, is due to the oxidation of nitrogen found in the combustion air known as nitrogen oxides (NOx). Nitrogen does not take part in the combustion process but the pressures and temperatures that prevail in the primary zone of the combustor result in a small amount of nitrogen being oxidised. This impact of pressure and temperature is so significant in its formation to the extent that any rise in these parameters, causes an exponential increase of NOx.

Therefore, in its interaction with the environment under which it operates, the marine gas turbine generates a pollution of the atmosphere through the emission of pollutant gases from the engine's exhaust. For this reason, modern combustor design is totally dominated by the need for low emissions, both of Oxides of Nitrogen (NOx), Carbon monoxide (CO) Carbon dioxide (CO_2) and unburned hydrocarbons (UHC). This has made the combustor to become a critical component that must be carefully designed to operate reliably at extreme temperatures so as to ensure the provision of a suitable temperature distribution at entry to the turbine in order to produce a minimum amount of pollutants over a long operating life. Based on this, this research has included an exhaust emission model within its framework through the implementation of the "APPEM" (Analysis and Prediction of Pollutant Emissions) simulation code, which has the capability of determining the off-design emission quantities of the gas turbine when operating in a marine environment.

3.1.2.1 Combustion of Hydrocarbon Fuels

By dividing the process of combustion into three distinct segments, the combustion chamber exit temperature can be controlled in order that the creep life of the turbine component is not compromised. The three distinct parts are as follows:

- The Primary zone, where the fuel is burnt and the heat from the fuel is released
- The Intermediate zone, where additional air is introduced in order to complete the combustion.
- Dilution zone, where the remaining air is introduced in order to reduce the combustion chamber exit temperature in line with that required for the turbine.

Liquid fuel must be vaporised in order to achieve a satisfactory combustion process and the fuel must be heated to a high enough temperature where the molecules are broken down into elementary parts called radicals. In this regard,

such fuels like HFOs possess a high carbon-hydrogen ratio as a result of which they require burning time to convert CO into CO_2. Atypical chemical equation governing the combustion of methane (CH_4) in oxygen is given by

$$CH_4 + 2O_2 \rightarrow (CO + OH + CH_3) \rightarrow CO_2 + 2H_2O \qquad \text{Equation (3-1)}$$

Thus the carbon and hydrogen content of any fuel determines the quantity needed for complete combustion of the fuel in air and poor atomization can lead to reduced combustion efficiency and the formation of pollutants such as CO and UHC. For liquid fuels therefore, atomization is required through the use of pressure swirl atomizers, air blast atomizers or fuel vaporizers as opposed to gaseous fuels. The formation of radicals and species such as CO and hydrocarbon radicals is responsible for the process of combustion. The intermediate zone therefore adds more air in order to form a chemical reaction for production of carbon dioxide and water. With the combustion efficiency usually between 98,5% and 99.5%, the associated loss is responsible for the formation of CO and UHC present in the exhaust gases. CO and UHCs are both toxic and they are promoted by the same conditions.

On the other hand, NO_x is formed due to the oxidation of nitrogen found in the combustion air around the primary zone and does not take part in the process of combustion. NO_x is a toxic pollutant that takes part in the formation of thermal smog and enhances the depletion of the ozone. It is clear therefore that the formation of pollutants is dependent on the combustion pressure,, temperature and the mixing of fuel with the combustion air. The higher the temperature and the pressure, the higher will be the reaction rate leading to lower CO and UHC while increase in NO_x formation. It is important to therefore, that combustion pressure and temperatures vary with engine load, decreasing when the load is reduced. In this investigation, increasing levels of CO and UHC and decreasing levels of NO_x were observed in the event of reductions in engine load.

3.1.2.1.1 Prediction of NO_x, CO, UHC and the calculation of CO_2

The three predominant factors that affect the formation of these pollutants have already been identified, including fuel-air ratio, fuel and air mixing, combustor geometry and residence times. Various correlations have been proposed and validated and are a very useful means of predicting gas turbine emissions. In the case of CO_2 however, it is a greenhouse gas that is thought to be responsible for global warming and its prediction is relatively straightforward and can be readily calculated once the carbon-hydrogen ratio of a fuel is known.

The correlations are as follows:

(a) NO_x correlation due to Lefebre [45] suggests the following:

$$NO_x = 9 \times 10^{-8}\, \mathrm{P}^{1.25}\, \mathrm{V_c}\, \exp(0.10\mathrm{T_{st}})\, \mathrm{T_{pz}}\, /\mathrm{m_a} \qquad \text{Equation (3-2)}$$

(b) For the prediction of CO emissions, Lefebre [45] still proposes the following equation

$$\mathrm{CO} = 86\mathrm{m_a} \times \mathrm{T_{pz}} \times \exp - \frac{(0.00345\mathrm{T_{pz}})}{(\mathrm{V_c} - \mathrm{V_e})} \left(\frac{\Delta \mathrm{P}}{\mathrm{P}}\right)^{0.5} \mathrm{P}^{1.5} \qquad \text{Equation (3-3)}$$

(c) The correlation for the prediction of UHC was highlighted in ref [46] as follows:

$$\mathrm{UHC} = 0.755 \times 10^{11} \exp \frac{\left(\frac{9756}{\mathrm{T_{pz}}}\right)}{\mathrm{P}^{2.5}} (\mathrm{t} - 0.35\mathrm{t_e}) \left(\frac{\Delta \mathrm{P}}{\mathrm{P}}\right)^{0.5} \qquad \text{Equation (3-4)}$$

The values are calculated as an emissions index, g/kg of fuel and where,

Vc combustion volume, m^3

Ve volume occupied by the evaporated fuel,' m^3

P The combustion pressure, kPa

ΔP Combustion non-dimensional pressure drop

m_a The combustion air flow, kg/s

T_{pz} Average primary zone temperature

t is Residence time

t_e is the evaporation time in seconds

(d) The equation governing the formation of CO_2 states that 1 molecule (mole) of the fuel will react with n moles of oxygen (O_2) to produce n_1 moles of H_2O in the following:

$$C_xH_y + nO_2 = n_1CO_2 + n_2H_2O \quad \text{Equation (3-5)}$$

Where

x/y is the carbon-hydrogen ratio of the fuel

$n_1 = x$; $n_2 = 0.5y$; $n = n_1 + 0.5\, n_2 = x + 0.25y$ and by substitution,

Equation (3-5, becomes

$$C_xH_y + (x + 0.25y)O_2 = xCO_2 + 0.5yH_2O \quad \text{Equation (3-6)}$$

3.1.2.2 Pollutant Emissions Modelling

The input parameters of the gas turbines earlier used in the TURBOMATCH uninstalled, off design performance simulation exercise were equally used as the input data required for running the “APPEM” code. The results were obtained in the form of a matrix of many parameters relating to the combustion process and were further corroborated into the performance spread sheet of the TURBOMATCH result file so as to integrate all of them together in the tables required for the process of interpolation later in MATLAB.

3.1.2.3 An Overview of the “APPEM” Scheme

This scheme is a FORTRAN program that has also been developed at the Department of Power and Propulsion in Cranfield University for the determination of combustor performance and exhaust emissions calculation of NOx, CO, CO_2 and UHC. In the process, exhaust emission quantities are calculated through the use of efficiency correlations and semi-empirical models as published by A. H. Lefebvre [45]. It is designed for the simulation of a single annular combustor (SAC) while incorporating a technology factor that provides the ability to calibrate the exhaust emission quantities to standards that apply to different combustor designs. This tool has been used in many Cranfield University projects requiring combustor performance simulation or exhaust emission analysis in the area of aero, marine and mechanical drive applications.

3.1.3 Hot Section Rotor Blade Creep Life Investigation

The durability of the hot section components has always been of interest to the operators of gas turbines and between one half and two thirds of the maintenance costs of the engine is attributable to the repair or replacement of these high-value parts. An investigation by Ref [47], found that virtually all hot section components are refurbished at part-life that may involve a combination of vacuum brazing, welding, recoating and reheat treatment. He found out that safety margins have to be incorporated because of the greater degree of uncertainty in material properties and the exact operating conditions of the components.

In [1], a model was developed for the prediction of the turbine rotor blade life consumption of the marine gas turbine hot section (the high pressure turbine) under the same range of off-design conditions already described in paragraph 3.1.1.2. It has been designed with a capability to quantify the creep life consumption of the blade depending on the changes in the off-design conditions expected to be encountered during a scheduled voyage subjected to the gas turbine. The model is integrated with the gas turbine performance model to obtain the required input parameters from it.

3.1.3.1 Larson-Miller Parameter.

The modelling methodology adopted for the blade creep life fraction t_f corresponding to the off-design conditions of the research gas turbines was based on the Larson-Miller criterion [48] as defined in equation

$$t_f = 10^{\frac{LMP}{Tb} - 20} \quad \textbf{Equation (3-7)}$$

Where t_f is the blade's time to failure, LMP is the Larson-Miller parameter while T_b is the blade temperature.

It is assumed that there is no bending stress occasioned by the gas pressure and momentum on the aerofoil, which makes the blade to be induced with centrifugal stress only. It is also assumed that the blade is of rectangular shape and that the creep life over a turbine stage is represented by the result obtained for one blade. Therefore the centrifugal stress σ_{cfd} at design point is defined as

$$\boldsymbol{\sigma_{cfd} = \rho_b \, x \, K_s \, x \, h_b x \left(\frac{2\pi N}{60}\right)^2 x \, r_{mb}} \quad \textbf{Equation (3-8)}$$

Where: ρ_b is the blade's material density, K_s is the shroud parameter, h_b is the height of the blade, N is the design point turbine shaft rotational speed and r_{mb} is distance from mid-shaft to mid-blade.

The blade's off-design centrifugal stress is calculated as follows:

$$\boldsymbol{\sigma_{cfo} = \sigma_{cfd} \left(\frac{N_{od}}{N}\right)^2} \quad \textbf{Equation (3-9)}$$

Where: N_{od} is the off-design turbine shaft rotational speed.

Assuming that the overall cooling effectiveness of the blade remains constant at all gas turbine off-design conditions, the gas temperature will then be the same with the turbine entry temperature (TET) and in the same vein, the compressor derived blade cooling air temperature will be the same with compressor outlet temperature as well, hence the following equation:

$$\mathbf{T_b = T_g - \varepsilon \times (T_g - T_c)}$$ **Equation (3-10)**

Where: T_g is the gas temperature, T_c is the blade cooling temperature and ε is the blade cooling effectiveness.

Therefore, having calculated and obtained the aforementioned values, the creep model for each of the gas turbines was established through the following input parameters:

- The shroud parameter K_s
- The blade height h_b
- The design point rotational speed of the turbine shaft N
- The distance from mid-blade to mid-shaft r_{mb} and
- The material density of the blade ρ_b

These form the family of input parameters required by the user before any scheduled mission can be embarked upon. The values of the blade cooling air temperature T_c, turbine shaft off-design rotational speed N_{od} and the gas temperature T_g are the variables that define the blade's life fraction t_f which have already been obtained from the gas turbine performance model.

3.1.4 Propulsion Power Investigation Model.

After successfully conducting the 'Uninstalled' performance investigation for each of the gas turbine models through the utilization of the TURBOMATCH code, the stage was now set for a so-called 'Installed' performance assessment to follow in which case, the ship models were to be modelled and integrated with the gas turbines to form the ship's propulsion machinery. Therefore, the results obtained in TURBOMATCH were further tabulated separately in 2-dimensional look-up tables in a MATLAB program environment (scripted M-files) so as to generate a single 3-dimensional table for each engine performance parameter. By means of linear interpolation between designated reference points, the rate of the required engine output parameter could be predicted. Figure 3:1 is an illustration of the transformation of the

TURBOMATCH performance spread sheet into tables contained in .txt files through which the “Installed” performance evaluation is made possible based on the following relationship:

Table 3:1 Sample values of power output variation of the 25MW ICR model at a TET of 1550K

$T_{amb}[^oC]$	Altitude				
	-400	**-200**	**0**	**200**	**400**
	Power Output [MW]				
0	31.2	30.703	30.163	29.646	29.113
2.5	30.9	30.314	29.791	29.265	28.751
5.0	30.5	29.946	29.422	28.904	28.394
7.5	30.1	29.578	29.056	28.551	28.045
10.0	29.7	29.213	28.706	28.2	27.699
12.5	29.4	28.855	28.352	27.85	27.357
15.0	29	28.504	28.006	27.513	27.022
17.5	28.7	28.159	27.662	27.173	26.693
20.0	28.3	27.82	27.327	26.845	26.371
22.5	28	27.482	26.997	26.522	26.048
25.0	27.6	27.151	26.674	26.199	25.735
27.5	27.3	26.823	26.351	25.884	25.422
30.0	27	26.507	26.036	25.572	25.117
32.5	26.7	26.19	25.727	25.268	24.819
35.0	26.3	25.859	25.425	24.967	24.52
37.5	25.9	25.508	25.074	24.65	24.234
40.0	25.6	25.16	24.733	24.313	23.898

$$P_i = f(T_{amb},\ P_{amb},\ TET)$$ **Equation (3-11)**

By iterating the value of TET in very small increments for the purpose of matching corresponding engine power output demanded by the ship the power plant performance parameters can be interpolated across the tables in line with the variation of the ambient conditions experienced along the vessel’s trade route. In all cases, each of the two dimensional interpolation tables represents a 50^{o}C increment of the turbine entry temperature (TET) while the rows are at intervals of 200m increment of altitude and the columns represent a 2.5^{o}C increment in ambient temperature. Samples representing the effect of the ambient conditions on engine power output as described above are illustrated for the 25MW ICR gas turbine model in Table 3:1 and Table 3:2

This further illustrates the fact that the gas turbine is greatly favoured to perform better at lower ambient temperature regimes more than in hot weather conditions as would be further shown while undertaking the different voyages designed for each of the ships involved.

Table 3:2 Sample values of power output variation of the 25MW ICR model at a TET of 1150K

$T_{amb}[^oC]$	Altitude				
	-400	**-200**	**0**	**200**	**400**
	Power Output [MW]				
0	5.90	5.793	5.689	5.587	5.488
2.5	5.84	5.739	5.635	5.537	5.435
5.0	5.78	5.676	5.574	5.475	5.375
7.5	5.72	5.618	5.517	5.416	5.319
10.0	5.66	5.559	5.459	5.361	5.262
12.5	5.60	5.499	5.401	5.304	5.207
15.0	5.54	5.445	5.345	5.248	5.153
17.5	5.49	5.39	5.292	5.194	5.101
20.0	5.43	5.335	5.236	5.143	5.046
22.5	5.38	5.283	5.185	5.09	4.997
25.0	5.33	5.23	5.133	5.039	4.947
27.5	5.27	5.178	5.083	4.99	4.897
30.0	5.22	5.128	5.032	4.94	4.849
32.5	5.17	5.079	4.985	4.892	4.801
35.0	5.12	5.031	4.938	4.846	4.754
37.5	5.08	4.983	4.891	4.80	4.71
40.0	5.03	4.936	4.845	4.755	3.278

The ship Power Prediction Model is designed to simulate the hydrodynamic and aerodynamic resistance experienced by a marine vessel for the purpose of calculating the brake power expected to be generated by the vessel's power plant. The ability for any ship to sustain its speed under ideal and adverse weather and sea conditions on account of the different seasons of the year is the main focus of the current investigation.

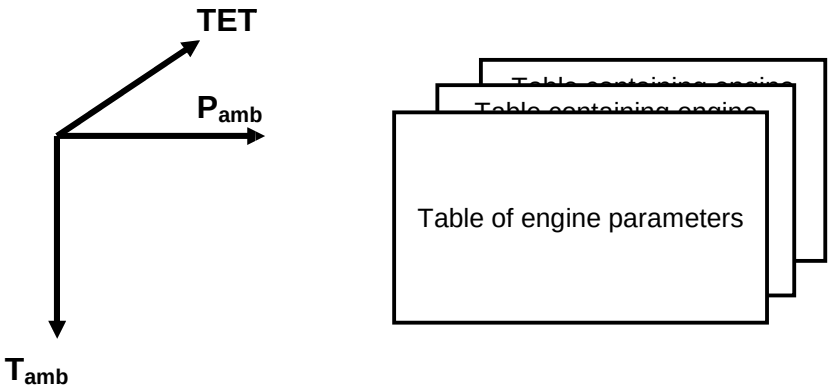

Figure 3:1 Basic structure of the interpolated GT performance parameters

A summary of the of the structure of the power plant investigation model is illustrated in Figure 3:2

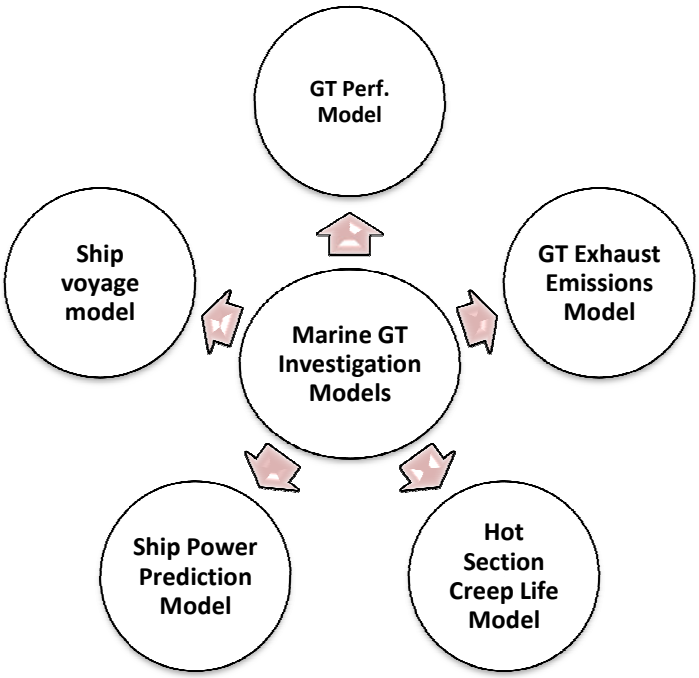

Figure 3:2 Key Modules of the Marine Gas Turbine Investigation model

Depending on the type of vessel involved, a comparative analysis of the behaviour of the selected GT cycle configurations according to the different conditions that are likely to be encountered at sea are considered.

3.2 Selection of the Transit Routes

Table 3:3 summarises the details of the different fixed ship routes that were selected for each of the vessels and Figure 3:3 illustrates the actual track to be followed as the ship transits from port of loading to that of delivery.

Table 3:3 Voyage profiles of the vessels

Type of vessel	Port of Loading	Port of discharge	Range [nm]	Ship speed [knots]	Trip duration [hrs]
LNG Carrier	Algiers	Portsmouth	1619	19.5	84
Cargo ship	Cape Town	Rotterdam	6342	25	254
Cruise ship	Lagos	Jeddah	5687	22	259
Fast Ferry	Malta	Marseille	639	30	22

3.2.1 The LNG Carrier Trade Route

In recent years, LNG has grown to become a significant component of the energy landscape, linking once distinct gas markets around the world and starting the process of unifying the global gas market place.

The UK became the first country in the world to commercially transport natural gas through an LNG Carrier from Algeria in 1964. This has continued ever since then. Therefore it was not by coincidence that the choice of the trading route for the LNGC was fixed between the Algerian port of Arzew and Portsmouth as shown in Figure 3:3.

3.2.1.1 Characteristics of LNG

The LNG Carrier however, is a purpose built ship, specially designed and principally used for transporting natural gas in liquid form to markets where it is re converted to its original state (gaseous state) through re-liquefaction and distributed as pipeline natural gas to the end users. While it has been found to produce less pollutant emissions, it offers an energy density comparable to gasoline and diesel fuels. Also, an important aspect of this type of fossil fuel is

that its density is between 0.41kg/L and 0.50kg/L which is much less than that of water at 1.0kg/L. Because it has the lowest CO_2 emission per unit of energy, it is considered as the most environmentally friendly fuel and is especially suitable for use in ship propulsion of LNG Carriers where the natural Boil off Gas (NBOG) would otherwise be flared. Therefore the economic potential of using the NBOG is one of the major benefits to be tapped by the application of the gas turbine as an alternative propulsion prime mover in LNG Carriers.

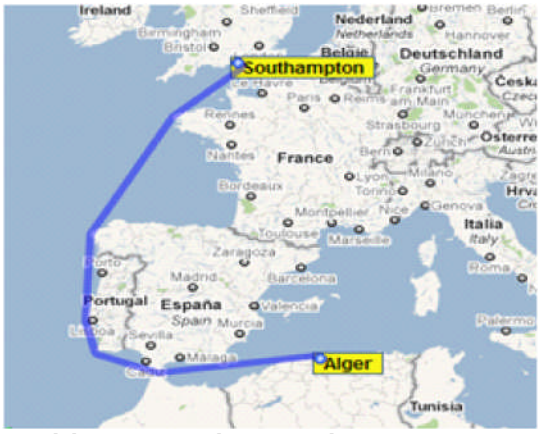

(a) LNG Carrier Transit Route

(b) Cargo ship Transit Route

(c) Passenger Cruise Liner's Transit Route

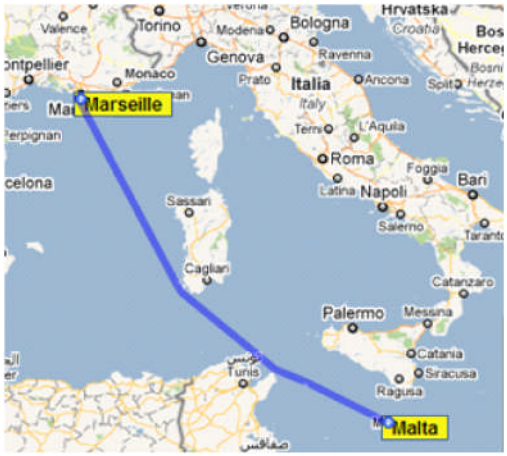

(d) Passenger Ferry's Transit Route

Figure 3:3 Scheduled Trade Transit Routes of the vessels Selected for Investigation [49]

3.2.1.2 LNG International Trade Routes

In the history of the LNG trade and transportation by oceangoing LNG vessels, the international trade route between the UK and Algeria is one of the very first

to be established in 1964. The use of natural gas as a primary energy source has increased over the years and there is a worldwide demand in which many countries are now involved as can be seen in Figure 3:5 [50]. Among the leading natural gas exporting countries of the world as contained in data released in 2008, Qatar was dominating as number one on the list followed by Malaysia and Indonesia while Nigeria and Algeria occupied the fourth and fifth positions respectively. On the import side, Japan, South Korea and Spain are leading in which the UK possesses a substantial share of the market through the trade route between it and Algeria as it still exists. This route has however been selected for the investigation of the gas turbine propulsion of the KLNG carrier.

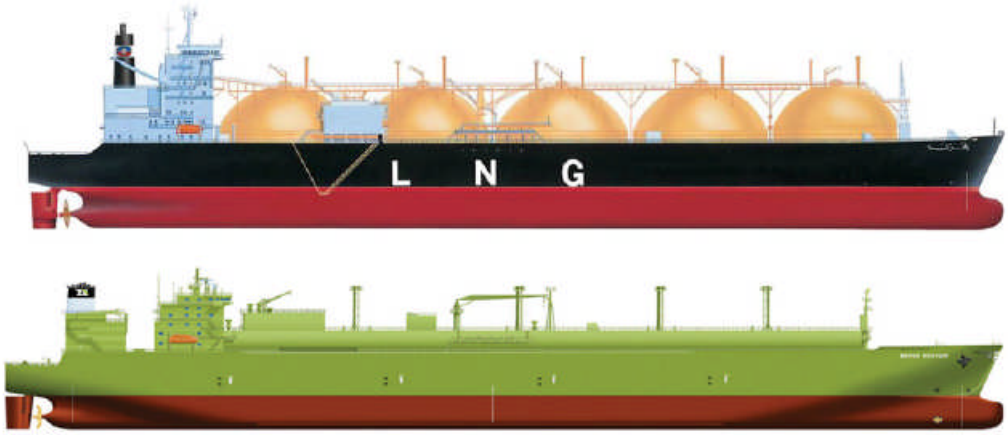

Figure 3:4 Main types of LNG Carriers: Moss spherical tanks (top) membrane tankers (bottom) [51]

The distance between the Algerian port of Arzew and the UK port of Portsmouth was found to be 1619 nautical miles and at a service speed of 19.5 knots, the transit time in ideal weather conditions was found to be 83 hours (about 3 and half days). The varying weather conditions during the different seasons and in adverse weather conditions does grossly affect propulsion engine performance that results in significant increase in the estimated transit times thereby imposing grave economic penalties on the ship operator. In this regard, the assessment seeks to extend the investigation in consideration of several

operating scenarios in order to achieve a wide variety of results and draw up reasonable conclusions in the final analysis.

3.2.1.3 Liquefaction and Boil off Gas

In order to facilitate the transportation of natural gas where pipeline transmission is not possible, it is cooled down to approximately -163^{o}C at atmospheric pressure and at which point it condenses to a liquid. Therefore, the tanks onboard the LNG Carrier effectively function as thermoses to keep the liquid gas cold during storage and transportation at sea. However, no insulation is very so perfect and as a result, the liquid is constantly boiling during the voyage, which in turn results in about 0.1% to 0.25% of the liquid cargo converting to gas each day. This boil off rate depends on the efficiency of insulation and the roughness of the voyage in which for a typical 20 day voyage, about 2% to 6% of the total volume of LNG could be lost. This small amount of 'boil off' is needed to maintain the pressure and temperature inside the vessels within operating limits. And this has made the steam turbine to remain as the traditional prime mover that conveniently utilizes the gas as fuel for its boilers to generate steam for driving the turbines. In spite of the success of the steam turbine however, the application of modified low speed diesel engines as an alternative for improved thermal efficiency has proved to be successful coupled with an emerging scarcity of trained personnel in the field of steam turbine technology.

3.2.2 The Search for Alternative LNGC Propulsion Systems

Even though most recent orders for new LNG carriers still favour steam turbine driven ships, the lack of its qualified seagoing engineers and the more attractive financial returns in using marine-grade fuel oil are factors that seem to be driving the change from steam turbines to other alternatives. One of those alternatives is the gas turbine which has already been successfully applied using the Rolls Royce MT30 [15] and in this work, an attempt is being made to assess the techno economic and environmental benefits while taking into account the many factors that may affect performance depending on

circumstances. In this regard, an LNG ship model, developed by the Korean Institute of Ships and Ocean engineering, “KRISO” [52] was selected and its principal design parameters and technical features have been adopted for the purpose of investigating the behaviour of the gas turbine when installed as the main propulsion engine of a liquefied natural gas tanker. Nicknamed as KLNG, the KRISO design had been projected to sustain a loading capacity of 138 000m^3 of the LNG product. Its other principal particulars and geometry are represented in Table 2:5 and Figure 3:4 depicts a typical LNG Carrier undertaking a trade mission on the high seas

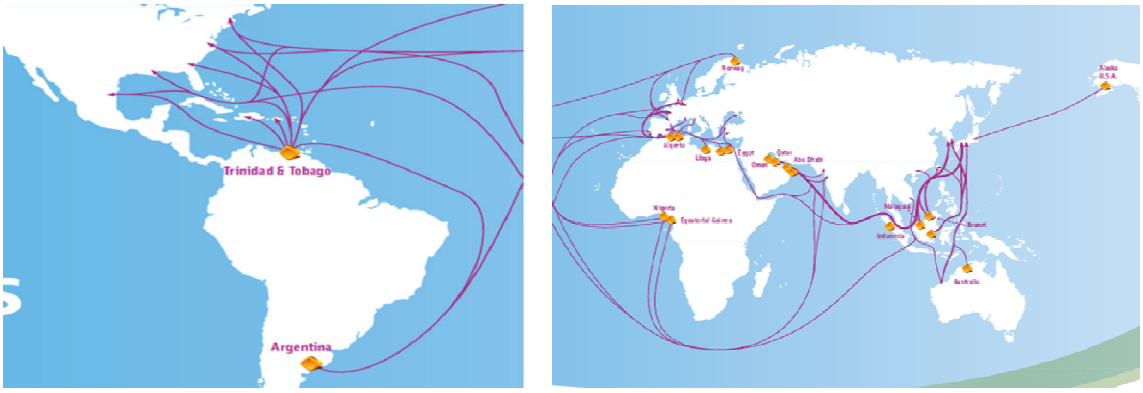

Figure 3:5 A representation of the world's LNG trade routes and contracts [50]

3.2.3 Impact of Ambient Conditions

The effect of ambient conditions on the performance of gas turbines can be quite significant and must be considered in their selection and application on any ship. Therefore, the variation of engine performance under varying operating conditions has been considered as a very important economic issue in the assessment of the models under investigation. This is more so because the power output of any gas turbine is directly proportional to the airflow rate through the machine [21]. Using the modelling and simulation platform, and having selected the aforementioned basic input parameters outlined in section 3.1.1.1, their performance was described by representing compressor

characteristics through the variation of non-dimensional mass flow along constant speed lines plotted against pressure ratio. Through this, it can be observed that the gas turbine pressure ratio increases as the non-dimensional mass flow increases but only up to the point of maximum efficiency where it reaches its maximum value [42] [43]. The lines representing the locus of maximum efficiency forming a curve by which the compressor should closely operate in a state of equilibrium.

In order to properly account for the effect of ambient conditions that are expected to be encountered at sea, three key variables needed as the basic inputs for modelling the OD performance including the Turbine Entry Temperature (TET), the ambient temperature (the compressor inlet air temperature), T_{amb} and the ambient pressure, P_{amb} were chosen.

3.3 Major Scenarios of the Case Study

With the expected variation in weather and sea conditions, the propulsion plant for each of the ships was to be made up of each of the gas turbine in turns and be operated to transport the cargo from the loading terminal to the port of discharge while monitoring the performance of the gas turbine throughout the voyage. The ‘installed’ performance would then be conducted in five different scenarios as follows:

3.3.1 Speed and Power in Waves

Arising mainly from the increased resistance experienced by the ship hull and appendages, the power needed for its propulsion at a given speed increases with increase in the severity of the wave system. If the propulsion machinery is already producing full power, it follows that there must be an enforced reduction in speed. Past a certain severity of waves, the motions of the ship or slamming may become so violent that the captain may decide to reduce speed below that possible with the power available. This is a voluntary speed reduction and might be expected to be made in merchant ships of fairly full form at Beaufort numbers of 6 or more [53].

3.3.2 Calm weather (IWC)

Ideal weather conditions were assumed to exist when the mean wind speed is between 0 and 2 knots with sea states of not more than 2 on the Beaufort scale, giving a wave height of not more than 0.1 metres high. In addition, this scenario accounts for a clean ship, giving a hull surface roughness of not more than 30µm. This scenario was considered as Ideal Weather Condition (IWC)

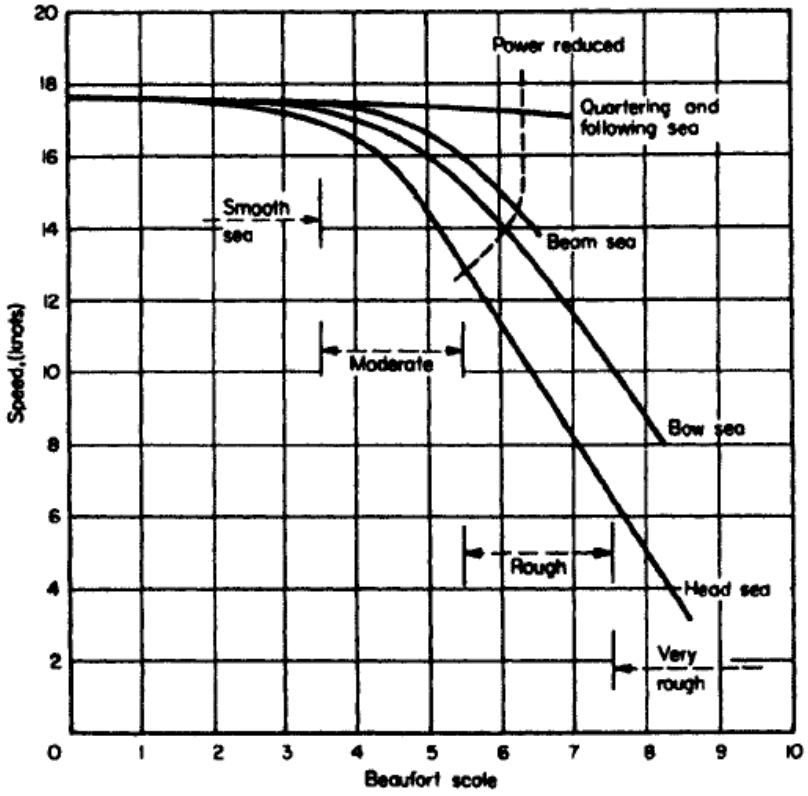

Figure 3:6 Effects of Waves on the Propulsion Power and Ship Speed [53]

3.3.3 Rough Weather (AWC)

Under this scenario, the mean wind speed is assumed to be above 4 knots capable of generating a wind speed of 3 and above on the Beaufort scale, while the submerged hull surface roughness remains at 30µm only.

3.3.3.1 Sea State Profiles

In order to determine the effect of the sea waves resulting from rough weather conditions on the performance of the ship and the gas turbine, there was the need to establish the adverse conditions that vessels were likely to encounter while in transit. As a result, data for daily tidal waves for the selected routes were obtained from the UK Hydro graphic Office (UKHO), which provides the services of forecasting hydrodynamic conditions for over 7000 ports worldwide [54]. Through the process, values for wave heights were estimated at intervals of one hour for each of the trade routes using the Beaufort [55] scale as illustrated in Figure 3:7.

The ocean wave statistics obtained were used to establish the magnitude of waves and the sea states for each trade route and according to the seasons under consideration.

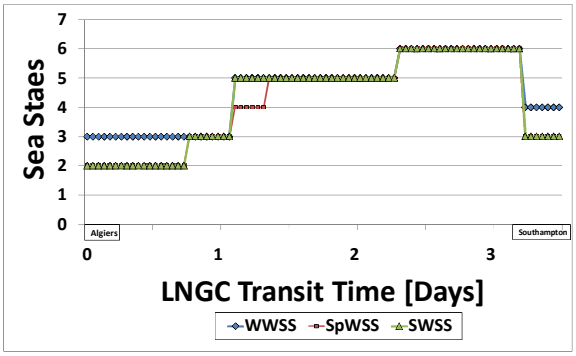

(a) LNG Carrier

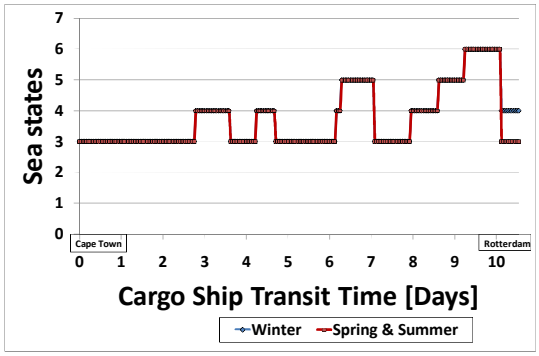

(b) Container ship

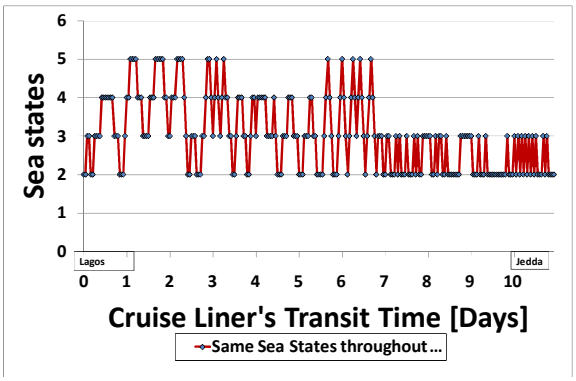

(c) Cruise Liner

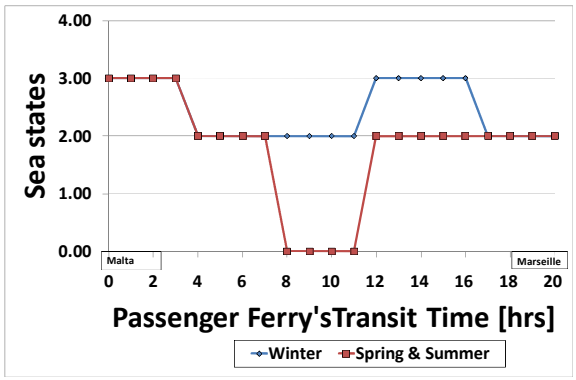

(d) Passenger Ferry

Figure 3:7 Sea State Variations for the Trade Route of each Ship

3.3.4 Hull Fouling Scenarios (HR1, HR2 and HR3)

Under these scenarios, the weather and sea conditions remain the same as in paragraph 3.3.3 but the values for the underwater hull surface roughness changes as we first consider a value of 120μm followed by 240μm and finally invoking a value of 360μm. The intension is to consider the wear and tear of the hull according to age and to evaluate the effect of increased resistance and loading of the propulsion system.

3.4 The Simulation Platform of 'Poseidon'

This code represents the platform for the prediction of marine vessels' propulsion power consisting of a numerical model to simulate the hydrodynamic and aerodynamic resistance and calculate the brake power that needs to be generated by the vessel's power plant that will sustain the its speed requirement under a variety of weather conditions. It does not yet take the effect of shallow water and propeller cavitations into consideration and it is fashioned as a combination of the following modules:

- Hull resistance prediction
- Propulsion factors prediction
- Propeller open water characteristics
- Hull fouling resistance
- Sea wave resistance
- Wind resistance

The Holtrop 1984 – resistance prediction method is one of the techniques used for the prediction of displacement and semi-displacement vessels [56] and as it is widely applicable in several marine vessel power prediction tools available in the market, its statistical correlations [3] were used in the development of the hull resistance module as detailed in ref [1]. In defining the basic range of hull form parameters of any vessel, the method identified an additional parameter

(Lambda) as a factor that should be checked to be in conformity with the illustration of Figure 3:8.

The hull's weight displacement Δ, and the Froude F_n, number were defined in Equation (3-12) and Equation (3-13)

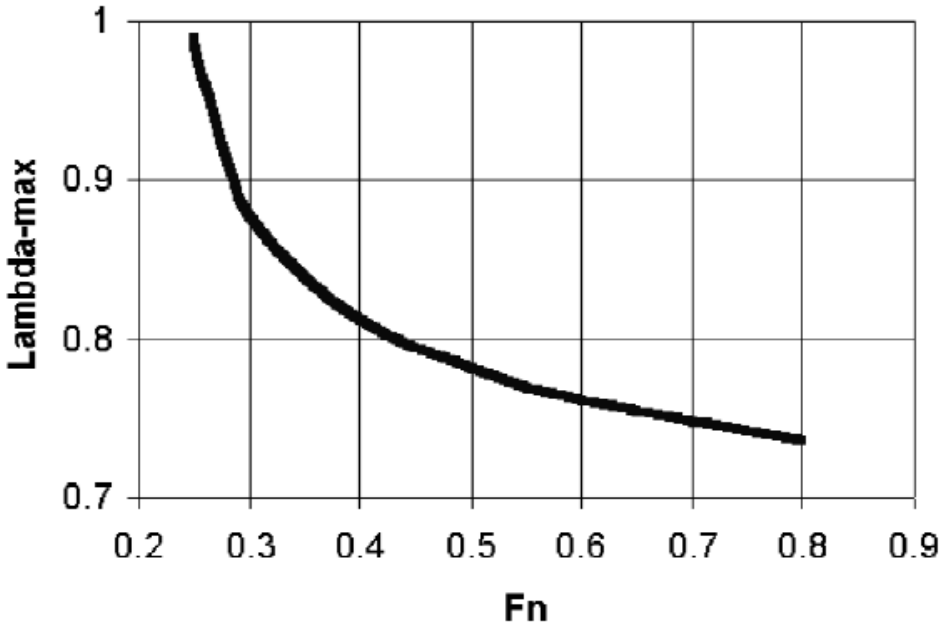

Figure 3:8 λ should always correspond to values below the line for a specified Froude number [56]

$$\Delta = \rho_s \, g\nabla$$ **Equation (3-12)**

$$F_n = \frac{V}{\sqrt{gL}}$$ **Equation (3-13)**

Where ρ_s is the density of sea water and g is the acceleration due to gravity

The introduction of long hauled voyages in the current research made it necessary to modify the weather module so as to facilitate the fluctuation of temperature likely to be encountered in the different environments of the oceans

through which the vessels may be navigating. The choice of the different ship models was based on the nature of their trade missions and design configuration.

3.5 Selection of the Ship Models

The main dimensions decide many of the ship's characteristics, e.g. stability, hold capacity, power requirements, and even economic efficiency. Therefore determining the main dimensions and ratios forms a particularly important phase in the overall design [57]. However, every design must achieve its unique balance of weight carrying capability and available volume for payload that will satisfy Archimedes principle which states that weight must equal displacement [32] as follows:

$$\Delta = \gamma LBTC_B(1-s)\ [tons] \qquad \textbf{Equation (3-14)}$$

Where the hull dimensions, length L, beam B and draft T, are the moulded dimensions of the submerged hull to the inside of the shell plating. γ is the weight density of water while C_B is block coefficient and s is the appendage allowance. Also in ref [58], it was noted that when a target displacement and an acceptable choice of vessel length-beam ratio, beam-draft ratio and block coefficient based upon vessel type and Froude number. This approach can provide a way to obtain an initial estimate of the vessel length and the above equation becomes

$$L = \{[\Delta(L/B)\text{^}2\ (B/T)/\gamma C\_B\ (1-s)\ ]\ \}^{1/3} \qquad \textbf{Equation (3-15)}$$

The ranges of feasible design characteristics for marine vehicles depend upon their intended use and based on economic comparisons with alternative modes of transportation. Table 3:5 represents the characteristic dimensions of the selected ship types for the project's investigation.

Table 3:4 Primary influence of Hull Dimensions [32]

Parameter	Primary Influence of Dimensions
Length	Resistance, Capital cost, Manoeuvrability, Longitudinal strength, Hull volume and Sea keeping
Beam	Transverse stability, Resistance, Manoeuvrability, Capital cost and Hull volume
Depth	Hull volume, Longitudinal strength, Transverse stability, Capital cost and Freeboard
Draft	Displacement, Freeboard, Resistance and Transverse stability,

Table 3:5 Main Characteristics of the Selected Ship Types

Ship types	LNGC	Cargo ship	Cruise ship	Passenger Ferry
Length at water level, L_{WL} [m]	266.0	287	283.5	188.54
Maximum Beam, B [m]	42.6	40.0	39.0	25.0
Average design draft, T [m]	11.3	14.0	9.0	6.40
Block coefficient, C_B	0.7493	0.65	0.65	0.55
Midship coefficient, C_M	0.9857	0.975	0.98	0.93
Water plane coefficient, C_{WP}	0.7848	0.75	0.78	0.69
Service speed, V_s [knots]	19.5	25.0	22.0	30
Froude Number, F_n	0.1964	0.4746	0.4172	0.34687
Displacement, Δ [tons]	965604.88	22215031.21	1636347.992	166978.368
Wetted surface, S_w [m^2]	13831.0	24592.051	20662.695	4916.588
Lambda, λ	0.93	0.84	0.91	0.63
Prime mover Brake power [KW]	29801.96	87242.59	64428.72	46576.05
Effective power [KW]	16126.95	38786.30	26803.82	24481.29
Total resistance [N]	1.607743e+006	3.427321e+006	2.605348e+006	1.641101e+006

Literature reveals that the frictional resistance of a hull increases with hull length while the wave resistance decreases with longer ship hulls and since the hull cost also increases with length, it is an economic choice to use a length that does not influence such.

3.5.1 Non Dimensional Ratios

The Length-Beam ratio is used to check independent choices of L and B or with an initial L, the choice of a desired L/B can be used to obtain an estimated beam B. From this, [59] recommended the following:

$$\frac{L}{B} = 4.0 \; for \; L \leq 30m \qquad \textbf{Equation (3-16)}$$

$$= 4.0 + 0.025(L - 30), \qquad for \; 30 \leq L \leq 130m$$

$$= 6.5, \text{for } 130 \leq L$$

3.5.2 Other Factors

The ability of a ship to ferry cargo at the required speed so as to get to its terminal port of discharge at the right time and with the right payload are the factors that seeks for higher ship speeds. This may result in increased power requirements which further entail additional operating expenses (e.g. fuel consumption). The factors that need to be considered in merchant ship design characteristics include:

- Payload (cargo or passenger capacity and description)
- Sustained sea speed and endurance
- Limits to overall ship dimensions (length, beam and draft) for operation in the intended service
- Loading-discharging methods and capacities
- Number of holds, tanks or other cargo spaces for balanced service
- Crew or manning requirements/level of automation
- Hotel requirements such as heating, ventilation, air conditioning, gallery, public spaces, power and lighting
- Special requirements for navigation and communication

- Manoeuvrability requirements (steering, handling and mooring)
- Reliability and logistics support objectives

The research vessels outlined in Table 2:5 were selected and modelled based on the above criteria.

3.5.3 The Cargo ship model

A cargo ship or freighter is any sort of ship or vessel that carries cargo (goods or materials) from one port to another. Often being equipped with loading and unloading machinery and specially designed for the task they are meant for, they handle international trade across the world's seas and oceans every year.

Traditionally, cargo ships carry various types of cargo in different shapes and sizes, and have been in use since the 1900s. However, because of their high operating costs, the use of such ships is steadily decreasing and giving way to container ships. These ships are designed in a manner that optimizes space restricting their capacity to be measured in Twenty-foot Equivalent Units (TEU) as standard. The number of these 20-foot containers, measuring 20 x 8.0 x 8.5 feet (6.1 x 2.4 x 2.6 metres) is limited by the overall capacity of the ship. [60]

A Panamax container ship with a carrying capacity of about 5000 TEU has been selected as the cargo ship model for this research and Table 3:6 along with Figure 3:9 describes the technical features and historical development of the container ship industry. The standard size classification developed by Lloyd's Register relates to the ship's ability to pass through either the Panama or Suez Canal respectively.

The gas turbine propulsion system alternative has not been prominent with this type of ship but by highlighting its capability for achieving higher speeds and facilitating more available space for additional cargo carrying capacity to generate more revenue and ensure a an environmentally friendly operating environment when compared to traditional diesels, many proposals abound.

Table 3:6 Classification of Container ships according to size [60]

Vessels' Design Characteristics	Twenty-foot Equivalent Units (TEU)			
	6,000 Post-Panamax	**8,000** Post-Panamax	**12,000** Suezmax	**18,000** Post-Suezmax
Deadweight [DWT]	70,000	93,000	137,000	200,000
Length overall [m]	305	355	400	470
Length between pp [m]	290	340	380	450
Breadth [m]	43.0	43.0	52.5	60.0
Design draught [m]	12.5	14.6	14.6	15.7
Block coefficient	0.59	0.61	0.62	0.62
Sea margin [%]	15	15	15	15
Engine margin [%]	15	15	15	15
Ship speed [knots]	25.0	25.3	25.5	25.5
Propulsion power [KW]	2x26,900	2x33,000	2x42,800	2x51,400

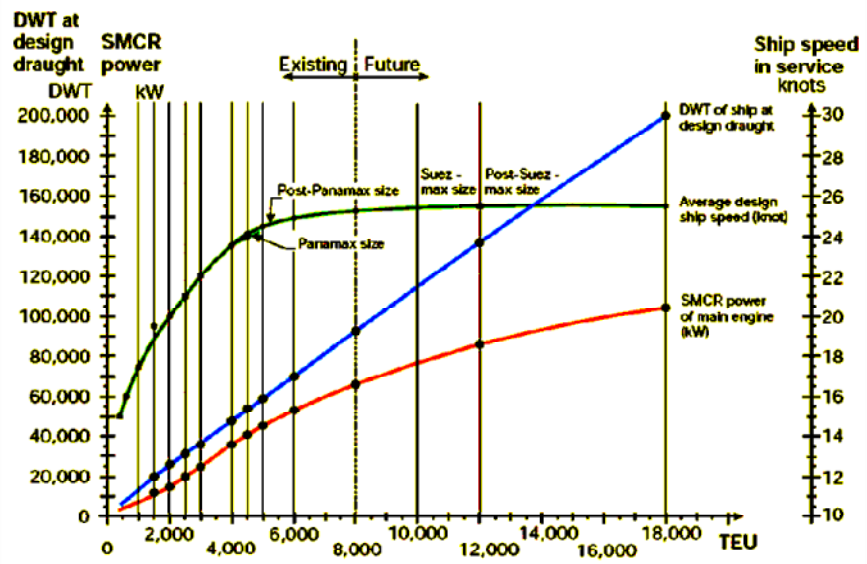

Figure 3:9 An Illustration of Existing and future Categories of the Container ships [60]

3.5.4 The Cruise Liner

Generally speaking, a Cruise ship or Cruise Liner is a passenger ship used for pleasure voyages, where the voyage itself and the ship's amenities are part of the experience in which transportation may not be the prime purpose of the journey.

In this research however, the transportation of passengers (Muslim faithfuls) on a long haul from the port of Lagos (Nigeria) to the port of Jeddah for a pilgrimage in Saudi Arabia is the main objective. This is suggested as an option to the incessant complications frequently associated with air travel during the annual hajj operations and the gas turbine is proposed as the main propulsion prime mover of the selected vessel at a speed of 22 knots (40.74 km/hr) covering a distance of 5687 nm in about 11 days. The ship that has been chosen for the purpose of this investigation has been correlated to the "*Voyager of the Seas*", operated by the "*Royal Caribbean*" [61], whose main features are included in the table of existing Cruise ships, Table 3:7. The required propulsion power for this ship was found to be 42MW in addition to a ship service power requirement of 34MW, bringing the total installed power to 76MW. Engine size and power requirement are a function of prime mover brake power predicted from the hull total tow rope resistance.

The research assumes configuration of identical gas turbines in forming the power plants of the various vessels being considered for providing the propulsion power and onboard service power requirements of the various vessels.

3.5.5 Choice of Route

The selected route for the cruise liner was viewed as a better option than going through the 'Cape of Good Hope' via the southern African tip and through the Indian Ocean in order to avoid the following:

- It would take a voyage time of 13 days and 16 hours to cover a distance of 7226 nm instead of 13 days and 16 hours needed for the chosen route that passes through the Mediterranean covering only 5690 nm.
- The security concerns around the horn of Africa due to the current level of piracy could not be taken for granted.
- The waiting times and delays necessary for crossing the Suez Canal has potential for longer travel times and additional expenses [62].

Table 3:7 Characteristics of some recent Cruise ships [61]

Name	Seaborne	Columbus	AIDAcara	Crystal Symphony	Grandeur of the Sea	Carnival Density	Voyager of the Seas
Gross Tonnage	9961	13950	38530	50202	73817	101353	137276
Passengers	212	410	1186	960	1950	2642	3138
Cabins	106	205	593	480	975	1321	1557
Delivery (Year)	1988	1997	1996	1995	1996	1996	1999
Length O.A. (m)	134	144	193	238	178	272	311
Beam (m)	19	22	28	30	32	36	39
Draft (m)	5	6	6	8	8	8	9
Depth (m)	12	10	20	20	22	20	21
Installed power (MW)	11	18	31	39	50	63	76
Propulsion power (MW)	7	11	22	23	34	40	42
Service speed (knots)	16	19	21	22	22	22	22
Crew	154	170	526	545	776	1058	1180
Deadweight (tonne)	800	1300	3752	5869	7600	11171	9154

3.5.6 The Passenger Ferry

The role of a ferry is the routine and continuous transportation of people and their associated baggage and in Europe alone, more than 100 million people travel every year on car ferries with many millions more travelling as commuters on passenger only ferries [63]

The passenger ferry under investigation in this research is assumed to be propelled by marine gas turbines across a distance of 639 nautical miles per voyage and at 30 knots within 22 hours of transit time between Malta and Marseille in France. This could be a substitute to coach and rail transportation for tourists transiting between the two international destinations.

The compact nature and the environmental friendly operation of the aero-derivative gas turbine make it a preferred alternative to the conventional diesel propulsion machinery. The gas turbine propulsion of a ferry achieves its highest potential when operating at full power through which its problem of low fuel efficiency at part-load operation could be eliminated

3.6 Limiting Factors of the Gas Turbine

The gas turbine cycle is a continuous flow process in which a fluid flows through a system at a steady rate while transferring work and heat with the surroundings. As obtained in much academic literature, its governing equation is the steady flow energy equation that satisfies the first law of thermodynamics as follows:

$$Q = W - \Delta H \qquad \textbf{Equation (3-17)}$$

Where,

Q = heat input into the system

W = Work done by the system

ΔH = Change in gas energy and it is the change in stagnation or total temperature

For an ideal gas, the change in enthalpy can be represented by

$$\Delta \mathrm{H} = m \times C_p \times \Delta T \qquad \textbf{Equation (3-18)}$$

where

m = Mass flow rate and

C_p = specific heat of the gas at constant pressure while

ΔT = total temperature change in the thermodynamic system.

By substitution, the energy equation becomes:

$$Q - W = m \times C_p \times \Delta T \qquad \textbf{Equation (3-19)}$$

In order to illustrate the thermodynamic processes that make up the gas turbine, a temperature-entropy diagram is required from which the adiabatic compression work can be determined:

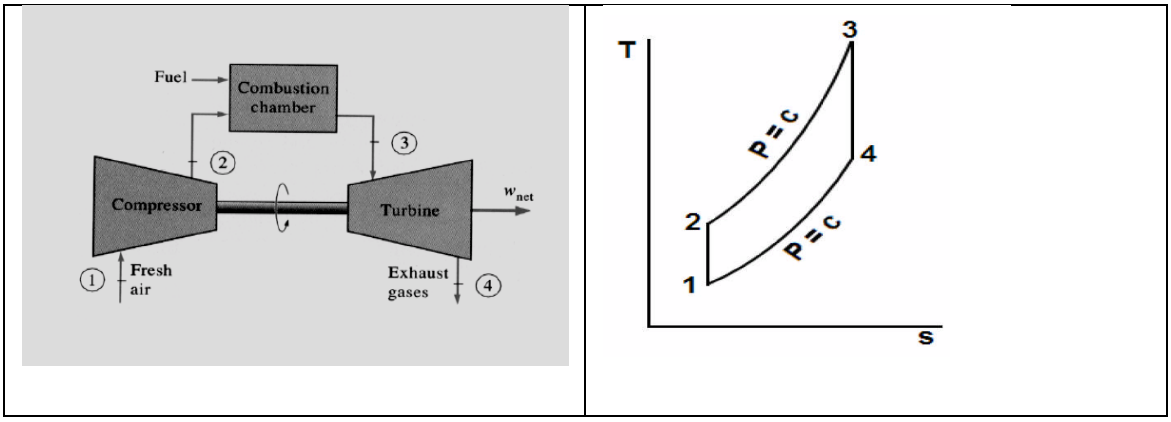

Figure 3:10 (a) Simple cycle gas turbine (b) Temperature-entropy diagram of a simple cycle (Source: The aircraft engine book – Rolls-Royce UK)

$$W_{12} = C_p\,(T_2 - T_1) \qquad \textbf{Equation (3-20)}$$

The compressor discharge temperature from the isentropic compression of the gas (process 1-2) can be found from the following:

$$T_2 = T_1 \left(\frac{P_2}{P_1}\right)^{\frac{\gamma-1}{\gamma}} \qquad \textbf{Equation (3-21)}$$

where

$\gamma = C_P/C_V$ which the ratio of the specific heats and is usually referred to as the isentropic index. On the other hand, the adiabatic expansion work may be foind by:

$$W_{34} = C_P\,(T_3 - T_4)$$ **Equation (3-22)**

where

$$T_4 = T_3\left(\frac{P_4}{P_3}\right)^{\frac{\gamma-1}{\gamma}}$$ **Equation (3-23)**

Since work done by the system is zero, the heat input can be expressed as:

$$Q_{23} = C_P\,(T_3 - T_2)$$ **Equation (3-24)**

Therefore the net work done by the cycle per unit mass flow rate (specific work, W_{net}) is the difference between the expansion and compression work:

$$W_{net} = C_P\,(T_3 - T_4) - C_P\,(T_2 - T_1)$$ **Equation (3-25)**

The thermal efficiency of the cycle can be expressed as the ratio of the net work done by the cycle and the heat input:

$$\eta_{th} = \frac{W_{net}}{Q_{23}}$$ **Equation (3-26)**

Which, when substituted, will emerge as

$$\eta_{th} = \frac{C_P\,(T_3 - T_4) - C_P\,(T_2 - T_1)}{C_P\,(T_3 - T_2)}$$ **Equation (3-27)**

$$= \frac{(T_3 - T_2) - (T_4 - T_1)}{T_3 - T_2}$$

$$= 1 - \frac{T_4 - T_1}{T_3 - T_2}$$

By substituting the equations for of T2 and T4, the thermal efficiency becomes

$$\eta_{th} = 1 - \frac{T_1}{T_2}$$ **Equation (3-28)**

Hence the ideal gas turbine thermal efficiency is dependent only on the compressor pressure ratio but is less than the Carnot efficiency since T_3 is greater than T_2

$$\eta_{\text{th}} = 1 - \frac{T_1}{T_3}$$ Equation (3-29)

When Equation (3-29 is expressed as the compressor pressure ratio, then

$$\eta_{\text{th}} = 1 - \frac{1}{c}\ , where\ c = \left(\frac{P_2}{P_1}\right)^{\frac{\gamma-1}{\gamma}}$$ Equation (3-30)

It then means that thermal efficiency will increase with increase in pressure ratio and maximum possible thermal efficiency is achieved when T_2 tends to T_3 and will be zero as the pressure ratio tends to 1

The equation for the specific work can now be re-written as

$$\text{W}_{\text{net}} = C_P\, T_1 \left(\frac{c-1}{c}\right)\left(\frac{T_3}{T_1} - c\right)$$ **Equation (3-31)**

Thus, for a given gas, the specific work of the ideal gas turbine cycle depends on the compressor pressure ratio P_2/P_1, the maximum and minimum temperature ratio T_3/T_1 and the compressor inlet temperature T_1 and as such, increasing the ratio T_3/T_1, will increase the specific work, whereas increasing pressure will lead to an increase in the specific work initially but will later decrease at high pressure ratios. Therefore an optimum pressure ratio can be expressed as follows:

$$\text{C}_{\text{opt}} = \sqrt{\frac{T_3}{T_1}} = \left(PR_{opt}\right)^{\frac{\gamma-1}{\gamma}}$$ **Equation (3-32**

$where\ \left(PR_{opt}\right)\ is\ the\ optimum\ pressure\ ratio$

At the optimum pressure ratio, when the specific work is a maximum, the turbine exit temperature T_4 should be equal to the compressor discharge inlet temperature. Advanced gas turbines operate at very high maximum cycle temperatures and achieve very thermal efficiencies.

The current research is interested in the performance variation that occurs in the marine gas turbine when T_1 is varied.

.

4 RESEARCH PRELIMINARY INVESTIGATIONS

This chapter seeks to evaluate each of the gas turbine models before installing and operating them as propulsion prime movers for the vessels that have been selected to be integrated for carrying out a variety of voyages along selected trade routes. This uninstalled evaluation was undertaken by simulating each of the models under a variety of ambient temperatures so as to ascertain their performance when they are eventually installed and operated under any climate in any of the oceans of the world. It also evaluate the best combination and total number of engines that may be required to form the propulsion plant for each of the vessels based on their cargo capacities and voyage profiles. The rated power capacities and cycle configuration of each gas turbine model have been taken into consideration in the simulation and in order to formulate the basis for selecting any engine combination that will allow for a reliable redundancy and proper management of the available propulsion power for each of the vessels.

A number of ship models have also been developed in order to ingrate the simulation of the gas turbine models in a variety of ship propulsion systems.

4.1 Uninstalled Engine Performance Investigations

The performance evaluation of a variety of gas turbine cycle configurations is the main subject of this research. Under the assumption, four designs were modelled and simulated at the uninstalled stage and values for some of their vital performance parameters were obtained through the use of the digital simulation of TURBOMATCH and are presented in Table 4:1.

4.1.1 TURBOMATCH Simulation

A total of four gas turbine cycles have been modelled and simulated based on existing thermodynamic cycle configurations. Among them is a 25MW simple cycle, single spool model, 2 other different simple cycles but with dual spools rated at 19MW and a 36MW respectively and the fourth is an intercooled recuperated (ICR) cycle also rated at 25MW. To determine the effect of different

operating conditions that were expected to be encountered in the marine environment, they were simulated to determine their off design performance at varying ambient temperatures. The effect of sea states and ship hull surface degradation was later to be considered through a variety of investigated scenarios. In addition to the prediction of engine performance, the investigation was also aimed at predicting the percentage of engine life consumed and the quantities of exhaust pollutant emissions for every voyage completed in all the scenarios.

Table 4:1 Basic performance parameters of the investigated marine gas turbine engines at design point

GT Model/Design Parameter	36MW DSSC	25MW ICR	25MW SSSC	19MW DSSC
TET [K]	1550	1500	1505.5	1480
OPR	24	15.52	18.75	26.3
Intake Mass Flow [kg/s]	105	70	72	61
Exhaust Mass Flow [kg/s]	107.157	71.36	73.54	62.12
Exhaust Gas Temperature [K]	778	660	804	780.84
Thermal Efficiency [%]	39.27	42.58	37.78	39.35
SFC [g/KWh]	213	196.6	221.65	212.76

4.1.2 36MW Simple-Cycle, Dual Spool

The 36 MW was conceived based on the simple thermodynamic cycle configuration but with a layout consisting of two different spools (LP and HP). The dual spool arrangement of the gas generator splits the compression and expansion processes in order to provide a substantial increase in specific work output of the gas turbine. The output shaft of the engine is aerodynamically coupled to the gas generator through a power turbine. The low pressure spool of the gas generator consists of a low pressure compressor (LPC) at the intake side connected to a low pressure turbine (LPT) at the outlet of the gas generator through a shaft that allows the compressor to be driven by the turbine. The design of the HP spool also consists of a HPC and HPT connected through a hollow configuration inside which the LP shaft rotates and the two spools rotate independently of each other. By allowing the LP and HP

compressors to rotate optimally, this configuration gives higher compression ratios and efficiencies over the entire speed range. The reduced work of compression leads to an increase in the overall thermal efficiency of the simple cycle.

The TURBOMATCH modelling and assumed process established an overall pressure ratio of 24:1 and a turbine entry temperature (TET) of 1550K at design-point. A thermal efficiency of 39.3% was achieved through a corresponding intake air mass flow of 105 kg/s and the design point fuel flow for this engine was also found to be 2.132 kg/s giving a SFC of 213 g/KWh.

An off design simulation conducted under different ambient (intake) air temperatures the effect of the environment on the principal performance parameters of this engine was predicted as illustrated in Figure 4:1

4.1.3 25MW Intercooled-Recuperated Cycle

This advanced cycle aero-derivative marine gas turbine engine was modelled as an Intercooled-Recuperated (ICR) cycle at a rated output power of 25MW with a similar spool and shaft layout to the 36MW model. It differs from the dual spool simple cycle (DSSC) models by the incorporation of a system of heat exchange that consists of an intercooler and a recuperator. The recuperator is used to transfer heat from the exhaust gas to the compressed air entering the combustor thereby, causing a reduction in the amount of fuel required to be burned in the combustor. This increases the thermal efficiency of the gas turbine cycle by 20 to 30% but a further addition of an intercooler (usually a water-cooled heat exchanger), reduces the air temperature between the low pressure and the high pressure compressors so as to reduce the work of compression.

Evaluating the thermodynamic process of this cycle revealed that the combined effect of inter-cooling and waste heat recuperation effectively reduces the amount of work required to deliver the same pressure ratio due to a reduction in the volume of gas in the system. Inter-cooling also reduces the discharge

temperature of the HPC and allows the recuperator to effectively transfer heat from the exhaust gases back to the compressor discharge air. In the case of this model, the intercooler output temperature was simulated at 310K.

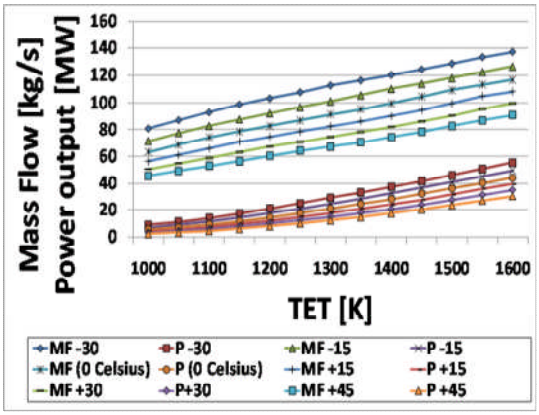

(a) Mass flow and power output

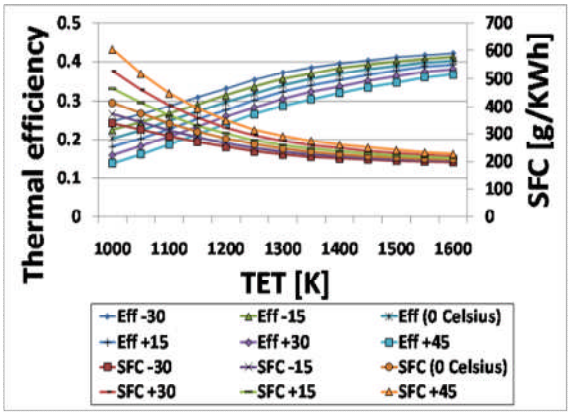

(b) Thermal efficiency and SFC

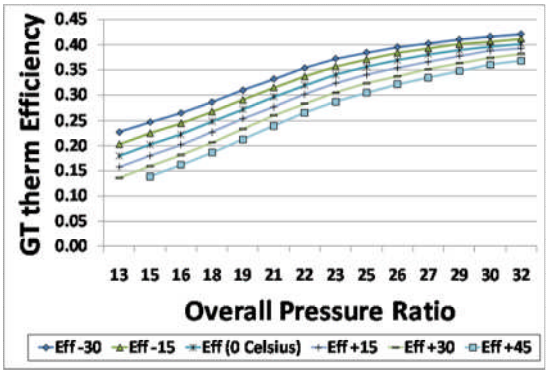

(c) Thermal efficiency over OPR

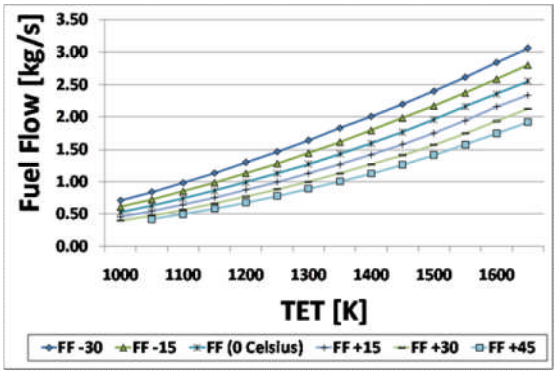

(d) Fuel flow over TET

Figure 4:1 Effect of varying intake air (ambient) temperature on the performance of the 36MW marine gas turbine model.

The combination of inter-cooling and recuperation in this particular model significantly resulted in a higher thermal efficiency and SFC compared to the simple cycle models of the research.

The substantial increase in specific work output gained by the addition of a heat exchange system led to an estimated 30% improvement in fuel efficiency. At design point, a pressure ratio (PR) of 15.5:1 and TET of 1500K converged with an intake air mass flow of 70 kg/s and a fuel flow of 1.36 kg/s was achieved

giving a thermal efficiency of 42.6% at design point. Figure 4:2 illustrates the behaviour of the ICR at off design due to variation of ambient temperatures.

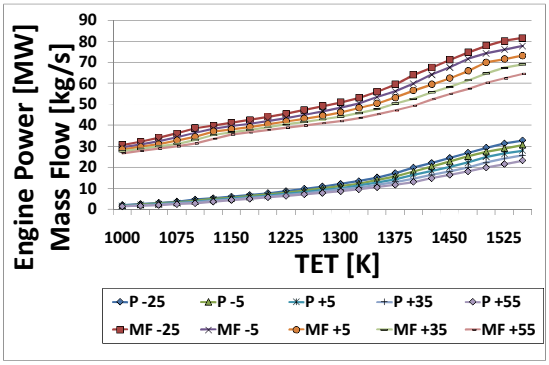

(a) Variation of Mass flow and power output

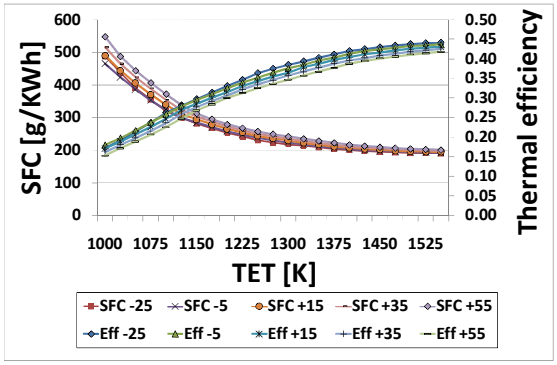

(b) Variation of Thermal efficiency and SFC

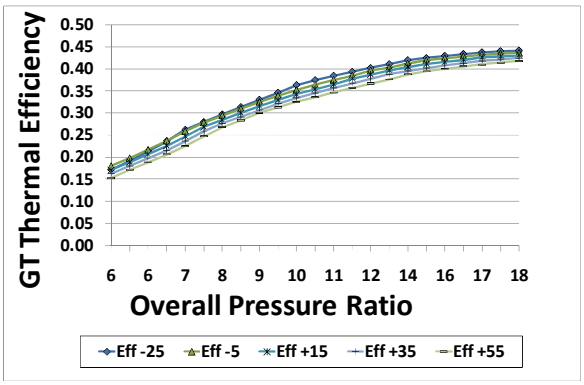

(c) Variation of Thermal efficiency over OPR

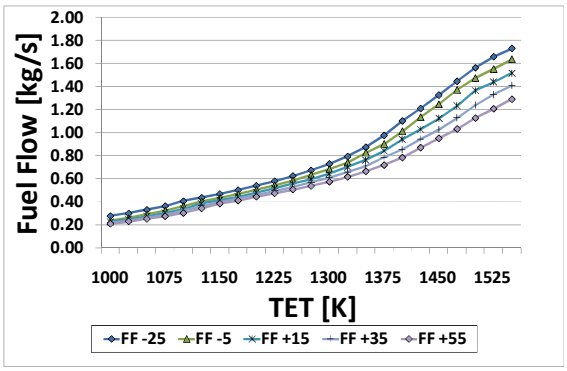

(d) Variation of Fuel flow over TET

Figure 4:2 Effect of ambient temperature variation on the performance of the 25MW ICR model.

4.1.4 25MW Simple-cycle, Single Spool

The third gas turbine model involved in the research was modelled based on the simple cycle configuration but with a single spool gas generator unit (GGU) aerodynamically coupled to an output shaft through a power turbine. Existing literature reveal that it is well suited for naval application because of its simple design and easy operation. Comprising of a compressor and turbine with a combustor in between, it was also found to be the most common gas turbine cycle in use. Its free power turbine has an independent shaft that uses the

excess energy at the discharge of the gas generator turbine to produce output shaft power. The input parameters for this simple cycle model used a pressure ratio of 18.75:1 and a TET of 1505K with a mass flow of 72 kg/s, the engine was simulated at design point in which a thermal efficiency of 0.378 and a fuel flow of 1.54kg/s were obtained. Figure 4:3 is an evaluation of the simulated its behaviour of when operated off design at various ambient temperature regimes.

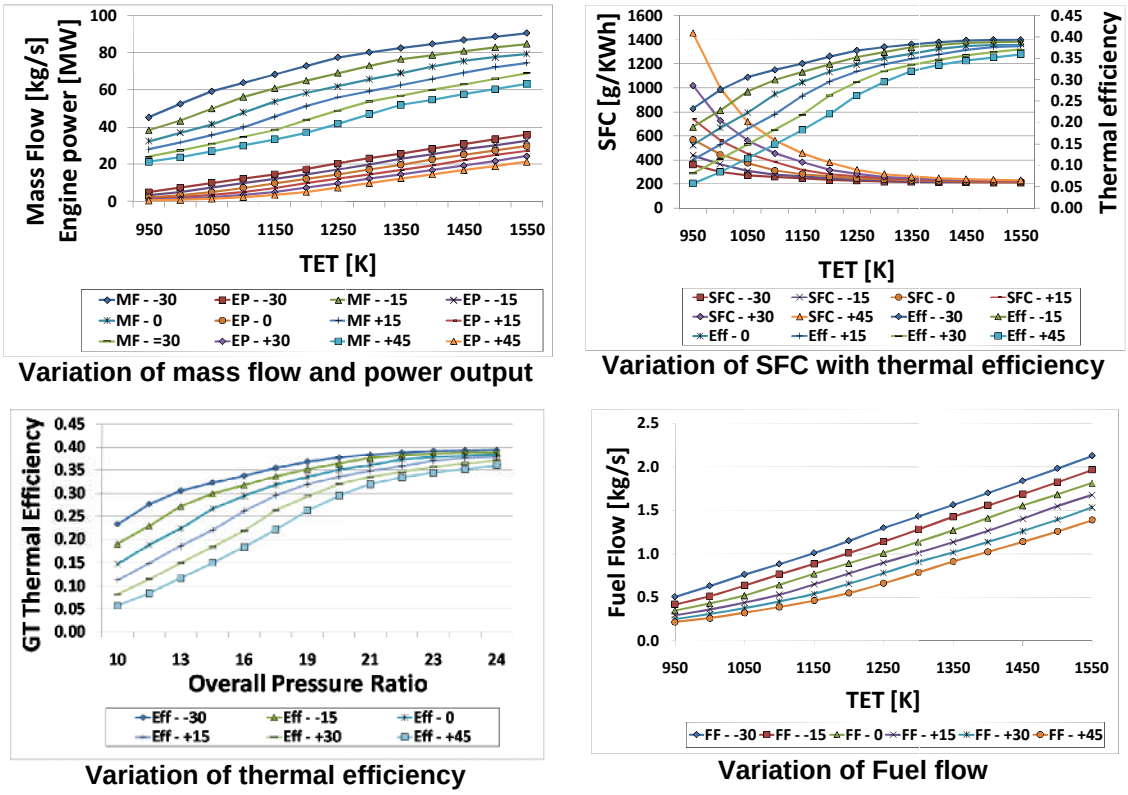

Variation of mass flow and power output

Variation of SFC with thermal efficiency

Variation of thermal efficiency

Variation of Fuel flow

Figure 4:3 Effect of ambient temperature variation on the performance of the 25MW Simple Cycle model.

4.1.5 19MW Simple-Cycle, Dual Spool

Many aircraft-derivative gas turbines utilize two-spool gas generators and a free power turbine in which the use of multi-spool compressors allows higher compression ratio designs to operate efficiently over the entire speed range. In terms of cycle configuration and shaft layout, the 19MW model of this research was conceived as a smaller version of the 36MW and is the least rated among the four. Its input parameters simulated at design point include a pressure ratio of 26.3:1 giving a TET of 1480K following an intake air mass flow of 61 kg/s, the

thermal efficiency was found to be 0.393 with a fuel flow of1.124kg/s. Figure 4:4 is an illustration of the its behaviour when subjected to varying ambient conditions.

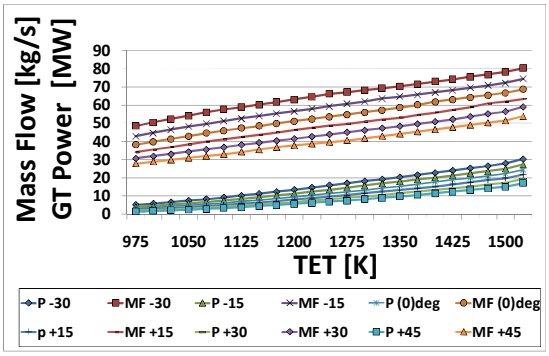

(a) Mass flow and power output

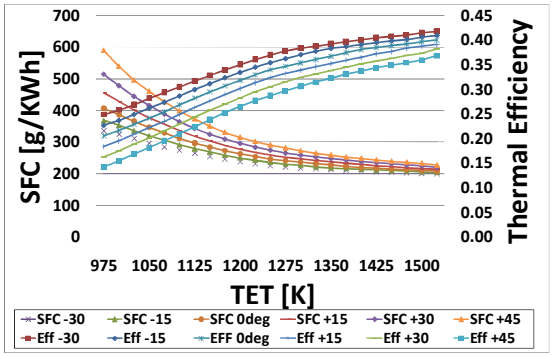

(b) Thermal efficiency and SFC

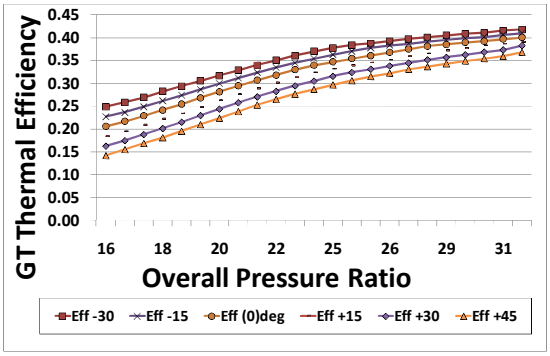

(c) Thermal efficiency over OPR

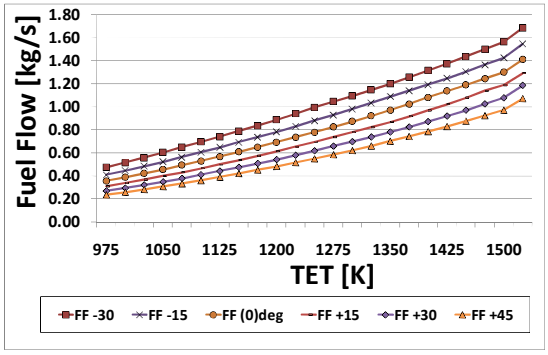

(d) Fuel flow over TET

Figure 4:4 Effect of ambient temperature variation on the performance of the 19MW marine gas turbine model.

4.1.6 Preliminary Comparative Analysis of the Gas Turbine Models

In order to effectively evaluate the performance of each of the marine gas turbine models of the project, a comparative assessment is presented in Table 4:2. The assessment of various parameters when the gas turbines are operated under very cold weather conditions compared to hot weather operations at off-design under ambient temperature intervals of between -30^{o}C and +45^{o}C. Within the limits identified, the maximum and minimum output values for some valuable performance parameters were identified as a measure of their capability under the limiting operating conditions. Comparatively, the SC model was found with a slightly higher overall power output capability (Redundancy) the advantage of the ICR is in its part load performance capability as

demonstrated by the narrower gap exhibited between its cold day and hot day thermal efficiencies.

Table 4:2 Comparative analyses of the Gas turbine models

GT model	T_{amb} [^oC]	Power [MW]		Efficiency [%]		FF [kg/s]		MF [kg/s]	
		Max	Min	Max	Min	Max	Min	Max	Min
36MW	-30	55.4	6.9	42.1	22.7	3.06	0.71	137.1	74
	45	30.4	2.4	36.7	13.9	1.9	0.42	90.8	45.7
19MW	-30	30.3	4.5	41.8	23.9	1.68	0.44	80.3	46.5
	45	17	0.7	36.8	7.8	1.1	0.21	54	25.5
ICR	-25	32.8	2	44.1	**17.2**	1.72	0.28	81.6	30.7
	30	23.2	1.4	41.8	**15.2**	1.29	0.21	64.5	26.7
SC	-30	33.15	6.16	38.2	26.1	2	0.55	90.6	48.6
	45	21.5	0.53	35.9	5.8	1.4	0.21	63.4	21.5

4.2 Weather Variation and Voyage Profiles

Having selected a projected trade route for each of the ship models under investigation, the environmental impact of the weather and sea conditions were considered as important factors to determine how well the gas turbine propulsion machinery was going to perform and yield a good return on investment (ROI) for the operators after making their choice. This is because the effect of ambient conditions on the performance of gas turbines can be quite significant and they must be considered in the selection and application of gas turbines on any ship [21]. It is also considered that its effect can be so severe that a change of 5^oC to 6^oC in ambient temperature can change the power output of the gas turbine by as much as 5%. This investigation will later show the variation of other engine parameter needed in keeping with the ship's power demand as it travels along its trade route.

The ambient temperature values along each of the selected trade routes were obtained online from daily temperature forecasts of the UK meteorological office (UKMO) website, [4]. The service provides daily weather forecasts for all major cities of the world including sea ports Therefore, the data needed for determining the weather conditions along each route was obtained and used as

input values to simulate the ambient temperature effect in all three selected seasons of winter, spring and summer and in all cases.

In order to effectively capture the variation of ambient conditions according to the different climates that the vessel is expected to encounter along its transit route, the entire voyage needed to be broken into separate segments at locations where the temperature regimes were established to be within the same range as obtained for the cargo ship transit route in Table 4:3. The same procedure was adopted in determining the voyage profiles for the other vessels of the research as shown in Table 4:4 and Table 4:5.

Table 4:3 Maximum and Minimum Variation of Ambient Temperature according to Segments along the Cargo Ship Route

Distance of same temp variation [nm]	Winter		Spring		Summer	
	Max Temp [^{o}C]	Min Temp [^{o}C]	Max Temp [^{o}C]	Min Temp [^{o}C]	Max Temp [^{o}C]	Min Temp [^{o}C])
699	27	16	20	10	18	7
914	31	24	28	22	28	19
1397	33	23	29	23	28	22
896	30	21	30	25	27	15
1260	21	15	25	20.2	27	21
362	15	8	22	13	26	16
814	8	2	19	7	23	12

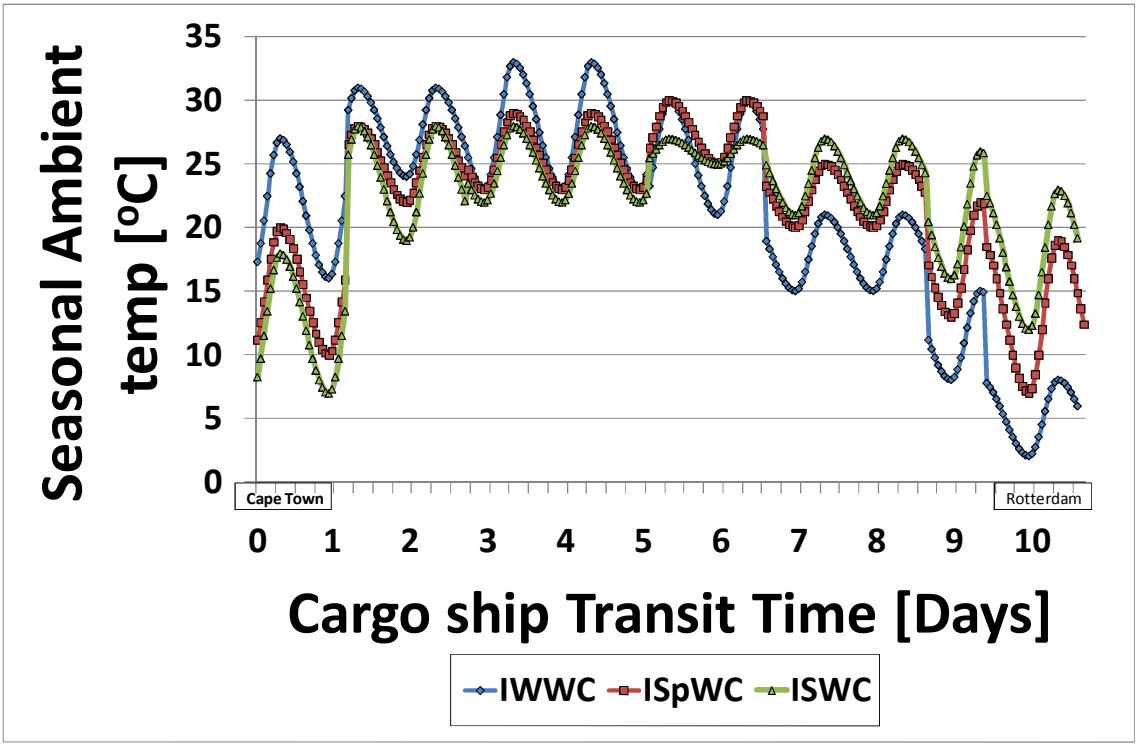

Figure 4:5 Ambient Temperature variation along the Cargo Ship Trade Route

Table 4:4 Maximum and Minimum Variation of Ambient Temperature according to Segments along the Cruise Liner's Route

Distance of same temp variation [nm]	Winter		Spring		Summer	
	Max Temp [°C]	Min Temp [°C]	Max Temp [°C]		Max Temp [°C]	Min Temp [°C]
911	33	21.7	29	23	28	22
896	21	15	25	20	27	21
1251	16.6	7.3	23.8	13.4	30.3	20.5
224	16.7	5.1	23.9	13.2	31.6	20.1
204	16.7	5.5	23.9	12.3	32.2	19.8
500	15.2	9.2	23.3	14.9	30.7	21.8
852	18.4	29.1	26.5	16.6	2330.4	23.1
849	28.7	18.2	31.8	24	38.3	26.7

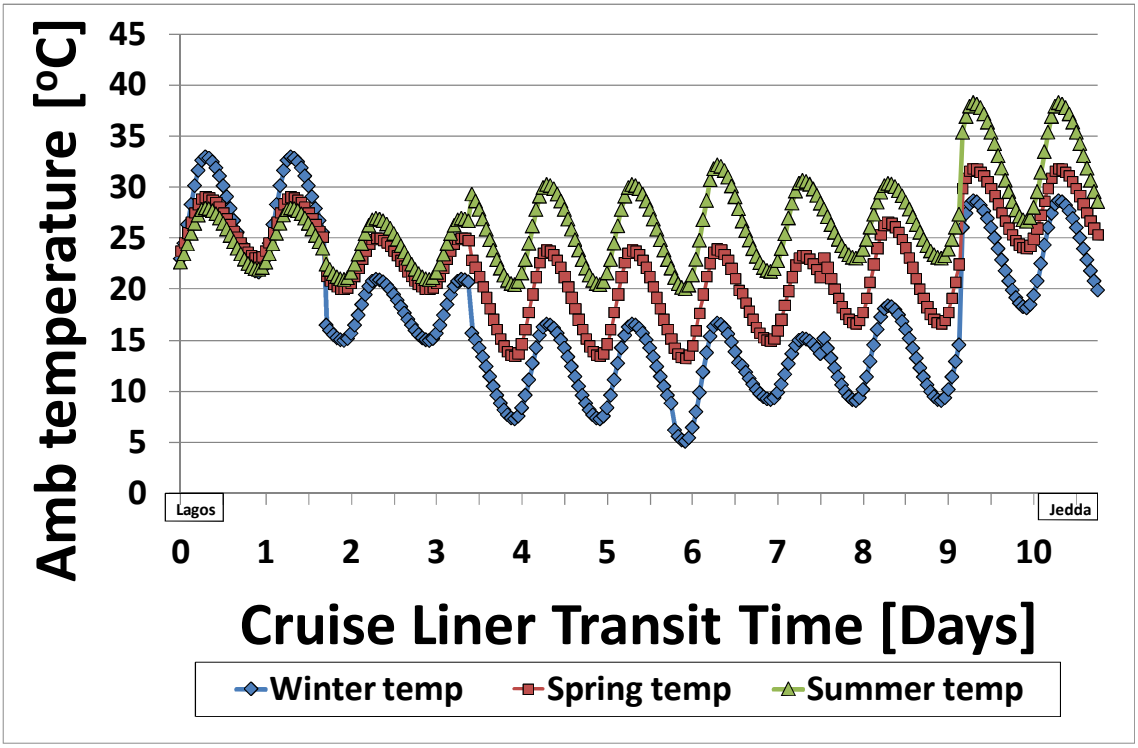

Figure 4:6 Weather variations along the Cruise Liner's Route

As expected, the changes in weather results in higher temperatures during the summer and lower temperatures during winter. A mid season was assumed in which the temperatures were lower than those of the summer season but lower than those of winter on the other hand. In the case of the cargo ship however, it would be observed that when hot weather conditions are experienced by the vessel at the beginning of the voyage from Cape Town in summer season for instance, by the time the vessel gets to Rotterdam in the northern hemisphere, it will be winter as shown in Figure 4:5.

On the other hand, the voyage selected for the Fast Speed Ferry (FSF) happens to be the shortest with only 2 temperature segments and taking only about 22 hours from beginning to end.

Table 4:5 Maximum and Minimum Variation of Ambient Temperature according to Segments along the Passenger Ferry's Route

Distance of same temp variation [nm]	Winter		Spring		Summer	
	Max Temp [°C]	Min Temp [°C]	Max Temp [°C]		Max Temp [°C]	Min Temp [°C]
311	15.2	9.2	14.9	23.3	30.7	21.8
388	10.2	3	22.2	12.6	29.2	18.7

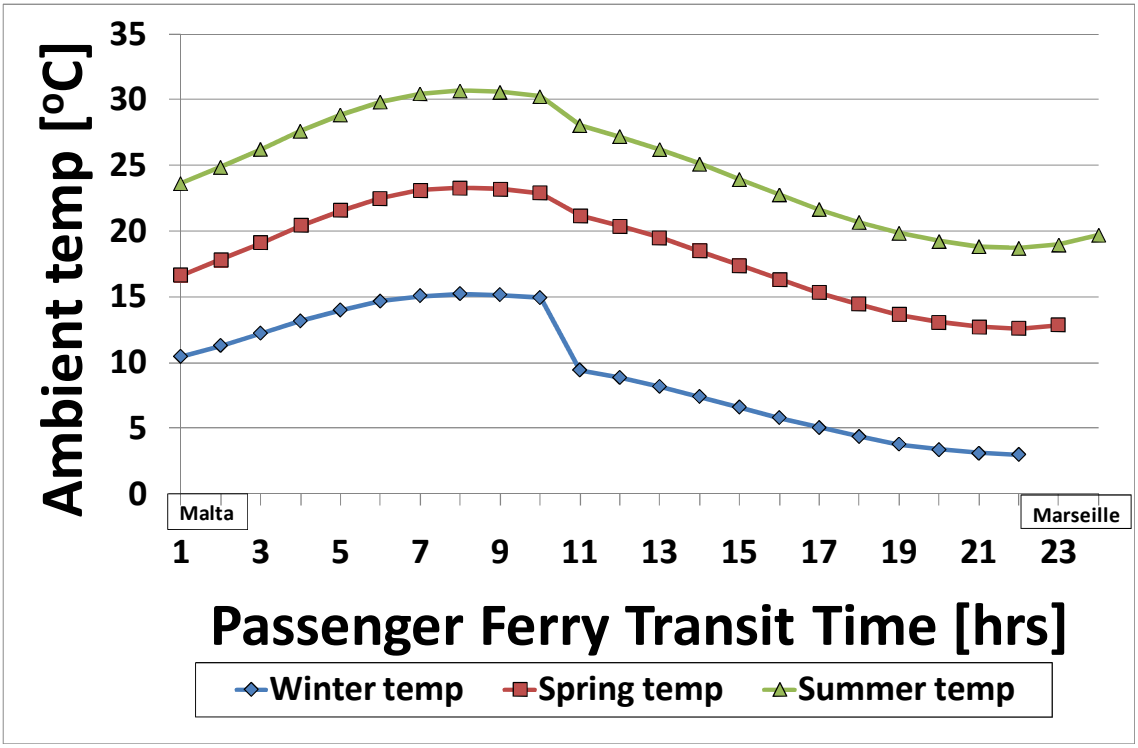

Figure 4:7 Ambient Temperature Variations along the Transit route of the Passenger Ferry

4.3 Management of Propulsion Power and Redundancy

Considering that the ship propulsion power required at any point during the voyage is dependent on such factors as the ambient (GT intake) air temperature, roughness of the sea water surface in line with its waves' characteristics, the condition of the ship hull surface, the roughness of the propeller blades among others, and that each ship is designed with an installed capacity to meet the sustained service speed, it is necessary to allow for a certain margin of power to be available in cases when the resistance increases., It became necessary for a preliminary evaluation of the different propulsion system configurations for each GT model so as to determine the redundant power and capacity to overcome the limiting factors that are likely to be encountered during the sail. The exercise revealed the maximum speed and how early each of the GT models was capable of completing a particular voyage in comparison with the others. The composition of the number of gas turbine that were needed for configuring each power plant to meet the power requirement for overcoming expected increased resistance due to changes

arising from ambient temperature and rising sea waves were determined as listed in Table 4:6. The COGAG method of combining different marine gas turbines for the propulsion machinery of the vessels is adopted for the investigation in this research.

4.3.1 Number of Installed GTs per Vessel

In order to meet the requirement to power each of the vessels, a COGAG arrangement was adopted and depending on the ship's load characteristics, a multiple engine setup was necessary in most of the cases. Table 4:6 shows the required number of gas turbines for each power plant according to cycle configuration and power rating. It is important to note that the arrangement of the prime movers facilitates the boosting of the plant's power so as to meet the speed requirement and tackle hard propulsion instances occasioned by form, wind or wave resistance as the case may be.

Table 4:6 Installed Capacities of the Propulsion Plants

Type of Vessel	19MW TSSC	25MW SC	25MW ICR	36MW TSSC
LNG Carrier	3	2	2	1
Cargo ship	5	3	3	2
Cruise Liner	4	3	3	2
Passenger Ferry	3 (2)	2	2	1

4.3.2 Availability of Power for the Cargo Ship

As highlighted in Table 2:5, the selected cargo ship model is represented by a container ship whose trade route involves a long-hauled voyage from the port of Cape Town in South Africa and terminates at Rotterdam in Nederland and vice versa. It sustained sea speed was estimated at 25 knots and was expected to cover an approximate distance of 6342 nautical miles in a transit time of 254 knots during ideal weather conditions. Under ideal weather conditions (IWC) and assuming the estimated auxiliary power margin to be 3.5MW needed for onboard service, the total estimated installed capacity was evaluated to be 56.727MW.

An assessment of the COGAG configuration of the propulsion machinery for the cargo ship capability to overcome the expected adverse conditions along its designated trade route was conducted through which a comparison of the power margin available in each case was observed. The variation of the brake power in relation to ship speed at every point was used to determine the number of engines required to meet the ship's peak power demands. The behaviour of each of the gas turbines in terms of their brake power, thermal efficiency, TET and the pollutant emission of NO_x as the cargo ship transits between a lower speed range and the maximum available power for achieving the highest ship speed possible were predicted. With its design speed at 25 knots under ideal weather conditions and with ambient air temperature assumed to be at ISA level, the power margins in the case of the cargo ship were investigated and are as shown in Table 4:7.

Among the variety of engines under investigation, the highest efficiency for this ship was achieved through the 25MW intercooled recuperated cycle with specific fuel consumption (SFC) of about 195 g/KWh. The preliminary assessment is also capable of assessing the pollutant emissions while the ship is in transit.

Table 4:7 Cargo ship Power management Profile

GT Models [Cargo ship]	Max No. of GTs	Min Available Capacity		Deficiency (Min No of GTs)	Max Available Capacity		Redundancy (From extra GT)
		Speed [knots]	PB [KW]	[%]	Speed [knots]	PB [KW]	[%]
19MW	3	24	44630	4	25.4	57106	1.6
ICR	2	22	30912	12	25	53226	0
SC	2	22	30912	12	25	53226	0
36MW	2	24	44630	4	27	76561	8

With the arrangement of the power plant in a COGAG configuration, it is assumed that the power requirement at low speeds and low power settings can be augmented by the inclusion of a smaller gas turbine or diesel engine(s) in order to improve the part load performance covering the entire speed range

from the beginning of the voyage in each case. When comparing all four gas turbines,

It found out that the 36MW engine has the capacity to operate with a single engine up to the limit of the sustained sea speed under ideal weather conditions (IWC) and its two engines combine together can propel the cargo ship up to a maximum speed of 27 knots and with a maximum efficiency of 39.6%.

4.3.3 Availability of Power - Cruise Liner

The journey involving the Cruise Liner is one of the two long-hauled voyages under this investigation. It is designed with capacity to cover a nautical distance of 5687nm (10,532km) from Lagos-Nigeria through the Mediterranean Sea at a cruise speed of 22 knots and terminate at Jeddah in Saudi Arabia. It is expected to take about 11 days under ideal weather conditions. The expected delay in the process of crossing the Suez Canal has not been considered in this thesis and it assumed to have enough capacity to endure and cope with the requirement to meet the fuel quantity needed to cover the entire voyage without refuelling. The preliminary performance investigation for each gas turbine engine is shown in Table 4:8

Table 4:8 Cruise liner Power management Profile

GT Models [Cruise Liner]	Max No. of GTs	Min Available Capacity		Deficiency (Min No of GTs)	Max Available Capacity		Redundancy (From extra GT)
		Speed [knots]	PB [KW]	[%]	Speed [knots]	PB [KW]	[%]
19MW DSSC	3	14	6710	36	22.4	29120	2
25MW ICR	3	22	29120	0	26	53976	18
25MW SC	3	16	10086	27	25.1	47144	13
36MW DSSC	2	14	6710	36	24.8	45079	13

4.3.4 Availability of Power for the Passenger Ferry

As with the other ship types, the preliminary investigation in the case of the Fast speed ferry was conducted under the assumption IWC while anticipating

adverse climatic and hydrodynamic conditions to persist during the voyage along its designated trade route. Intake air temperatures were assumed to range from 0^{o}C to 40^{o}C and the power margins were observed. All the models showed capacity to develop enough power to propel it up to its designed service speed of 30 knots.

Table 4:9 Power management Profile of the Fast speed Ferry

GT Models [Ferry]	Max No. of GTs	Min Available Capacity		Deficiency (Min No of GTs)	Max Available Capacity		Redundancy (From extra GT)
		Speed [knots]	PB [KW]	[%]	Speed [knots]	PB [KW]	[%]
19MW DSSC	2	26	21962	13	30.1	39364	0
25MW ICR	2	28	28759	7	32.2	55111	7
25MW SC	2	26	21962	13	32	53697	7
36MW DSSC	1	30	38753	0	30	38753	0

The results in Table 4:9show that the 36MW model when configured in a single engine layout, its power output is sufficient to meet the demand for IWC but without any redundant power for AWC. At the same time, the 19MW model single engine configuration of the power plant was unable to meet the demand unless two of its units were combined together and yet without any redundancy. However, when the 25MW versions were installed, each single unit was capable of delivering power with a deficit of 7% for the ICR and 13% for the SC model respectively.

4.4 Preliminary Installed Performance Prediction

In line with the ambient conditions found for each of the selected fixed trade routes, the operating temperature range earlier considered in the uninstalled “Turbomatch” design and off design investigation of the gas turbine models ranged from 0^{o}C up to 40^{o}C and as first step, the gas turbine thermal efficiencies were evaluated across the same operating temperature range under the assumption of ideal weather conditions.

The preliminary evaluation analysed the cycle efficiency and the TET for each of the gas turbines under standard ISA conditions and for each of the vessels, it showed how the performance can vary when the ship speed gradually increase from lower speed settings to their maximum possible limits.

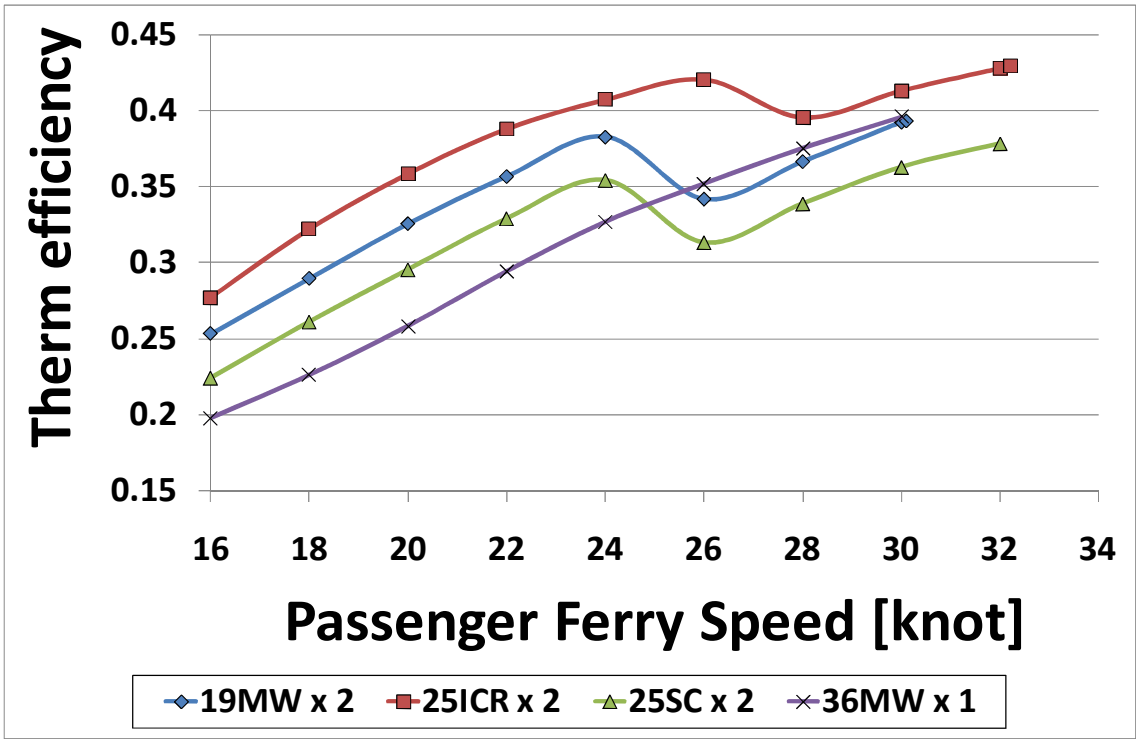

Figure 4:8 Variation of thermal efficiency of the GT models vs ship speed

The operating temperature profile of any marine gas turbine is a significant factor in assessing its life. It is normal practice however, to design the machine with enough allowance for off design operation at the upper limit of its operating temperature, namely, the turbine entry temperature (TET). The “Poseidon” simulation code was used to facilitate the prediction of the variation of this parameter as an important factor with implications in the investigation of the metallurgical limit of the GT models.

The creep model embedded in the integrated simulation platform facilitates the limitation of the maximum TET for operating each of the gas turbine models as control measure to limit the hot end life consumption.

4.4.1 Cruise Liner

A comparison of the performance installed power plants configured according to the different GT models shows the 3-engine configuration of the ICR model on the cruise liner as a more fuel efficient combination. With only 2 engines in operation, this model was capable of operating well over 40% in efficiency at speeds that were as low as 6 knots. The preliminary investigation also show that the requirement for the attaining the service speed along with the onboard auxiliary power requirement and hotel load can be met if only two of the ICR model were to be installed. The rest of the models showed a loss of efficiency especially at the points of engaging the augmented power from an additional engine.

The preliminary evaluation of the power plants was conducted at 0^{o}C, 15^{o}C (ISA) and at the maximum ambient temperature regime of 40^{o}C as illustrated Figure 4:9 to Figure 4:11.

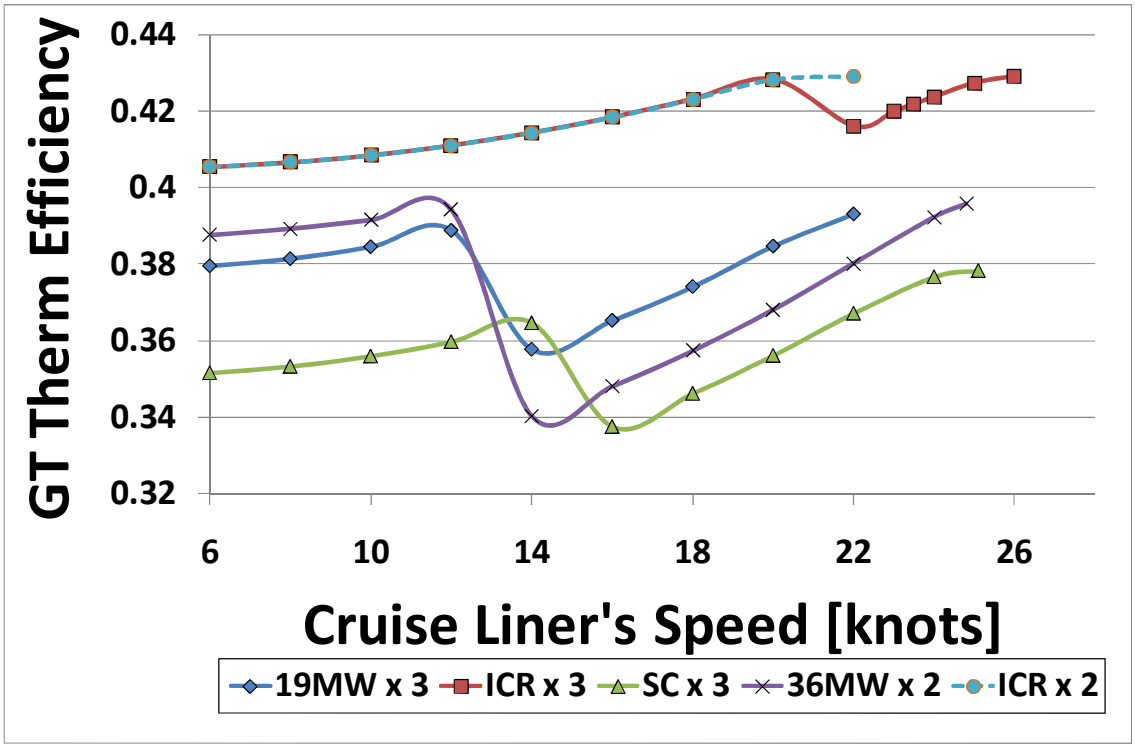

Figure 4:9 Preliminary evaluation of the cruise liner's GT efficiency when operated at 15^{o}C (ISA) conditions

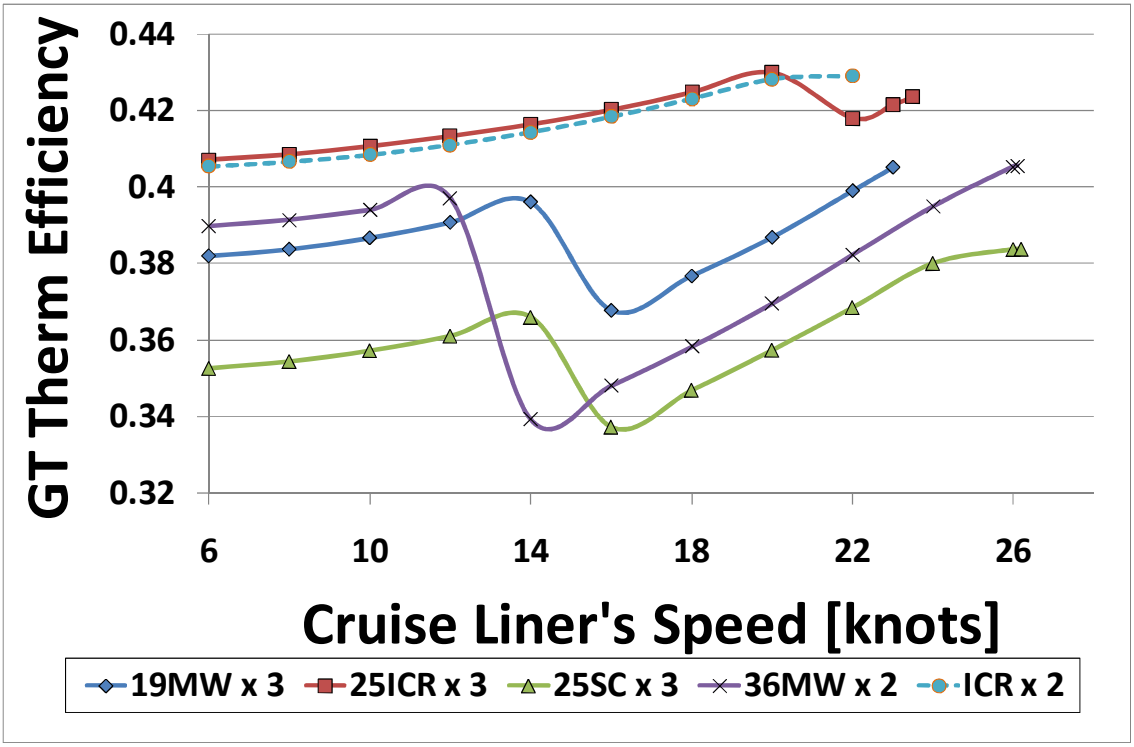

Figure 4:10 Preliminary evaluation of the cruise liner's GT efficiency when operated at an ambient temperature of 0°C

While the ICR model was capable of propelling the cruise liner with an efficiency of over 40% at a minimum speed of 6 knots and rose up to 43% at a speed of 20 knots, the 25MW simple cycle model could only achieve about 35% efficiency at a minimum ship speed of 6 knots with two engines and steadily rose up to only about 36.5 thereby requiring the power to be supplemented through a third engine at a speed of 14 knots only. It is important to note that the efficiency of the gas turbine is grossly affected by the hot weather conditions as illustrated in Figure 4:11.

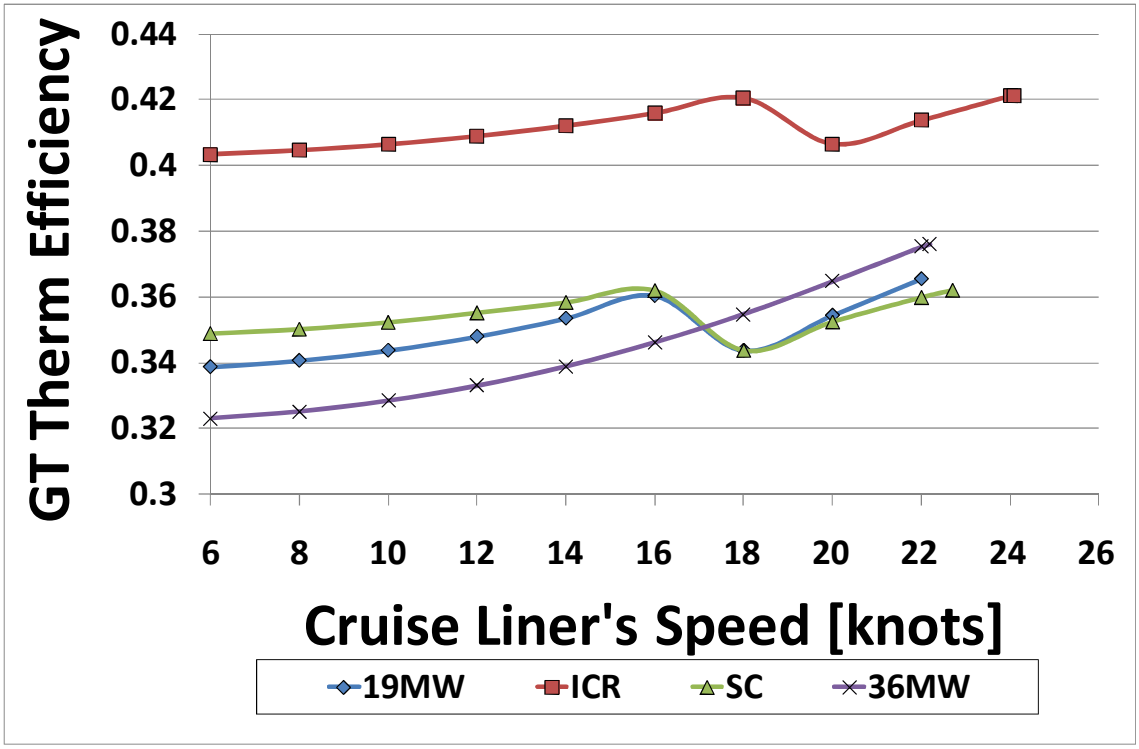

Figure 4:11 Preliminary evaluation of the cruise liner's GT efficiency when operated at an ambient temperature of 40°C

4.4.2 Cargo ship

With the service speed of 25 knots for the cargo ship, the dual engine configuration with the 36MW model was able to propel the ship up to a speed of 22 knots before a demand for boost power from a second engine became necessary. This model affords the cargo ship's power plant enough redundant power that is capable of propelling it up to a maximum cruising speed above 27 knots. Its downside however is that it operated at lower efficiency during low speed operations which can easily be overcome by the addition of a smaller gas turbine or diesel engine in a COGOG or CODOG configuration.

The ICR in this application still showed considerable advantage over the others in terms of efficiency and spare or redundant power for possible application in times of high power requirements. In the case of the smaller engine, 19MW model, the result is similar to that of the 36 MW but with the advantage of more flexibility for low speed transition. It demonstrated how the first engine is capable of being operated alone without any requirement for boost power until

the ship attains a speed of 18 knots but a second engine will only boost it up to 22 knots before the third is engaged in order to attain the MCR speed and without any redundancy. For this reason therefore, the constitution of the cargo ship power plant with the 19MW model consisted of 4 units as shall be seen later in chapter 5.

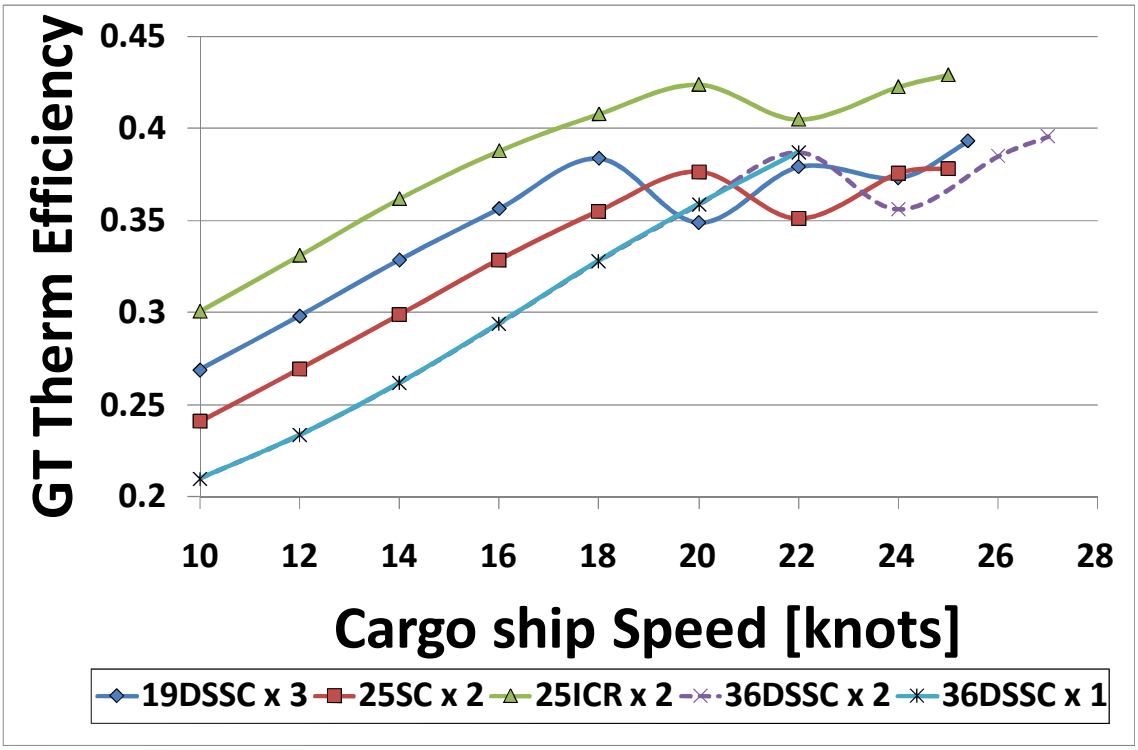

Figure 4:12 Preliminary assessment of the gas turbines for installation on the cargo ship measured at ISA conditions.

The prediction of the performance of a single 36MW engine model was included as shown in Figure 4:12 showing its capability to propel the cargo ship up to 22 knots before additional power was required to boost the speed to its MCR status meaning that the dual 36MW engine power plant will possess enough power to spare whenever the need arose.

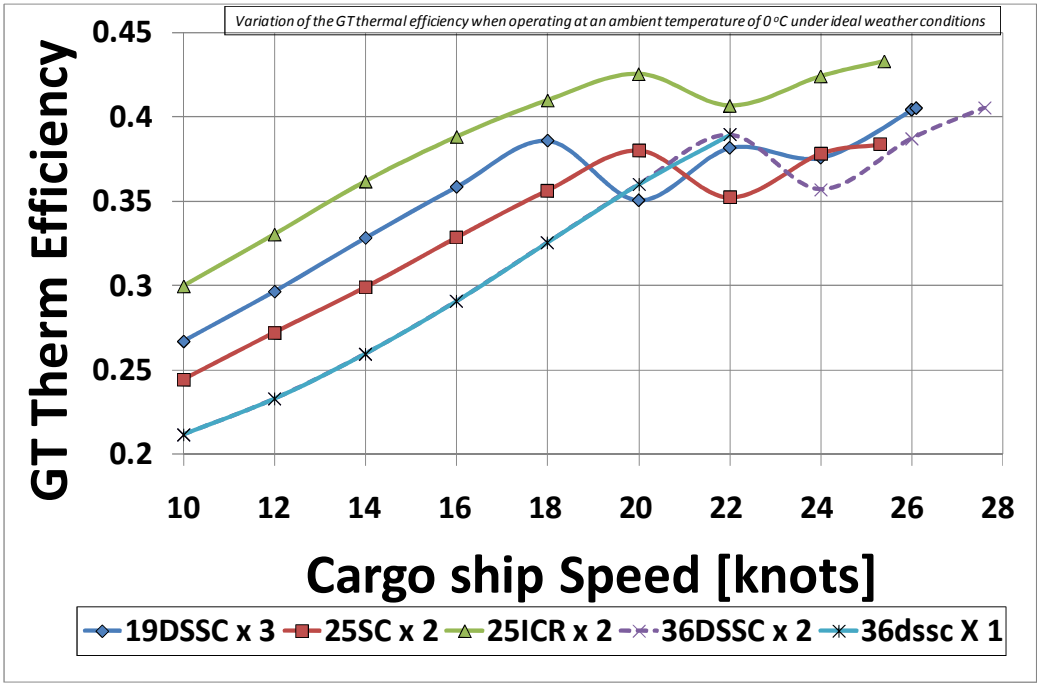

Figure 4:13 Prediction of the efficiency of the gas turbines for the cargo ship propulsion at an ambient temperatures of 0^{o}C.

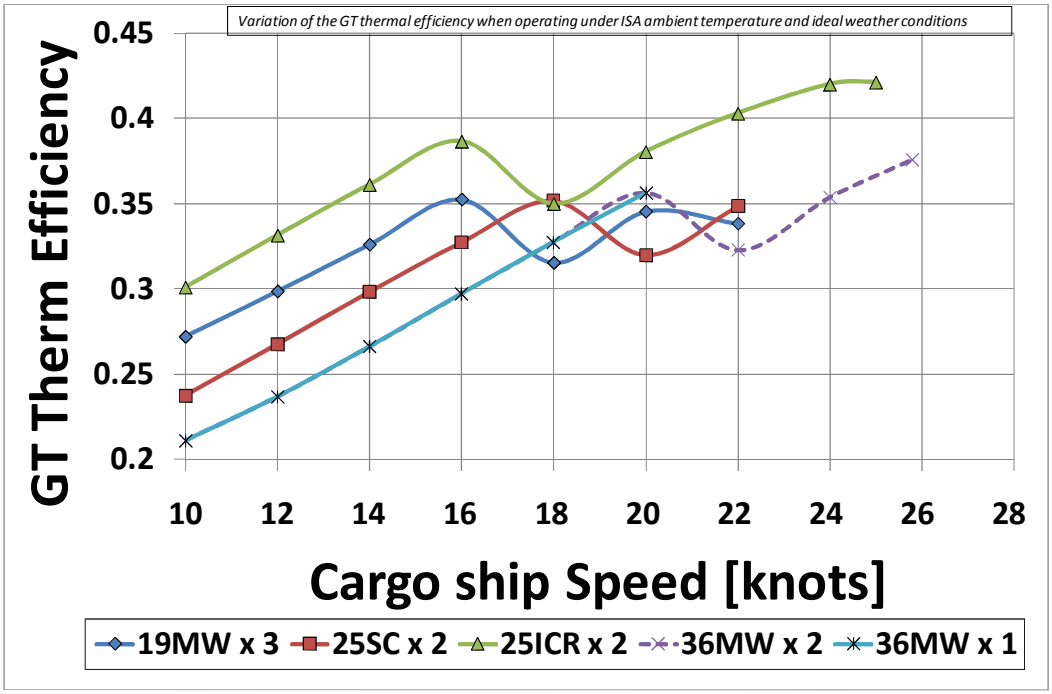

Figure 4:14 Prediction of the efficiency of the gas turbines for the cargo ship propulsion at an ambient temperatures of 40^{o}C.

Figure 4:13 and Figure 4:14 are a further illustration of the effect of operating the cargo ship under the two extreme ambient temperatures of 0^{o}C and 40^{o}C as considered in the research. At 40^{o}C the capability of the gas turbines to acquire

maximum speed with enough redundancy was grossly affected and in particular, the ICR could not match its SC counterpart during hot weather operation as its single unit was unable to propel the vessel up to 16 knots before losing its superiority in terms of efficiency. It can be seen in Figure 4:14 that it was able to meet the demand up to a speed of 22MW while maintaining its superior efficiency when operated at 0^{o}C.

4.4.3 The Fast speed Ferry

The performance of all the models on the Ferry was also evaluated and the behaviour of all the models was predicted. A single engine configuration was assumed in the case of the 36MW model while the flexibility of the 19MW model makes it possible to install 3 of its units in the power plant, only two units were assumed and the pattern of its variation could be compared to that of the 25MW SC model as illustrated in Figure 4:16and Figure 4:17. The ICR and SC models were combined in a COGAG configuration of two engines each and were able to demonstrate effective capability to propel the Ferry beyond its service speed with the ICR still featuring better performance compared to the SC model.

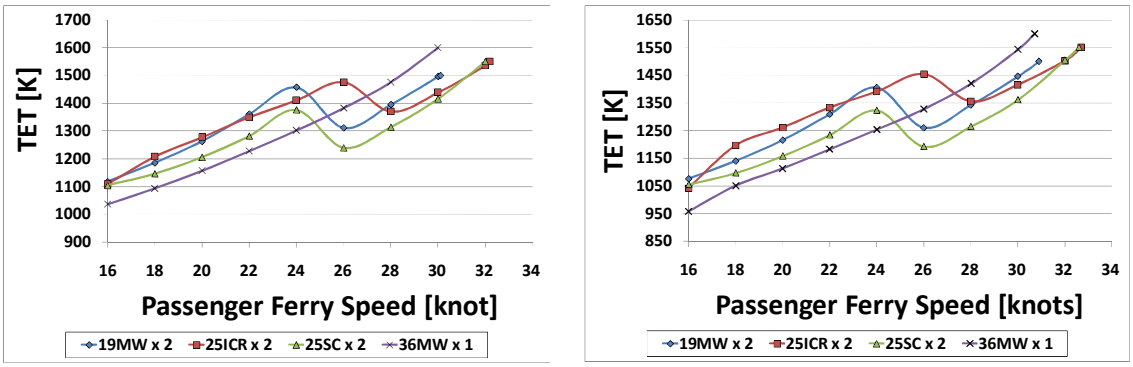

Figure 4:15 Prediction of the TET variation when the gas turbines operate as propulsion prime movers for the Ferry at ambient temperatures of 15^{o}C and 0^{o}C respectively.

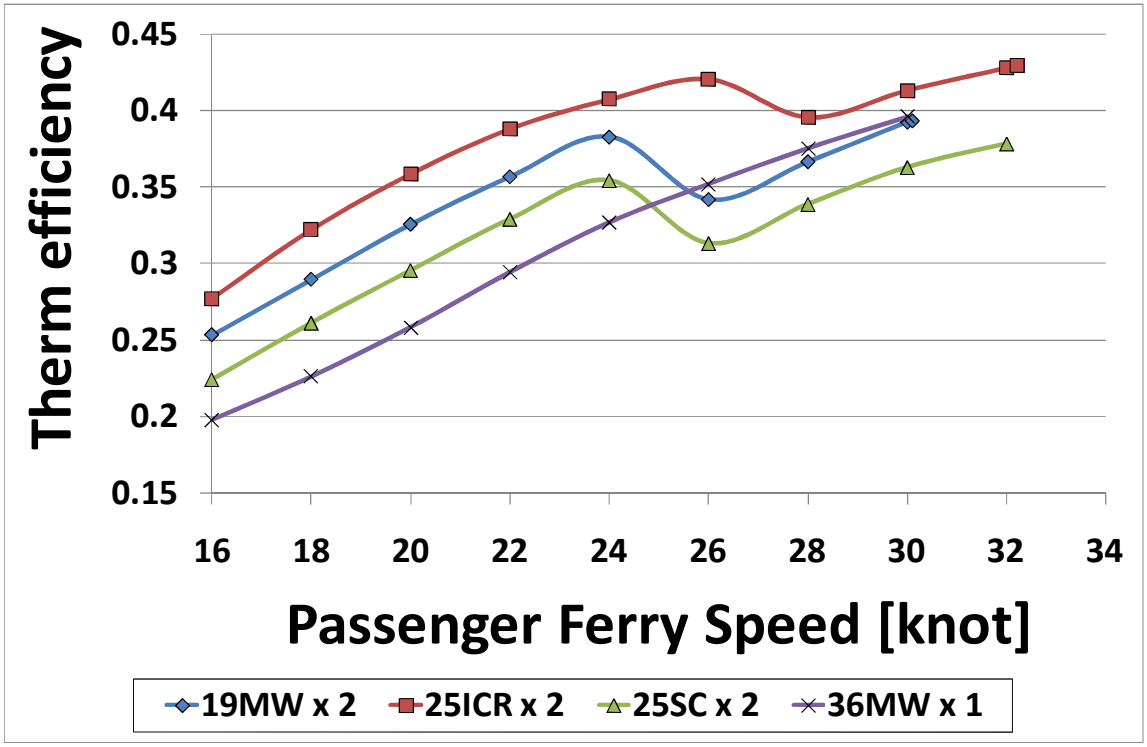

Figure 4:16 Prediction of the efficiency variation when the gas turbines operate as propulsion prime movers for the Ferry at an ambient temperature of 15°C.

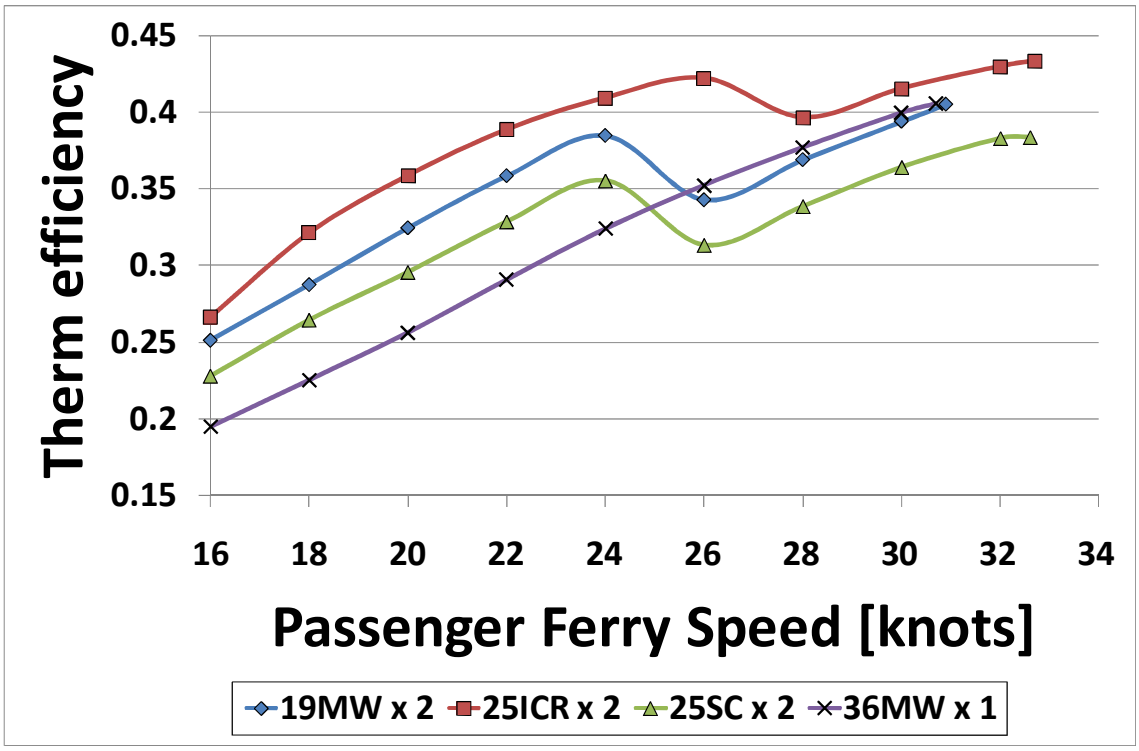

Figure 4:17 Prediction of the efficiency variation when the gas turbines operate as propulsion prime movers for the Ferry at an ambient temperature of 0°C.

The effect of hot weather can be seen in the illustration of the TET and the P_B variation in Figure 4:15 and Figure 4:18 when measured at 0^oC and 15^oC respectively.

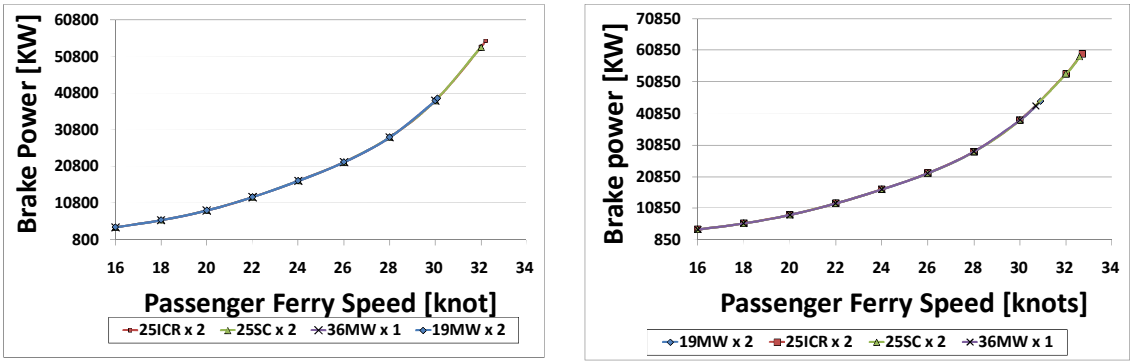

Figure 4:18 Prediction of the PB variation when the gas turbines operate as propulsion prime movers for the Ferry at ambient temperatures of 15^oC and 0^oC respectively.

4.4.4 Prediction of Exhaust Pollutant Emissions

Similarly, the exhaust pollutants were investigated and it shows that the emission quantities rise to higher values with increases in ship speed. The curves demonstrate the relationship with proportionate growth in the TET values.

Although results for CO_2, CO, UHC and NO_x were obtained, NO_x and CO_2 have been considered as most important parameters that have attracted worldwide attention and they now constitute considerable economic implications when evaluating the operating cost of any gas turbine engine. The estimation of these quantities has been attempted and the variation for NO_x is represented in Figure 4:20

When ambient temperatures get as high as 40^oC, the performance of the 19MW and 36MW units drops to the extent that an increase in the number of engines for the power plant becomes mandatory in order to sustain the sea speed designed for the Ferry. This gave rise to the number of engines from two to three in the case of the 19MW model while that of the 36MW became two instead of one. It is well known that the gas turbine technology suffers

degradation in terms of performance when higher ambient temperatures are encountered which is expected to lead to increased maintenance costs.

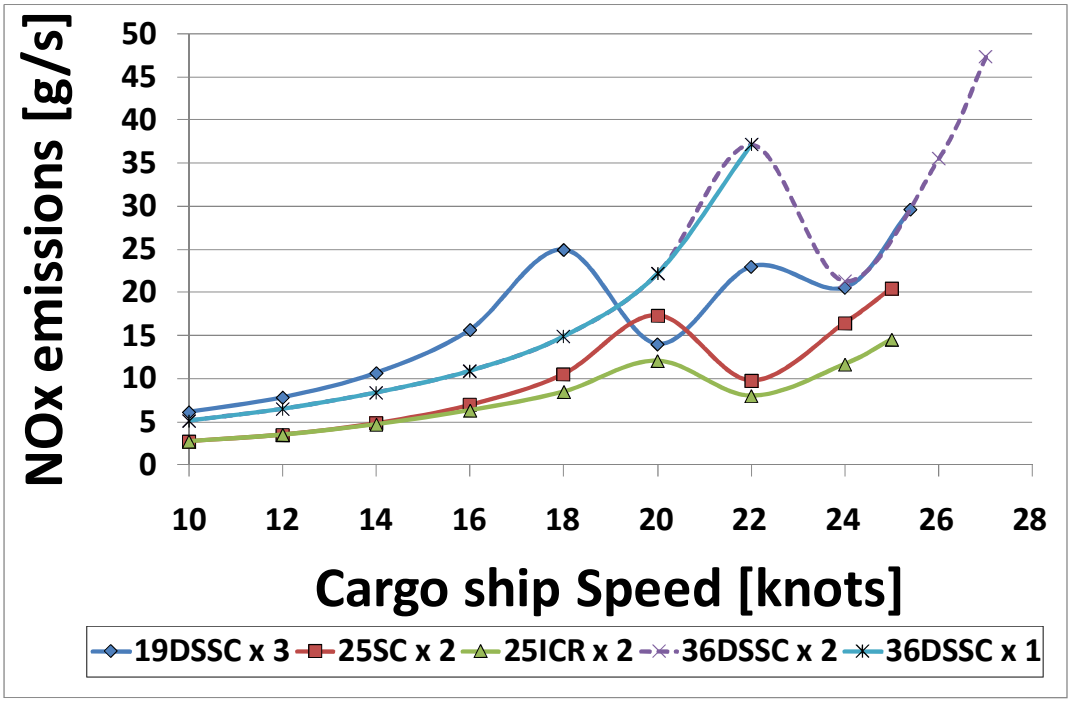

Figure 4:19 NO_x emission profiles of the four GT models for the cargo ship

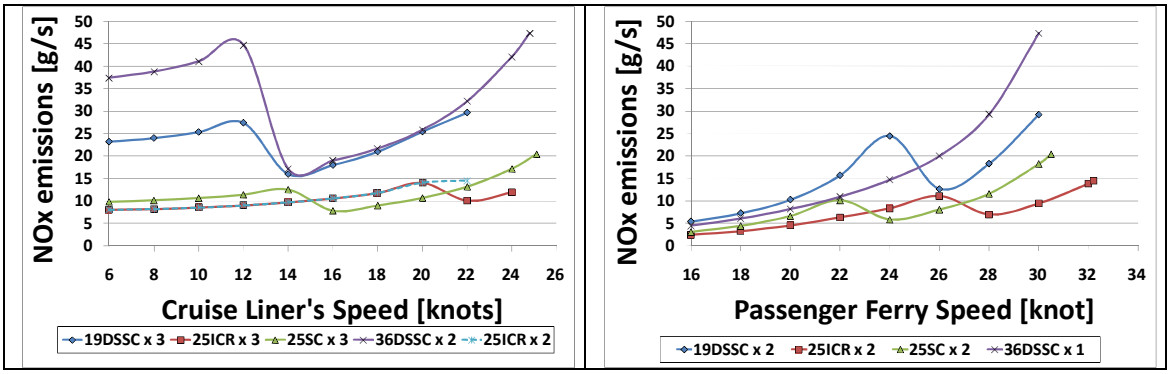

Figure 4:20 NO_x emission profiles of the four GT models for the Cruise Liner and the Passenger Ferry.

5 ANALYSIS OF THE LNG CARRIER

This chapter seeks to analyse the behaviour of all the gas turbine models when operated as the propulsion prime movers of the LNG Carrier by comparing their performance according to the different environmental operating conditions as the vessels travel along the fixed trade route that has been selected for the investigation. An analysis of the overall effect of the limiting factors was conducted and the benefit of using the boil-off gas as fuel was evaluated while comparing and predicting the quantities of fuel burned (FB), pollutant emissions and estimation of engine life consumed in each case.

5.1 The Gas Turbine Propulsion Alternative

The application of slow and medium speed diesel engines and marine gas turbines are currently the most favoured propulsion systems being proposed main alternatives to the conventional steam turbine that has dominated the LNG Carrier industry. So far, the DFGE (Dual-fuel Gas turbine Electric) propulsion system, which incorporates a heat recovery steam generator (HRSG) has been the most proposed. Its configuration is such that the hot exhaust gas is used to drive a steam turbine for the generation of additional electrical power with the overall benefit of raising the thermal efficiency of the installation to competitive levels with the diesel engine. The HRSG is also fitted with burners for auxiliary firing with either the liquid fuel or the BOG. The analysis of the LNG carrier therefore is aimed at evaluating the performance of each gas turbine model in terms of the quantity of fuel burned, pollutant emissions released into the atmosphere and the estimated engine life consumed per every voyage. In addition, the quantity of the expected BOG was estimated at the rate of 0.15% of the vessel's cargo capacity per day and the amount was compared with the values of the voyage quantities of FB in order to determine how much liquid fuel back up was needed in an efficient operation of the LNGC. A comparative analysis of the gas turbine models was realised and the outcomes are the main subject being discussed further.

5.2 Composition of the Power Plants

Based on the rated power of each of the projected gas turbines, the number of engines required for operating the vessel while maintaining its cruising speed was established for each case scenario. The variables considered in the composition of the power plant based on the engine models include the seasonal weather conditions, sea states and hull fouling. Under ideal weather conditions (IWC), two units of the 19MW model were needed to operate in such a way that a third one would be required whenever there was the need for boost power due to changes in the operating environment. On the other hand, the SC and the ICR which are both rated at 25MW each could effectively meet the demand under IWC with a single engine installation while a second unit was to be deployed whenever severe operating conditions were experienced. As a result of the high rated power of the 36MW model, a single engine installation was the only option available to cater for both IWC and AWC. A profile of the LNGC power plant according to the different gas turbine cycle configurations of the project are detailed in Table 5:1.

Table 5:1 Composition of GT models for the Propulsion plant

GT models [Rated Power]	No. of Engines Required	
	Ideal Conditions	Adverse Conditions
25MW	1	2
25MW ICR	1	2
36MW	1	1
19MW	2	3

5.3 Voyage Analysis

Following the typical marine practice, the following characteristic phases were observed to be part of the round trip voyage profile of the LNG vessel:

- Voyage in full load condition from loading to the off-loading terminal (port)
- Voyage in ballast condition from the off-loading and back to the loading terminal

- Manoeuvring during approach to both the loading and off-loading terminals
- LNG loading period at the loading terminal
- LNG delivery period at the off-loading terminal

However, this research focuses on operating profile of each gas turbine within the first two phases mentioned above. This mainly so because of the fact that the proposed COGAG installations can only be beneficial when the vessel in utilizing full power at its service speed during which the vessel is expected to cruise continuously by using the dual fuel facility of the BOG or the liquid marine diesel oil (MDO).

As a matter of safety, the use of boil-off gas during the other three phases listed above is prohibited as a result of which only the liquid fuel could be put to use. It is noteworthy to state that a significant fraction (about 5%) of the LNG cargo known as the heel volume cannot be practically off-loaded and a fraction of it must then be evaporated and used as BOG fuel during the ballast voyage. This heel volume is also used for cooling the cargo tanks during the ballast trip.

A combination of the outgoing voyage in full load condition and the ballast voyage combine to make up the duration of the round trip used for the evaluation of the economic benefits of using BOG for fuelling the LNG carrier.

5.4 Voyage Profile of the LNG Carrier

The trade route selected in this research and assumed for the transportation of LNG cargo by a gas turbine propelled LNG Carrier between the Algerian port of Arzew and the UK port of Portsmouth is one of the oldest LNG trade routes in existence since 1964.

In order to effectively predict the behaviour of the projected gas turbine engines, the distance and duration of the voyage between the two terminals based on the service speed of the vessel were established. Furthermore, the environmental conditions that that were expected to affect engine performance such as ambient temperature needed to be evaluated and daily forecasts of

maximum and minimum values were obtained[4] and are contained in Table 5:2.

Table 5:2 Maximum and Minimum Variation of Ambient Temperature according to Segments along the LNGC Route

Distance Between Sea Ports (nm)	Winter		Spring		Summer	
	Max Temp (^oC)	Min Temp (^oC)	Max Temp (^oC)	Min Temp (^oC)	Max Temp (^oC)	Min Temp (^oC)
366	16.6	7.5	23.9	12.1	32.2	19.8
509	14.5	5.1	21.7	10.6	27.9	14.6
499	13.5	4.2	19.4	8.5	25.0	13.0
245	7.2	2.4	17.0	10.7	21.9	11.4

Using the modified version of “Poseidon”, a voyage from the loading port to the terminal discharge port was simulated and the ambient temperature variation along the selected transit route was generated for all three seasons of winter, spring and summer as shown in Figure 5:1.

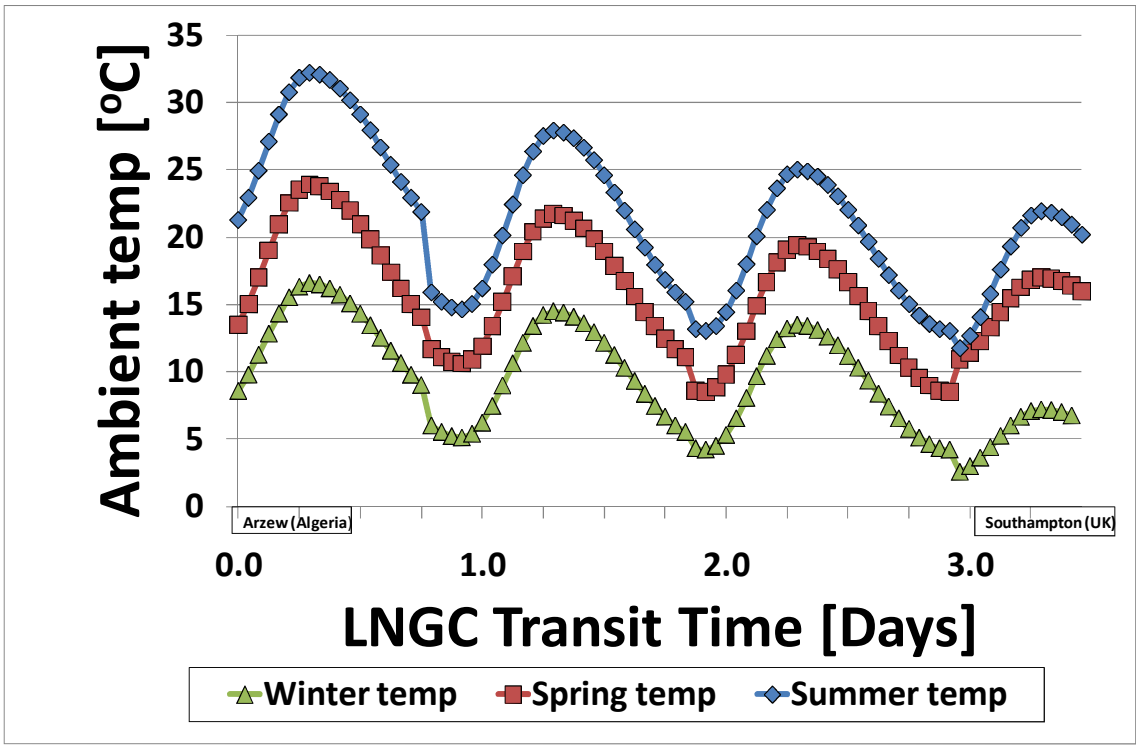

Figure 5:1 Ambient Temperature variations along the LNG Carrier Transit Route

5.4.1 Predicted Performance of the models

The behaviour and performance output of the 25MW rated simple cycle and ICR models were operated and compared under the same conditions and in the same way the 36MW and the smaller 19MW models were also paired in order to predict the derivable merits from each cycle configuration.

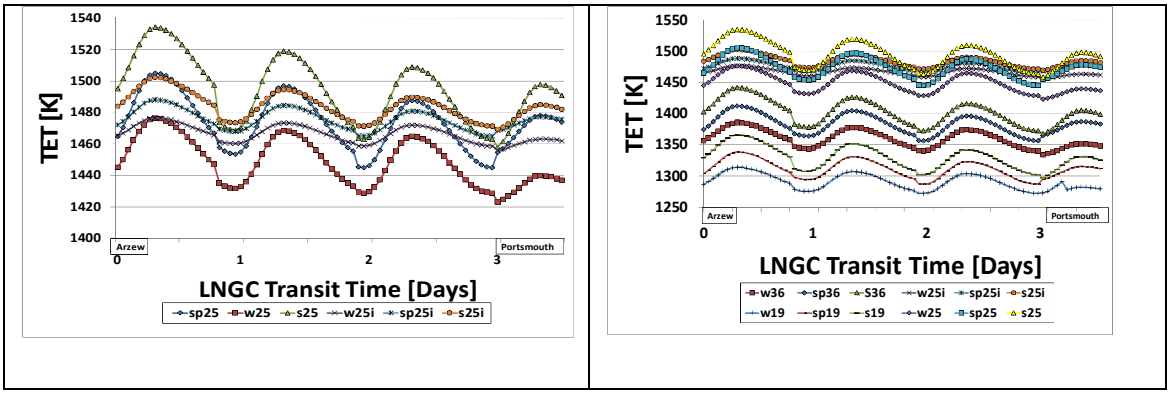

Figure 5:2 Seasonal variation of TET for the (a) 25MW ICR and SC models (b) All 4 models

An evaluation of the SFC showed the benefits to be gained by using the ICR as a better option to the other models throughout the voyage as outlined in Figure 5:3 and Table 5:3. The required propulsion power under IWC was found to be steady at about 22MW but was raised to over 60MW when the ship encountered adverse limiting conditions. Therefore, in all cases except for the 19MW model, the LNGC carrier was able to cruise with only one engine until the vessel encountered abnormal operating conditions.

The disadvantage of a very poor part-load performance at low power setting for the 36MW model can be eliminated through the installation of two of the 19MW model in a COGAG arrangement.

Table 5:3 Performance profiles of the models under IWC

GT model	Average output values of Performance Parameters			
	Efficiency [%]	SFC [g/kWh]	PR	Fuel Flow [kg/s]
19MW	34	245	20	1.55
SC	37	224	18	1.41
ICR	42	197	14.8	1.26
36MW	35	236	19	1.48

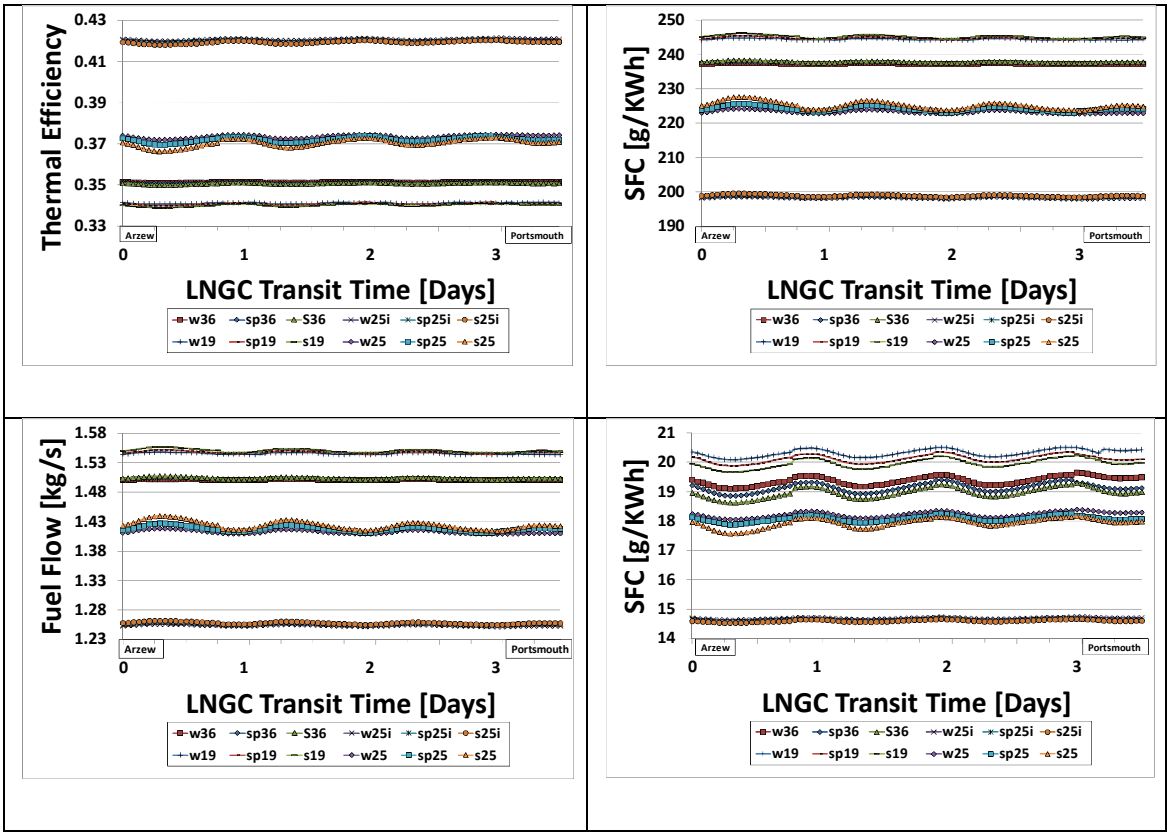

Figure 5:3 Variation of the gas turbine performance parameters in all seasons under IWC

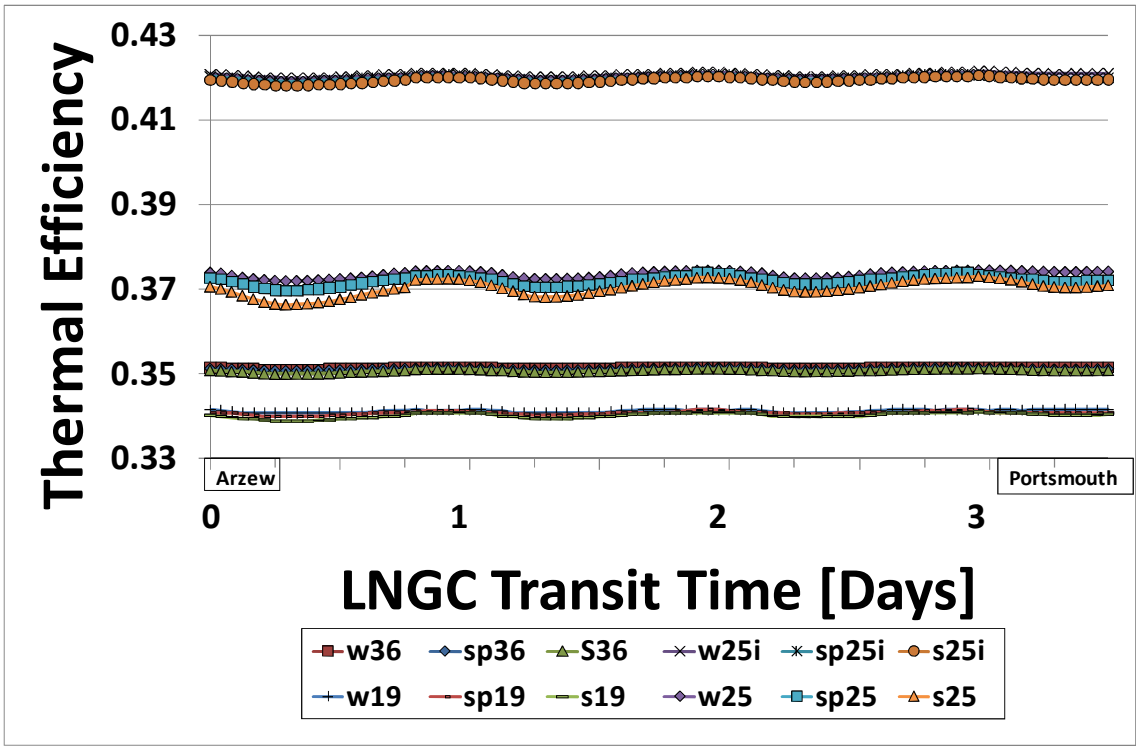

Figure 5:4 Profile of the thermal efficiencies of the GT models in all seasons under IWC

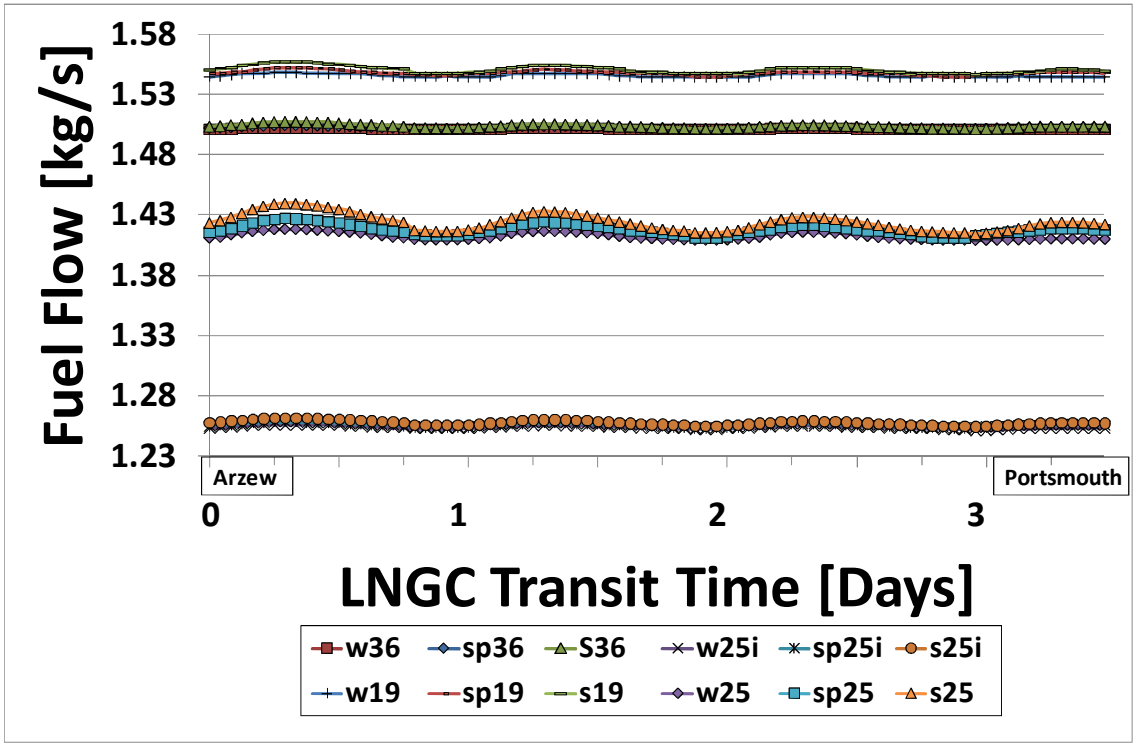

Figure 5:5 Profile of the Fuel flow of the GT models in all seasons under IWC

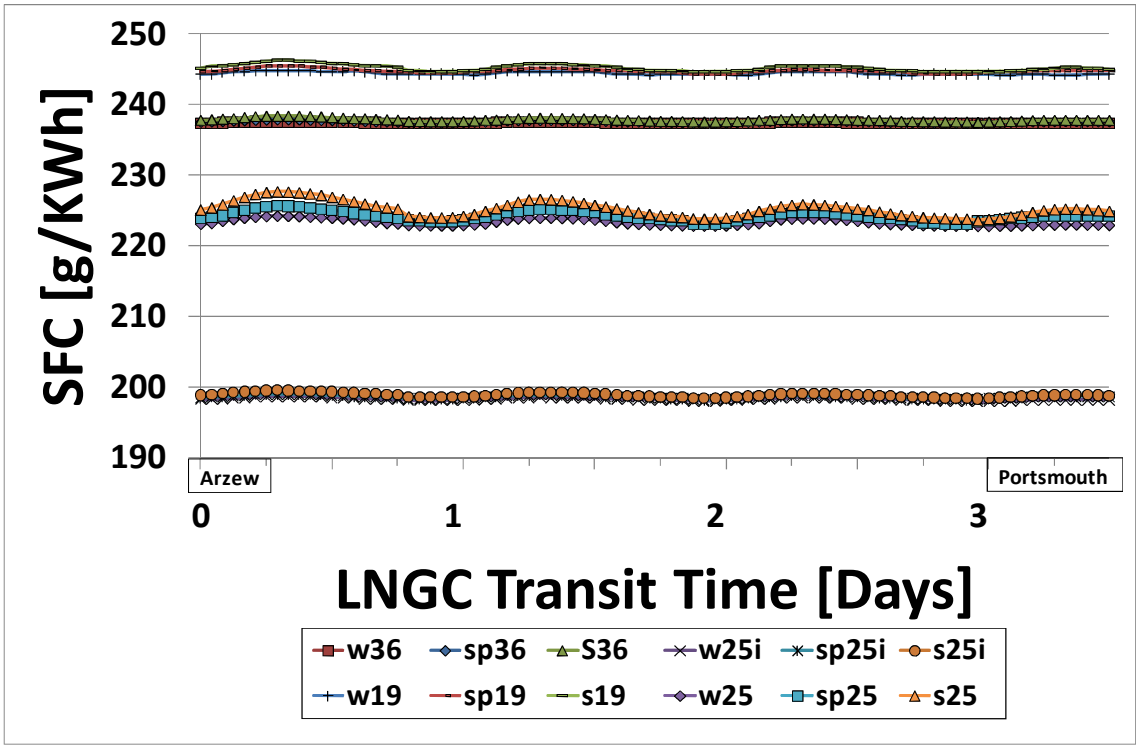

Figure 5:6 Profile of the SFC of the GT models in all seasons under IWC

5.4.2 Impact of Hull Roughness on the Propulsion System

Expectedly, the ship hull surface roughness resulting from fouling and possible corrosion of the submerged part of the ship influences degradation of the GT performance parameters even further. Therefore, the consequences of allowing the ship hull underwater surface to be degraded by fouling and corrosion were evaluated and effect on performance predicted in each case scenario. The hull fouling investigated scenarios were made possible by the implantation of hull roughness values of 120μm (HR1), 240μm (HR2) and 360μm (HR3) as has been the case in the investigation of the other merchant vessels of the research. Under IWC and AWC, a clean hull was assumed as having a maximum roughness value of 30μm for all voyages.

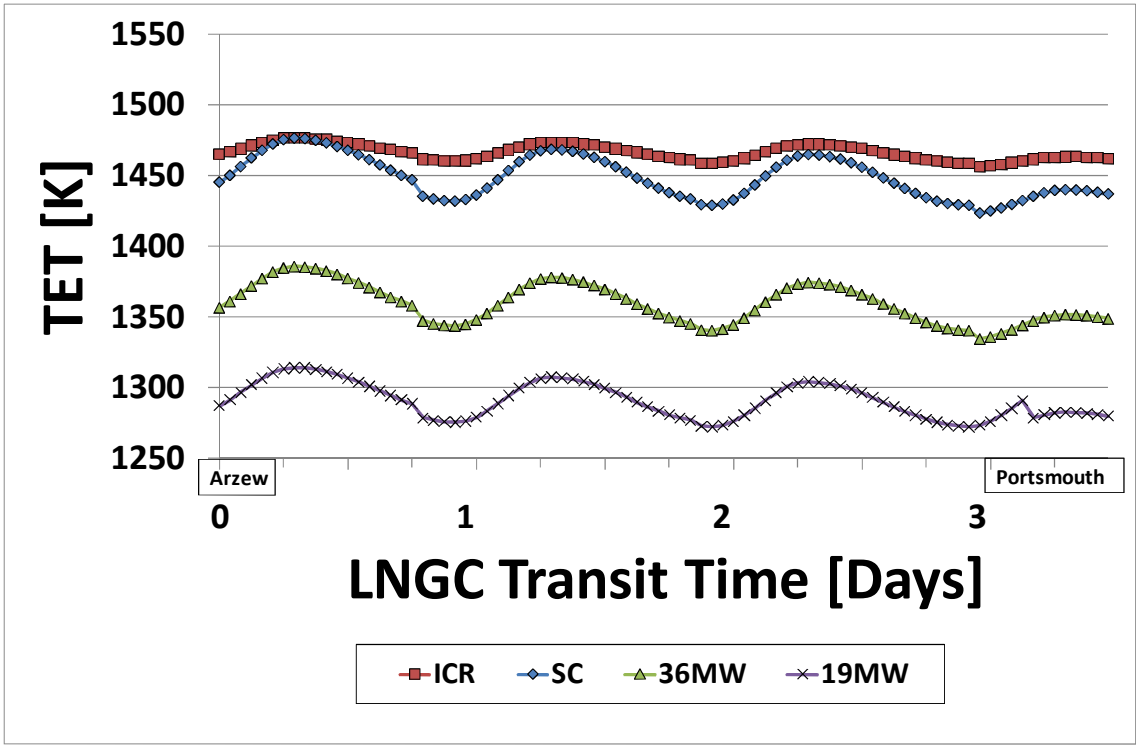

Figure 5:7 Profile of the TET in winter for the respective GTs

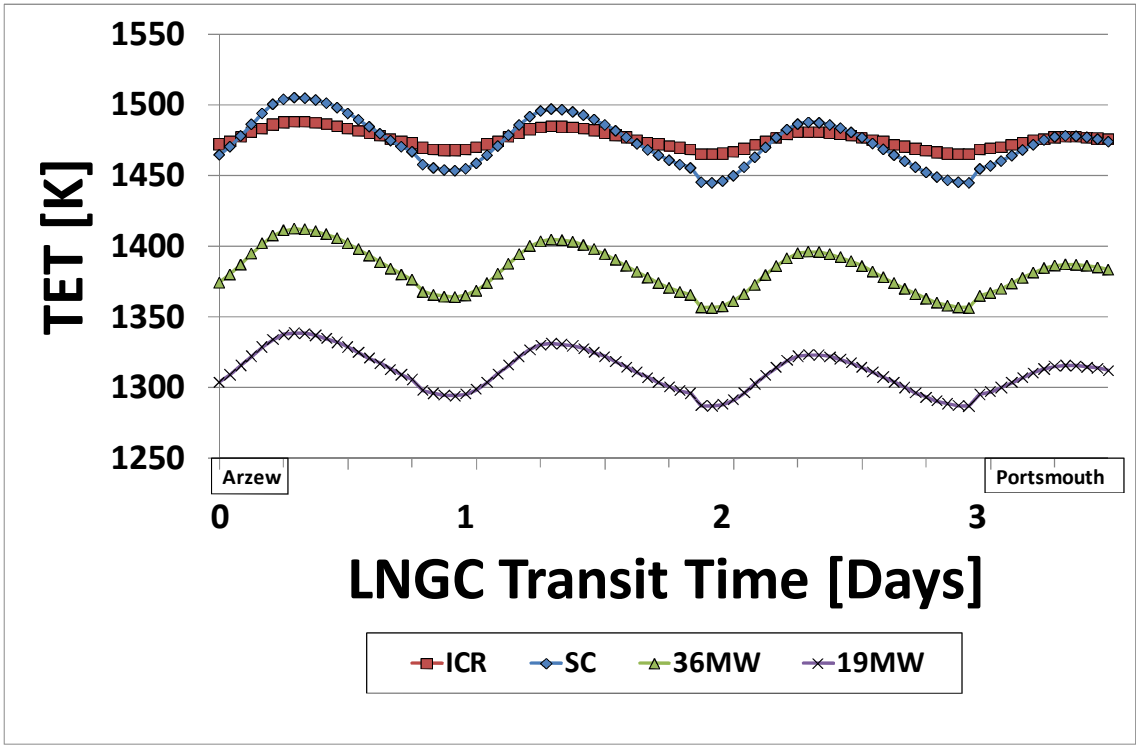

Figure 5:8 Profile of the TET in spring time for the respective GTs

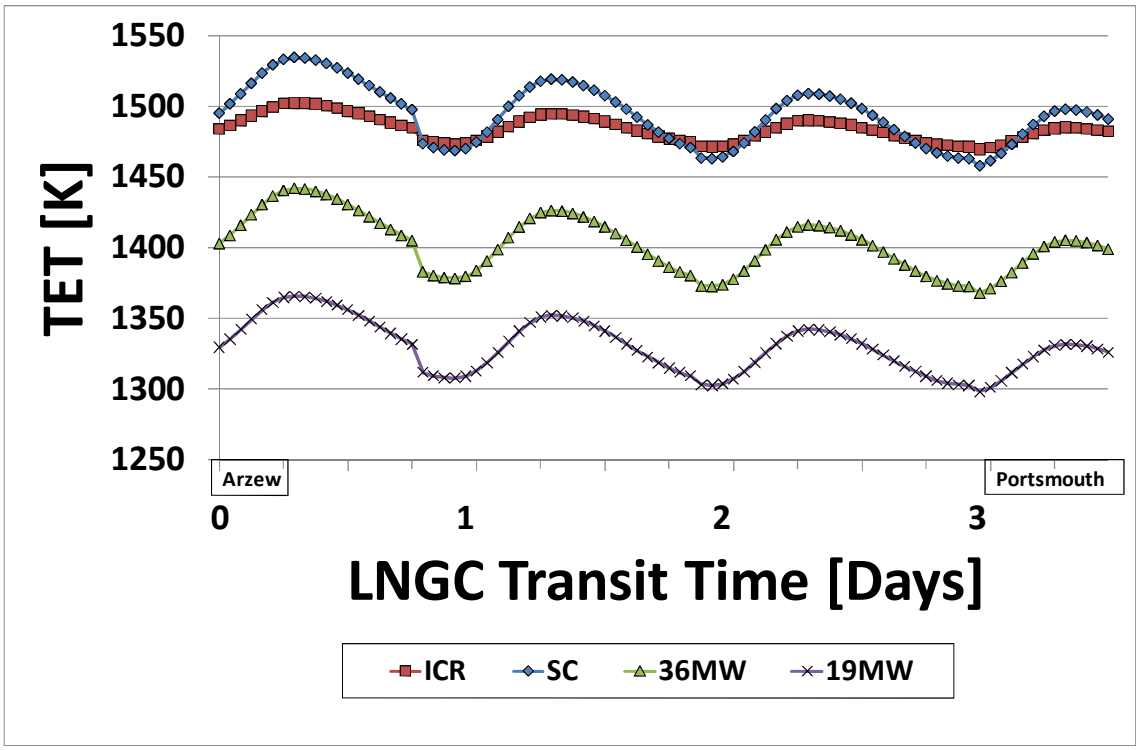

Figure 5:9 Profile of the TET in summer time for the respective GTs

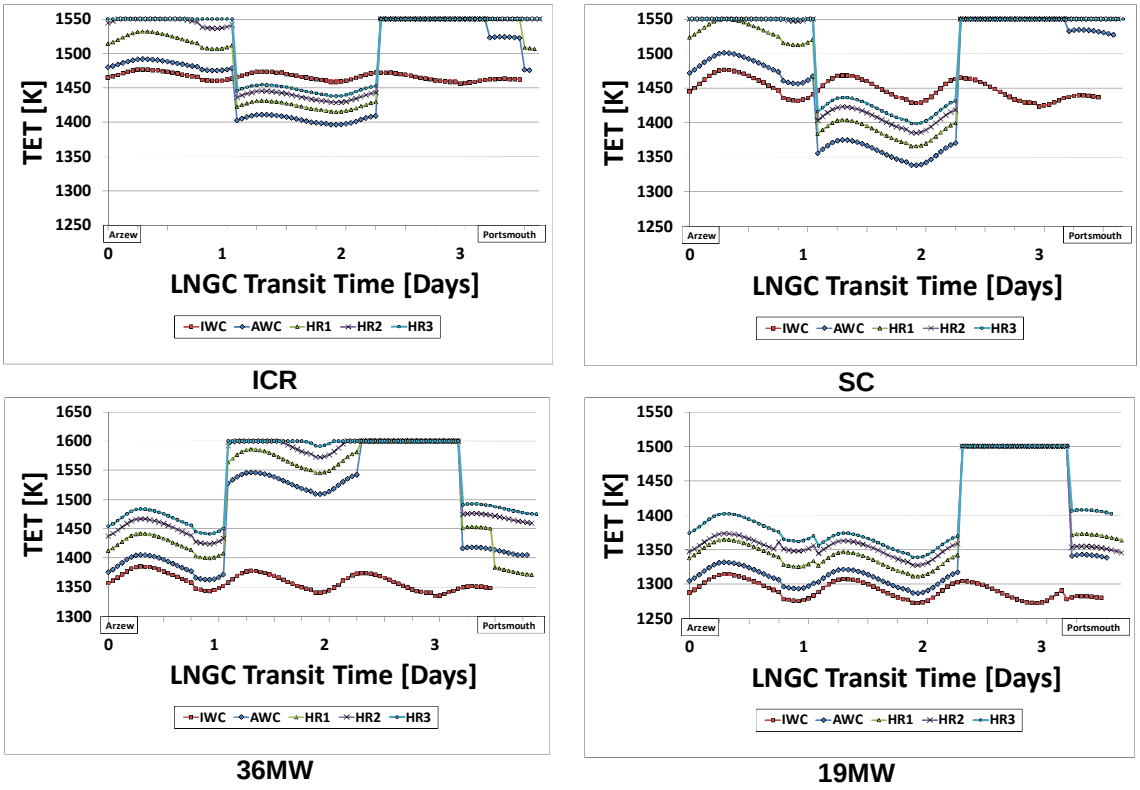

Figure 5:10 TET profile for each of the gas turbines when operated under the selected investigated scenarios

The turbine entry temperature has been used as the parameter for analysing the behaviour of each of gas turbine models and from Figure 5:7 to Figure 5:9 the engine profiles for winter, spring and winter are illustrated. Each of them was found to respond to the adverse conditions in a very unique way such that the ICR was able to steadily operate within a very narrow margin of high TETs (almost maintaining a straight line curve) especially when compared with the SC model. The analysis shows how the gas turbine is compelled to operate at elevated temperatures when the weather is hot. It further reveals the lower operating temperature (TET) of the 19MW model mainly because of the use of 2 engines instead of one.

Figure 5:10 also illustrates how each of the models responds to the severe operating conditions of the vessel when sea states and hull fouling are involved. It should be noted that for the sake of controlling the engine life, the TET was pegged to a maximum limit for each of the models. The most important

parameter that was worth predicting is the fuel burned (FB) in each case scenario.

5.4.3 Specific Fuel Consumption (SFC) Profiles

The specific fuel consumption profiles for each model were analysed under the four selected adverse environmental conditions of operation as shown in Figure 5:11. The 25MW models were found to operate efficiently during the first stage of the voyage where the sea states were less that 5 and the propulsion system required only one engine to satisfy the demand but at Beaufort wind scale 5, the second engine in the power plant came into action and the SFC rose from around 225 g/kWh to about 235 g/kWh. However the efficiency immediately improved to around 220 g/kWh when the ship encountered a sea state of 6 even with the two engines still running.

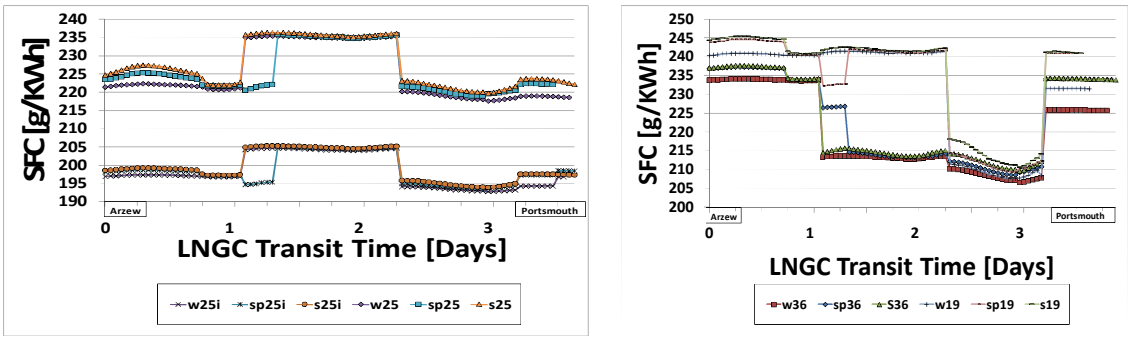

Figure 5:11 Comparative Seasonal effect of winter, spring and summer on the SFC for all the models

The second plot in Figure 5:11 show the performance of the 19MW and 36MW models. In both cases, the part load operation in location with lower sea states below 5 generated a SFC above 235 g/kWh. The pattern for the 19MW engine however remained very poorly between 240 and 245 g/kWh until the sea states became 6 before it could come down to about 220 and below. This shows how economically disadvantage it is to operate the marine gas turbine in regions where sea states are not favourable particularly in the case of the multi-spool cycle configuration of the simple cycle models.

5.4.4 Variation of Power Output

The ICR gas turbine model was used for the assessment of the power output of the models as it varies with the changes that occur in ambient temperature and rough sea conditions in combination with ship hull surface roughness illustrated in Figure 5:12 and Figure 5:13. It was normal to observe that the output power reduced when ambient temperature became higher during hot weather sails in spring and summer. It revealed the output of higher powers in winter when compared to the spring and summer seasons.

For all the GT models except the 19MW, one engine alone was enough to power the LNGC all through the entire voyage until AWC conditions were encountered during the sail. This condition led to the need for boost power when sea states above 4 were encountered during the second day of the voyage thereby satisfying the requirement for maintaining the service speed. During the period of AWC, the two engines were able to operate at nominal power setting and at part load efficiency. They could only peak up and operate with higher fuel efficiency when the sea states rose up to the Beaufort scale level of 6. Towards the final phase of the voyage, the sea state values dropped from 6 to 4 in winter and down to 3 in spring and summer so that the normal operation with a minimum number of engines could economically satisfy the power demanded. It will be noted that none of the gas turbines was able to satisfy the requirement for the power needed for overcoming severe sea states of 6 which enforced a reduction in speed,

It is important to note that a normal voyage under IWC should take only 83 hours (about 3 and half days) while a voyage under AWC would cause a prolonged duration of the voyage.

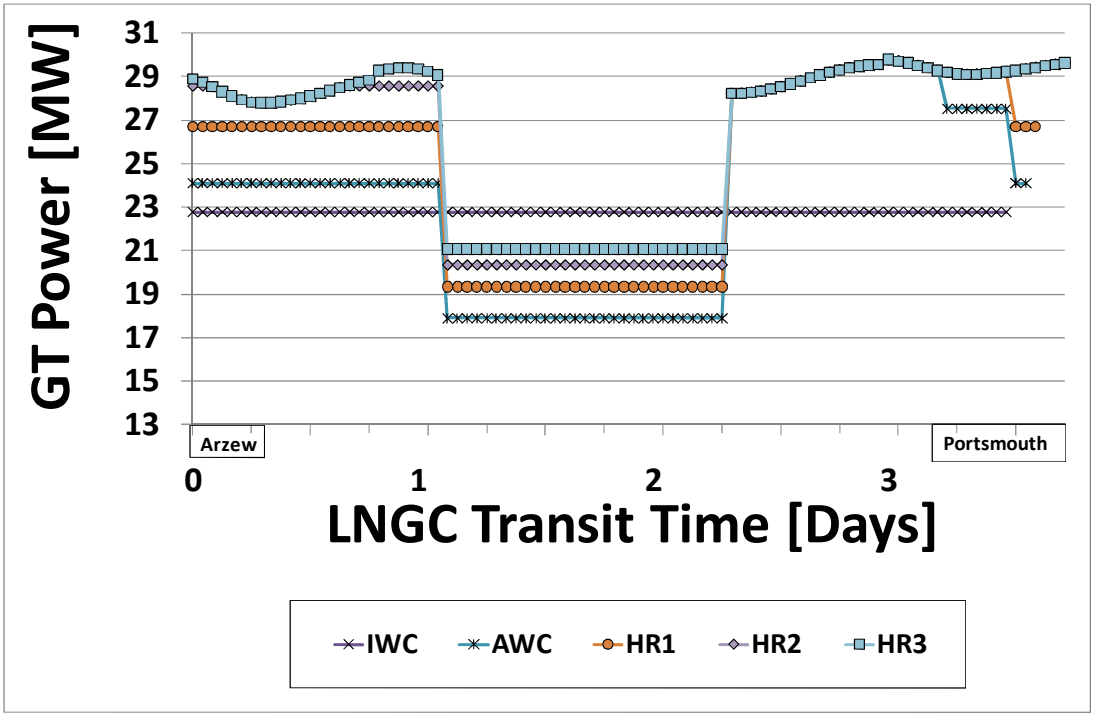

Figure 5:12 Comparison of the power output variation for the ICR under the investigated scenarios during a voyage in winter

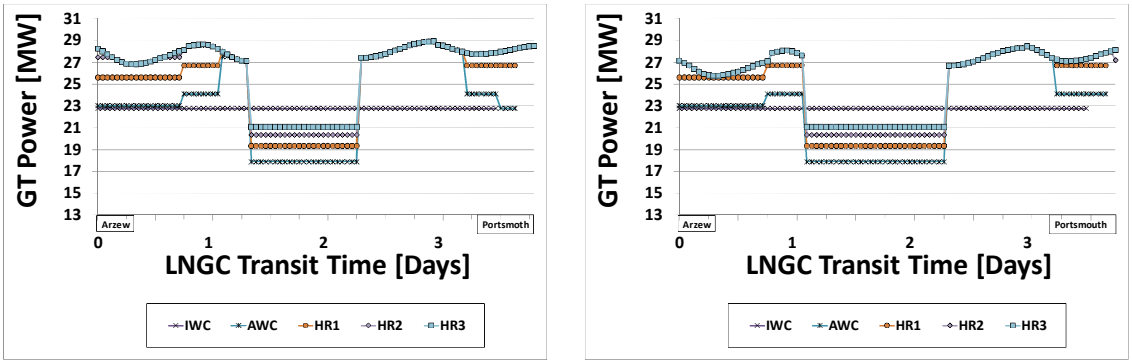

Figure 5:13 Comparison of the power output variation for the ICR under the investigated scenarios during a voyage in spring and summer

5.4.5 Prediction of Ship Speed Variation

It would be observed in Figure 5:14 and Figure 5:15 that a combination of irregular weather and sea conditions in addition to increased drag due to ship hull surface irregularities can affect the ship speed significantly. The curves reveal that the variation of speed occurs in different locations of the voyage as a result of encounters with higher than normal ambient temperatures in combination with sea waves and hull surface roughness resulting from fouling.

5.4.5.1 25MW models speed variation

Comparing the two equally rated but differently configured 25MW cycles, it shows that the ICR retains its advantage over the simple cycle model.

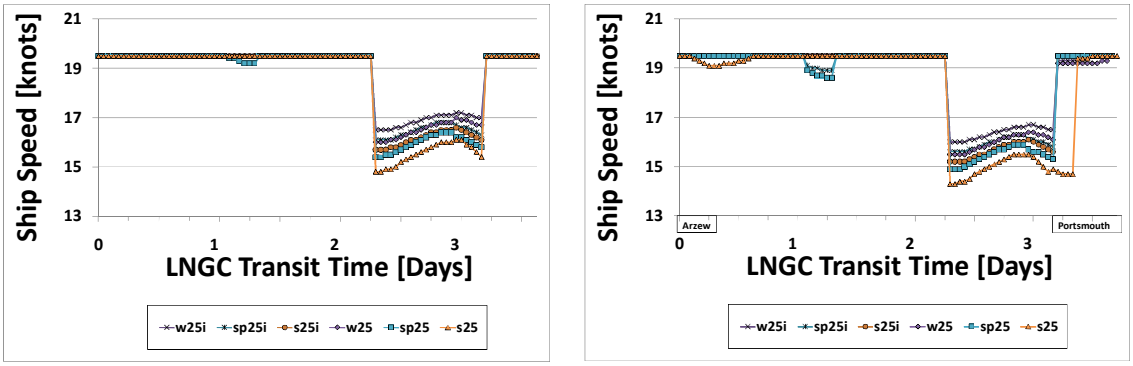

Figure 5:14 Ship speed reduction patterns of the SC and ICR models in AWC and HR1 conditions

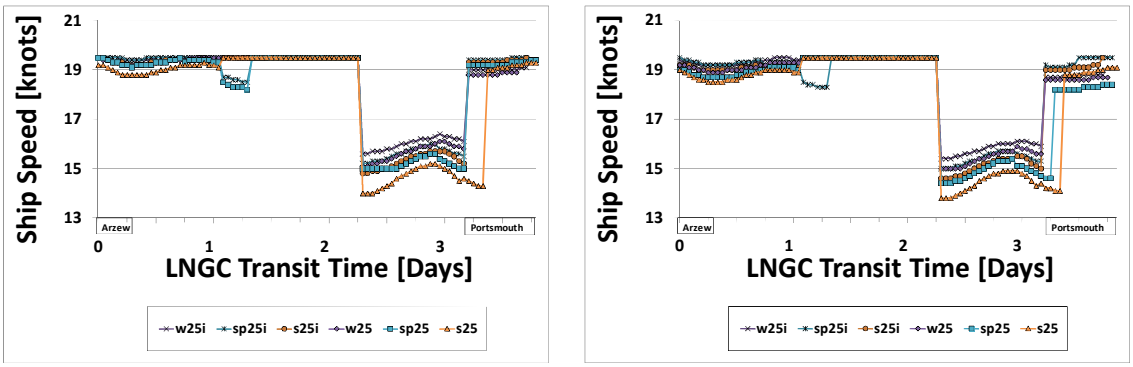

Figure 5:15 Ship speed reduction patterns of the SC and ICR models under HR2 and HR3 conditions

5.4.5.2 19MW and 36MW speed variation

The SFC of the 19MW engine was found to be much better compared to that of the 36MW model as illustrated in Figure 5:11. Comparing the installed power in each case, the 19MW engine combines together for a total capacity of 38MW higher than the 36MW single engine configuration. The speed profile showed a steady trend until adverse weather conditions characterized by sea states above 5.

When sea states of above Beaufort wind scale 4 were encountered, the brake power required was elevated such that an additional engine had to be engaged in order to boost the power. At Beaufort scale of 6 however, the cube law became more pronounced even with the availability of boost power and a speed loss was imposed. As such, the 2-engine layout of the 19MW model experienced less speed loss when transiting AWC than all the other models and could deliver the cargo in good time. A comparison of the transit times for each of the engine models is predicted in Figure 5:18 and Figure 5:19 Comparison of the transit times in summer

Table 5:5 to Table 5:7 also help to reveal the extent to which the selected scenarios can affect the ship speed based on the transit times that were predicted in the case of each model.

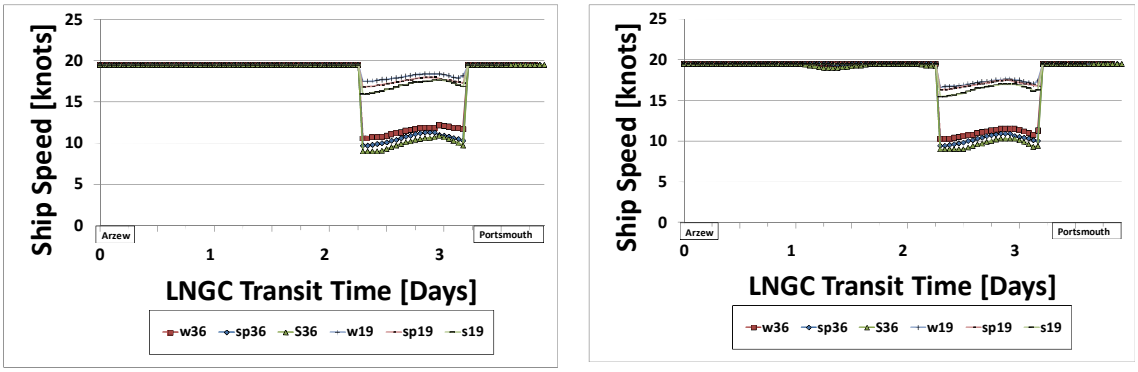

Figure 5:16 Comparative variation of the ship speed with the 19MW and 36MW gas turbines in winter under AWC and HR1

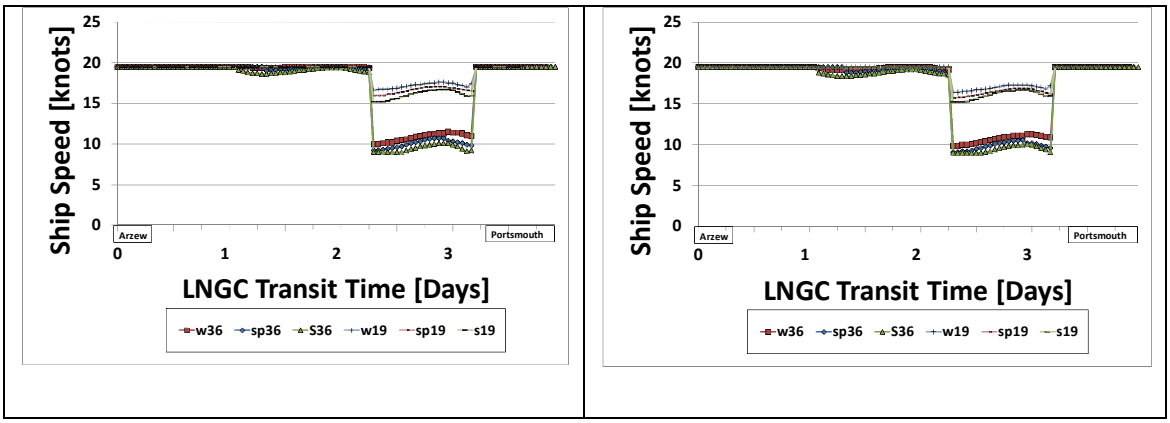

Figure 5:17 Comparative variation of the ship speed with the 19MW and 36MW gas turbines in winter under HR2 and HR3

Two engines are required whenever the vessel encounters environmental and climatic conditions that deviate from the ideal but even with a combined power output of 50MW coming from the two engines, the increased resistance still caused a speed loss at the location where the sea states rose to Beaufort 6. When it is equal to “5” and below, the twin engine operation with all the models except the 36MW is capable of providing enough power to satisfy the requirement for service speed. This becomes unsustainable the moment the sea states are elevated to 6 and above. The results reveal a drop of about 18% in winter and 24% in summer for the simple cycle, while the intercooled recuperated model experiences a lower drop of 15% and 19% respectively.

Table 5:4 Percentage reductions in ship speed for each of the GTs due to adverse weather conditions

GT models [Rated Power]	Ship Speed Reduction [%]		
	winter	spring	Summer
25SC	18	21	24
25 ICR	15	17.5	19
36MW	46	50	54
19MW	10	14	18

Table 5:4 is a detail of the speed loss experience by each model during the seasons under investigation. Among all the models it is the single 36MW gas propulsion plant configuration that suffers the most degradation in terms of speed loss whenever the operating environment becomes unsustainable. Its poor part load (OD) performance causes the ship speed to drop to a low of 9 knots instead of 19.5 knots. Other hand however, the single engine configuration would have been the most economical if initial and installation costs were the only governing factors to be considered.

The consequence arising from any speed loss lies in prolonged transit time causing undue delay in the delivery of the cargo. Therefore, the issue of hull roughness and possible routing that may avoid zones of rough weather conditions must be given special attention through the application of anti fouling techniques.

5.4.6 Assessment of Transit Times

For any voyage undertaken under ideal weather conditions IWC, the transit times were calculated from Equation (5-1) below:

$$\Delta_t = \frac{Sailing\ distance(nm)}{Ship\ speed\ (\frac{nm}{hr})} = \frac{S(nm)}{V_s \times 24}[Days] \qquad \textbf{Equation (5-1)}$$

where;

Δ_t = Voyage duration [hr]

V_s = Vessel's speed [knots]

The power and speed variations have already been analysed and from Equation (5-1), it can be understood that the duration of the voyage of the LNGC in any scenario will depend on the speed profile based on the performance of any of the GT models.

Table 5:5 Influence of Speed limiting factors on transit times in spring

GT models	Winter season Transit Times [Days]				
	IWC	AWC	HR1	HR2	HR3
19MW	3.5	3.54	3.58	3.58	3.58
SC	3.5	3.63	3.67	3.67	3.71
ICR	3.5	3.58	3.63	3.67	3.67
36MW	3.5	3.83	3.88	3.88	3.92

Table 5:6 Influence of Speed limiting factors on transit times in winter

GT models	Spring season Transit Times [Days]				
	IWC	AWC	HR1	HR2	HR3
19MW	3.5	3.54	3.58	3.63	3.63
SC	3.5	3.63	3.67	3.71	3.79
ICR	3.5	3.63	3.67	3.67	3.71
36MW	3.5	3.88	3.92	3.92	3.96

Table 5:7 Influence of Speed limiting factors on transit times in summer

GT models	Summer season Transit Times [Days]				
	IWC	AWC	HR1	HR2	HR3
19MW	3.5	3.58	3.63	3.63	3.67
SC	3.5	3.67	3.75	3.79	3.79
ICR	3.5	3.63	3.67	3.67	3.71
36MW	3.5	3.92	3.96	3.96	4.00

The 19MW installation shows the most economic potential as it is able to propel the LNGC to its final destination faster than any of the other models in all cases.

Table 5:5 to Table 5:7 indicate that the ideal duration of the voyage in IWC is three and half days but when the operating environment becomes unbearable for the propulsion system, the ship speed would drop thereby, causing the cargo to be delivered behind schedule. The worst case scenario is that of the 36MW model, which possesses higher redundancy under ideal conditions but is unable to meet the requirement for overcoming the adversities of the trade route at higher sea states. Later in the analysis, it will be seen how this phenomenon affects the overall quantities of LNG cargo delivered, fuel consumed, BOG and pollutant emissions released.

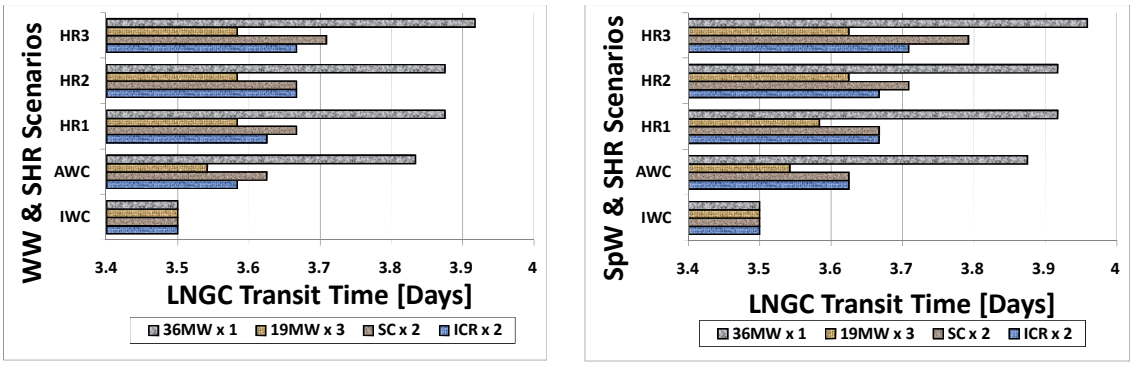

Figure 5:18 Comparison of the transit times in winter and spring

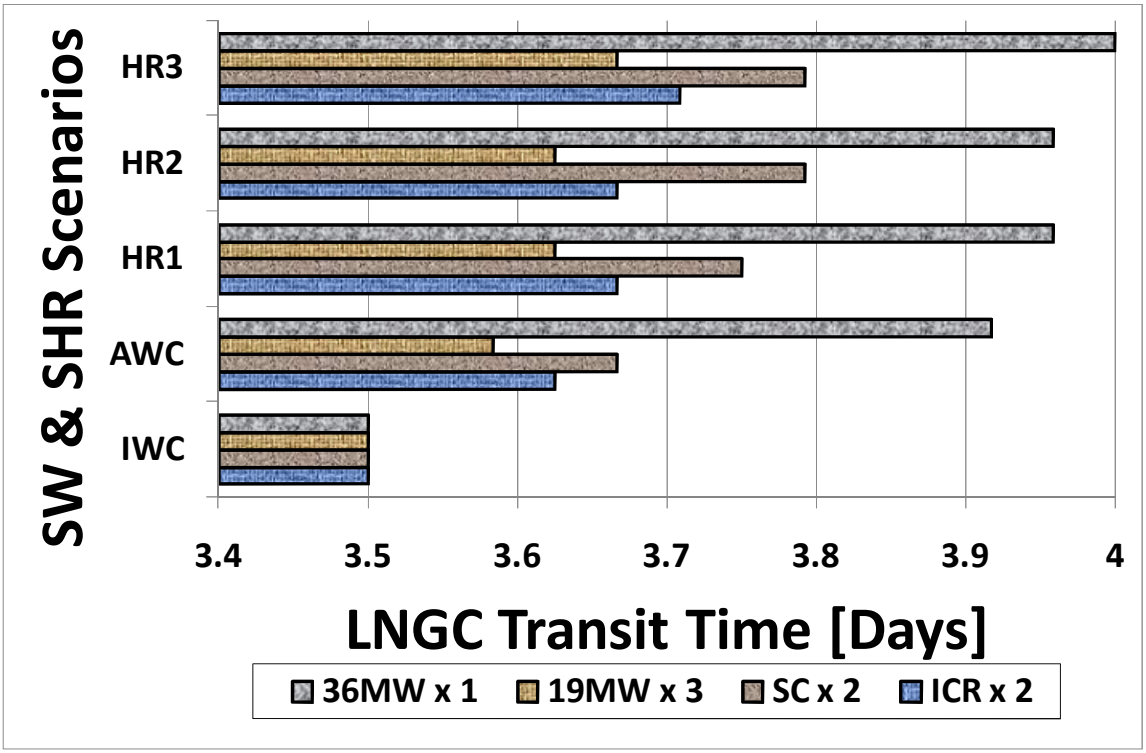

Figure 5:19 Comparison of the transit times in summer

5.4.7 Estimated Number of Round Trips

It is a widely accepted assumption that only about 75% of the total number of the days in a year that any LNG Carrier fully engages in cruising at the service speed of the vessel to ferry the LNG cargo, while the rest of the 25% time is spent on loading and discharging, manoeuvring in and out of port and maintenance downtime etc [5]. Table 5:8 is an illustration of how the LNGC reacts with each of the propulsion engine options in different seasons and under the defined investigation scenarios through.

$$N_{RT} = \frac{0.75 \times 365}{\Delta_t}$$ **Equation (5-2)**

Table 5:8 Predicted annual number of round trips in winter

GT models	Number of LNG deliveries per year				
	IWC	AWC	HR1	HR2	HR3
19MW	39	38.65	38.20	38.20	38.20
SC	39	37.76	37.33	37.33	36.91
ICR	39	38.20	37.76	37.33	37.33
36MW	39	35.71	35.32	35.32	34.95

Table 5:9 Predicted annual number of round trips in spring

GT models	Number of LNG deliveries per year				
	IWC	AWC	HR1	HR2	HR3
19MW	39	38.65	38.20	37.76	37.76
SC	39	37.76	37.33	36.91	36.10
ICR	39	37.76	37.33	37.33	36.91
36MW	39	35.32	34.95	34.95	34.58

Table 5:10 Predicted annual number of round trips in summer

GT models	Number of LNG deliveries per year				
	IWC	AWC	HR1	HR2	HR3
19MW	39	38.20	37.76	37.76	37.33
SC	39	37.33	36.50	36.10	36.10
ICR	39	37.76	37.33	37.33	36.91
36MW	39	34.95	34.58	34.58	34.22

It shows that the most efficient propulsion engine combination is the 19MW model capable of making a minimum of 37.33 deliveries in the worst case scenario of summer while the worst performing model still remains the 36MW single engine installation where the lowest number of deliveries of 34.22 was made.

5.4.8 Predicted Quantities of Fuel Burned (FB)

The fuel burned per voyage was obtained from the results of the simulation exercise and was analysed as presented in **Error! Reference source not found.Error! Reference source not found.**.

Under IWC the benefit of the ICR model was further established showing how it is far more fuel-efficient than other models of the research. It still assumed a leading role even under severe limiting factors present in the other scenarios. Relating this to the results of the transit times makes it easier to understand how the 19MW engine is capable of delivering a greater quantity of LNG cargo than the ICR due mainly to its 3- engine configuration of the power plant.

By comparison, the results show that the more severe the operating conditions encountered during the voyage, the higher the quantity of fuel burned as contained in Table 5:11. The impact of changes in seasonal weather conditions on the fuel consumption can be observed to be quite minimal when compared to that of sea waves and hull fouling. For instance, the difference between the fuel consumed in winter appear to remain the same for the other seasons in all the scenarios but between AWC and the scenarios of hull fouling, the quantities continue to rise higher and higher for each of the engine models.

Table 5:11 Quantities of fuel burned per voyage according to GT models and seasons under ideal weather conditions

IWC Fuel Burned per voyage [tons]				
	ICR x 2	**SC x 2**	**19MW x 3**	**36MW x 1**
Winter	379.1	427.0	467.4	453.9
Spring	379.7	428.7	468.0	454.2
Summer	380.3	430.6	468.8	454.7

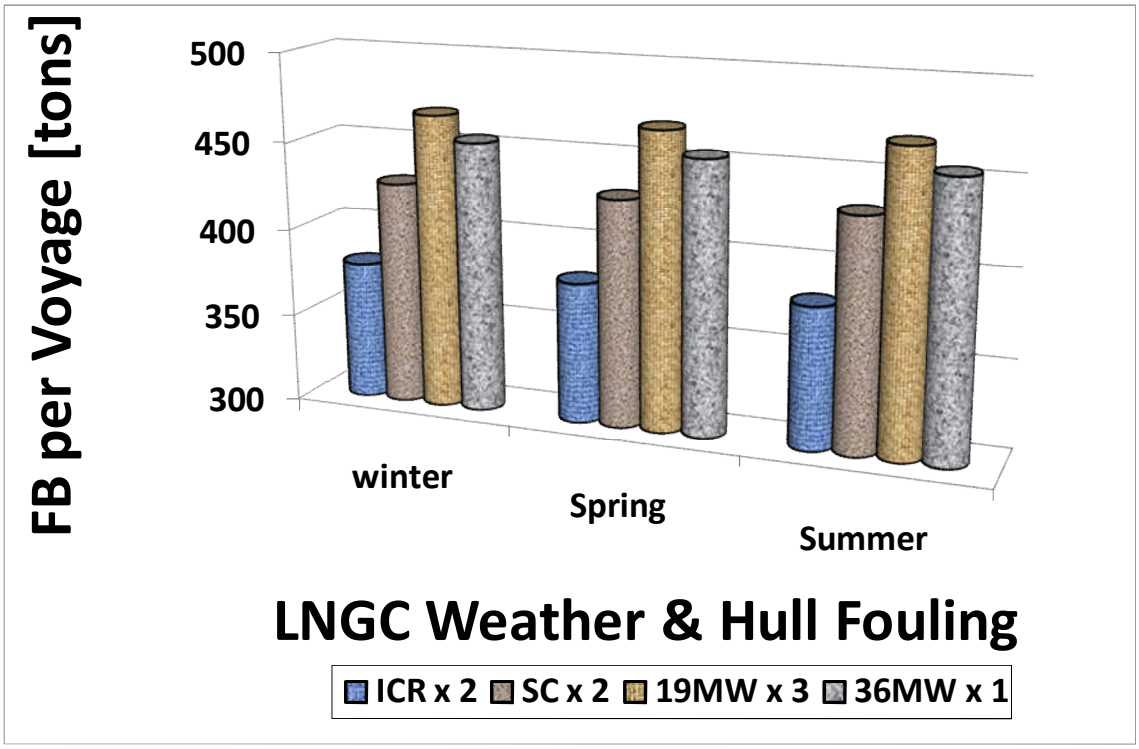

Figure 5:20 Predicted quantities of FB by the gas turbines when operated under IWC

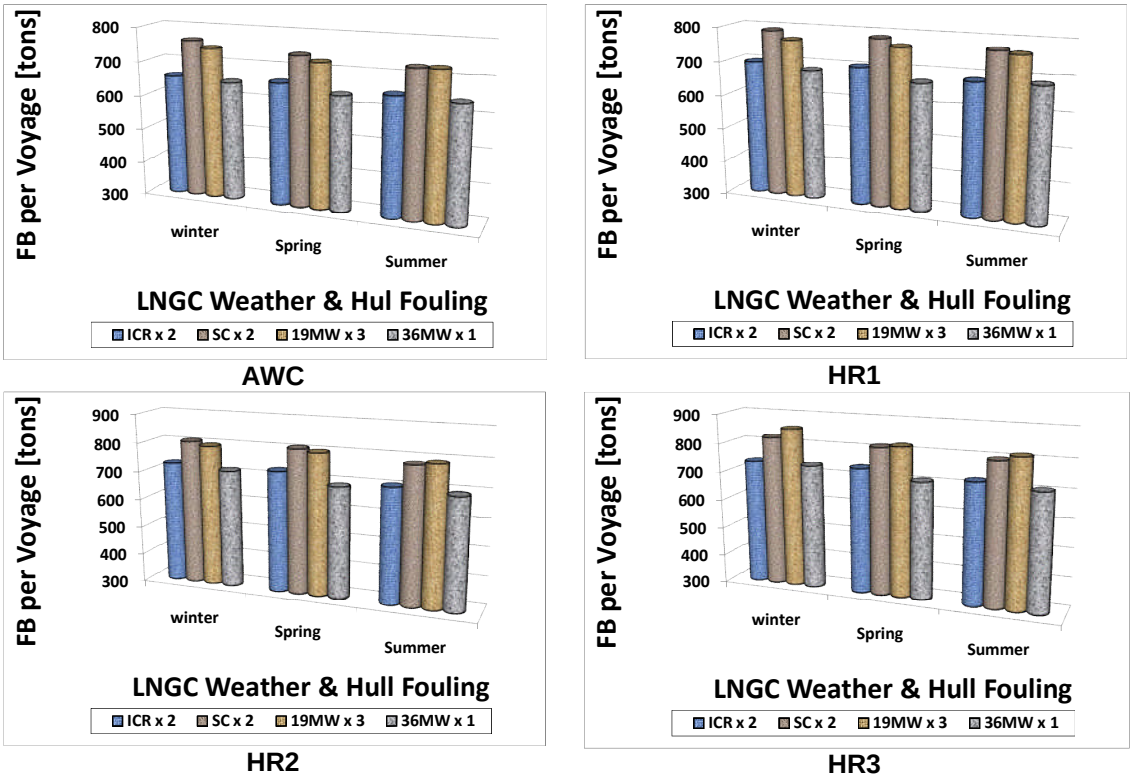

Figure 5:21 Predicted quantities of FB by the gas turbines when operated under the indicated adverse scenarios

The specific gravity of marine diesel oil was researched and found to be between 820 and 950 kg/m^3 while that of natural gas (Methane) was 464.54 kg/m^3 [70]. Therefore, the quantities of fuel burned needed to be converted from units in tons to units in cubic metres (m^3) to natural gas so as to relate same with the expected BOG quantities.

$$FB_V = \frac{FB_W \times 1000}{SG_{fuel}} [kg \div kg/m^3] \qquad \text{Equation (5-3}$$

where;

FB_V = Volume of fuel burned [tons]

FB_W = Weight of fuel burned [m^3]

It is assumed that the propulsion machinery in each case has a dual fuel facility that makes it possible to switch between Marine diesel oil (MDO) and BOG (Natural gas). The volume of the fuel consumed per voyage was obtained by converting quantities from tons to cubic metres by using the specific weight of

natural gas (450 kg/m^3) and that of marine diesel oil (900 kg/m^3) as outlined in Equation (5-4) and Equation (5-5). As a result, one metric tonne of MDO was found to occupy a volume of 1.1m^3 and a volume of 2.2 m^3 for every metric tonne of LNG [71] respectively.

$$FB_{MDO} = \frac{Q_{MDO}(tons) \times 1000}{900} [m^3]$$ Equation (5-4

$$FB_{BOG} = \frac{Q_{BOG}(tons) \times 1000}{450} [m^3]$$ Equation (5-5

Where;

F_{MDO} = Volume of diesel fuel [m^3]

Q_{MDO} = Weight of diesel fuel [tons]

F_{BOG} = Volume of LNG fuel [m^3]

Q_{BOG} = Weight of LNG fuel [tons]

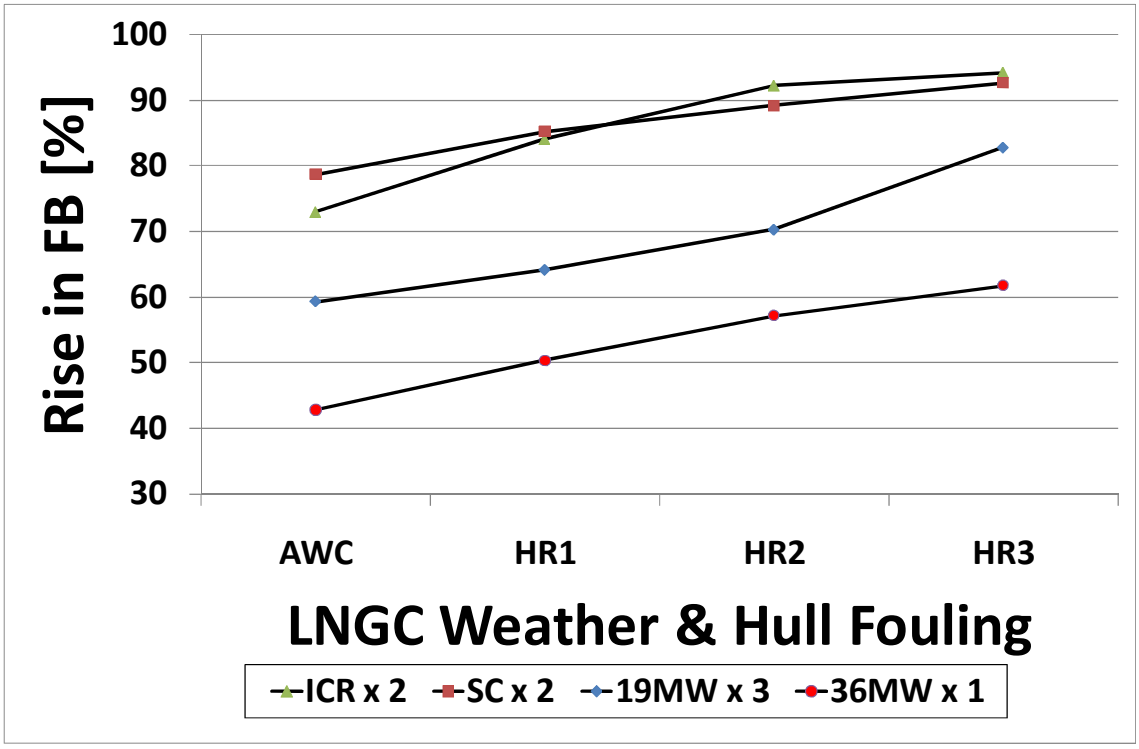

Figure 5:22 Comparison of the influence of adverse environmental conditions during winter voyage and under IWC

Having established the number of round trips each of the gas turbine models is capable of achieving, the quantity of loaded LNG per annum could then be calculated using the respective transit times in the following:

$$Q_{AL} = T_{RT} \times Q_c \ [m^3] \qquad \textbf{Equation (5-6)}$$

Where;

T_{RT} = Duration of round trip

Q_{AL} = Annual loaded LNG cargo

Q_c = Installed cargo capacity of the LNGC (138,000m^3)

Table 5:12 Annual Loaded LNG cargo based on the investigated Scenarios

GT models	Annual Loaded LNG cargo [m^3]					
		IWC	AWC	HR1	HR2	HR3
19MW	Winter	5396786	5333294	5271279	5271279	5271279
	Spring	5396786	5333294	5271279	5210690	5210690
	summer	5396786	5271279	5210690	5210690	5151477
SC	Winter	5396786	5210690	5151477	5151477	5093596
	Spring	5396786	5210690	5151477	5093596	4981648
	summer	5396786	5151477	5037000	4981648	4981648
ICR	Winter	5396786	5271279	5210690	5151477	5151477
	Spring	5396786	5210690	5151477	5151477	5093596
	summer	5396786	5210690	5151477	5151477	5093596
36MW	Winter	5396786	4927500	4874516	4874516	4822660
	Spring	5396786	4874516	4822660	4822660	4771895
	summer	5396786	4822660	4771895	4771895	4722188

5.5 BOG Analysis

In order for the gas turbine to be able to meet the requirement to power the vessel at the required speed under any of the scenarios being investigated, the exact quantities of BOG needed to be established. The results obtained from the voyage analysis with regards to the quantities of fuel burned per voyage was the used as a basis for assuming the expected values of BOG as outlined in Figure 5:23.

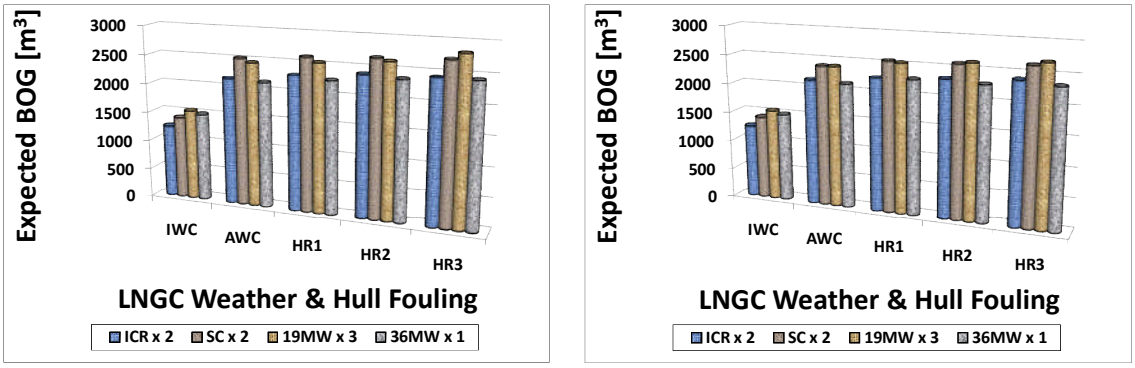

Figure 5:23 Natural BOG required per round trip in winter and summer seasons

5.5.1 Estimated Natural BOG

A significant fraction of the LNG cargo volume (about 5%) cannot be practically off- loaded. This is usually called the heel volume. Therefore, a fraction of this amount of LNG is evaporated during ballast voyage and is used as BOG fuel. The heel volume is also used to keep cargo tanks cool during the ballast voyage [5].

Since the launch of the first LNG carrier in the 1960s, natural boil-off gas (NBOG) has been used as fuel for power generation on the vessels. Depending on the size and quality of the LNG containment system, boil-off rates are typically in the area 0.11 to 0.15 percent per day of the ship's cargo capacity during laden voyage and approximately half during ballast voyage [72].

In this work therefore, it is assumed that equal amounts of natural BOG are released during the delivery and the ballast voyages. The boil-off rate is estimated at 0.15% of the fully loaded LNG cargo as outlined in Equation (5-7).

$$Q_{BOG} = \left(\frac{0.15}{100}\right) \times (1.5 \times Q_c) \times T_v \; [m^3] \qquad \textbf{Equation (5-7)}$$

where;

T_v = the duration of one voyage (Days)

Q_c = Installed loading capacity of the LNGC (138,000m^3)

Based on the above therefore the assumption is that only about half the normal quantity of BOG is released for fuel during the ballast voyage as can be seen in Equation (5-7). The result is presented in Figure 5:25.

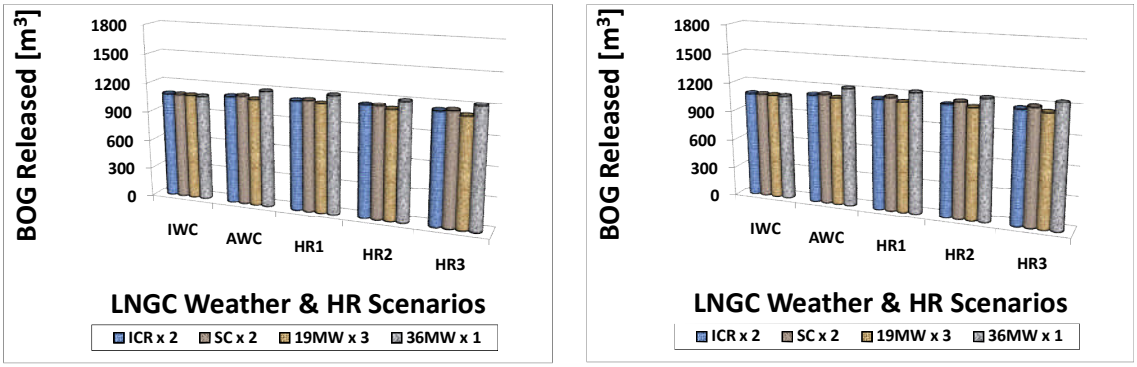

Figure 5:24 Example of the quantities of estimated BOG released in winter and summer

Table 5:13 BOG released and converted to fuel per every round trip

GT models	BOG Released per every Round Trip [m^3]					
	Seasons	**IWC**	**AWC**	**HR1**	**HR2**	HR3
19MW	Winter	1087	1100	1113	1113	1113
	Spring	1087	1100	1113	1126	1126
	summer	1087	1113	1126	1126	1139
SC	Winter	1087	1126	1139	1139	1151
	Spring	1087	1126	1139	1151	1177
	summer	1087	1139	1164	1177	1177
ICR	Winter	1087	1113	1126	1139	1139
	Spring	1087	1126	1139	1139	1151
	summer	1087	1126	1139	1139	1151
36MW	Winter	1087	1190	1203	1203	1216
	Spring	1087	1203	1216	1216	1229
	summer	1087	1216	1229	1229	1242

When the values in Table 6:13 were multiplied by the total number of round trips in each case scenario, the annual quantity of BOG predicted to be released was predicted to be 42499.69 m^3.

Examples of the pattern of the BOG quantities estimated to have been released are illustrated in Figure 5:24.

5.5.2 Required Back up Fuel

In order to establish whether the natural BOG will be adequate enough to power the gas turbines, the quantities of fuel burned per voyage was analysed and compared with the estimated BOG released. Figure 5:23 is an illustration of the estimated BOG expected to be released so as to be able to effectively power all the gas turbine models under investigation. This was obtained by converting the fuel quantities predicted from the voyage analysis.

The estimation of a 0.15% BOG rate per day was found to be inadequate for fulfilling the obligation of the gas turbines, hence the need for fuel back up in all the scenarios.

There are two options available there are two options resolving the problem of fuel back up and one of them is to increase the quantity of BOG by pumping more BOG (FBOG) in addition to the natural BOG so as to meet the power requirement of the vessel from the gas turbines. The other option is to have a mixture of MDO and BOG being supplied at the same time.

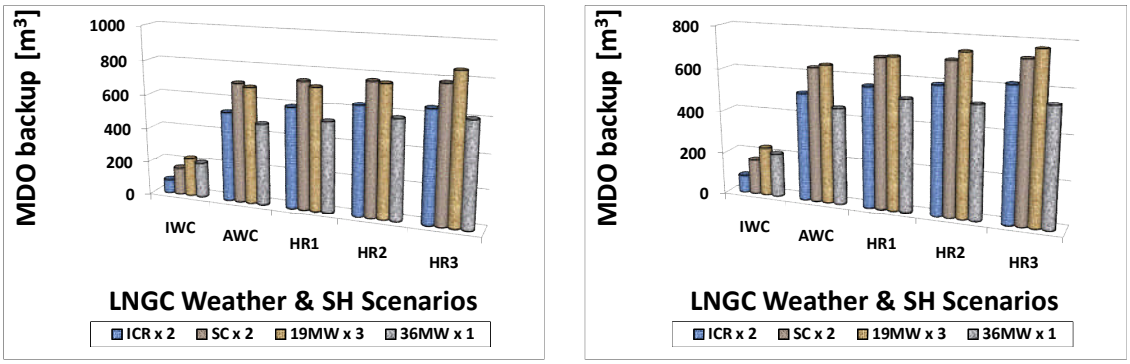

Figure 5:25 Example of the required MDO backup for winter and summer

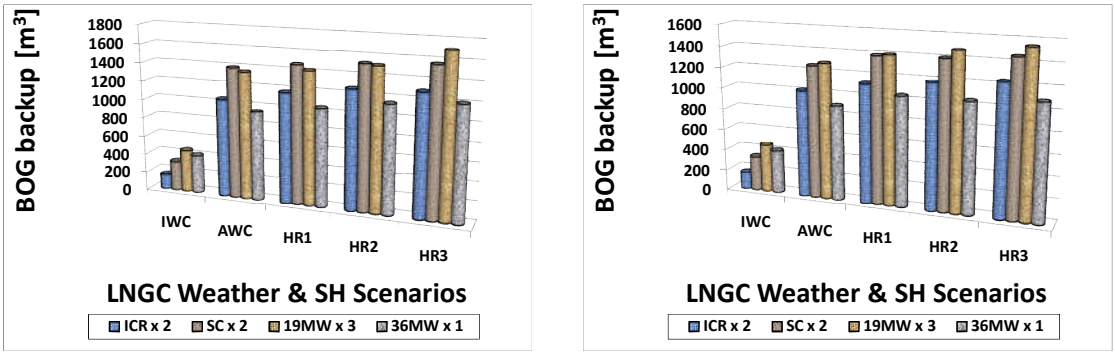

Figure 5:26 Example of forced BOG back up for winter and summer

5.5.3 Predicted Quantity of Annual LNG Delivered

The loss of LNG cargo occasioned by the natural escape of BOG affects the quantity of LNG that originally loaded for delivery and although such losses are assumed to have been converted to fuel, the difference between the original quantity and delivered quantity still remained.

$$Q_{Del} = Q_{lOAD} - Q_{BOG}\ [m^3] \qquad \textbf{Equation (5-8)}$$

where;

Q_{Del} = Delivered LNG [m^3]

Q_{Load} = Loaded LNG from production terminal [m^3]

Q_{BOG} = BOG lost in transit [m^3]

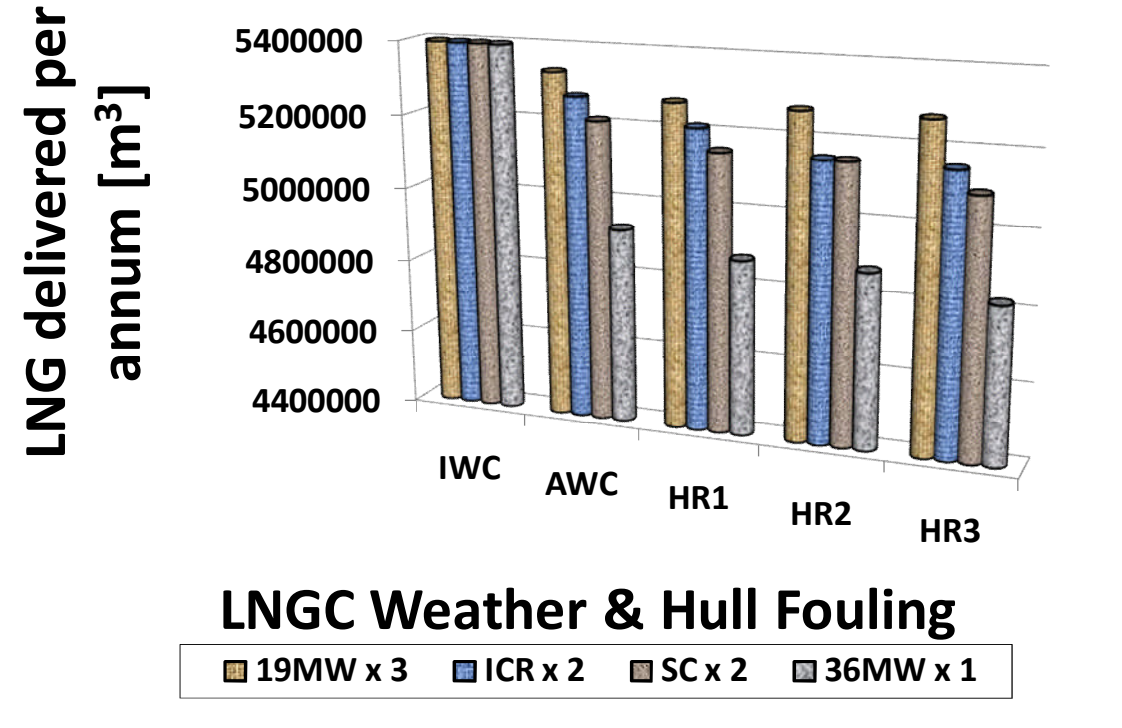

Figure 5:27 Consequence of AWC and hull fouling on the quantity of LNG cargo delivered during winter.

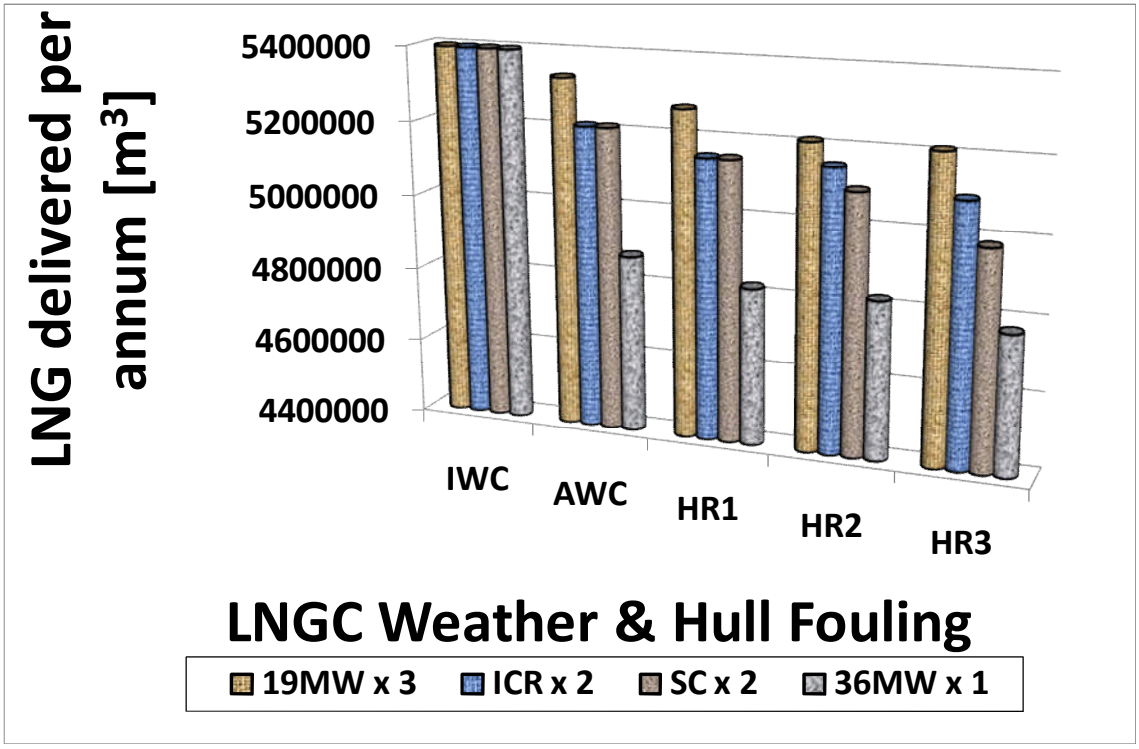

Figure 5:28 Consequence of AWC and hull fouling on the quantity of LNG cargo delivered during spring.

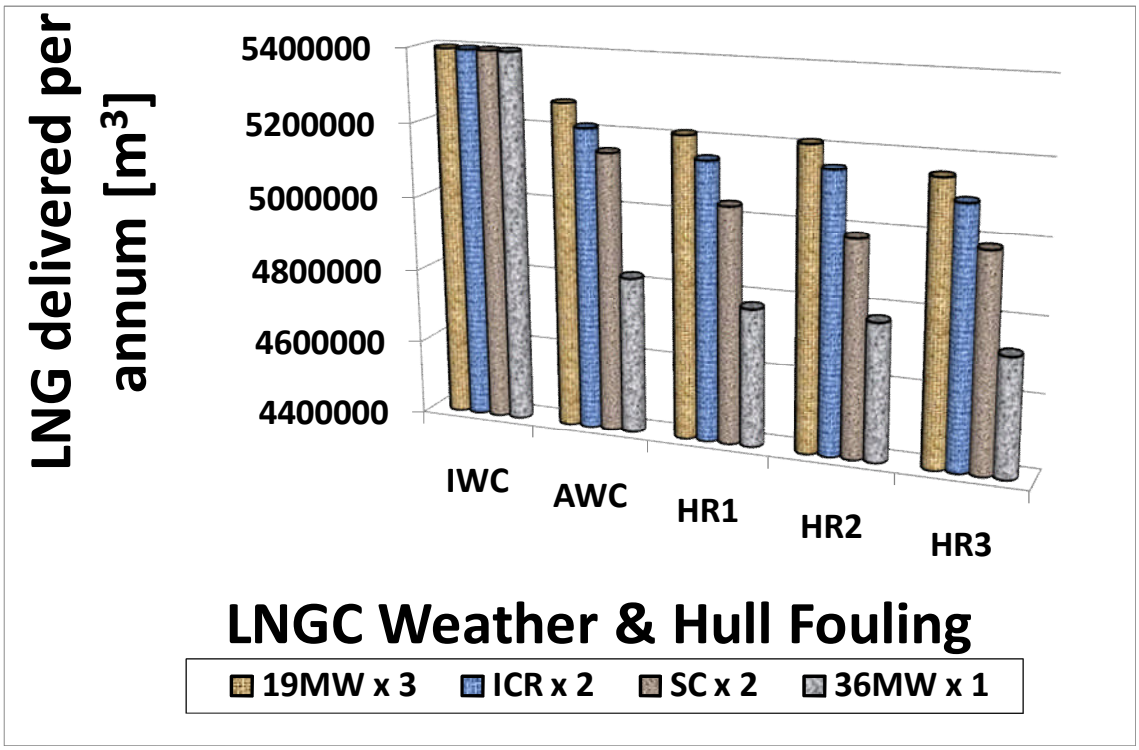

Figure 5:29 Consequence of AWC and hull fouling on the quantity of LNG cargo delivered during summer.

The results of the BOG analysis show that under higher ambient temperature regimes and increased hydrodynamic resistance caused by sea waves and hull fouling, the duration of the journey was bound to increase. Extended voyage duration due to inadequate matching of the propulsion power with speed may lead to:

- More quantity of BOG released.
- Increased fuel consumption cost for the propulsion engines
- Increased delivery losses
- Penalty cost due to delayed delivery

A comparative evaluation of the quantity of delivered LNG was conducted against the fuel consumed by the gas turbines as illustrated in

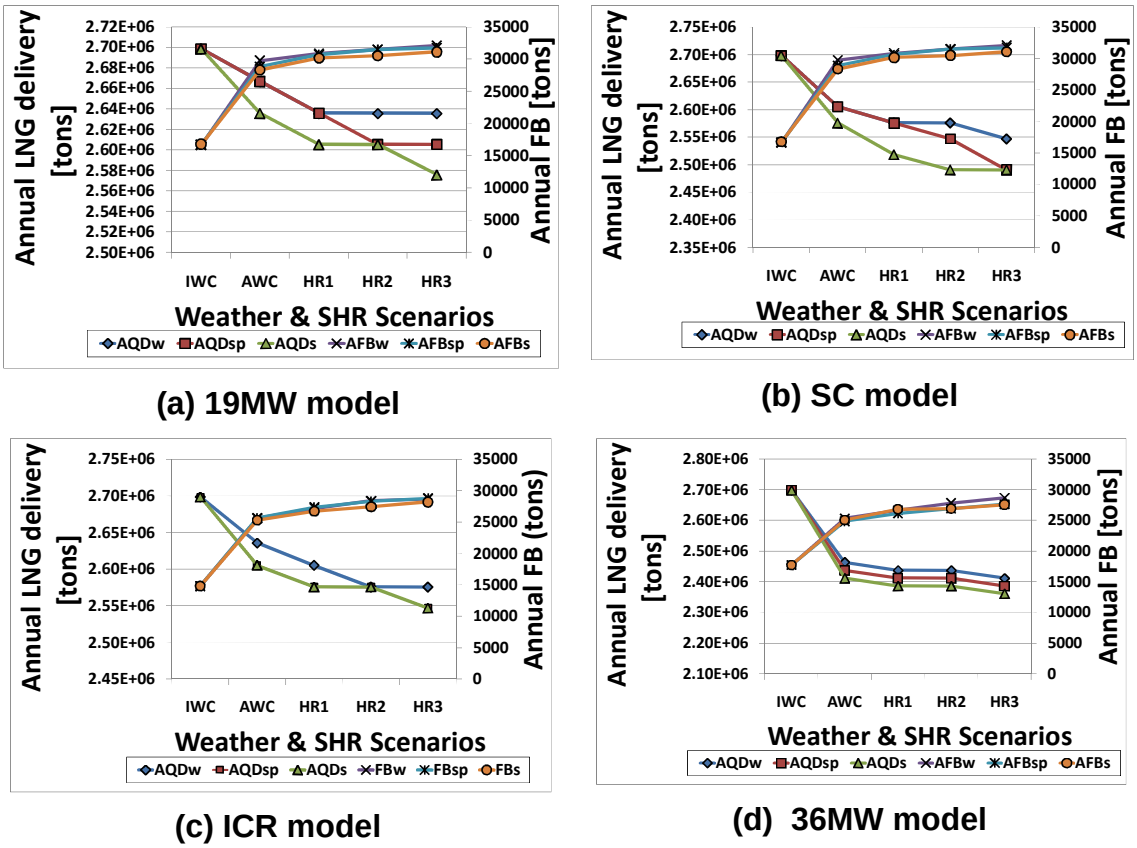

(a) 19MW model

(b) SC model

(c) ICR model

(d) 36MW model

Figure 5:30 Comparison of the annual LNG cargo delivery and annual Fuel burned for the different GT models

5.6 Exhaust Emission Evaluation

The correlations for the evaluation of gas turbine pollutant emissions were discussed in paragraph 3.1.2.1.1 and a sample of the emissions analysis for one of the vessels under investigation was briefly presented in paragraph 6.6.2. This section aims to discuss the pattern of the four major pollutant emissions of the LNGC marine gas turbine propulsion power plants involved in the research.

In order to effectively identify the behaviour of each of the engine models, the variation of NOx, CO2, CO and UHC pollutants was investigated through the voyage analysis according to seasons and under the investigated scenarios of the LNG carrier sailing from the port of production to its terminal port of discharge.

5.6.1 Pollutant Emissions of NO_x

Figure 5:31 shows the variation of NO_x pollutant emissions during the voyage of the LNGC when propelled by the variety of gas turbines. It reveals how the ICR model emits less NOx compared to the other models under the varying weather and sea conditions being considered due to the lower combustion temperatures resulting from the presence of the heat exchange layout of the design. It illustrates how the requirement for higher propulsion power results in the generation of excessive NO_x emissions at locations of higher sea states

The simple cycle model was found to be generating up to 40g/s of NO_x while that of the ICR remained around 30g/s even when the vessel encountered rough seas at a higher value of Beaufort wind scale of 6. Figure 5:32 illustrates the variation occurring at the different scenarios under consideration.

In the investigation, the 36MW and 19MW models were equally compared but due to their lower operating temperatures and design configuration during the early stages and towards the end of the voyage, their NO_x emission patterns were observed to be much higher particularly for the multiple engine configuration of the 19MW power plant, hitting a value of over 90g/s in the worst case scenarios.

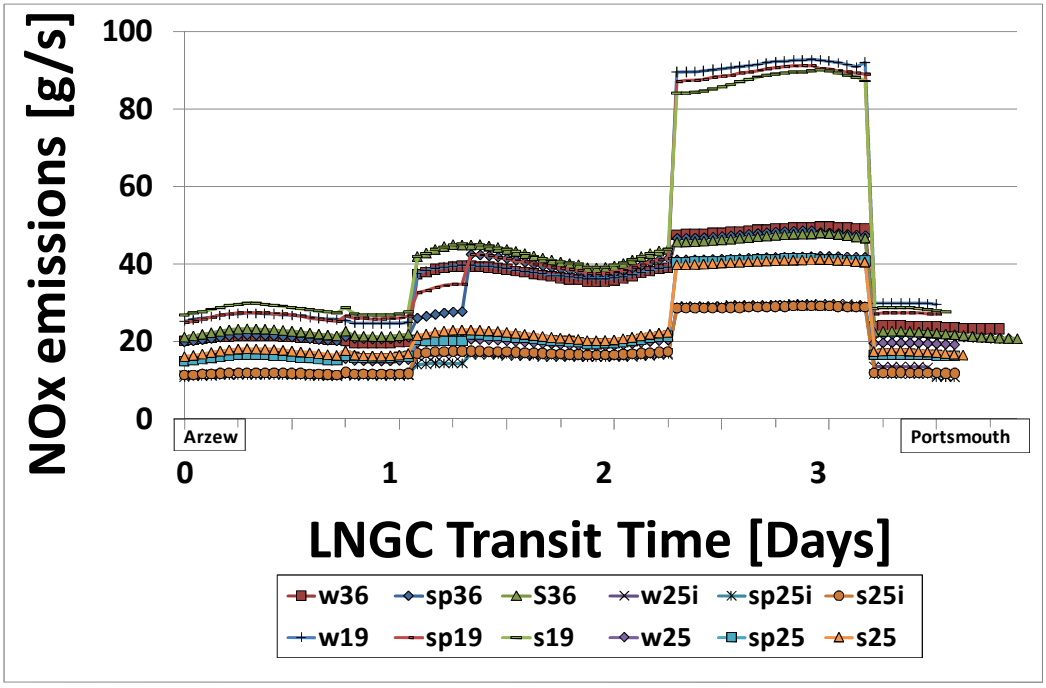

Figure 5:31 Comparative variation of NO_x emissions for all the models along the LNGC trade route conducted for all weather conditions under AWC

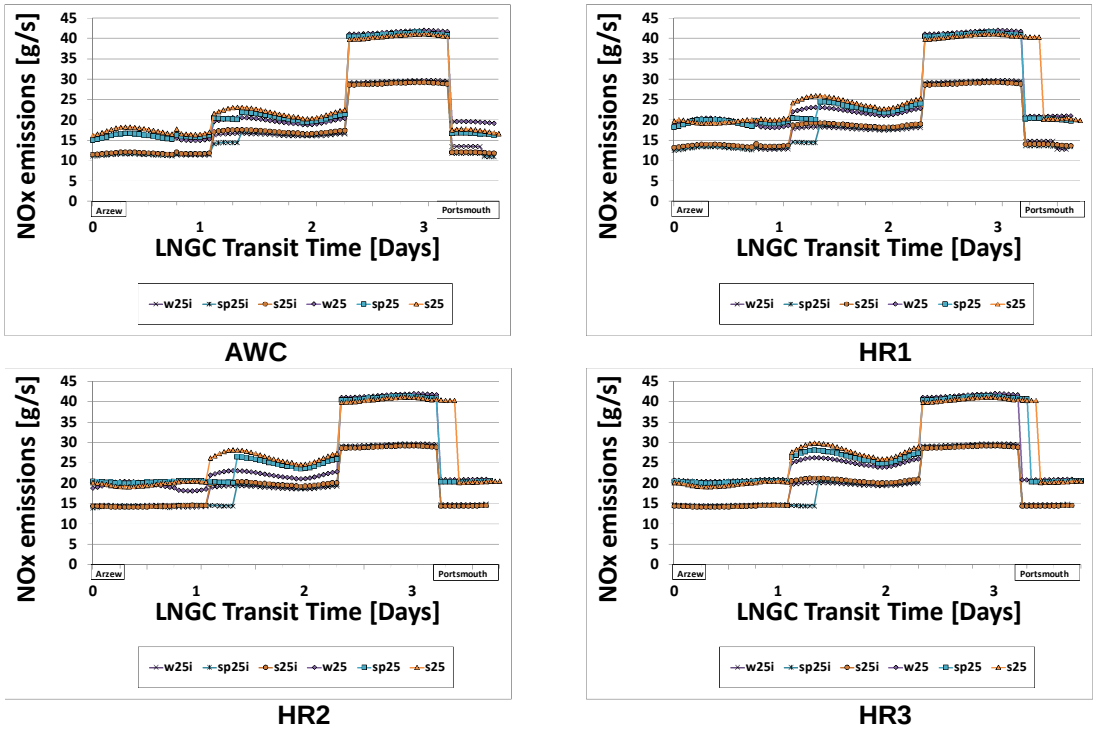

Figure 5:32 Comparative variation of NO_x emissions for the ICR and the SC along the LNGC trade route

On the other hand, the 36MW model maintains a fair emission of not more than 50g/s at the locations of higher sea states being represented in Figure 5:33.

The predicted quantities of NO_x emissions for each of the gas turbines when operated under each of the investigated scenarios in winter and summer seasons are illustrated in Figure 5:34. Accordingly, the values obtained correspond to the pattern of variations already discussed and naturally, the multiple engine combination of the 19MW model showed the highest volumes emitted. Therefore, part of the earlier benefits gained through shorter transit times which culminated into a higher throughput for the delivered LNG cargo could be compromised by the cost penalty likely to be incurred by the NO_x emissions from this particular model.

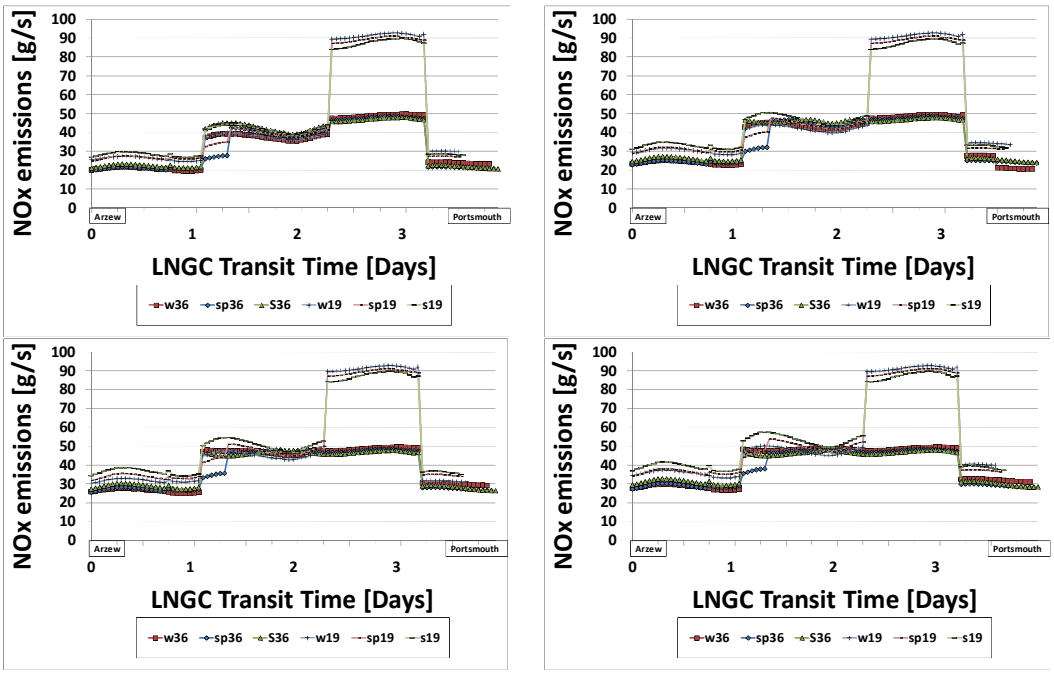

Figure 5:33 Comparative variation of NO_x emissions for the 19MW and the 36MW models

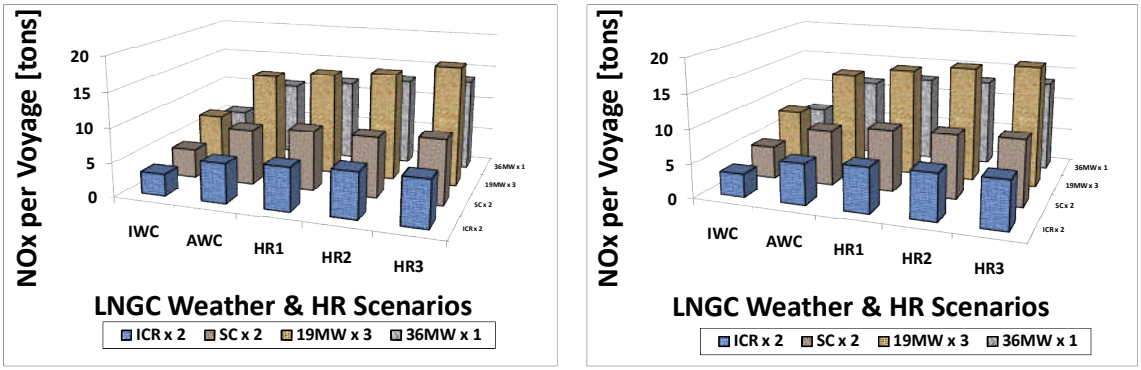

Figure 5:34 Predicted Quantities of NO_x emissions in winter and summer

5.6.2 Pollutant Emissions of CO_2

The pattern of variation for the CO_2 emissions was not found to be any different from that of NO_x. Comparing the emissions of this pollutant from the variety of gas turbine models, the 19MW could still be seen to be generating more that the rest. Again this is understood to be as a result of the lower operating temperature creating a rich mixture in combustion chamber and in its trail, an incomplete combustion of fuel.

The investigation was conducted determine the difference between the various engine behaviour under the scenarios of the investigation and in winter, spring and summer seasons as well. It was observed that the dual spool simple cycle models generated CO_2 emissions up to 6000g/s in IWC and up to 12000 under AWC with hull fouling. The SC and the ICR however produced slightly lower values.

The quantities of volume of CO_2 emissions were evaluated and analysed for winter and summer seasons as presented in Figure 5:37.

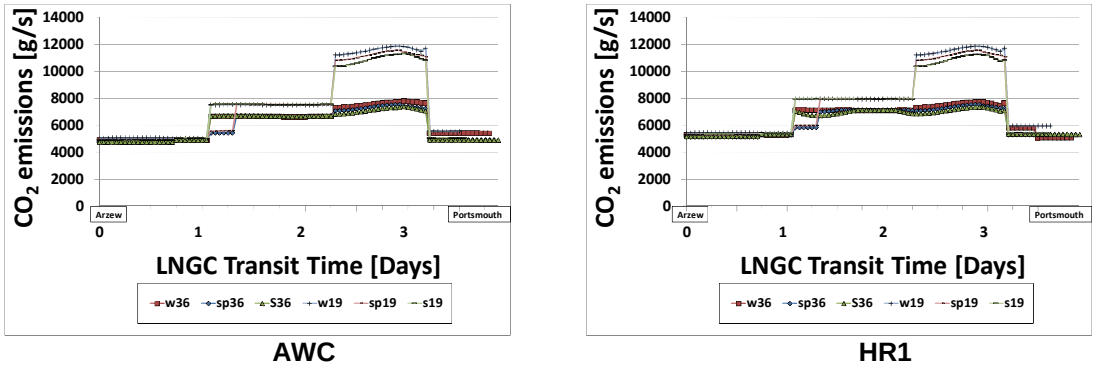

AWC **HR1**

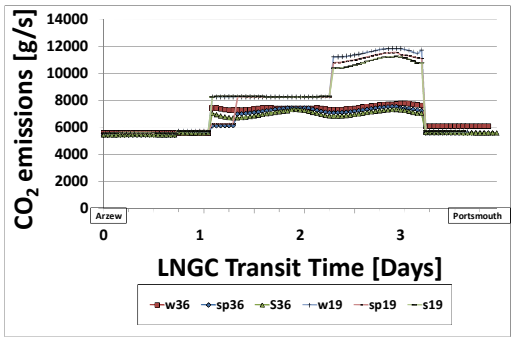

HR2

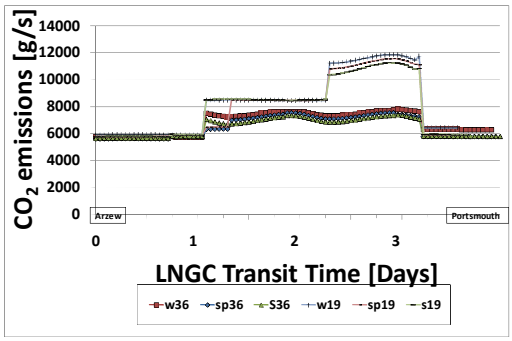

HR2

Figure 5:35 Variation of the CO_2 emissions for the 19MW and 36MW models according to different scenarios

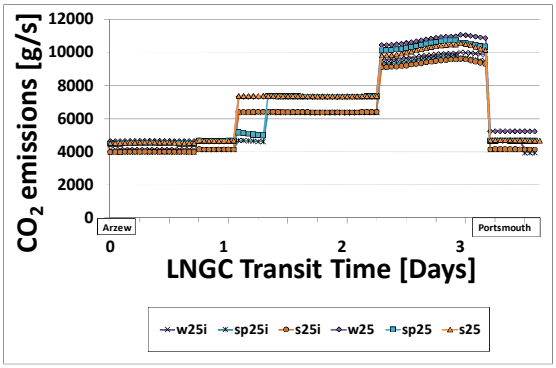

AWC

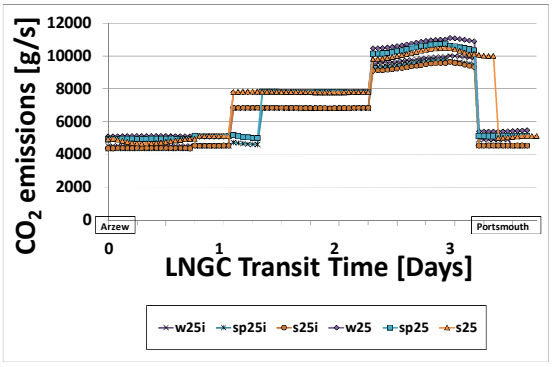

HR1

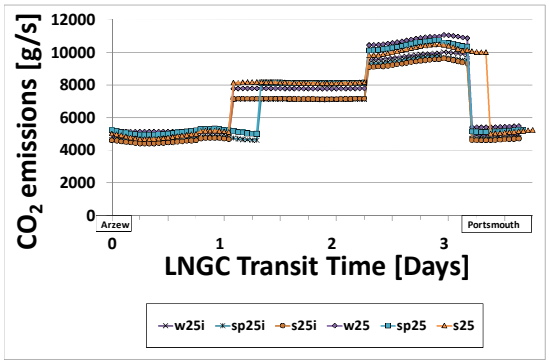

HR2

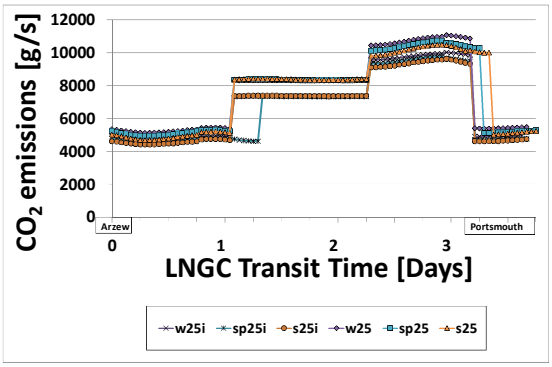

HR3

Figure 5:36 Variation of the CO_2 emissions for the ICR and SC models according to different scenarios

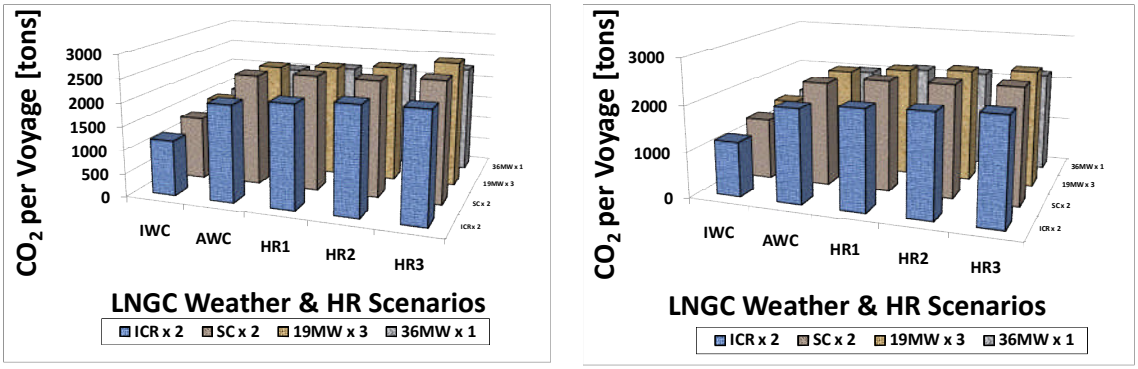

Figure 5:37 CO_2 emissions for winter and summer respectively

5.6.3 Pollutant Emissions of CO

Similar to the other pollutants, the investigation of the emission of carbon monoxide by the various gas turbine models was conducted according to seasons and different environmental and climatic scenarios. It was observed that more CO was produced in regions where the sea states rose to 5, prompting the propulsion system to engage the maximum number of engines for the ICR, SC and the 19MW models and to operate them at part-load until the vessel encountered the maximum sea state. The SC model generated more than the ICR.

In the case of the single engine configuration of the 36MW model, the engine operates at maximum power when the vessel encounters rough weathers conditions with sea states of 5 and 6 as a result of which less CO was being generated within that portion of the voyage.

The actual quantities of CO pollutant emissions that were generated by each of the gas turbine models in winter and summer are presented in Figure 5:40. The influence of AWC and ship hull surface degradation on this emission parameter can be seen to be fairly constant and different from its output when operated voyage is under IWC.

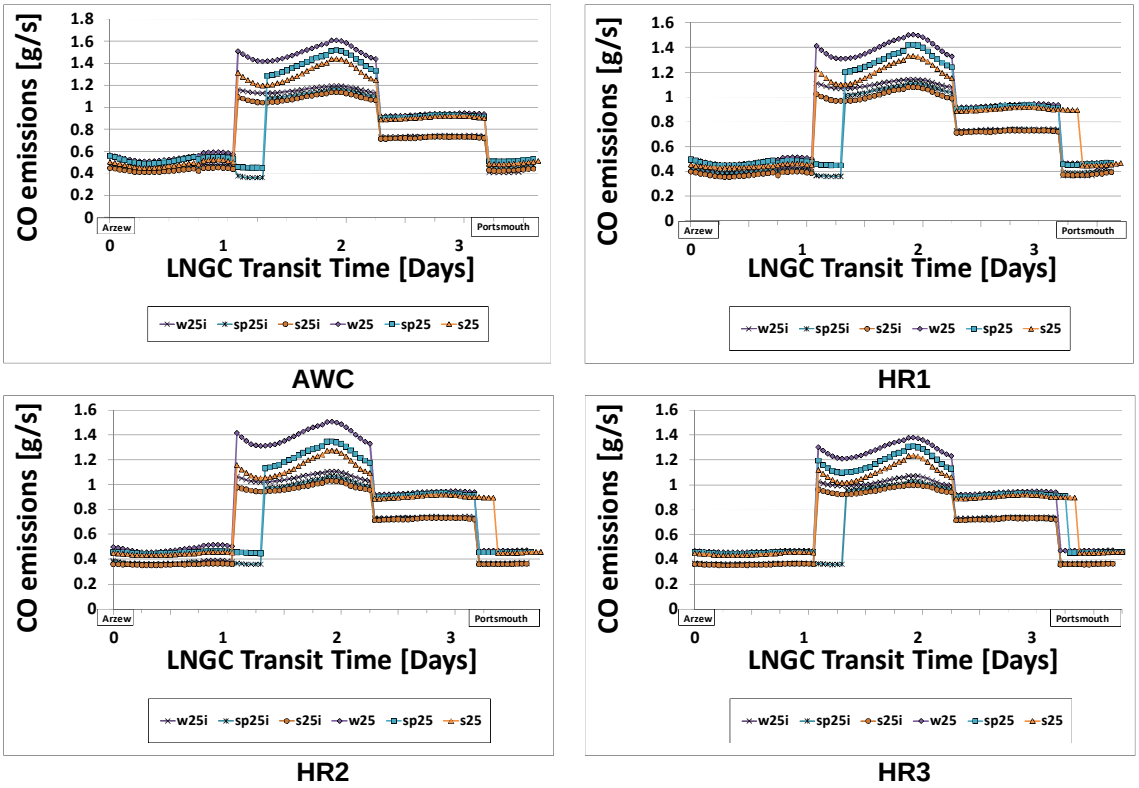

Figure 5:38 Variation of CO emissions for the ICR and the SC models

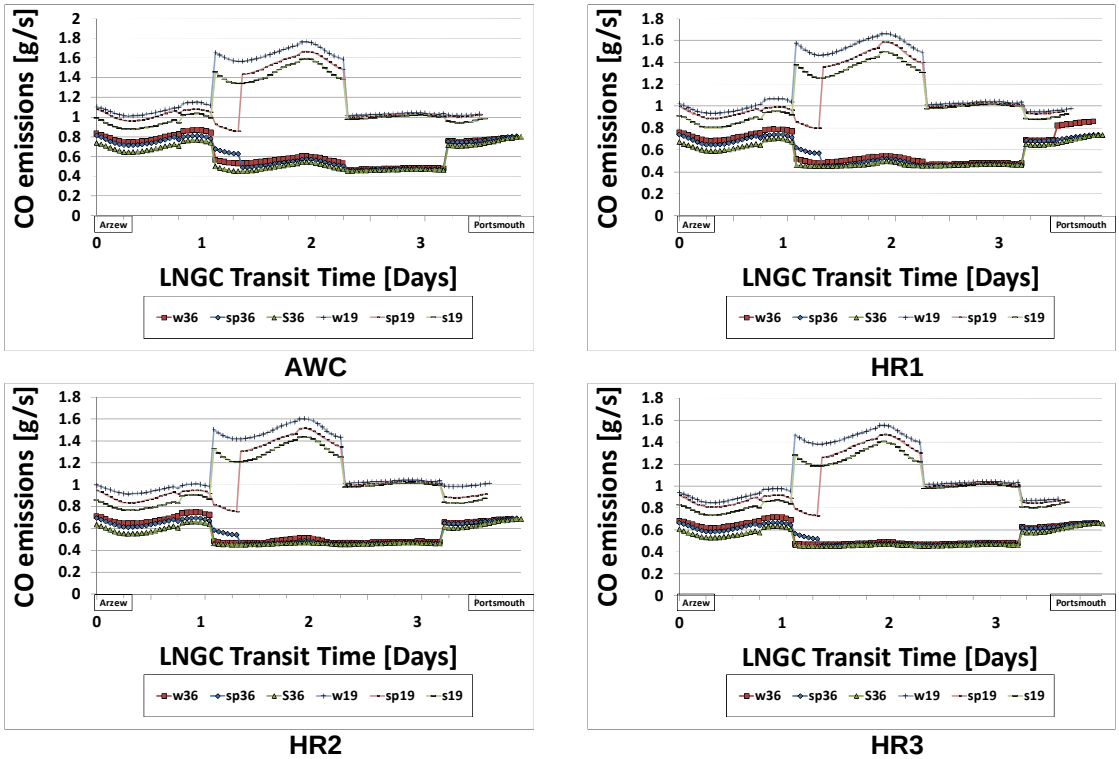

Figure 5:39 Variation of CO emissions for the 19MW and the 36MW models

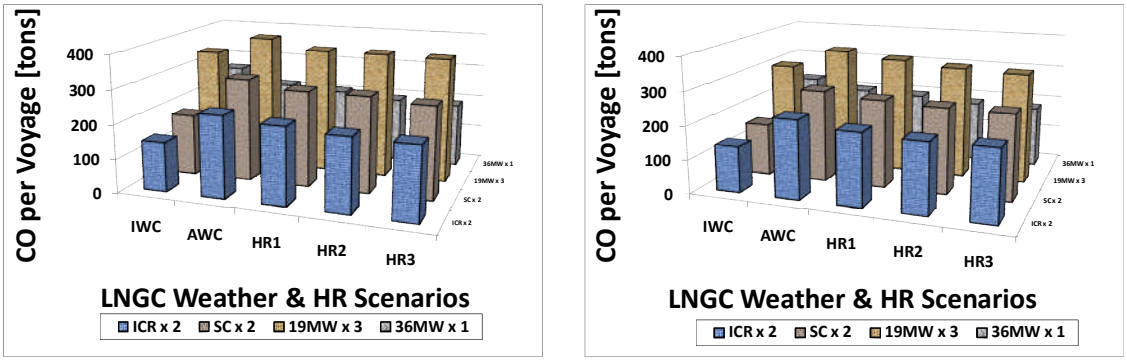

Figure 5:40 CO emissions in winter and summer respectively

5.6.4 Pollutant emissions of UHC

The SC and ICR models behaviour in relation to the emission of UHC pollutants is presented in Figure 5:41in which it can be observed that the SC model generates more of it than the ICR model in zones where the power requirement cannot be satisfied by a single due to the higher resistance experienced by the ship hull from fouling. The propulsion plant must operate at full capacity by engaging the two engines at the same time yet at lower TET. This continues when the resistance is increased which then causes the two gas turbines to fire at full power and at maximum TET. As for the ICR model, the CO emissions are lowest as a result of the lower operating temperatures due to the effect of inter-cooling and recuperation.

The voyage analysis of the 19MW and 36MW gas turbine models is illustrated in Figure 5:42. It shows how the 19MW model releases higher quantities of unburned hydrocarbons than the single engine power plant configuration of its 36MW counterpart as the LNGC undertakes its voyage. It is the model with the lowest emission of UHC pollutants among all the models of the project.

The quantities of UHC released by each of the gas turbines are illustrated in Figure 5:43 in which a significant amount is that due to the 19MW power plant in which the effect of hot summer weather causes it to generate more than in winter season. This demonstrates that the air density is a factor to be considered in the evaluation of UHC pollutants.

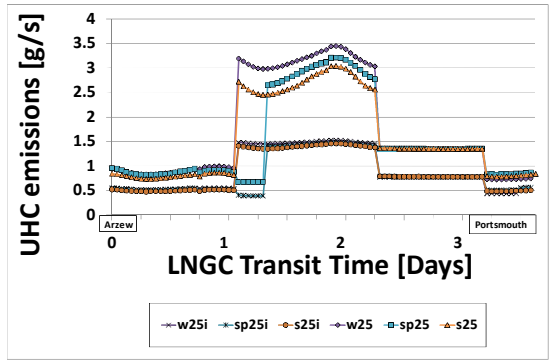

AWC

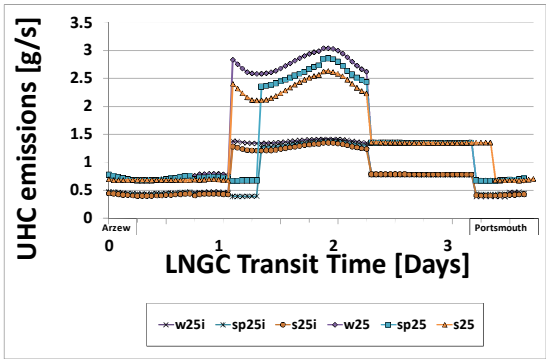

HR1

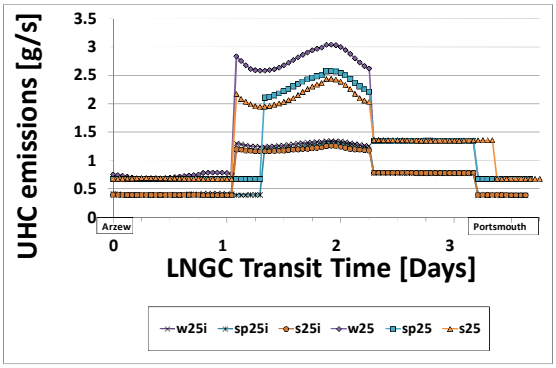

HR2

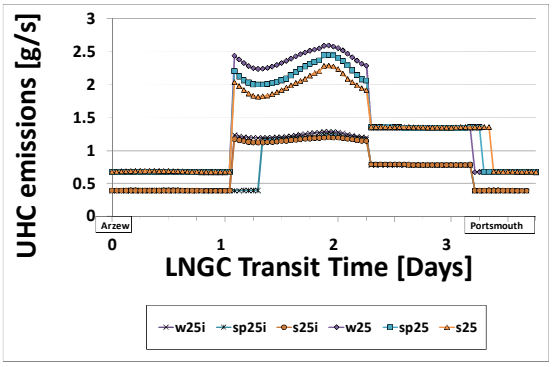

HR3

Figure 5:41 Variation of UHC emissions for the ICR and the SC models

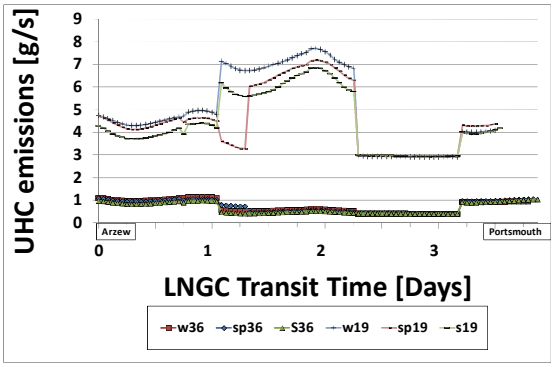

AWC

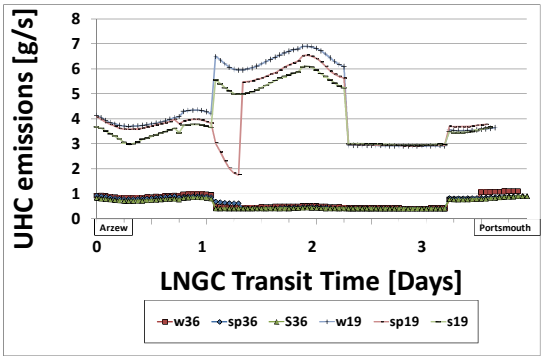

HR1

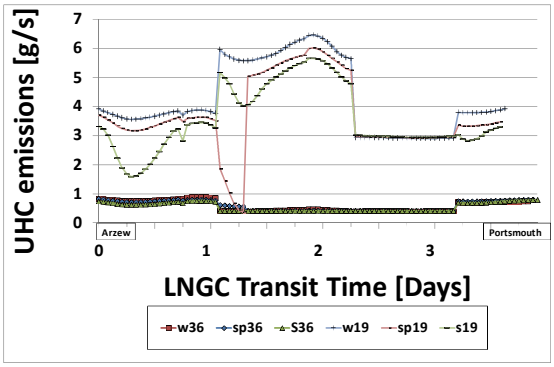

HR2

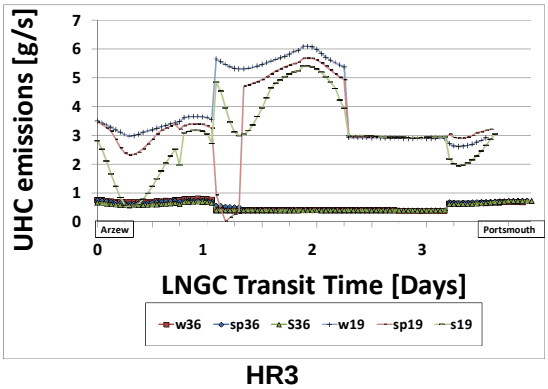

HR3

Figure 5:42 Prediction of the UHC emissions for the 19MW and 36MW models

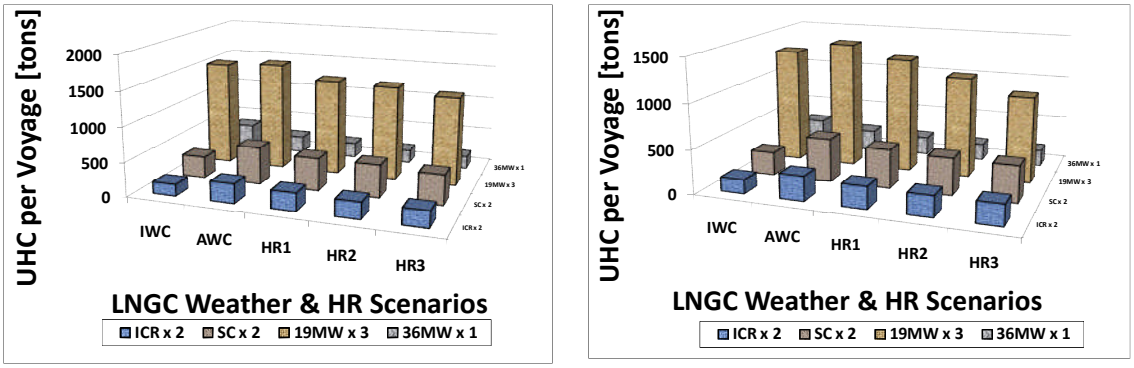

Figure 5:43 Predicted quantities of UHC emission for the various gas turbine models for winter and summer seasons

5.7 Assessment of the Turbine Creep Life Consumption

The turbine creep life model described in paragraph 3.1.3 was implemented for the prediction of the HPT rotor's blade life consumption of the hot section. The model has the ability to quantify the blade's creep life consumption during a scheduled journey undertaken by a vessel propelled by a gas turbine prime mover. Among the steps involved are the calculation of centrifugal stresses through the use of inputs from the results of the uninstalled gas turbine performance investigations and the calculation of the gas path geometry according to [73]. In addition, the creep life fraction t_f was calculated according to the Larson-Miller criterion [48]. In addition to the variation estimation of the blade's time to failure at each interval, the percentage of the hot section rotor blades life consumed after each LNGC voyage was obtained from the liner damage summation law or Miner's law [48]

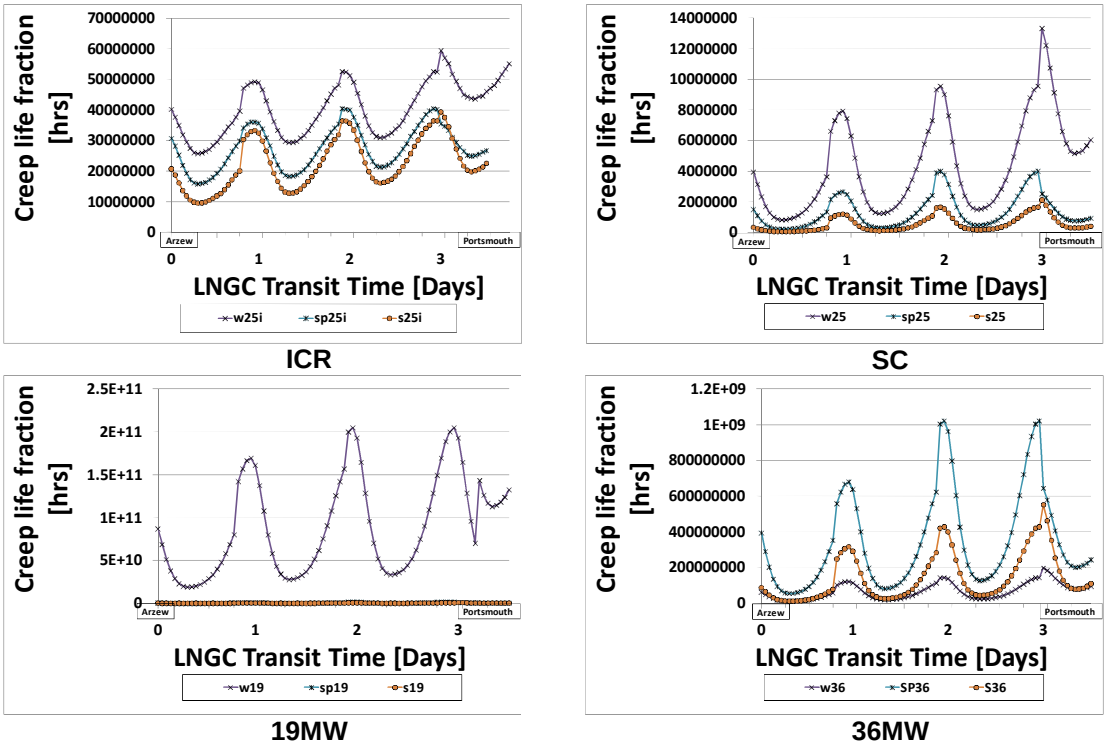

Figure 5:44 Comparative variation of the creep life factor for each of the models in IWC for winter, spring and summer

5.7.1 Variation of Creep Life under IWC

According to the voyage scenarios that have since been in place for the investigation in this work, the variation of the creep life fraction was analysed for each of gas turbine models when the LNGC was assumed to be undertaking its voyage under IWC in the different seasons as presented in Figure 5:44.

Under IWC naturally, there is no added resistance to the ship hull as it manoeuvres through the water with a clean hull surface as earlier suggested. The power required for propulsion of the vessel at its service speed is in accordance with the design criteria of the LNGC. However, each gas turbine model behaved differently according to cycle configuration and power rating thereby affecting the engine time-to-failure differently.

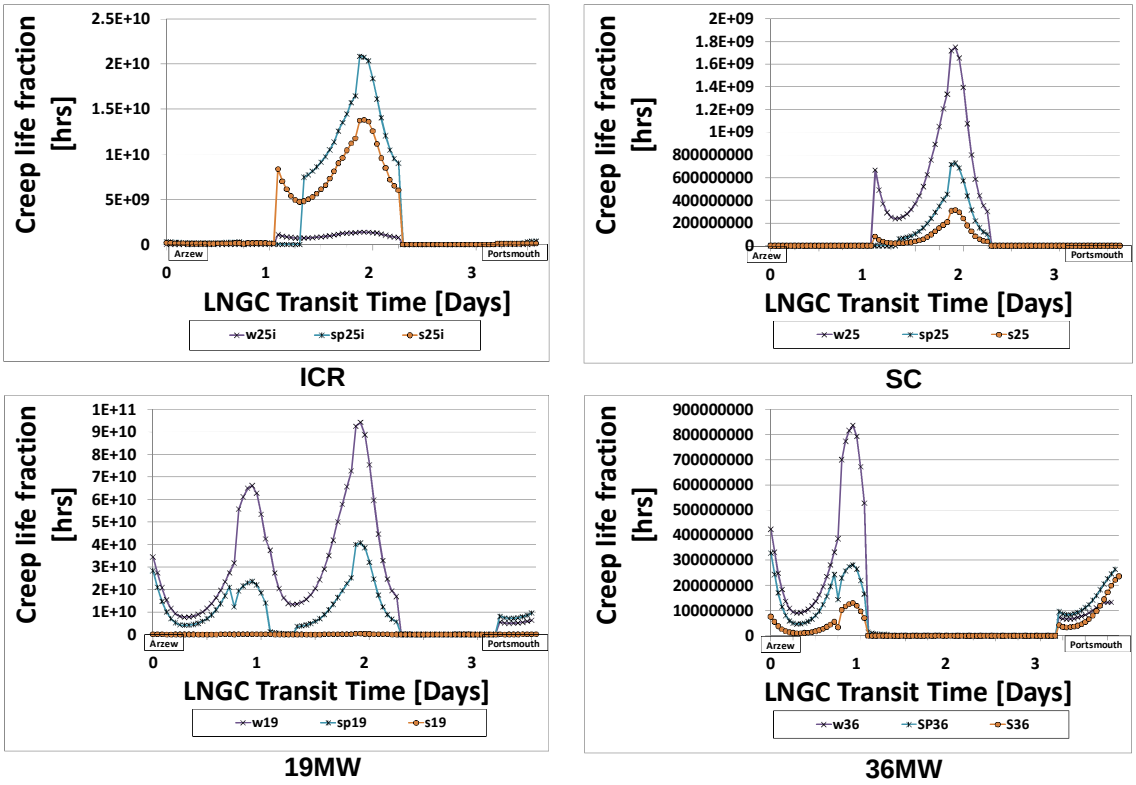

Figure 5:45 Comparative variation of the creep life factor for each of the models in AWC in winter, spring and summer

The simulated times in the curves were found to be slightly elevated and were assumed to be fairly acceptable only in comparison to each other and for the fact that values were considered at intervals and the engines are designed to withstand the most adverse conditions and for longer periods and still maintain their life cycle projections from conception. The results show that there is an adverse effect imposed on the blades' life when weather conditions change according to climate with the winter weather being the most favourable for all the models except in the case of the bigger 36MW model which favours the spring weather.

5.7.2 Variation of Creep Life under AWC

In Figure 5:45 the effect of the expected changes in weather conditions from IWC to AWC was analysed as the influence of sea states and wind can be seen to affect the operating conditions by demanding for more power to meet ship speed requirements at the locations where these changes were encountered

during the voyage. The deterioration can be observed to be more effective when a single engine was in operation but with the presence of sea waves, the higher power delivered triggered an elevated spool speed which affected the engine time to failure until a second engine was necessitated by higher sea states. However, the pattern remained fairly good until the sea states were further raised from 5 to 6 in which the life continued to be affected until sea states of 3 were encountered.

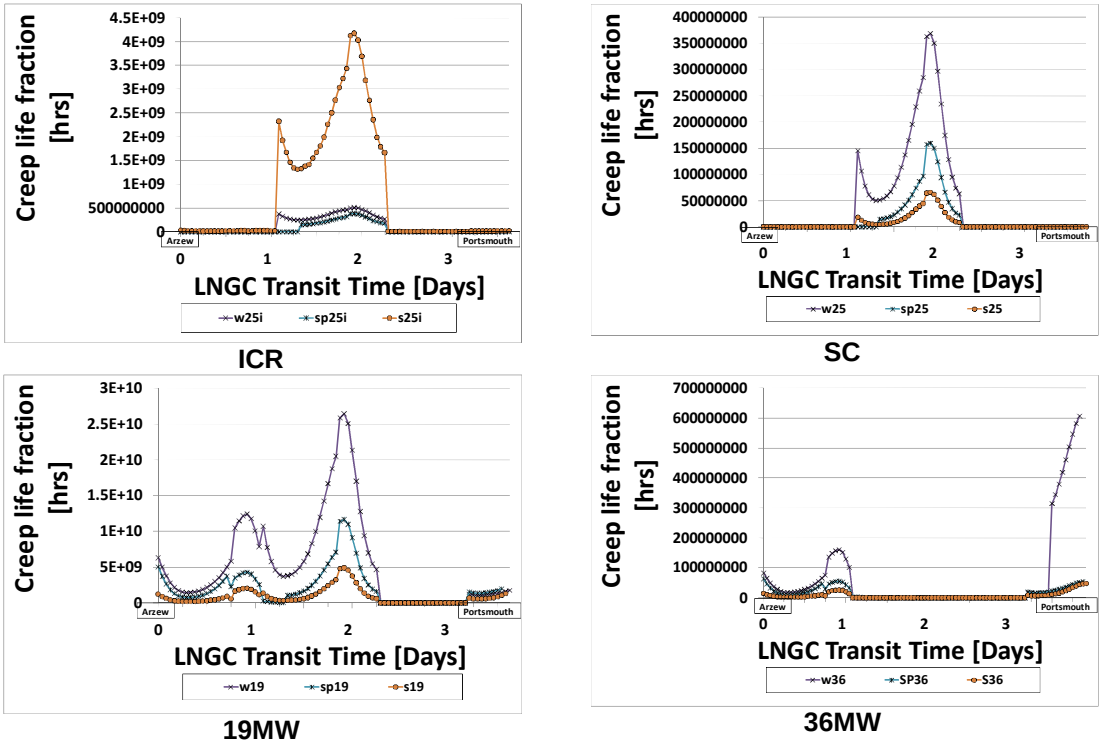

Figure 5:46 Comparative variation of the creep life factor for each of the models in HR1 in winter, spring and summer

Among the models, the 19MW model had earlier demonstrated a good time to failure in winter compared to the rest of the seasons under IWC but has now improved with the curves for both winter and spring seasons showing significant savings. It is also to be considered as the engine with the best redundant life if it use were to be limited to only IWC and AWC.

5.7.3 Effect of Hull Fouling on HPT creep Life

A further investigation was conducted through the implantation of a 120µm roughness on the submerged ship hull surface resulting from fouling and the

outcome for each of the models is illustrated in Figure 5:46. A further deterioration of the life can be seen due to the additional power output occasioned by the increased resistance.

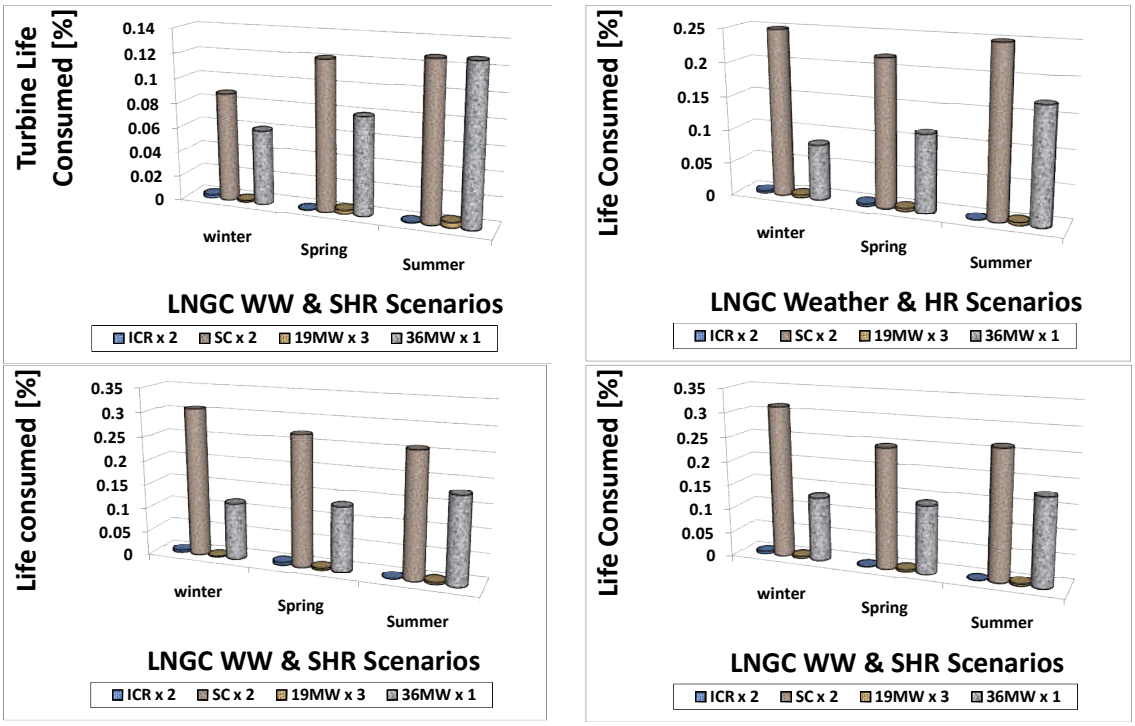

Figure 5:47 Predicted creep life consumption of the models in AWC and hull fouling scenarios

5.7.4 Percentage of Life Consumption

The life consumption per voyage was evaluated for each of the engine models and a comparative analysis of their individual ability to endure the stress caused by the different operating scenarios is presented. Figure 5:47 shows the effect of rough weather conditions on the hot section creep life for all the models in all seasons. It would be observed that the ICR and the 19MW models portray less life consumption than the SC and the 36MW models. The ICR benefits from its advanced cycle design while the 19MW model achieves this through the dual engine configuration of the power plant

6 OTHER SHIP PERFORMANCE PREDICTIONS

This chapter is an illustration of the voyage analysis of the variety of vessels aimed at evaluating the behaviour of the gas turbine models in response to the weather and sea conditions encountered along their transit routes. It analyses the effect of varying atmospheric conditions, high sea waves and ship hull fouling on the relevant performance parameters to determine the most economic gas turbine model for each of the vessels under investigation. It focuses on quantities of fuel burned (FB) and pollutant emissions released as well as the engine life consumption per every voyage undertaken under the selected investigated scenarios.

6.1.1 Engine Operating Limits

A gas turbine engine must incorporate two very important means of protecting it from excessive speeds and excessive temperatures among other safety features. Due to the fact that gas turbine blades are attached to disks that rotate with their spool shafts, the danger of an over speeding spool has the potential of causing the disks to rupture and release the blades with tremendous energy enough to drive them through bulkheads and decks with high possibility of destroying equipment or killing personnel [21]. Therefore, a gas turbine control system is required for the prevention of over speeding by the installation of over speed limiting functions. Also, as is the case with all the four engine models under investigation, the only connection between the power turbine and the rest of the engine is the hot gas that flows from the gas generator. In such a design, a torque limiting device is necessary due to the high toque capability that accompanies the combined effect of high air flow and low free power turbine speed. Shaft power increases with increase in air flow but a reduced spool speed can result in high torque with grave consequences.

Table 6:1 Maximum and minimum OPR values for the gas turbines as they operate along transit route of the Cruise Liner

GT models	Design Point -	Overall Pressure Ratio [OPR]					
		Winter		Spring		summer	
		Min	Max	Min	Max	Min	Max
19	26.3	23.605	25.058	23.855	25.086	23.052	25.088
25 ICR	15.52	13.93	14.80	13.88	14.02	13.84	13.964
25	18.75	16.97	17.62	17.011	17.411	16.782	17.251
36	24.0	21.90	22.681	21.93	22.43	21.75	22.244

Table 6:2 Maximum and minimum TET values for the gas turbines as they operate along transit route of the Cruise Liner

GT models	Max Limit	Design Point	Turbine Entry Temperature [K]					
			Winter		Spring		summer	
			Min	Max	Min	Max	Min	Max
19	1500	1480	1380.4	1477.6	1473.3	1408.7	1432.8	1497.0
25ICR	1550	1500	1440.9	1505.5	1452.1	1479.2	1461.6	1489.1
25	1550	1505.5	1401.2	1506.3	1431.3	1502.3	1457.5	1524.4
36	1600	1550	1462.0	1566.8	1492.3	1562.0	1517.4	1588.3

6.1.2 Prevention against Excessive Internal Temperatures

Operation of the marine gas turbine at higher-than-rated power produces higher operating temperatures and induces rapid failure of key turbine components such as the high pressure turbine (HPT) as a result of which engine output power is limited by materials consideration. Therefore, the gas turbine control system is required to protect the engine from excessive internal temperatures.

The flow of fuel and the flow of air are the only two basic parameters that can be controlled while a gas turbine is running. However, all turbine control systems have a fuel control function but not an air control function and the

temperature limiting function is inherently incorporated into the fuel control function. This regulates the flow of fuel into the engine, ensuring that the engine's power output matches the power output requested by the engine operator or the remote control system itself. Steady power demands therefore require the fuel control to provide a constant fuel flow whereas, power demands that are not constant require a change of fuel flow that closely conforms to the power requirement. The plots illustrating engine SFC for each of the engine models are presented in

Under ideal weather conditions, the off design operation for each of the gas turbine engines remained within the boundaries selected in each case. These boundaries were required to protect the hot end section from exceeding the metallurgical limits of the components. The TET variation follows the same pattern with the variation that occurs in the ambient temperature of the designated transit route selected for every vessel but the engine power output was dependent on that required for propulsion enough to keep the ship steadily cruising at its service speed. A distortion of the TET curves occurred only when the operating environment changed and caused a rise in power demand leading to higher operating temperatures but not exceeding the limits of TET that had been defined in the creep module of' Poseidon'.

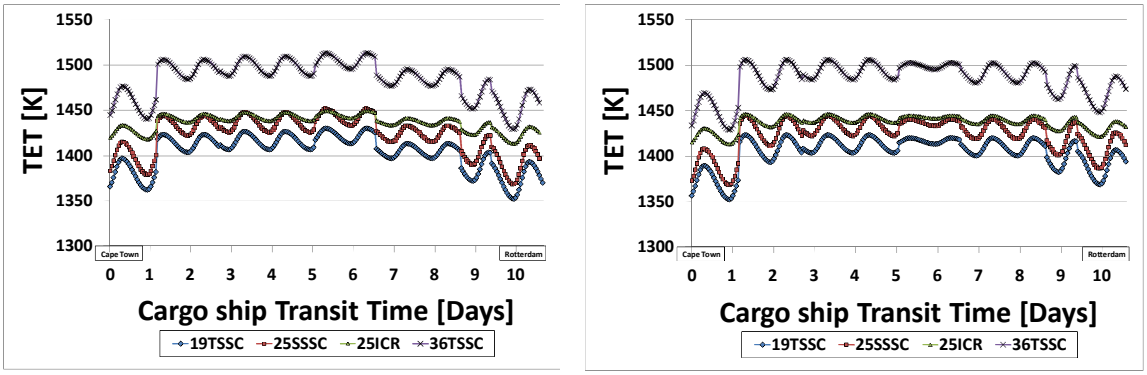

spring **summer**

Figure 6:1 Variation of the GT operating temperature (TET) for the cargo ship for spring and summer voyages.

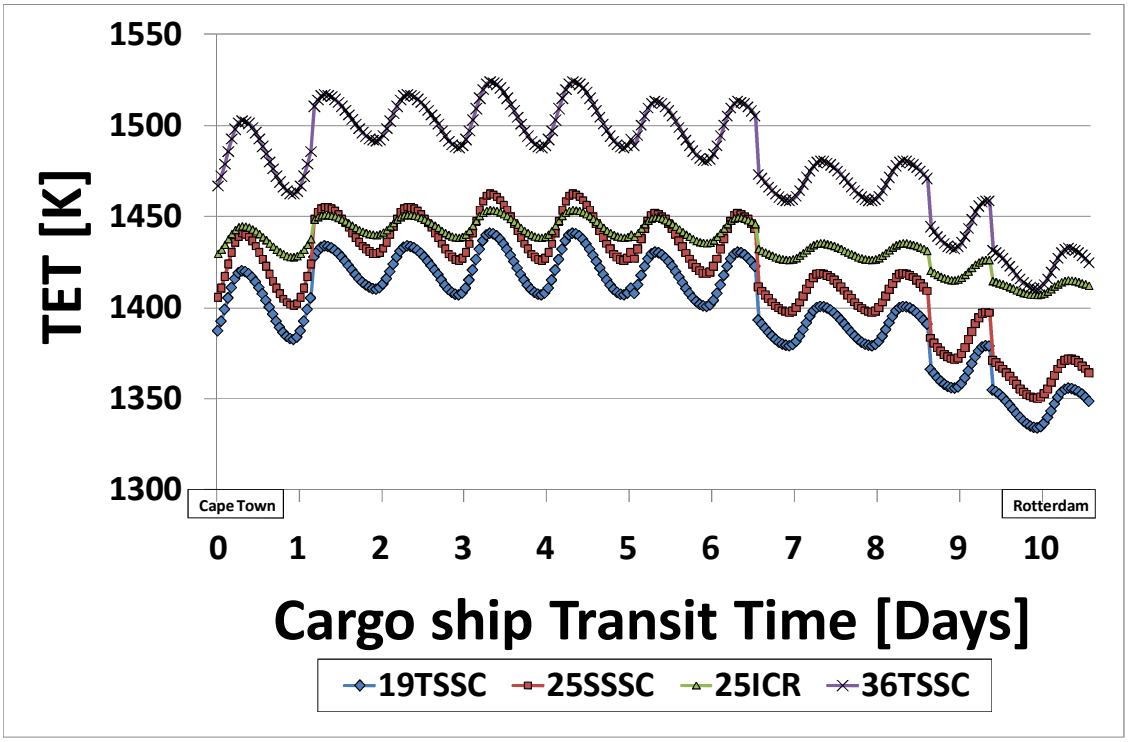

Figure 6:2 Variation of the GT operating temperature (TET) for the cargo ship during a winter voyage

6.2 Journey Profiles and Propulsion power Requirement

The key factor in defining the selected ship routes is the changing environmental conditions which affect gas turbine output due to increased drag caused by the adverse atmospheric and hydrodynamic conditions. The main scenarios that require greater attention focused on the effect of ideal weather conditions (IWC) when the weather is calm and the ship hull is fine and clean as well adverse weather conditions (AWC) in which the hull is assumed to be clean under rough weather accompanied by high sea waves. The input of the sea waves has been represented by sea state values using the Beaufort wind scale.

The ambient temperature profiles of each of the designated trade routes have already been defined in Chapter three and it is based on it that the variation of other significant engine/ship performance and emissions parameters will be analysed.

The results obtained for the cargo ship (container ship) with respect to four scenarios of adverse weather conditions and the power output of the individual

gas turbines are represented in Figure 6:4 under the following different case studies:

- Adverse Weather Conditions (AWC) under which the ambient temperature remains the same and the ship hull is assumed to be clean but there are sea waves present along the voyage route of the ship
- Same weather and sea conditions as above but in combination with a hull roughness of 120μm (HR1)
- Same weather and sea conditions as AWC but in combination with a hull roughness of 240μm (HR2)
- Same weather and sea conditions as AWC but in combination with a hull roughness of 360μm (HR3)

As a direct influence of the varying degrees of ambient temperature and sea states encountered along the aforementioned designated trade routes, a ship by ship investigation was conducted and the results are presented in the following

6.2.1 Ideal Weather Conditions

Under ideal weather conditions, it is assumed that the sea is calm without waves and as a result the total resistance on the ship hull and the profile of power output from each of the engines remains constant throughout the journey from beginning to end. However, the operating temperature of the gas turbines (TET), continues to vary according to the variation of the ambient temperature regime of the designated trade route. Under this condition, all other operating parameters of the gas turbine equally have to vary whenever there is a change in ambient temperature anytime and anywhere during the voyage. The parameters that have been taken into consideration include the following:

- Intake mass flow
- Thermal efficiency
- Fuel flow

- The HPT blade estimated time between overhauls
- The Specific Fuel Consumption (SFC)
- The Compressor outlet temperature and
- The variation of the HPT spool speed.

The anticipated variation in environmental conditions causes an increase in the resistance encountered by the ship with a tendency to slow it down while demanding for higher power in order to maintain it at the designed service speed. As result, the gas turbine power plant will be expected to meet the requirement for more power thereby, contributing to the overall running costs of the vessel.

Having ascertained the behaviour of each of the gas turbines for the propulsion of the ships and according to the aforementioned scenarios, the voyages were conducted in three different seasons and the different scenarios of IWC, AWC, HR1, HR2 and HR3. The gas turbine performance and emissions parameters were affected by the changes occurring due to ambient temperature changes. The adopted methodology facilitated the summation of the quantities of fuel burned (FB), quantities of pollutant emissions generated into the atmosphere as well as the percentage of engine life consumed. Results obtained through the cargo ship simulation are illustrated here as an example.

6.3 Profiles of Adverse Weather Conditions (AWC)

The transition of a ship through AWC induces speed losses for a given power output due to the less favourable working conditions of the propeller. The unpleasant features of operating in waves such as motions, slamming and wetness are generally eased by a reduction in speed so that an additional speed reduction may be made voluntarily [53]. Such a scenario increases the load on the propulsion machinery as the power output of the gas turbines in this investigation was found to be elevated in proportion to the sea states encountered during any of the voyages. With it, the performance parameters

also vary due to the combined influence of ambient temperature and sea state variation and ship hull surface degradation (see section 3.3.3.1).

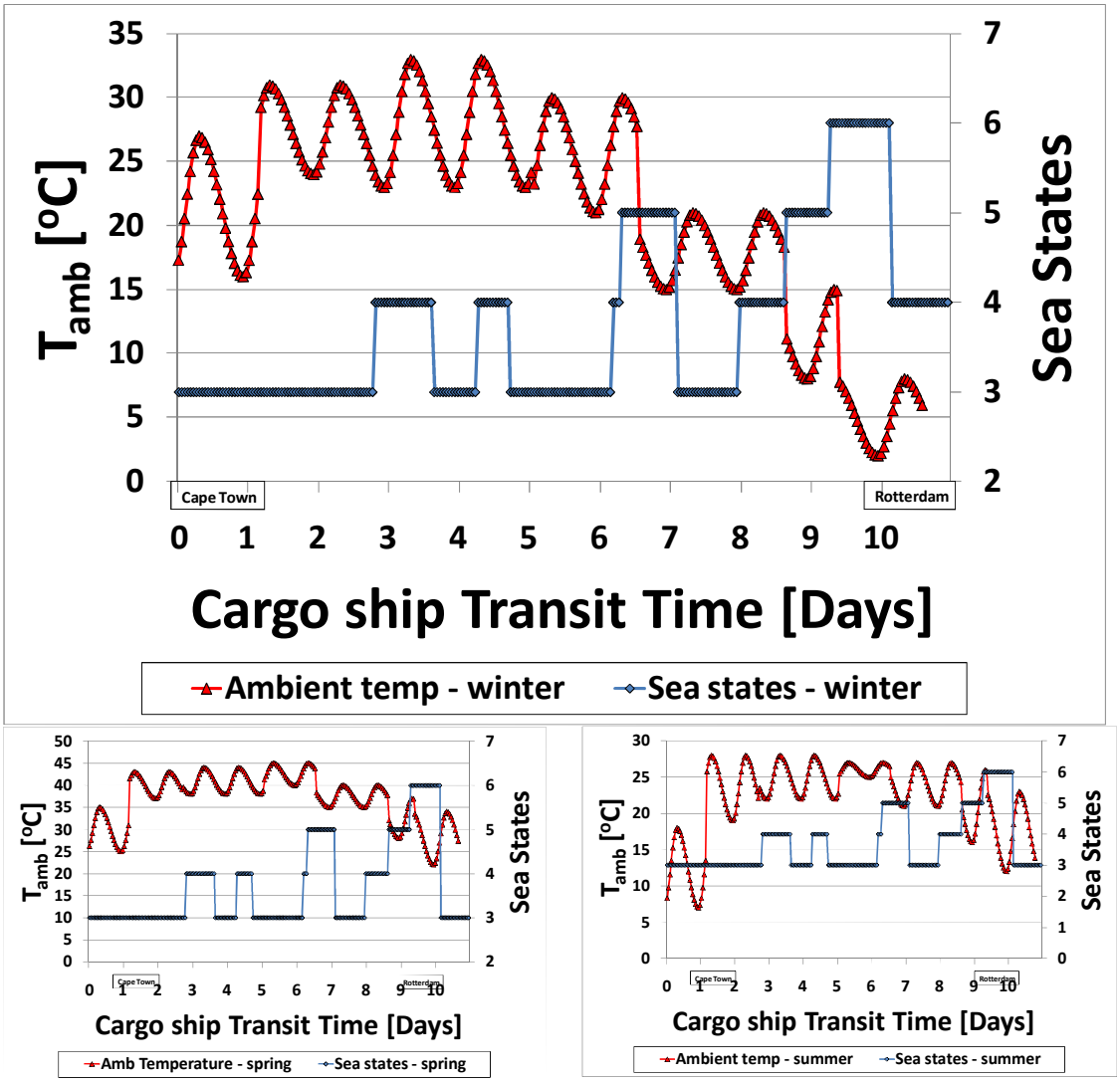

Figure 6:3 Factors that influence Adverse Weather Conditions (AWC) during the different Seasons under investigation along the cargo ship transit route

The effect of seasonal and climatic changes that occur along the transit routes are presented in Figure 6:3 and apart from the IWC, all other scenarios are affected by the presence of sea waves ranging between Beaufort wind scales 3 and 6 as illustrated.

6.3.1 Variation of GT Power output

The variation of each of the gas turbine output power was investigated and analysed while considering the effect of the off design conditions as they affect engine output power. The more degraded the conditions became, the higher the power required in order to be able to meet the speed requirement of the vessel. The number of gas turbines required for the configuration of the respective propulsion plants was determined by the most severe operating conditions to be encountered along the route of each vessel.

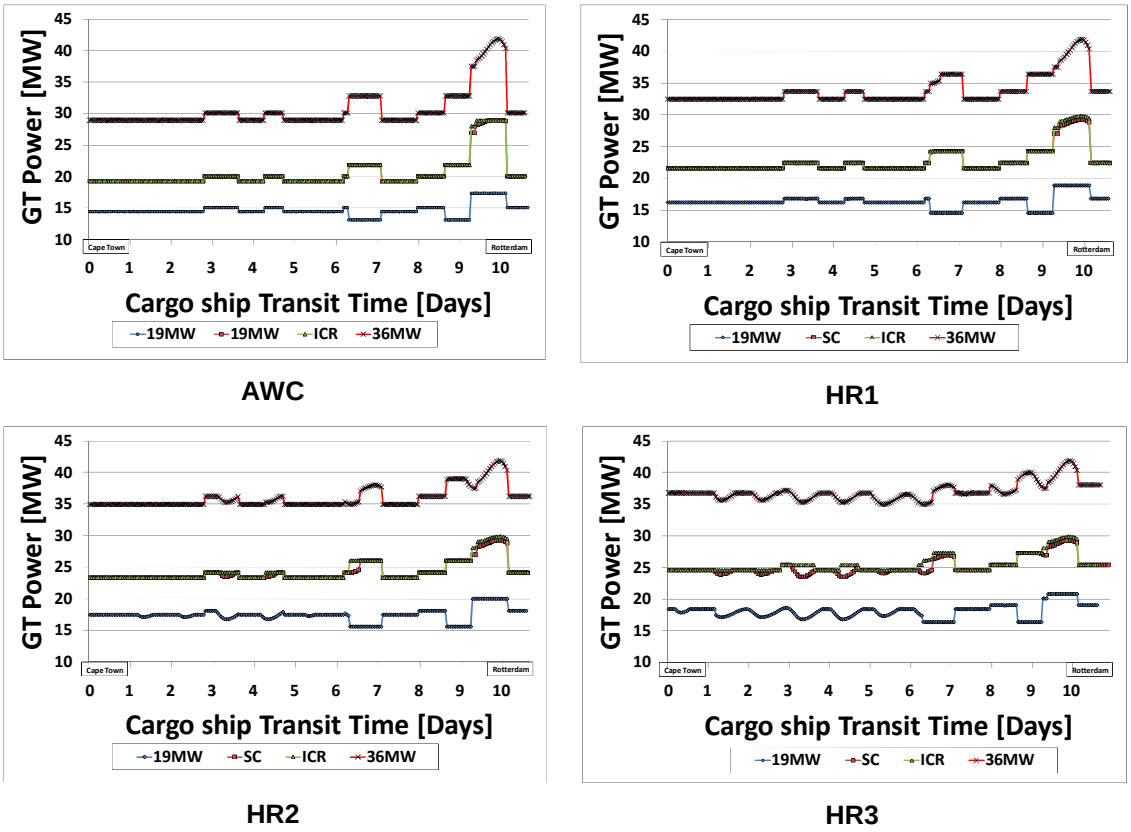

Figure 6:4 Variation of individual GT power output for the cargo ship under different adverse conditions during winter

6.4 Effect of Hull Fouling

The pattern of speed loss depreciated further as the rough weather effect was further complicated by degradation of the hull surface due to fouling. Further losses were experienced even at locations of less severe sea waves.

It would be observed that the performance of the 36MW model was affected mainly by the high sea waves but the others were affected by the hull surface roughness that grew beyond 120μm. The result affected the ship speed under the propulsion power generated by the 19MW model. It would be seen that the low rated GT model was more affected at locations of higher ambient temperatures.

6.5 Voyage Analysis of the Vessels

The brake power (P_B) capable of propelling each of the vessels at their designed cruise speeds was sustained during operations under IWC and remains fairly constant throughout the voyage. However, the emergence of adverse weather and sea conditions existing along each transit route aroused an elevated power requirement consequent upon the severity of the prevailing sea states and the level of hull fouling.

6.5.1 Voyage of the Cargo ship

The investigation showed that the cargo ship required about 53.3MW of brake power in order to keep the keep it cruising at its sustained sea speed of 25knots under IWC but this rose to 54.4MW when wave and wind resistance of Beaufort scale values of 3 began to persist. This represents a PB increase of 2% at sea states of 4, the percentage increased to 6.5% and later shot up to 16.6% and 56.3% when sea states of 5 and 6 were encountered respectively.

Table 6:3 Operating Profile of the cargo ship power plant

Installed Capacity of the Cargo ship		
	No. of GTs	**Power [MW]**
19MW	4 (5)	76 (95)
36MW	2	72
ICR	3	75
SC	3	75

The prediction of the power required for the effective operation of the cargo ship was conducted and the number of gas turbine units required in each case was

evaluated as contained in Table 6:3 and Figure 6:5. The flexibility of the 19MW model made it possible to adopt four of its units for operation under IWC, giving an installed capacity of 76MW and was inadequate to meet the power required for overcoming severe operating conditions. A fifth 19MW was to be brought online (95MW) whenever sea states of 6 were encountered by the vessel as illustrated in Figure 6:5.

It is noteworthy to state that the other models with installed capacities ranging from 72MW to 76MW lack this flexibility as so much undesirable redundancy could cause poor part load performance problems leading to unacceptable fuel economy.

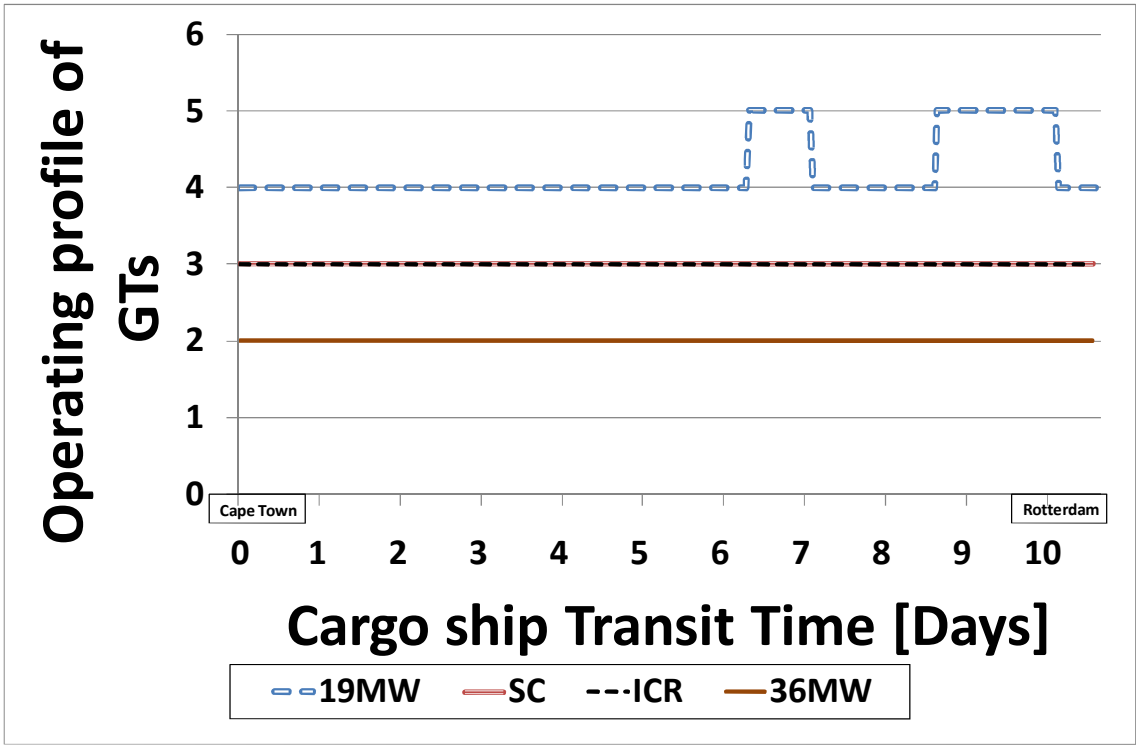

Figure 6:5 Operating profiles of the gas turbine models for the cargo ship

The HR1 investigated scenario represents a combination of rough weather and hull fouling that both cause significant increase in propeller drag and hull resistance with a roughness of the submerged surface measured at 120mμ at which the PB requirement increased by 15.3% with sea states of the magnitude of 4 and more than 31% when the sea states rose up to 5. The figure rose to 70% for sea states values of 6.

Figure 6:6 and Table 6:5 illustrate that arise when environmental operating conditions are worsened and shows the significant effect of hull fouling on the propulsion power and ship speed. The cargo ship experienced further power and speed losses in regions of higher ambient temperatures when engine performance could not meet power demand.

Table 6:4 Brake power increases imposed on the propulsion system by the investigated adverse scenarios in KW

Cargo ship Brake Power Required [KW]					
Sea States	**IWC**	**AWC**	**HR1**	**HR2**	**HR3**
0	53226.11	-	-	-	-
3	-	54409.12	61437.65	66483.82	70075.25
4	-	56793.27	63886.97	68977.21	72598.65
5	-	62160.89	69394.37	74577.1	78267.17
6	-	83297.4	91022.25	96544.46	100464.7

Table 6:5 Percentage increase of PB from IWC

Cargo ship Brake Power Required [%]					
Sea States	**IWC**	**AWC**	**HR1**	**HR2**	**HR3**
0	0	-	-	-	-
3	-	2.222616	15.42766	24.90828	31.65577
4	-	6.701893	20.02937	29.5928	36.39668
5	-	16.78646	30.37656	40.11376	47.04657
6	-	56.49726	71.01052	81.38552	88.75072

The investigation further revealed how each of the GT models performed under all the scenarios by evaluating the voyage duration in each case scenario as shown in the illustration from Figure 6:10 to Figure 6:12.

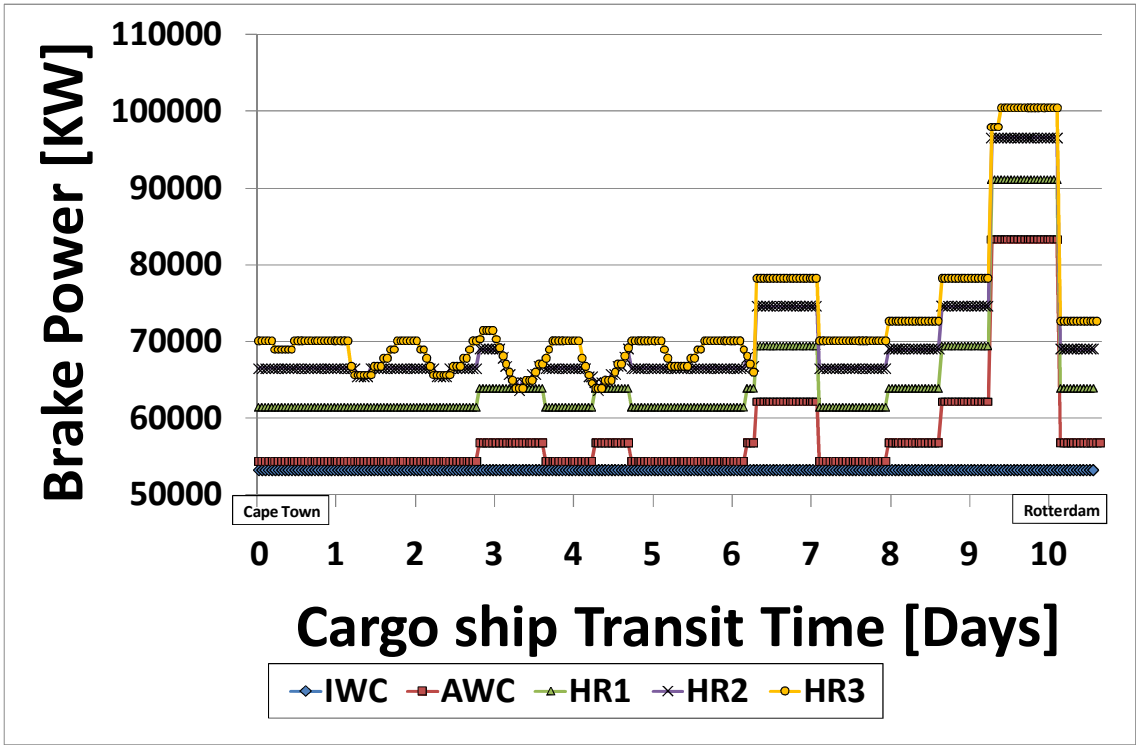

Figure 6:6 Variation of propulsion power of the cargo ship under the variety of investigated scenarios

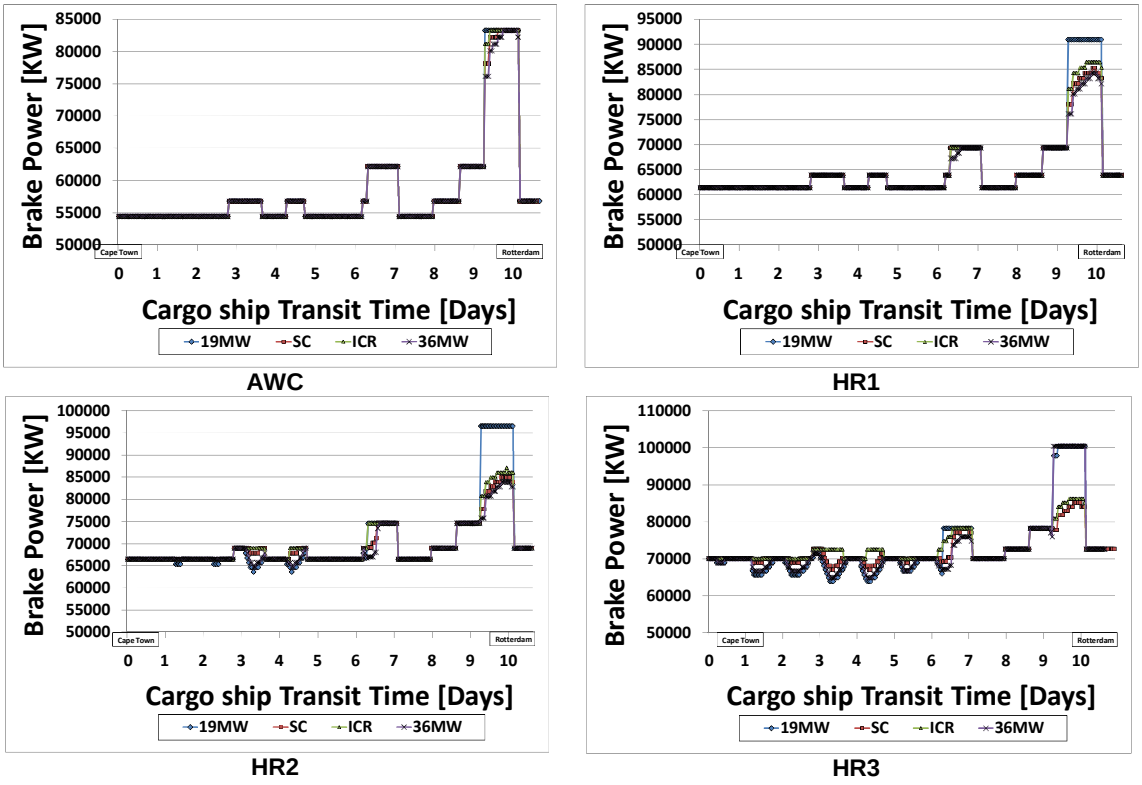

Figure 6:7 Consequence of variation in the operating environment of the cargo ship during its voyage along its fixed transit route in winter

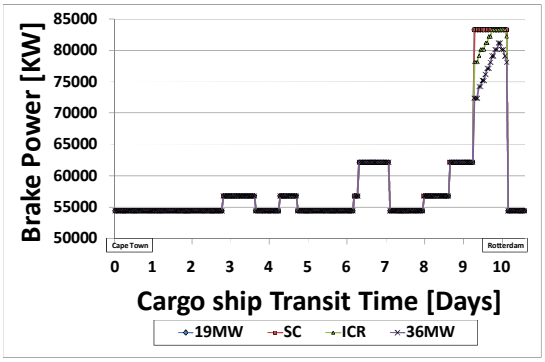

AWC

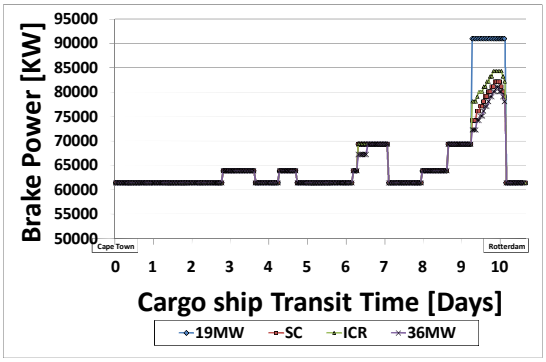

HR1

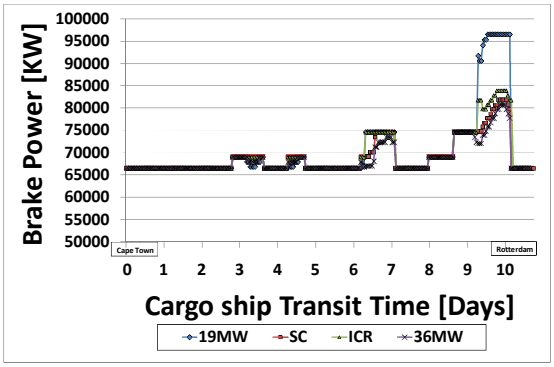

HR2

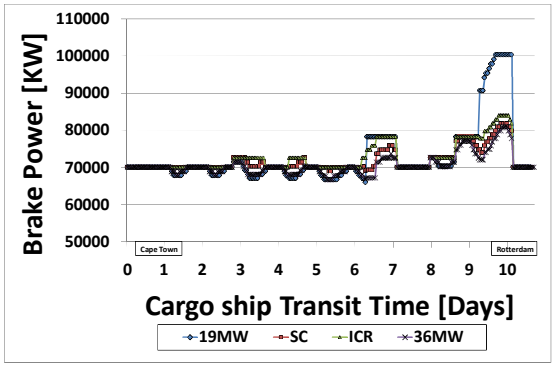

HR3

Figure 6:8 Consequence of variation in the operating environment of the cargo ship during its voyage along its fixed transit route in spring

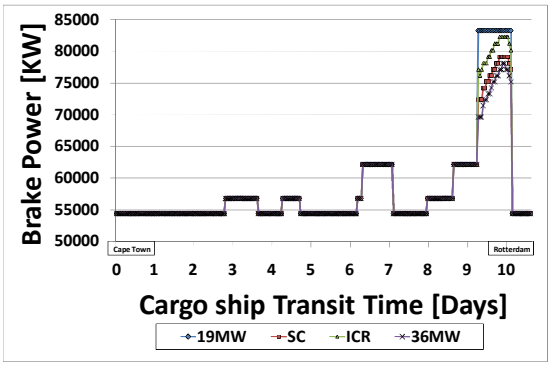

AWC

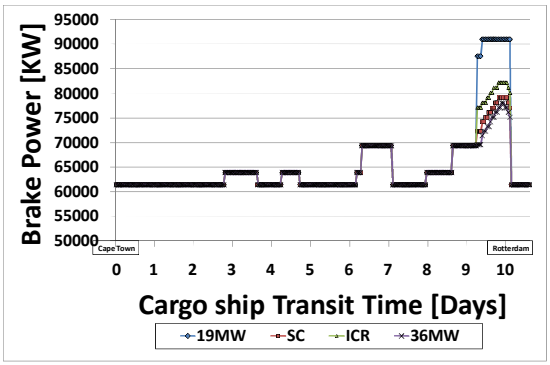

HR1

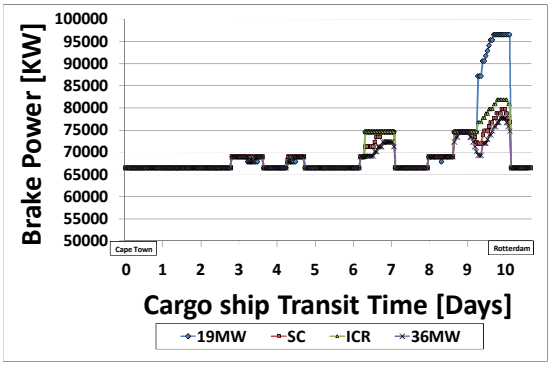

HR2

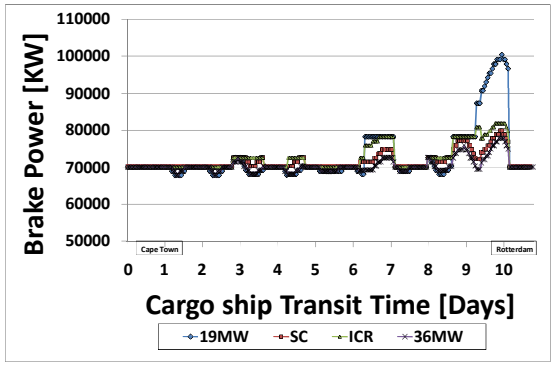

HR3

Figure 6:9 Consequence of variation in the operating environment of the cargo ship during its voyage along its fixed transit route in summer

The assessment of the investigated scenarios is illustrated in the analysis of the brake power as can be seen from Figure 6:7 to Figure 6:9 which represent the variations influenced by changes in seasons.

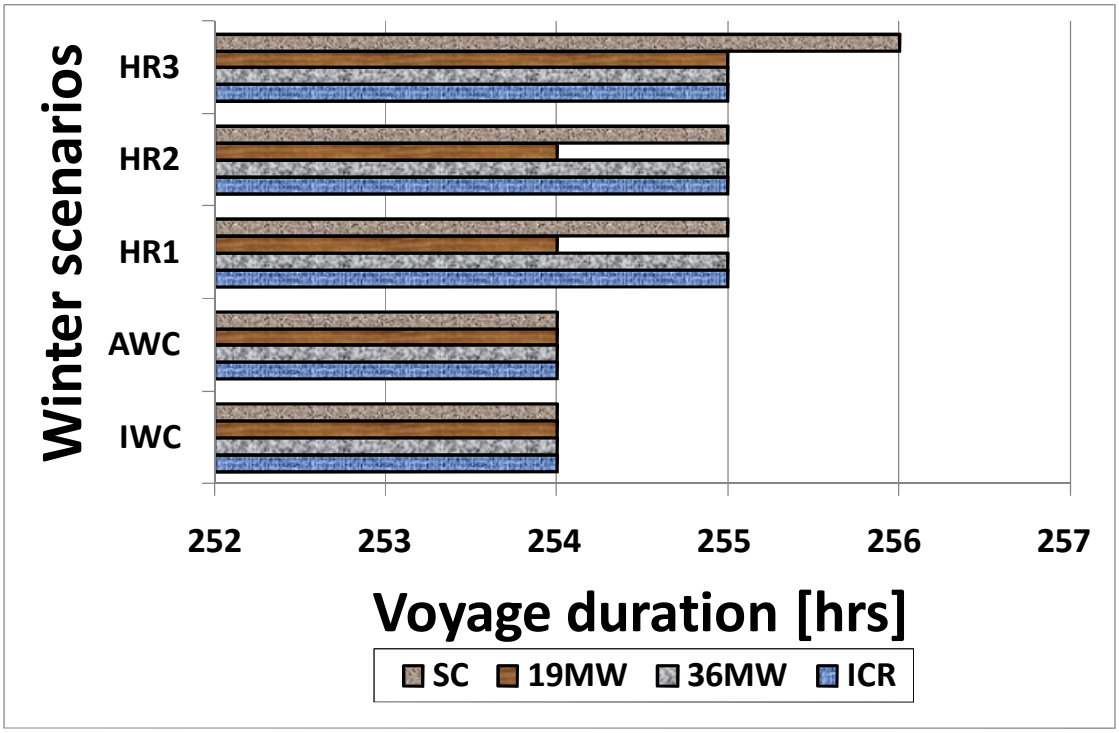

Figure 6:10 Cargo ship voyage duration in winter

Figure 6:10 illustrates the voyage analysis of the cargo ship in winter season showing how the various marine gas turbines are capable of propelling it well enough to arrive according to schedule and without delay. It illustrates the effect of hull fouling on the performance of each engine and in this case, the voyage duration of the 19MW model is the most satisfactory in all scenarios. Beyond a roughness of 240μm, the voyage duration was prolonged by one hour before arriving at its destination. The presence of hull fouling affected the other models more severely.

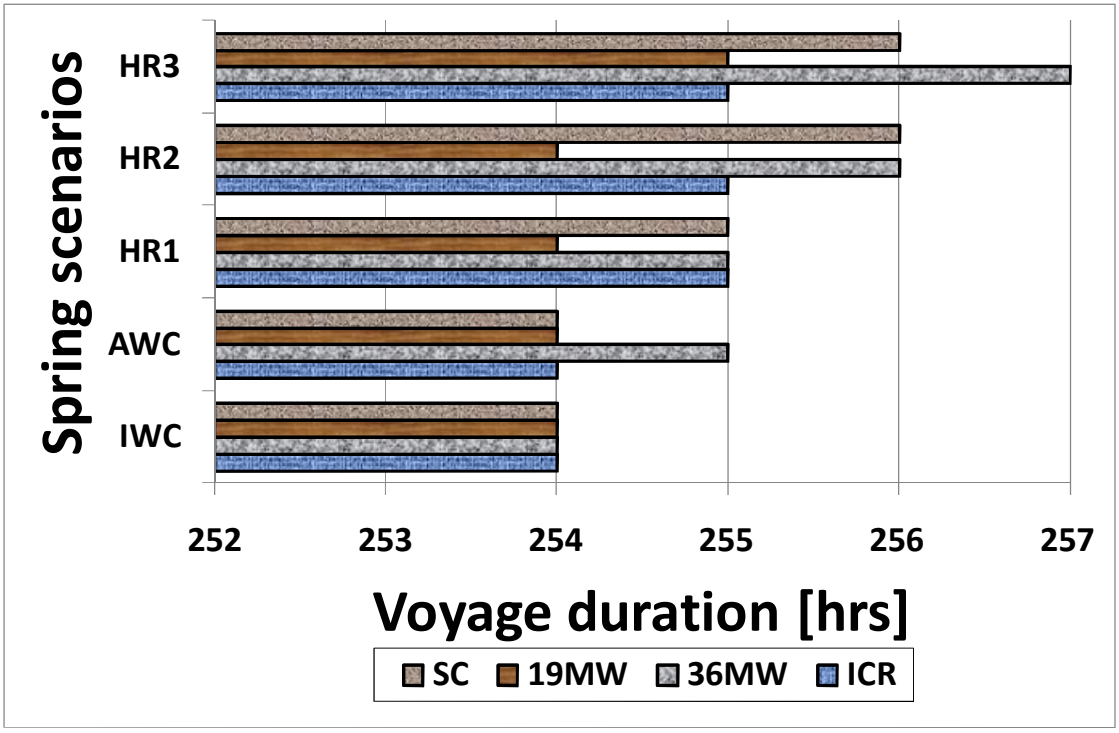

Figure 6:11 Cargo ship voyage duration in spring

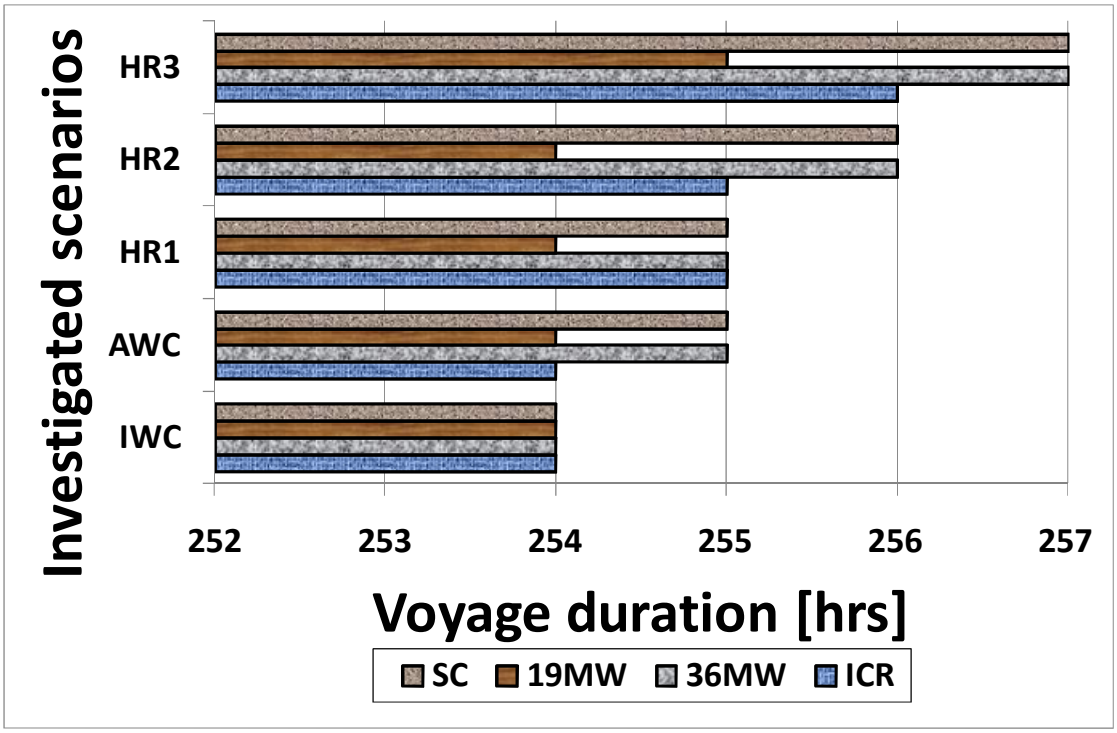

Figure 6:12 Cargo ship voyage duration in summer

In spite of the 75MW capacity of the SC power plant configuration compared to that of the 2-engine configuration of the 36MW model, its capability to overcome

the effect of hull fouling could not match the bigger sized engine model in winter. In spring however, it was found to be better than the 36MW model as it still propelled the cargo ship within 255 hours under HR1 and HR2 while the bigger engine took 256 hours under HR3 in summer season.

6.5.1.1 Ship Speed Losses

The presence of elevated wind speeds and high sea waves resulted in increased resistance and reduced ship speed as well as increased power demand. An investigation of how this combines with the effect of hull fouling to influence the ship speed losses was further conducted and analysed for a winter voyage for the cargo ship and the result is illustrated in Figure 6:13.

In contrast to the service power required for propelling the other vessels under investigation, the hotel power onboard the cruise liner accounts for about half of the total installed capacity of its power plant. As a result, only half of the power generated by the power plant is practically transmitted for its propulsion needs.

With respect to the ship's responses in ideal weather IWC, the investigation was conducted but showed that the ship cruises steadily at its specified service speed under its designed-point brake power, but the operating parameters of the gas turbines varied according to the fluctuation of the ambient air temperature based on seasons and geographical location.

Under AWC and during winter, the effect of sea states got more pronounced at locations of higher Beaufort wind scales causing the 36MW engine to generate the highest speed losses. This was followed by the 25MW SC model and was closely followed by the ICR model.

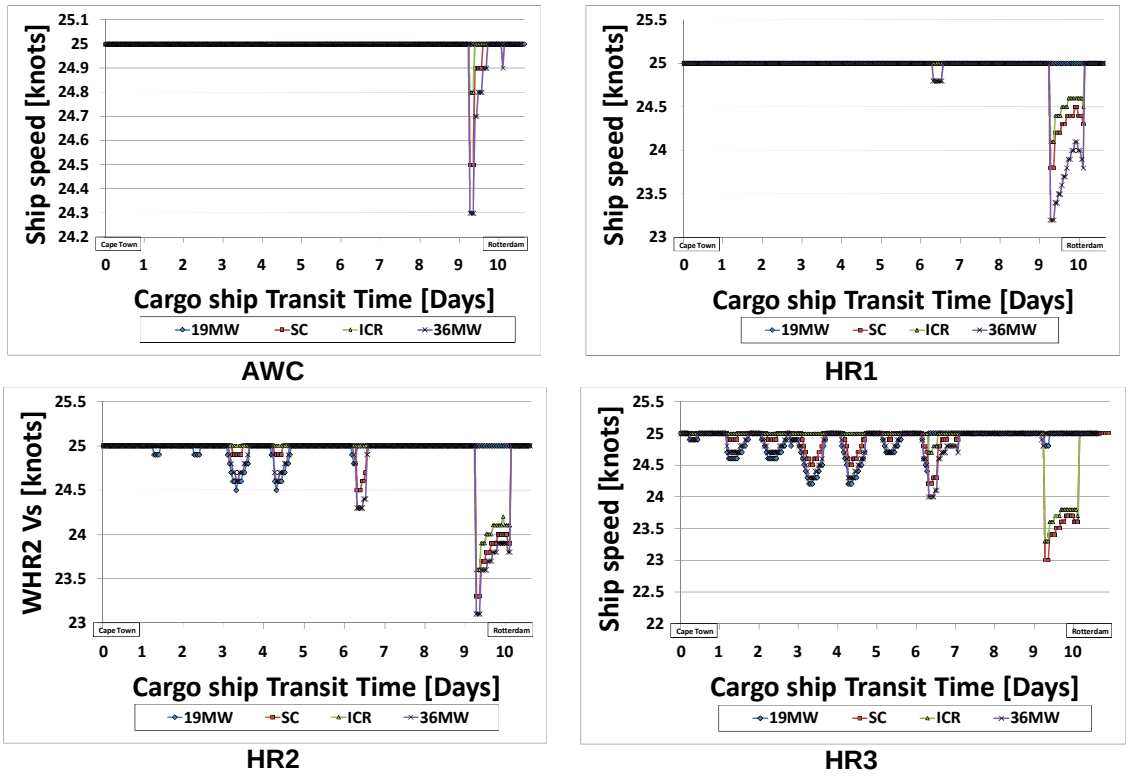

Figure 6:13 Variation of the Cargo ship speed as influenced by weather and sea conditions in winter season.

6.5.2 Voyage of the Cruise Liner

The matching of GT power output was similarly conducted for the Cruise liner to determine which of the models can best satisfy the propulsion power requirement under the variety of investigating scenarios. Table 6:8 shows the increases demanded by the cruise liner whenever it encounters any of the adverse operating conditions.

Unlike the case of the cargo ship, the propulsion power increased by only about 1% when the cruise liner encountered AWC with Beaufort scale of magnitude 2. It rose to between 3.6% and 20.5% for values of sea states between 3 and 5. A further deviation was experienced in the case of increased hull fouling which attracted close to 50% increase in power demand.

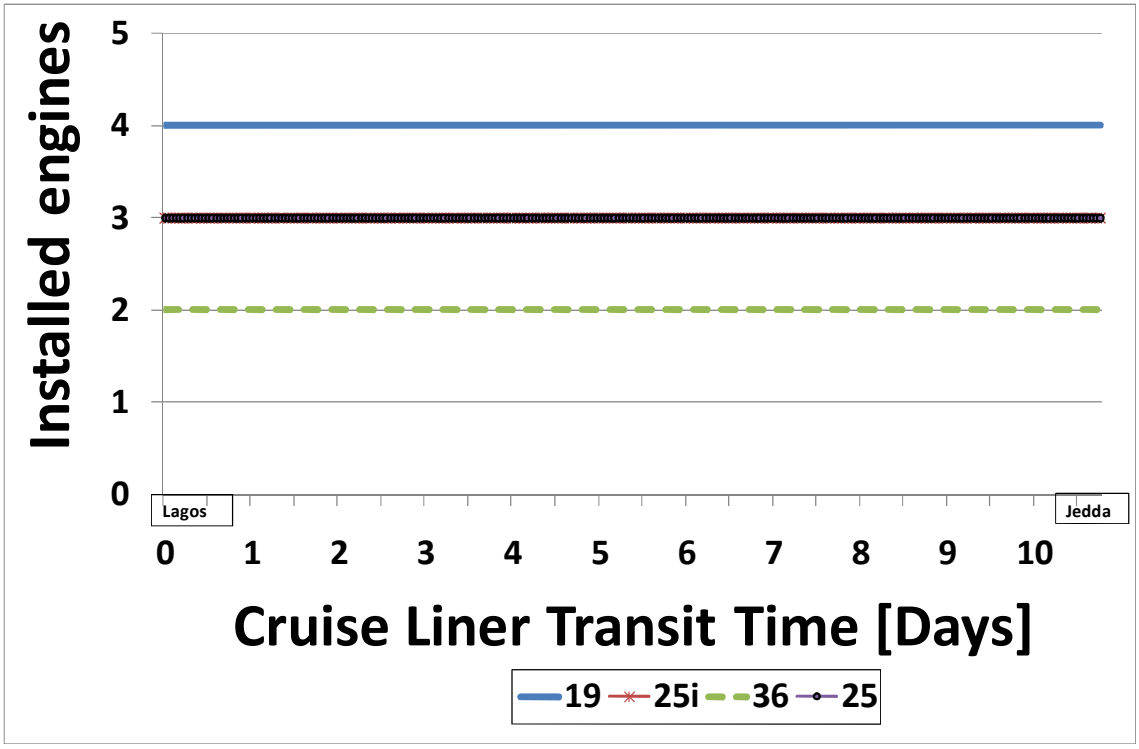

Figure 6:14 Illustration of the number of engines required to form the power plant of the cruise liner

6.5.2.1 Configuration of the power plant

The power plant configuration is illustrated in Table 6:6 showing the installed power capacity expected to be generated by each of the gas turbines. The configuration consisting of the 19MW model possesses the highest capability and enough flexibility to meet part load operating scenarios by engaging the lowest number of engines whenever the need arises. However, the combination of its four engines and full capacity does not compare well with the performance of the other models in the worst case scenarios. This is especially so under severe hull fouling conditions as illustrated in the plots for the variation of the brake power from Figure 6:15 to Figure 6:17. This scenario may be attributed to the transmission losses from the output shaft to the propeller.

An evaluation of the brake power was further conducted for voyages undertaken during the three different seasons covering all the investigated scenarios so as to determine the effect of deteriorating operating environment on the performance of each GT model as can be seen in the plots of Figure

6:15 to Figure 6:17. It was observed that under AWC conditions, each of them was able to satisfy the required propulsion power but when conditions were worsen by the different levels of hull fouling the 19MW and 36MW models were unable to meet the demand for PB. It shows how more of the brake power is required at each level of degraded operating condition and each of the gas turbines faired as detailed in Table 6:7and Table 6:8.

Table 6:6 Installed capacity and power plant configuration of the cruise liner

Installed Capacity of the Cruise Liner		
	Number of GTs	**Power**
19MW	4	76
36MW	2	72
ICR	3	75
SC	3	75

Table 6:7 Brake power increases imposed on the Cruise Liner's propulsion system under the investigated adverse scenarios in KW

Brake Power [KW]					
Sea States	**IWC**	**AWC**	**HR1**	**HR2**	**HR3**
0	29120.05	-	-	-	-
2	-	29487.79	33116.05	35706.27	37547.69
3	-	30185.93	33827.26	36430.04	38277.24
4	-	31748.28	35425.83	38050.27	39913.63
5	-	35096.39	38841.52	41515.13	43410.56

Table 6:8 Percentage deviation of the brake power from IWC

Brake Power [%]					
Sea States	**IWC**	**AWC**	**HR1**	**HR2**	**HR3**
0	0	-	-	-	-
2	-	1.259378	13.71859	22.61328	28.9366
3	-	3.653191	16.15686	25.09437	31.43733
4	-	9.01429	21.64189	30.65346	37.05168
5	-	20.50657	33.3658	42.54589	49.05402

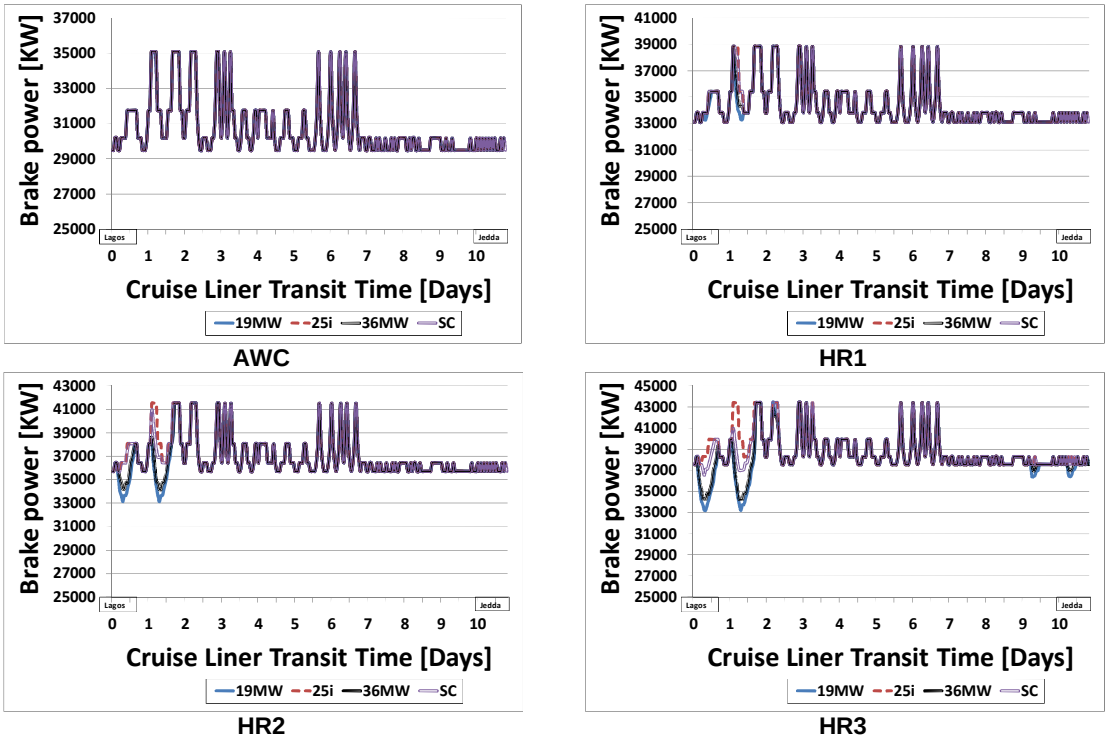

Figure 6:15 Consequence of variation in the operating environment of the cruise liner during its voyage along its fixed transit route in winter

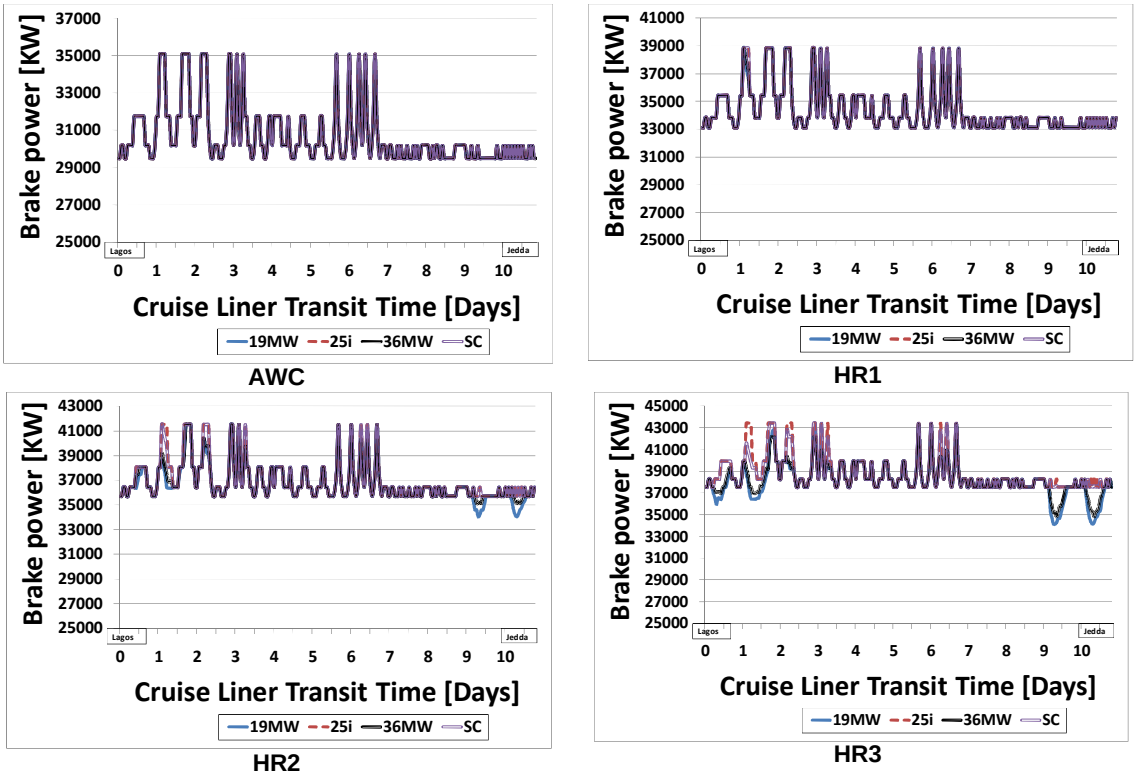

Figure 6:16 Consequence of variation in the operating environment of the cruise liner during its voyage along its fixed transit route in spring

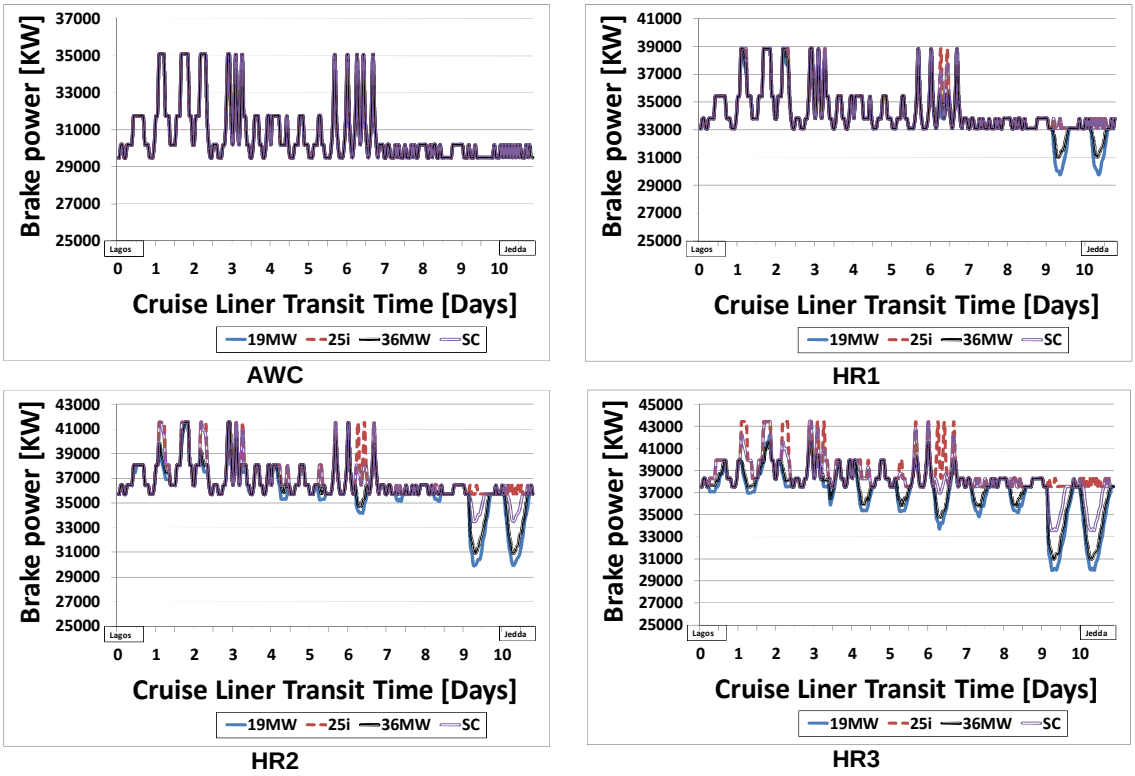

Figure 6:17 Consequence of variation in the operating environment of the cruise liner during its voyage along its fixed transit route in summer

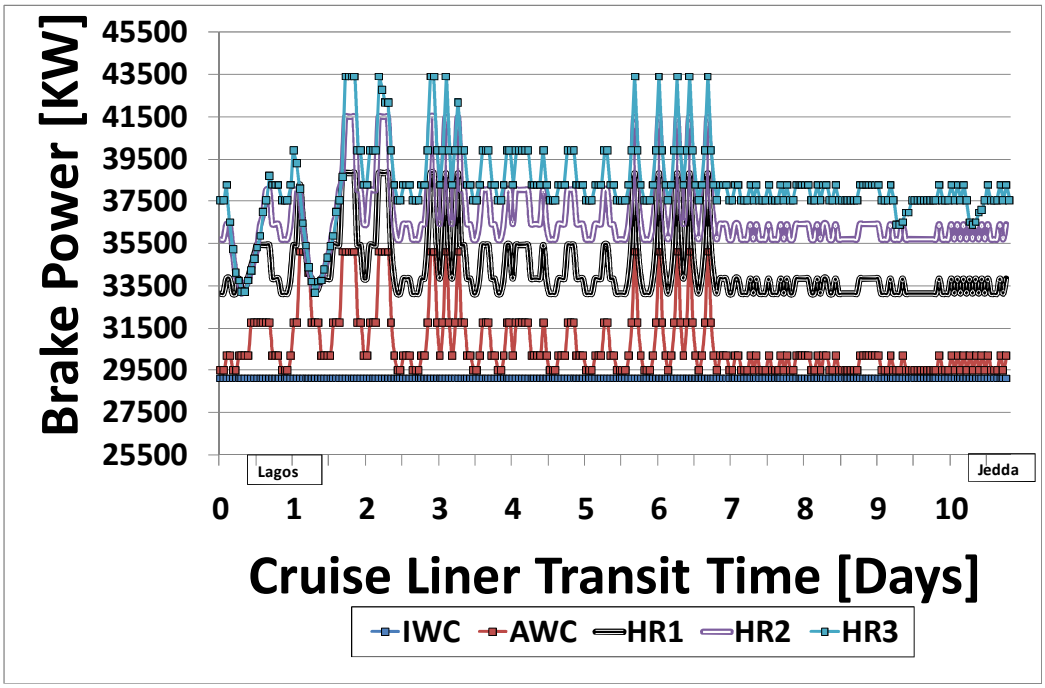

Figure 6:18 Variation of propulsion power of the cruise liner under the variety of investigated scenarios

The winter voyage shows how the 19MW and 36MW models were affected by a combination of higher ambient temperatures with sea states of 5 in addition to a hull fouling of 120µm during the second day of the voyage. This became more pronounced with increases in hull fouling at the HR2 and HR3 scenarios. The results show how the trend continued to deteriorate when the voyage is undertaken in spring season and worsens even further in summer due to temperature rise.

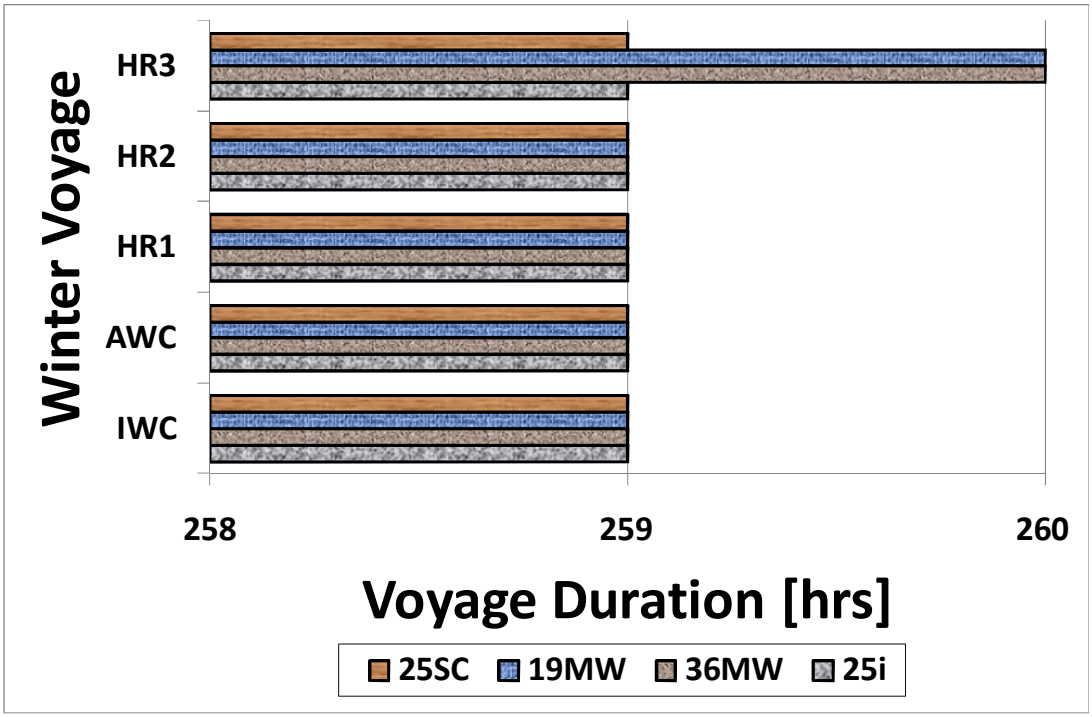

Figure 6:19 Voyage duration of the Cruise Liner in winter

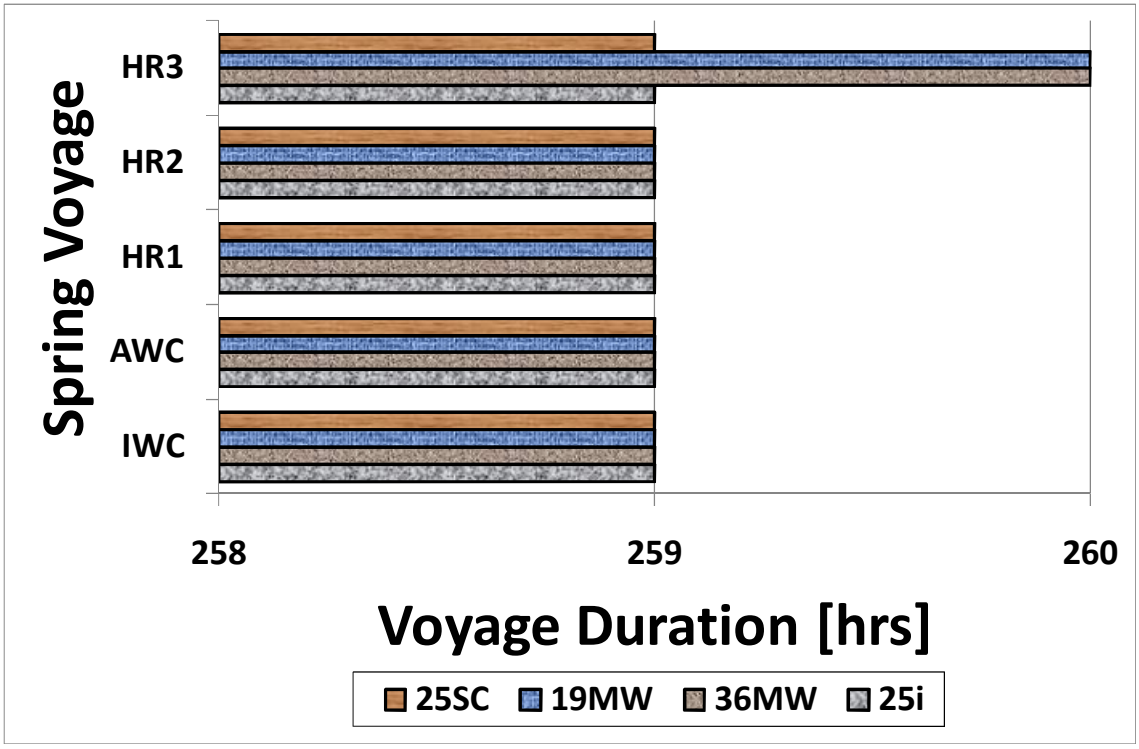

Figure 6:20 Voyage duration of the Cruise Liner in winter

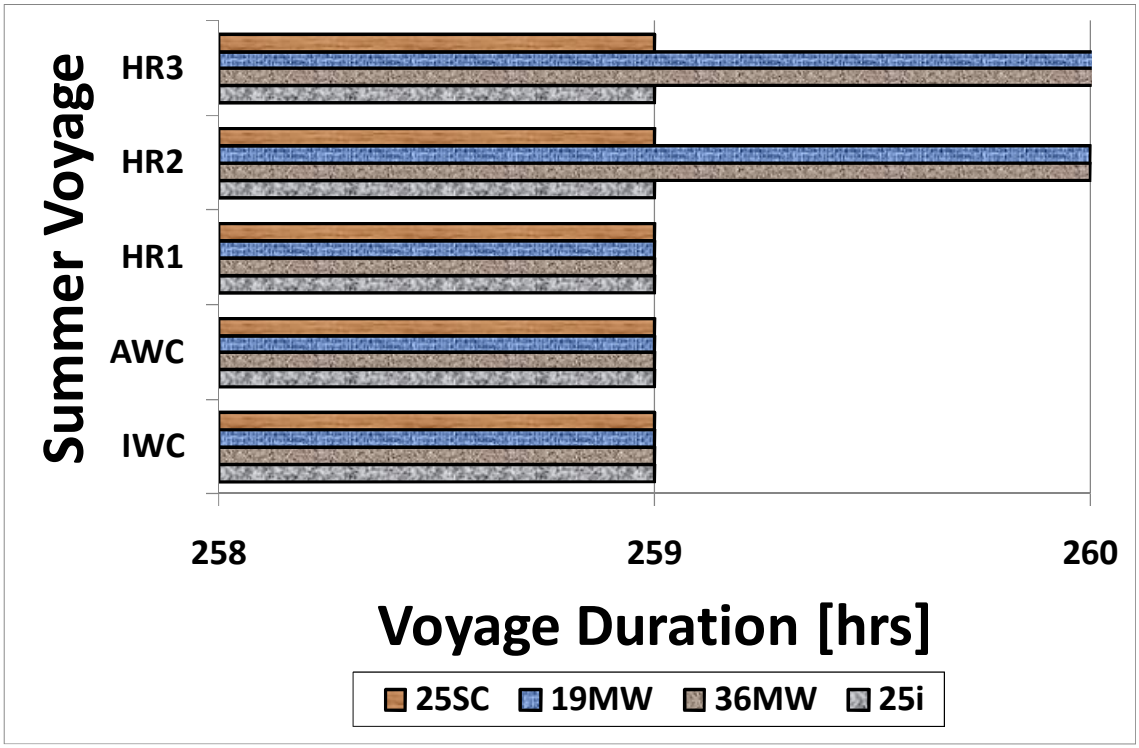

Figure 6:21 Voyage duration of the Cruise Liner in summer

6.5.3 Voyage of the Fast Speed Ferry

Under IWC, the PB demand is steady at 38753.46KW as influenced by the effect of rough weather in the Mediterranean Sea when the ferry transits between Malta and Marseille. The maximum severity expected to be encountered was found to be a sea state of Beaufort scale value of 3. The PB requirement rose to 39890.037KW at a sea state of 3 before dropping down to 39103.643KW at a sea state of 2 and hull fouling influenced an elevation of power requirement even further.

Table 6:9 Configuration of power plant for the FSF

Installed Capacity of the Fast speed Ferry		
GT models	**IWC**	**AWC**
	No. of GTs	**Power [MW]**
19MW	2 (3)	38 (57)
36MW	1	36
ICR	2	50
SC	2	50

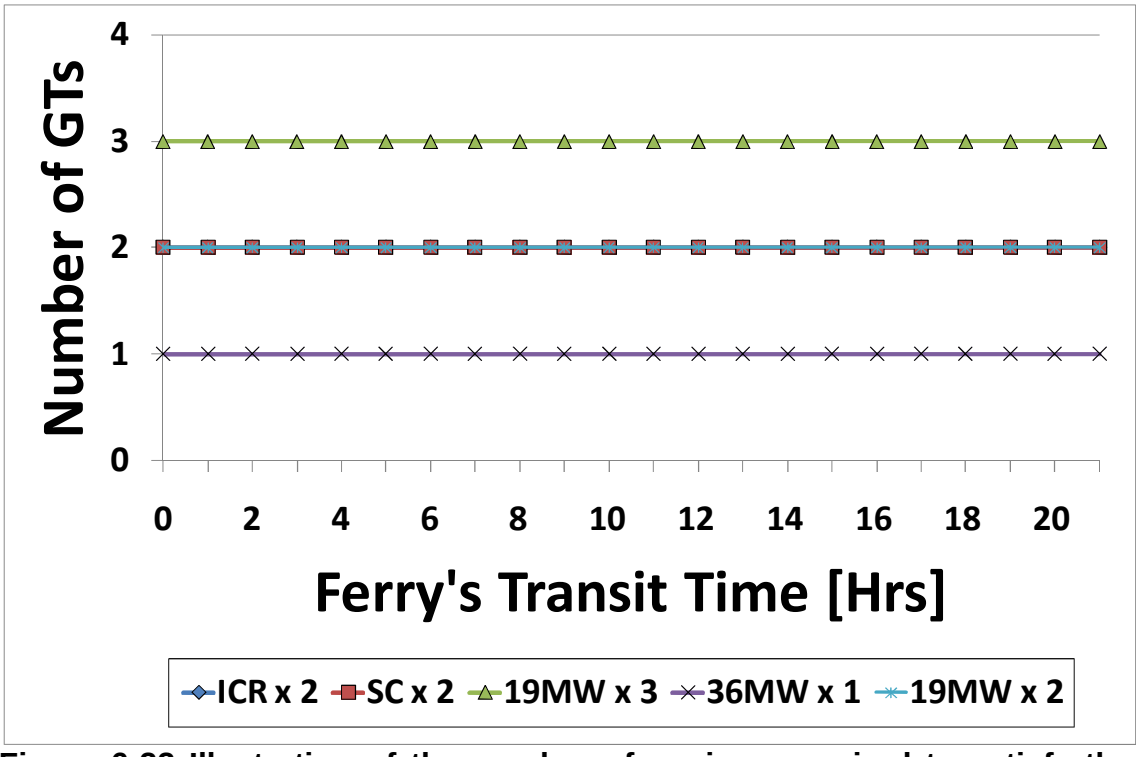

Figure 6:22 Illustration of the number of engines required to satisfy the propulsion power demand of the Fast Speed Ferry

The power plant profile illustrated in Figure 6:22 show the number of gas turbines that are appropriate for constituting the power plant of the fast ferry according to the different GT models of the research. For the 25MW models of the SC and ICR, only 2 units were found to be capable of meeting the propulsion power requirement. The investigation revealed that the combined installed capacity of 50MW was enough for overcoming the severe conditions expected along the fixed trade route of the Fast ferry without speed losses. The bigger 36MW unit however, could only be installed as a single unit and was only capable of sustaining the ship's service speed during IWC as well as AWC but significant loss of power and speed under hull fouling conditions. This GT model therefore was found to be incompatible when compared to the other models.

In the case of the 19MW model, the research evaluated two possible options in which two or three engines could be installed to add up to a total capacity of either 38MW or 57MW. Figure 6:23 to Figure 6:25 illustrate the variation of the brake power when either of the two options is selected as the propulsion plant for the Fast speed ferry. The flexibility with which any number of can be applied and the adequate redundancy for overcoming unexpected severe operating conditions are the advantages that endear the 19MW model to be a more favourable prime mover for the FSF among all the GT models of the research.

Figure 6:26 and Figure 6:27 illustrate the variation of the FSF speed when only 2 19MW gas turbines are utilized as the power plant.

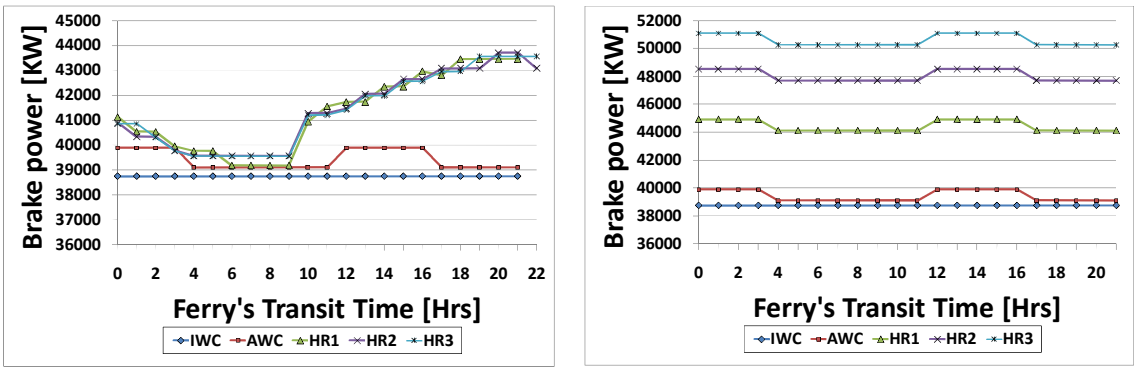

Figure 6:23 PB comparison of the 2-engine and 3-engine power plant configuration of the 19MW model in winter sail

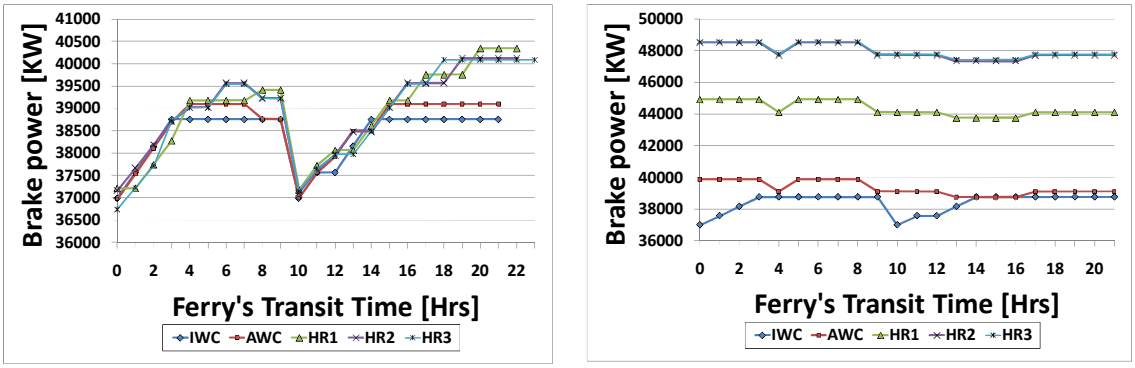

Figure 6:24 PB comparison of the 2-engine and 3-engine power plant configuration of the 19MW model in mid season sail

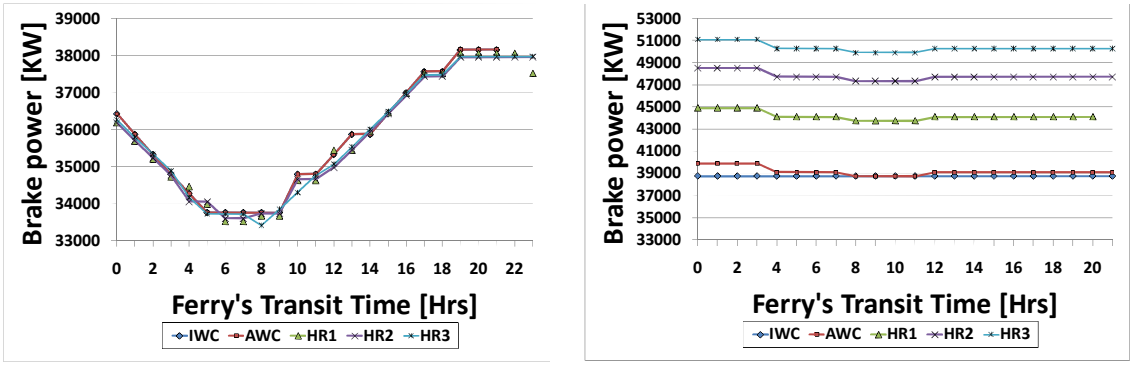

Figure 6:25 PB comparison of the 2-engine and 3-engine power plant configuration of the 19MW model in summer sail

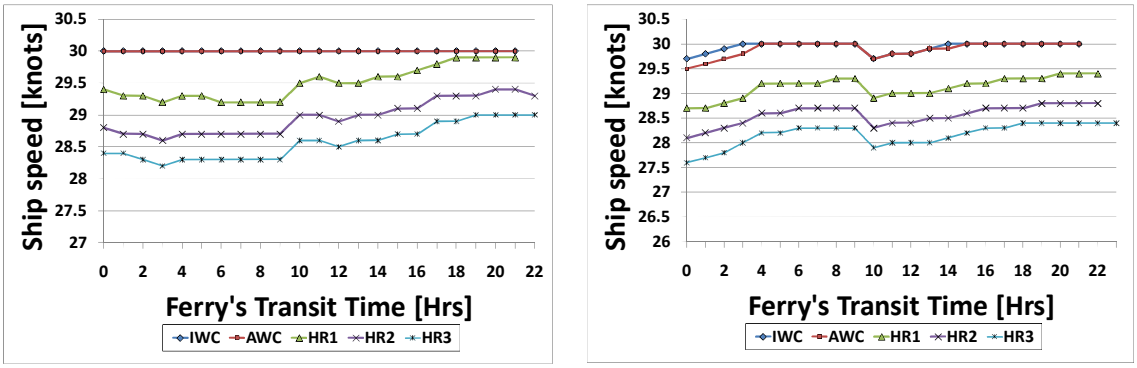

Figure 6:26 Comparison of the FSF speed variation between winter and mid season for the 2 19MW-GT option of the propulsion plant

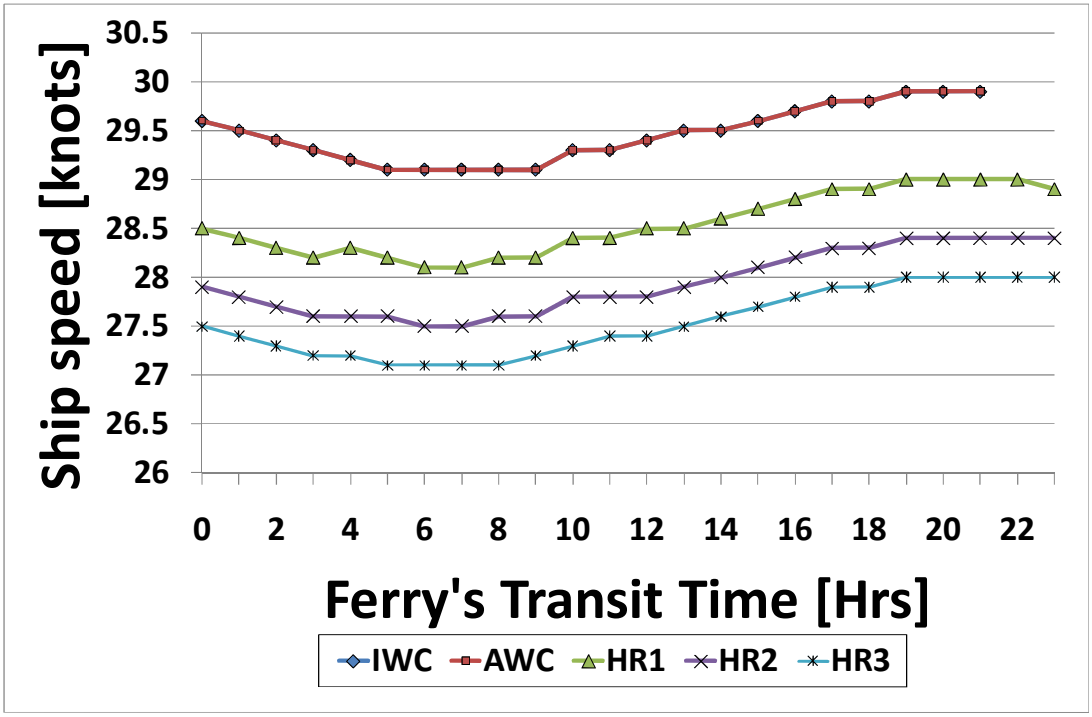

Figure 6:27 FSF speed variation in summer for the 2 19MW-GT option of the propulsion plant

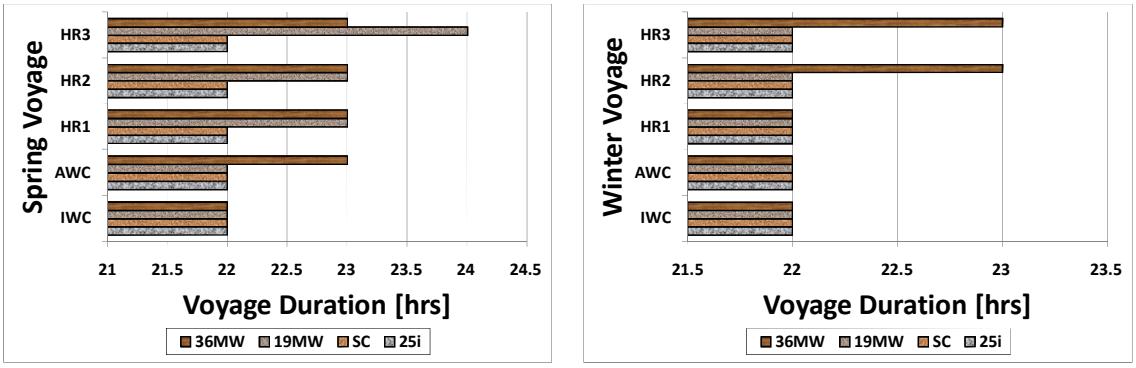

2 x 19MW 3 x 19MW

Figure 6:28 Comparison of winter voyage durations for the FSF with 2 or 3 19MW GT models are installed as prime movers.

An analysis of the voyage duration further revealed the benefits of the 2 options of the 19MW model along with the other models. It also shows how the single engine configuration of the 36MW model lacks the redundancy required to satisfy the power demand in severe adverse operating conditions.

6.5.3.1 Ship Routing

With a known or expected rough weather pattern on the ocean obtained from weather routeing departments, connected with meteorological institutes, an optimum ship's route, with respect to a minimum travelling time, fuel consumption or risk of damage, can be found. The prediction of the ship's reaction to wind and waves and the ship's speed in particular, is usually based on routeing experience with the ship under consideration, or with similar ships [64].

Since the ship's behaviour depends upon the presence or absence of waves, it may be reasonable to question whether overall performance can be improved by avoiding the more severe waves. The methodology involved in the conduct of this research therefore may be found to be useful in predicting ship speed losses in various ocean areas to help find an optimum route that could achieve significant savings in terms of voyage times and fuel burned.

In this investigation, the performance of gas turbines was monitored based on an hourly interval with the ship travelling along a designated route from the port of loading to the port of discharge and values the air mass flow, TET, thermal efficiency SFC, compressor outlet temperature (COT), pressure ratio (PR), etc were predicted. In addition, the pollutant emissions of NO_x CO_2, CO and UHC were also monitored and predicted as well as the HP turbine blade life. This was to ascertain effect of prevailing environmental conditions (pressure and temperature of the air at compressor inlet) on the gas turbine output [65; 66] [67]. An added input of the estimated auxiliary power necessary for onboard services was assumed for each of the vessels, the sum of which made the total power expected to be generated by the entire power Plant.

For each voyage completed however, the total quantities of fuel consumption (kg), HP blade life consumption (hrs), and all four pollutant emissions quantities (g/s), the voyage transit time (hrs) and its range (nm) were predicted. Each journey scenario was repeated for each of the three seasons under consideration in order to ensure a comprehensive evaluation of the results.

In addition to the different seasons and how they affected the gas turbine performance, the study also considered the effect of adverse weather over ideal weather conditions as well as the significant impact of hull roughness due to degradation caused by possible fouling and corrosion. The roughness caused by these factors was considered and simulated with values taken to be 120μm, 240μm and 360μm and repeatedly simulated accordingly. By this, the performance estimation and sea worthiness of each vessel installed with either of the gas turbines could be compared in each case scenario.

6.5.4 Effect of adverse Operating Conditions on Fuel Consumption

In the case of the cargo ship under consideration, the Specific Fuel Consumption SFC) of the fleet of gas turbines was investigated under IWC Figure 6:29, as well as the adverse conditions that make up the other scenarios of the investigation Figure 6:30. The results for winter simulation have mostly been selected for presentation in this text having considered it as the most severe season in comparison to the others.

6.5.5 Variation of the SFC

Under IWC, the OD performance output of the four models generated a SFC below 235g/KWh. Of particular interest that of the ICR model with a very high efficiency, giving a SFC of a little over 200g/kWh until they encountered severe weather conditions and when the underwater hull surface is fouled as a result of which the gas turbine operating temperatures had to be elevated to their highest limits.

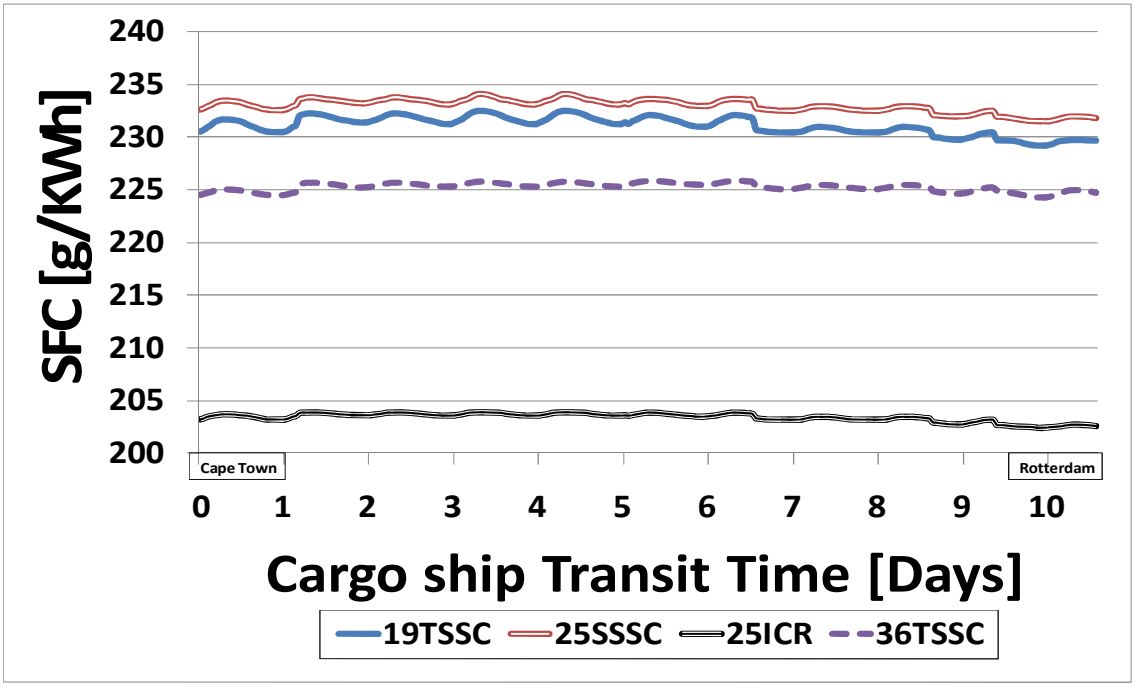

Figure 6:29 Variation of SFC under IWC with a clean ship hull in winter

6.5.6 Prediction of Fuel Burned

The quantities of fuel consumed per voyage was analysed to compare the efficiency of the gas turbine models in respect of the vessels and in consideration of the effect of weather and sea conditions. The results reveal how the operating costs of marine gas turbine propulsion systems can be affected by the cycle configuration based on the selected investigated scenarios of this research.

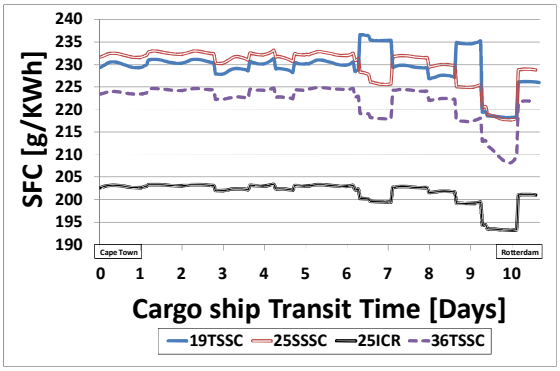

AWC with a clean hull

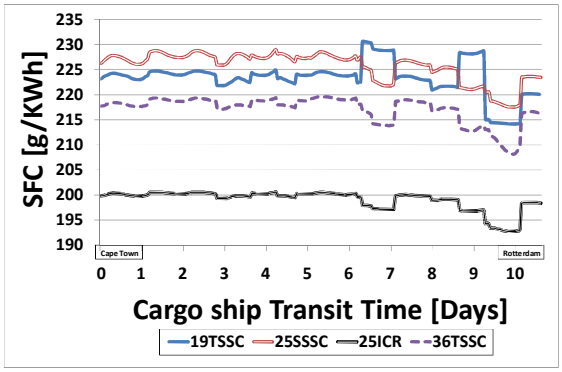

Fouled hull 120μm

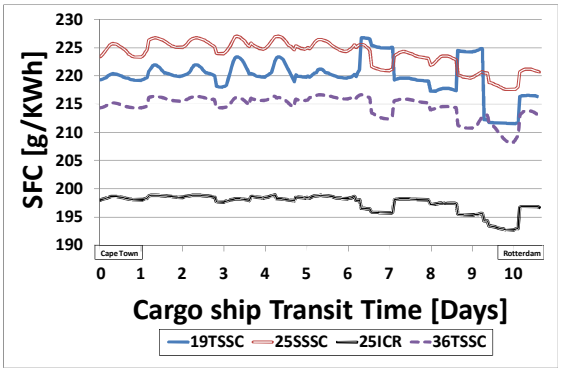

Fouled hull 240μm

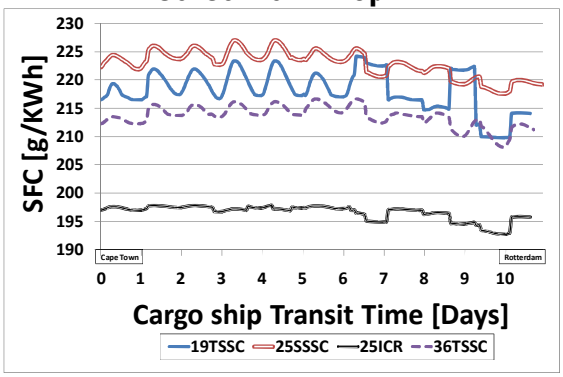

Fouled hull 360μm

Figure 6:30 Variation of the SFC of the GTs for the cargo ship under adverse weather and sea conditions

6.5.6.1 Voyage Analysis of Fuel Burned

As an example in this section, the analysis of the voyage of the cargo ship is presented for both IWC and AWC in Figure 6:31 and the daily consumption rates for every GT model is detailed in Table 6:10. Under IWC, the highest quantity of FB at 331.6 tons was consumed by the 5-engine power plant of the 19MW model and the least consumption was that of the ICR model at 250 tons only. The analysis show the effect of AWC as the consumption rate of the ICR jumped higher by 19% while that of the 19MW model recorded only about 3% increase between IWC and AWC scenarios. A further investigation revealed that hull fouling influences further degradation of the fuel consumption per voyage as exemplified by the details in Figure 6:32 for a voyage under HR1 and HR3 investigated operating scenarios. The difference between the FB quantities in winter and summer is predicted in Figure 6:33.

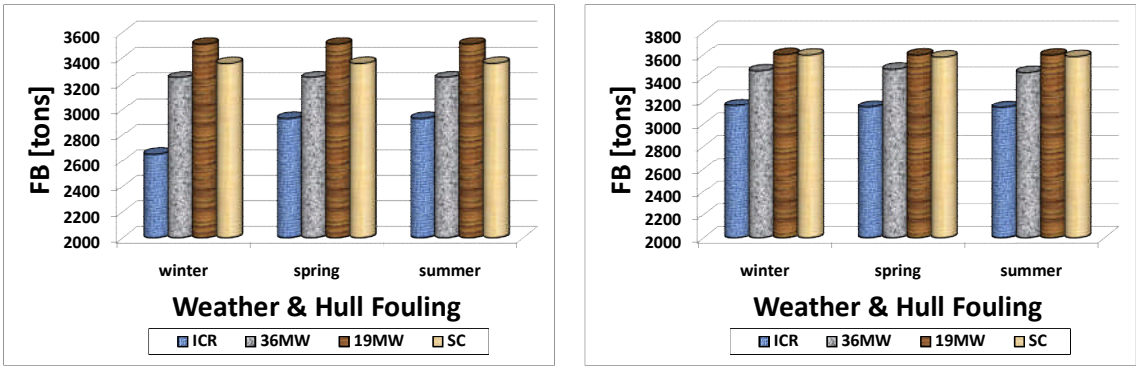

Figure 6:31 Comparison of the quantities of FB per the cargo ship voyage when operated under IWC and AWC.

Table 6:10 Quantities of daily FB for each of the GT models when operated under IWC and AWC

Cargo ship FB per day [tons]			
GT models	**IWC**	**AWC**	**% Increase**
SC	317.1	340.0	7.2
19MW	331.6	340.3	2.6
36MW	306.6	327.3	6.7
ICR	250.7	298.7	19.1

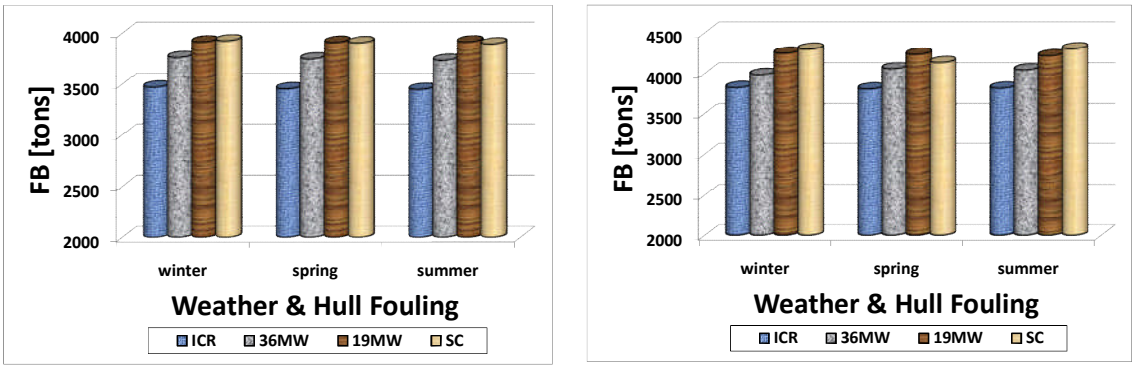

Figure 6:32 Voyage FB under HR1 and HR3 operating scenarios of the cargo ship in winter

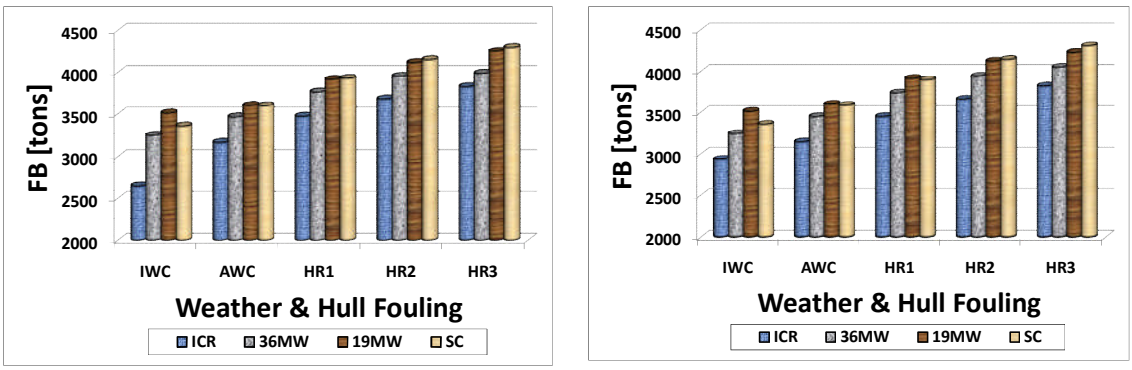

Figure 6:33 FB quantities between a winter voyage and that of summer

6.6 Analysis of Engine Exhaust Emissions

In the past when the gas turbine was known to have a clean and efficient steady flow process of combustion that burns fossil fuel by using a large amount of air in order to keep the turbine entry temperature (TET) at an appropriate value, there was little concern about their exhaust gas emissions for many years except to eliminate the visible smoke coming out from the exhaust. But this changed when the population of gas turbines increased and the issue of emissions control has now probably become the most important design and operating factor for land-based and marine gas turbines and more in the field of aeronautics. Although the combustion efficiency of the gas turbine is typically between 98.5% and 99.5%, the 0.5 to 1.5 percentage loss still results in the promotion of two toxic pollutants in the form of unburned hydrocarbons (UHCs) and carbon monoxide (CO). UHCs are known to have the characteristic smell usually found in airport environments while CO is both colourless and odourless. The correlations that define their composition including those of NO_x and CO_2 have already been explained in chapter 2.

6.6.1 Operational Considerations

The problem of how to control emissions is made more complicated by the fact that gas turbines can be operated over a wide range of power and ambient conditions. The off design performance prediction shows that the simple cycle and the advanced cycle configurations have widely varying operating characteristics by which the all behave differently.

6.6.2 Comparative Emissions Patterns under Ideal climate

The single most important factor that particularly affects the formation of NO_x, is the flame temperature which is theoretically at maximum at stoichiometric conditions and will fall off at both rich and lean mixtures [68]. The formation of this exhaust emission product can be reduced by operating well away from stoichiometric conditions but only at the risk of increasing the formation of both CO and UHC. Therefore the rate of formation of NO_x varies exponentially with

the flame temperature and reducing the value of this operating parameter is a key to the reduction of NO_x. Although it reduces the formation of both CO and UHC, another important factor that slightly affects the formation of NO_x is the residence time of the mixture in the combustor. Here again the pollutant emissions analysis code "APPEM", that was used in conjunction with TURBOMATCH and Poseidon is worthy of note.

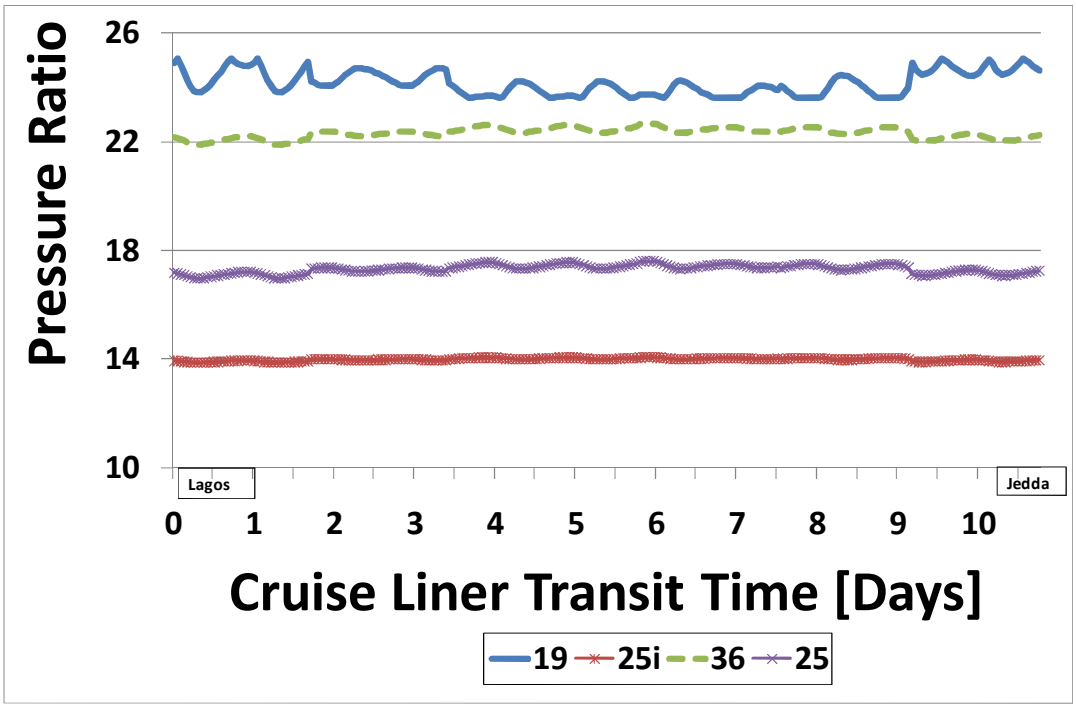

(a) winter

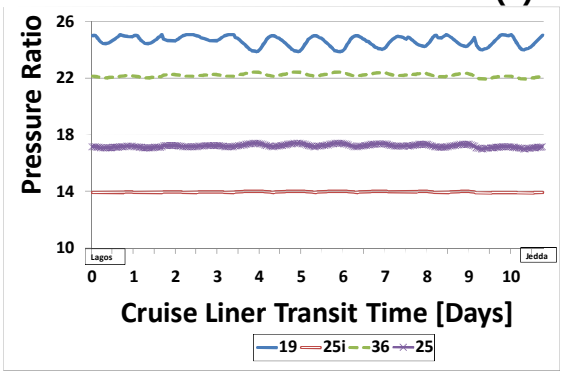

(b) spring

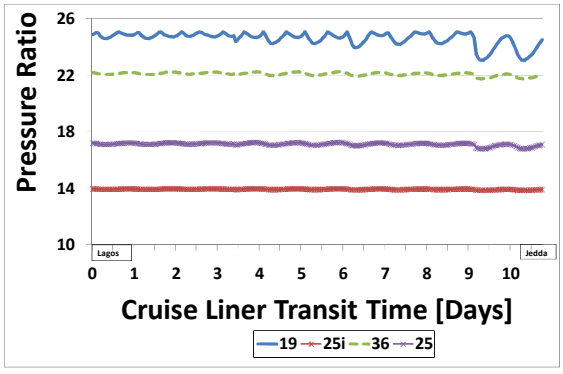

(c) summer

Figure 6:34 Comparison of the Pressure Ratio variation for the Cruise Liner under ideal weather conditions

As the rate of formation of exhaust pollutant emissions depends on the internal conditions of the combustor, this work seeks to realise the relationship between emissions and the key cycle parameters of pressure and TET as illustrated for

the Cruise liner in Figure 6:34 and Figure 6:35. This means that the emissions are a function of the basic cycle parameters as was discovered by Lipfert whose work revealed that NO_x emissions increased with combustor inlet temperature [69].

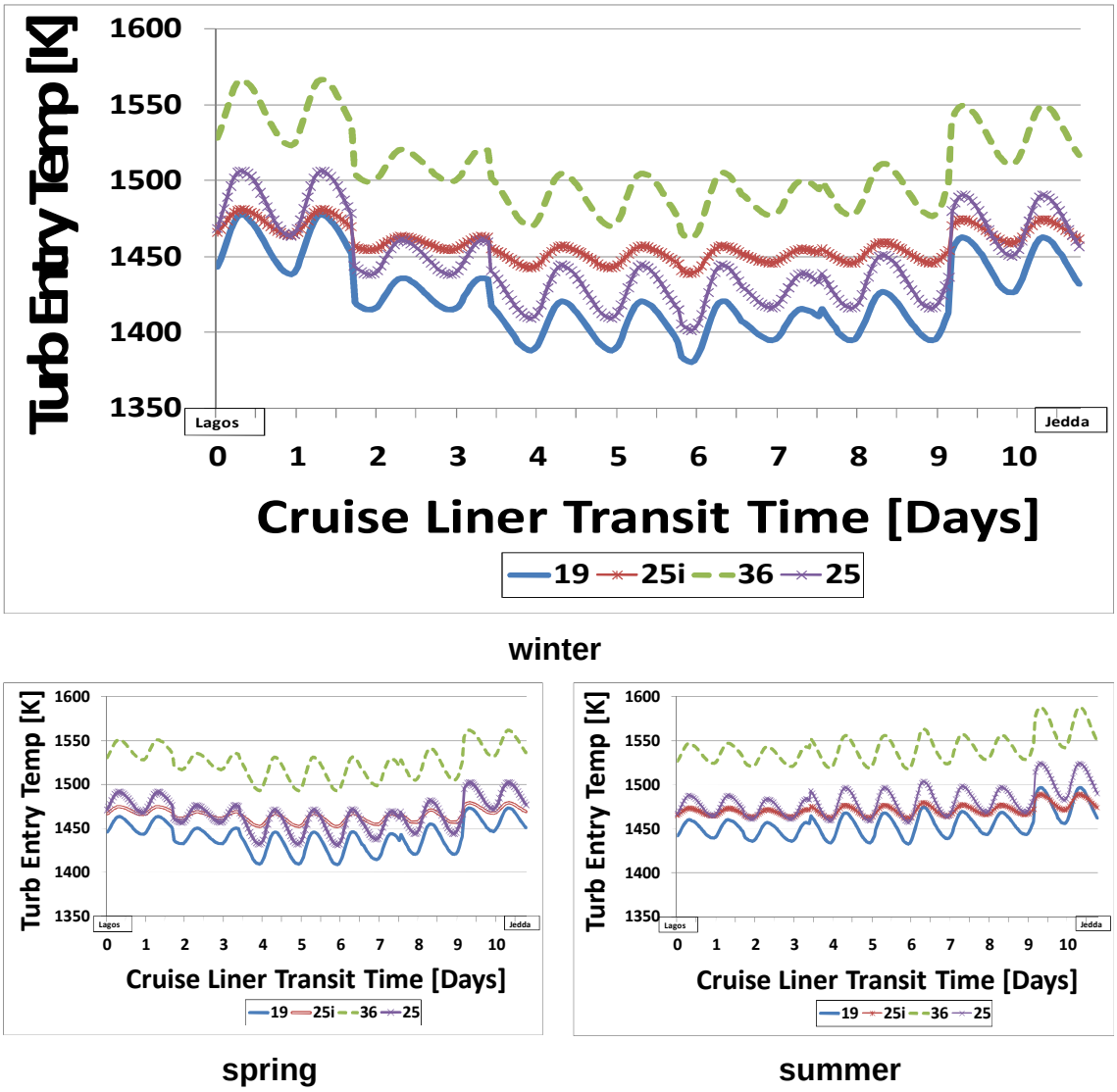

Figure 6:35 Comparison of TET variation for the Cruise Liner under ideal winter weather

6.6.3 Seasonal Comparison of Emissions

In Figure 6:37 the 19MW model in relation to its lower operating temperatures (TET) combined with higher pressure ratios, demonstrated a unique behaviour in the emission of UHCs when compared to the other models.

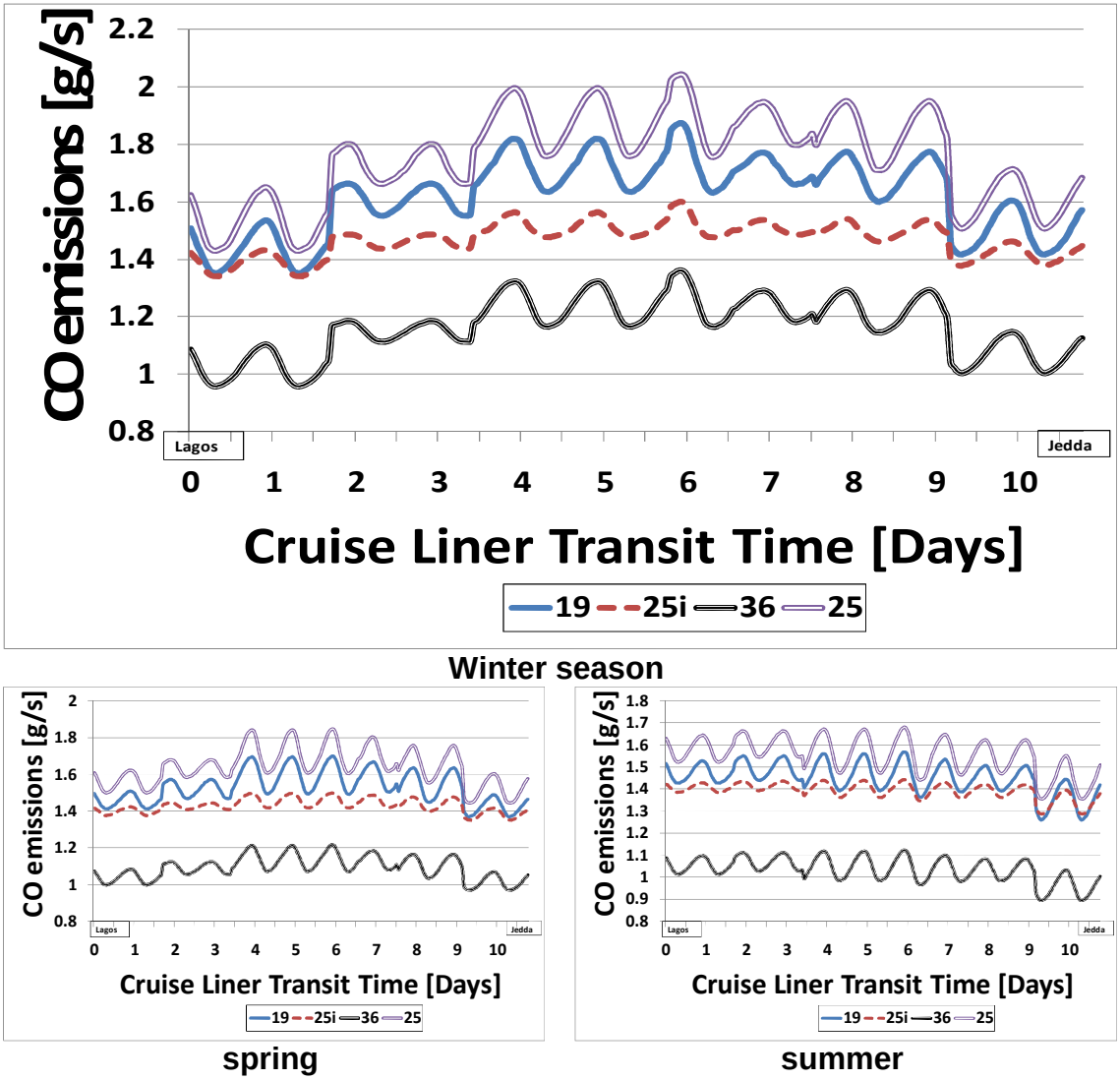

Figure 6:36 Emission of CO for the Cruise Liner in IWC.

The characteristic variation of the CO emissions appeared to be very interesting and still with particular focus on the 19MW two-spool, simple cycle model. In comparison with the other models, its operating pressure ratio is highest while the TET is lower than the design values.

The emissions output of the 25MW ICR model appears with relative stability in line with its favourable TET and OPR variations as it easily adapt any changes in weather or ship hull surface degradations.

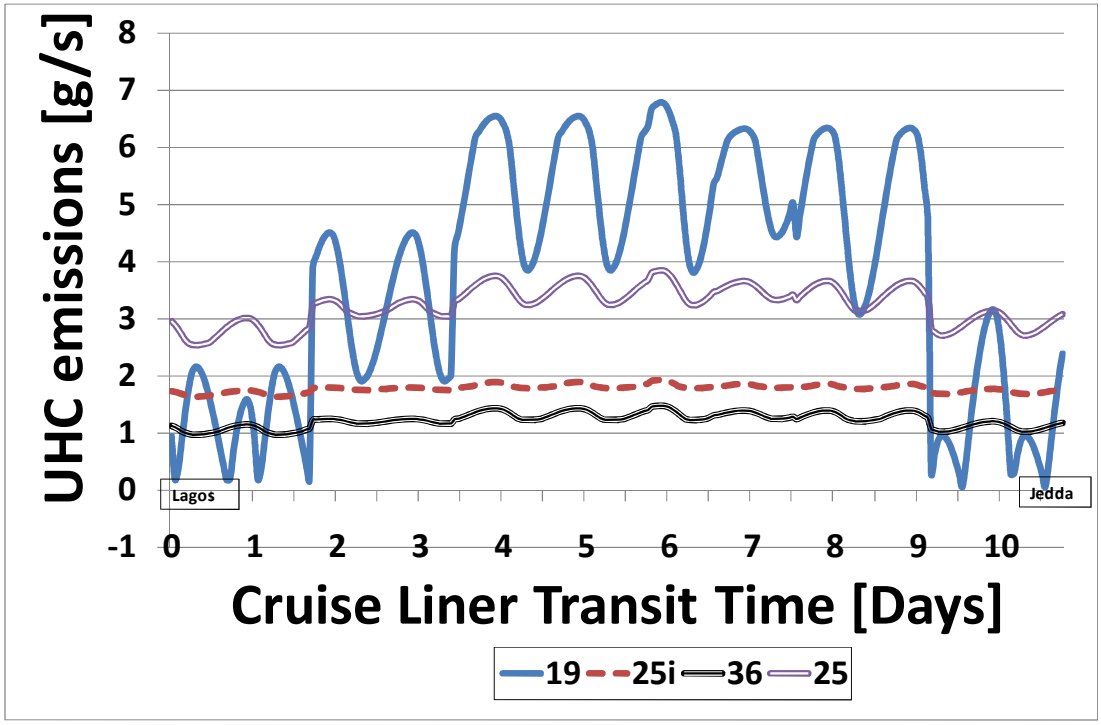

winter season

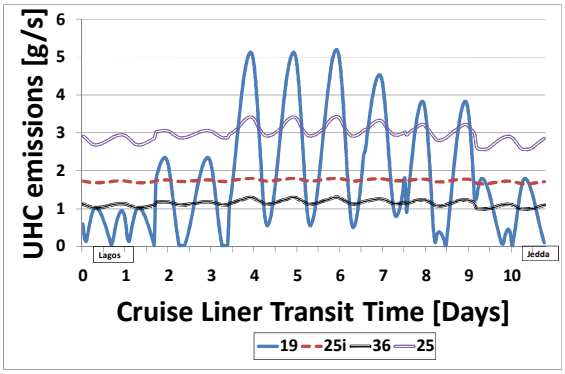

spring season

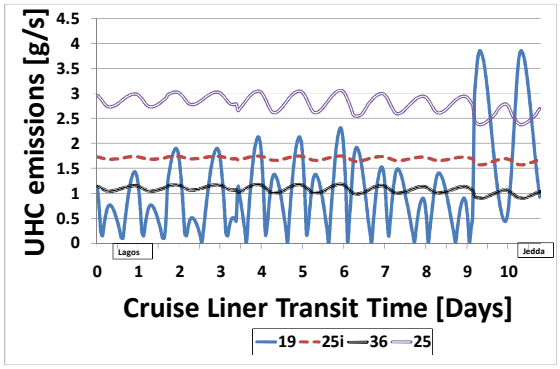

summer season

Figure 6:37 Emission of UHC for the Cruise Liner in IWC.

6.6.4 Predicted Quantities of Pollutant emissions

The cruise liner's pollutant emissions analysis is presented in this section to demonstrate how it was conducted for the other vessels of the research and Figure 6:38 illustrates the NO_x prediction per winter and summer voyages respectively. NOx emission levels were found to be lower with the ICR model followed by the SC mainly due to their lower overall compression ratios and higher TETs when compared to the dual spool simple cycle models of 19MW and 36MW respectively. The distinct design of the ICR with the incorporation of the inter-cooler and recuperator are the major factors that contribute to its low

pollutant emissions as it also records the lowest in terms of CO_2 as well. In the case of CO2 emissions for the other models however, the SC was found to emit more than the 19MW and 36MW models. In all., the difference between winter and summer emissions was predicted to be very insignificant.

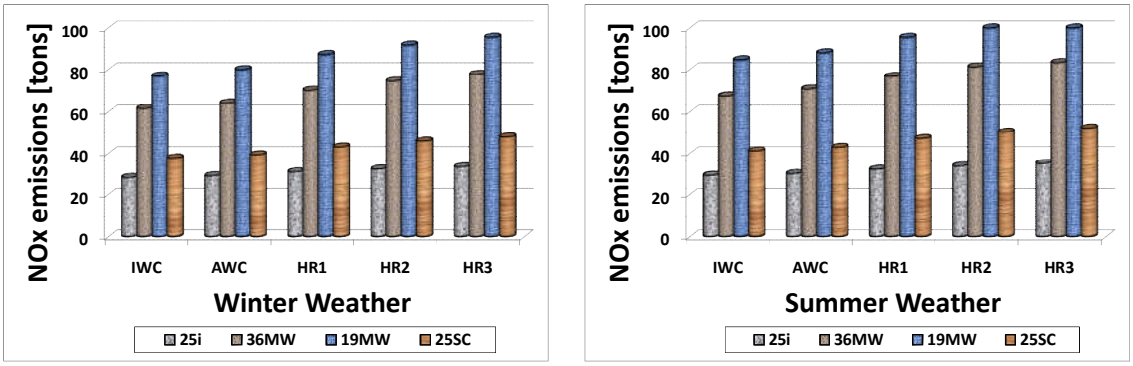

Figure 6:38 Pollutant emission of NOx for the Cruise liner in winter and summer seasons respectively

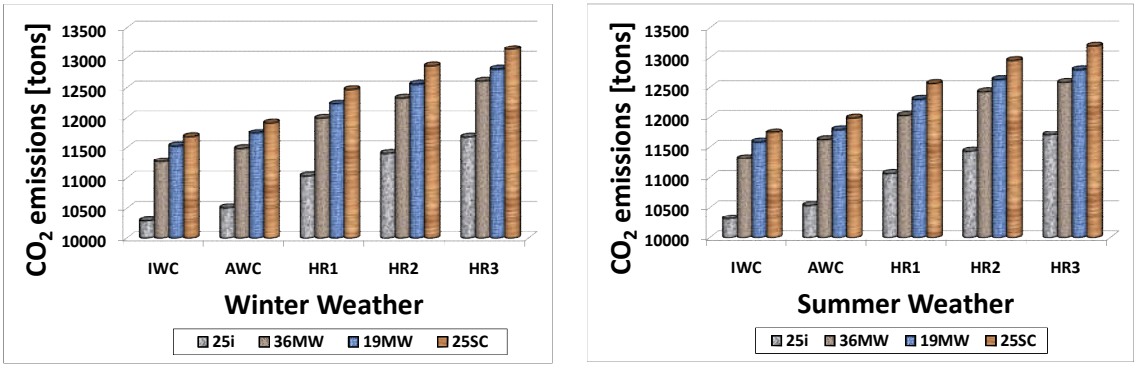

Figure 6:39 Pollutant emission of CO_2 for the Cruise liner in winter and summer seasons respectively

6.7 Analysis of HPT creep life

Temperature limitations are the most crucial limiting factors to gas turbine efficiencies and since the design of turbo machinery is complex and the thermal efficiency is directly related to material performance, material selection therefore is of prime importance. Comparing the three basic components that make up the gas turbine in its simplest form, compressor blades operate at a relatively low temperature but are highly stressed while the combustor operates at a relatively high temperature and low-stress conditions and the two contrasts with the turbine blades, which operate under extreme conditions of stress,

temperature and corrosion. Therefore, the required material characteristic in a turbine for high performance and long life include: limited creep, high-rupture strength, resistance to corrosion, good fatigue strength, low coefficient of thermal expansion and high-thermal conductivity to reduce thermal strain. The failure mechanism of a turbine blade is related primarily to creep and corrosion before considering the effect of thermal fatigue and satisfying these design criteria will ensure high performance, long life and minimal maintenance.

The creep-rupture phenomenon, which is a high temperature, time-dependent behaviour of a material was defined and modelled through the application of the “Larson Miller” parameter in section 3.1.3.1. This was included in the voyage analysis for all the ships and the gas turbine models of the project and aimed at determining the maintenance cost in each case. Apart from predicting the performance parameters through the voyage analysis, the primary assignment of this research is to determine the operating cost of the ships and the gas turbine models through a voyage analysis, the total fuel required for each single voyage was derived as has already been demonstrated. In order to be able to also predict the maintenance intervals and their associated costs, the life consumption per every trip were also predicted alongside the emissions as has alr5eady been analysed.

Considering the maximum operating pressures and temperatures given in Table 6:1 and Table 6:2, the failure time predictions for the different scenarios involving the cargo ship are presented in Figure 6:40. The plots reveal the environmental degradation of weather and sea resulting in variation of engine time-to-failure for the gas turbines whenever they operate along their scheduled transit route.

Another example of the prediction of HPT life consumption analysis is that of the passenger ferry as illustrated in Figure 6:41and Figure 6:42.

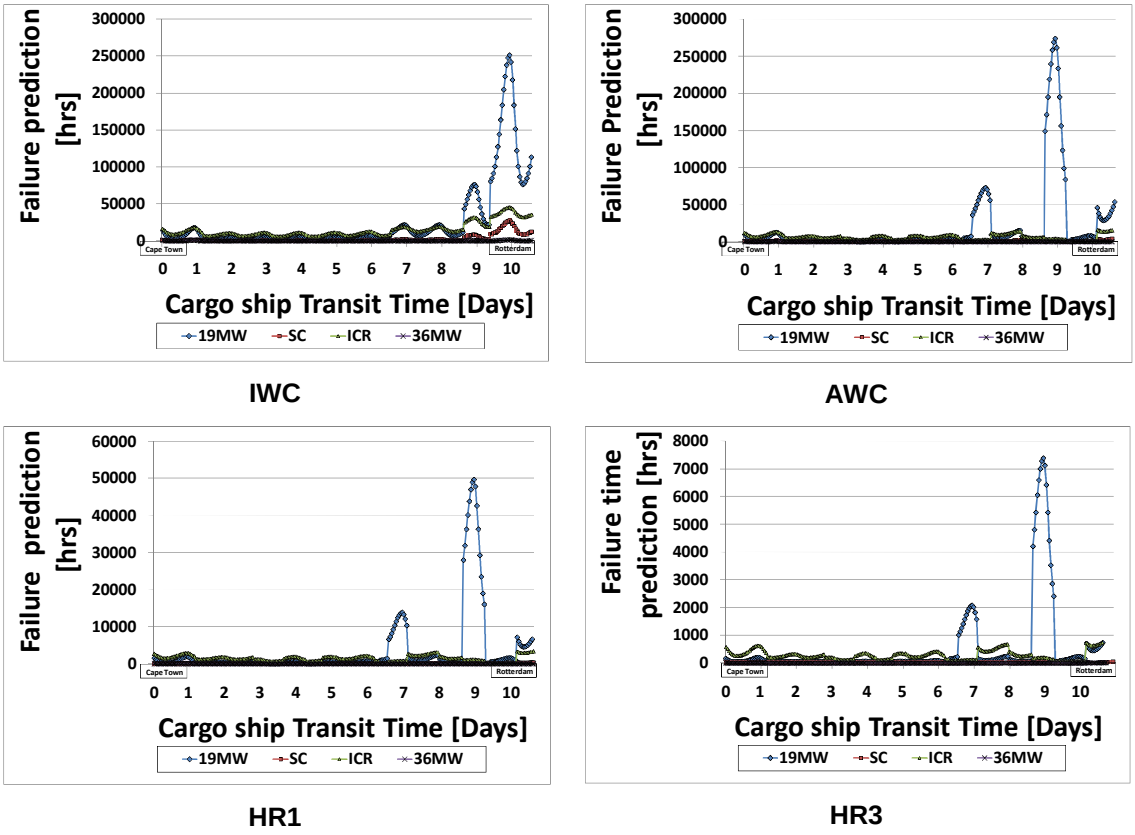

Figure 6:40 Prediction of engine Time-to-failure for cargo ship voyage under the designated investigated scenarios in winter season

The analysis reveal how the 19MW model operated on the cargo ship was found to be more economical in terms of its life consumption than the others due to the lower TETs under which it could operate. However, a penalty for this relative gain in the life consumption may be imposed by the installation costs due to the total number of engines in the layout of the propulsion power plant.

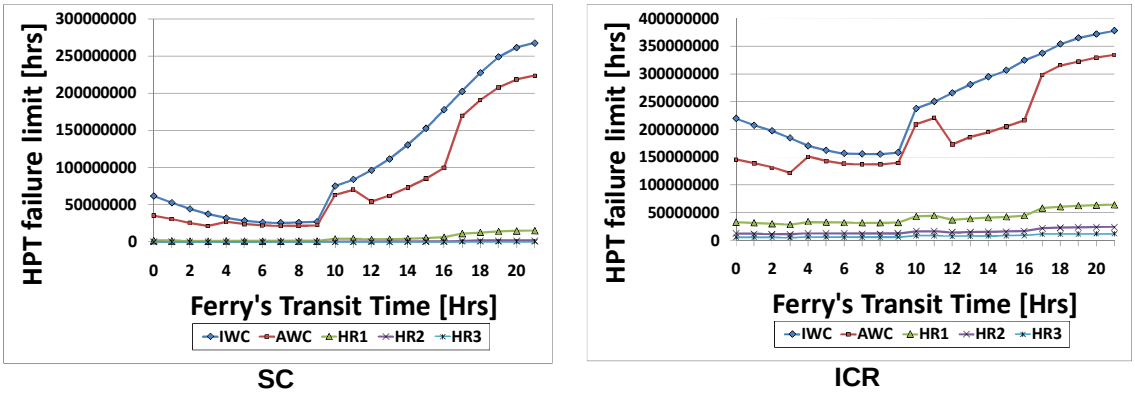

Figure 6:41 Engine failure limitations of the SC and ICR models of the passenger ferry

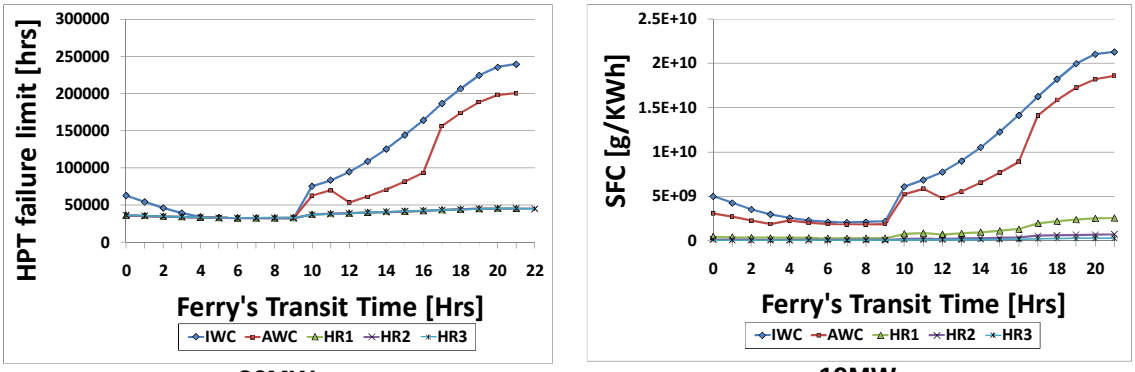

36MW 19MW

Figure 6:42 Engine failure limitations of the 36MW and 19MW models of the passenger ferry

6.7.1 Prediction of Life Consumption

The life consumption for each of the models was also investigated for each of the vessels of the project as analysed in some of the illustrations in Figure 6:43, Figure 6:44 and Figure 6:45. The result show how the 36MW is installed as a single engine power plant and as a result, it is compelled to operate at higher power setting thereby, consuming more of its life than necessary.

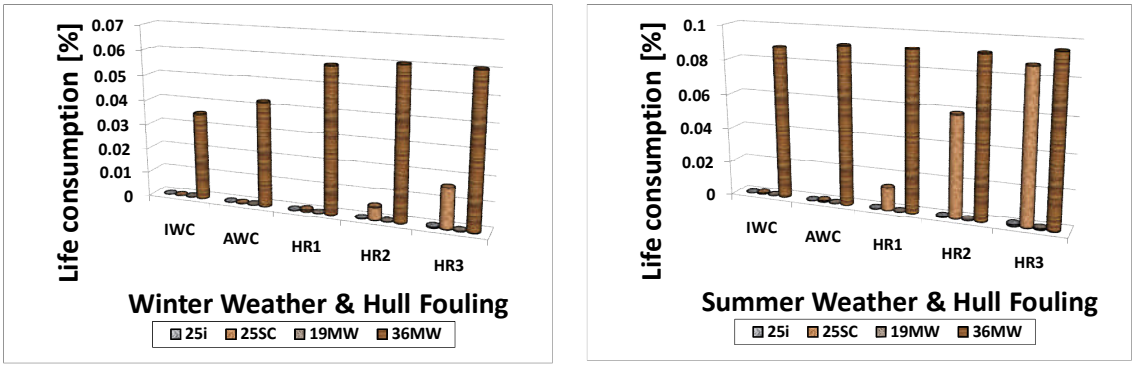

Figure 6:43 Comparison of the life consumption for the passenger ferry in winter and summer

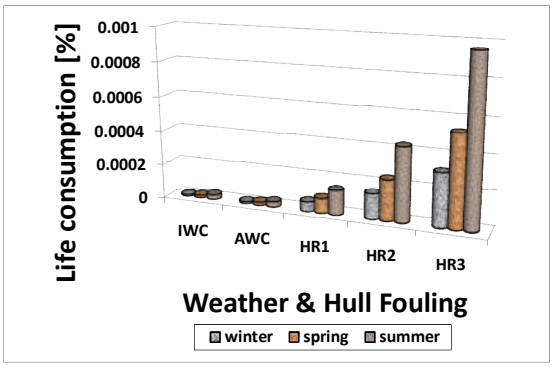

ICR

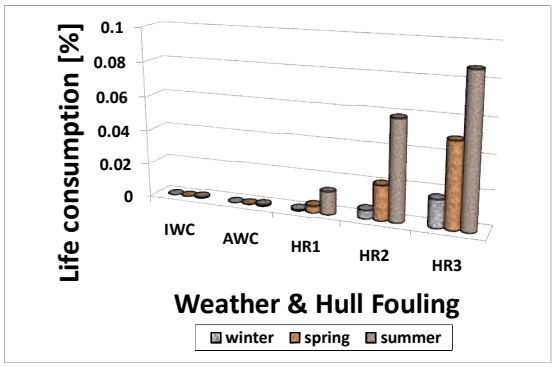

SC

Figure 6:44 Engine life consumption profiles of the ICR and SC models of the passenger ferry

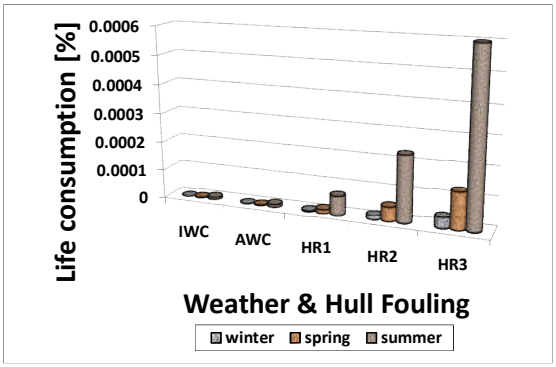

19MW

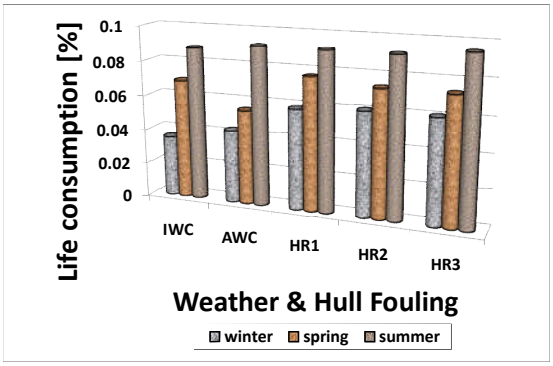

36MW

Figure 6:45 Engine life consumption profiles of the 19MW and 36MW models of the passenger ferry

7 CONCLUSION AND FURTHER WORK

7.1 Conclusions

The conclusions of the current research can be summarised as follows:

- The added complexity of the 19MW and 36MW dual-spool models of the research raised the thermal efficiency the thermal efficiency of the simple from 37% to 39.3% while the addition of a recuperator and an intercooler was able to achieve an efficiency of 42.6% when operated at standard sea level conditions.

- The evaluation of the effect of ambient operating conditions on gas turbine performance for the ICR model at a TET of 1550K showed generated a power output of 30.163MW when operated in cold weather at an ambient temperature of 0^{o}C but dropped to 24.733MW during hot weather operation at 40^{o}C.

- Among the variety of gas turbine cycles that constitute this research, the ICR model has demonstrated that when it is designed with the capability of recovering heat from the exhaust and aided by intercooling the compression process, the problem of part load operation can be overcome notwithstanding the disadvantage of added equipment and increased complexity.

- The use of an electric drive provides flexibility in the arrangement of the machinery since it is not mechanically linked to the propulsion shafting such that peak power requirements can be satisfied by multiple prime mover power generating sets. Such flexibility makes it possible for some of the prime movers to be taken offline thereby enabling the remaining ones to be operated within the range of their best efficiency.

- The hot and cold weather operation for each of the investigated GT models along the various trade routes conformed to the ratings of existing marine gas turbines of similar cycle configurations and power ratings. The 36MW

model was simulated at design point and a maximum power output of 55MW was generated when operated under an ambient temperature of -30^{o}C and at a maximum TET of 1600K but under a hot climate with an ambient temperature of +45^{o}C, the maximum power output dropped to 30MW only.

- The comparative voyage analysis of the variety of gas turbine models in this research shows how intercooling and exhaust heat recuperation elevates the thermal efficiency of the gas turbine thereby making its part load operation suitable even at low speed power requirements.

- A 50% gain in power output from the 36MW dual spooled simple cycle model also attracts about 40% increase in fuel flow when operated on a cold day.

- The brake power required for the propulsion of the 138,000m^{3} LNGC of the research at 19.5 knots was found to be 22.765MW when transiting through ideal weather conditions but this figure rose to 40MW when strong winds and high sea waves of Beaufort scale 6 were encountered in combination with a 360μm hull surface roughness existed due to fouling of the hull surface.

- In order to meet the power requirement necessary for overcoming the forecasted adverse weather and sea conditions expected to be encountered along the selected trade route, the assessment of the LNGC propulsion plant revealed that it required the installation of 2 units of both SC and ICR models, three 19MW but only a single unit of the 36MW.

- The investigated adverse conditions were capable of causing the LNGC speed to drop from 19.5 knots to the following values recorded during summer voyages:

    - Less than 9 knots with the 36MW model,

    - 14.6 knots in the case of the ICR

- 13.80 knots in the case of the simple cycle model
- 14.90 knots in the case of the three-engine configuration of the 19 MW model.

- Under the above conditions the duration of the voyage increased by:
  - 12 hours with the 36MW single engine configuration, making the vessel to take four days instead of three and half days before arriving at the discharge terminal thereby attracting a higher late delivery penalty than the rest of the models.
  - The three engine propulsion plant of the 19MW model generated the most satisfactory result compared to the other models of the research.

- A comparative analysis of the models with regards to fuel consumption showed that the ICR engine is capable of competing with the diesel alternative based on a SFC of between 192 g/kWh and 197 g/kWh.

- The natural BOG rate was estimated at 0.15% of the LNG cargo per day under ideal weather conditions, the quantity released per voyage was only 70% of the total fuel requirement for the gas turbines. Either the dual fuel configuration or a forced BOG system will have to supply the balance.

- The 36MW model was revealed as the most suitable for the propulsion of the cargo ship as a result of the redundant power left in reserve and was found to be capable of reaching a speed of over 26 knots against it service speed of 25 knots.

- The benefits of the ICR model were significantly demonstrated in all the scenarios of the investigation on all the ships. It was capable of propelling the cargo ship at a speed of 16 knots with a SFC of about 210 g/KWh while the a combination of two 19MW units generated a SFC of 235g/KWh, 250g/KWh and about 280g/KWh for the SC and 36MW models respectively.

7.2 Recommendation for Further Work

- The configuration of the various power plants investigated in this research only considered the use of the models without optimizing the performance through a COGOG layout. It is therefore recommended that the work can be continued by combining the different models in forming each of the power plants depending on the case study and selected trade route.

- The DFGE (Dual-fuel Gas turbine Electric) propulsion system is one of the most favoured gas turbine alternatives propulsion plant configurations of the LNGC. It combines a gas turbine with a heat recovery steam generator (HRSG in which the hot exhaust gas is used to drive a steam turbine for the generation of additional electrical power to raise the thermal efficiency of the installation to competitive levels with conventional systems. The models involved in the current research can be further investigated in this direction through a further development of the simulation platform.

- The GT models are also recommended for further investigation not only in the area of marine propulsion but can be investigated for power generation, offshore oil and gas platforms, oil and gas pipeline pumping stations etc.

- The current work did not include the effect of performance degradation of the gas turbine models, it is therefore recommended to be part the further work in this research.

- The development of Poseidon can be improved further by its implementation using other ship types that have not been considered in the current research.

- The simulation platform may also be manipulated to investigate CODOG, COSAG or CODLAG layouts of the propulsion systems.

- The economic assessment of the gas turbine models and the BOG of the LNG Carrier is an aspect that needs to be concluded in order to evaluate the economic rate of transport in each case scenario.

- The gas turbine is recommended for the propulsion of larger LNGCs of sizes above 250,000 m^3 capacity and a long-hauled voyage e.g. from Qatar to the US may be investigated so that the implications of having to pass through the Suez canal may be investigated as well.

- Although it will involve a much longer distance, the assessment of the cruise liner may be continued by considering a trade route going from Lagos but passing through the Cape of Good Hope in order to avoid the Suez canal.

- The effect of the waves and the wind can still be investigated in greater detail by considering the effect of the forces that cause rotation and translation of the ship hull in severe operating conditions.

- The effect of cavitations of the propeller is hereby recommended for further work in this thesis.

- The use of other types of propulsor e.g. water jets may be considered for further work in the research as well.

REFERENCES

[1] Tsoudis, E. and Pilidis, P. (2008), *Techno-Economic, Environmental and Risk Analysis of Marine Gas Turbine Power Plants* (unpublished PhD thesis), Cranfield University, United Kingdom.

[2] Rowen, A. L. (2003), "Machinery Considerations", in Lamb, T. (ed.) *Ship Design and Construction,* SNAME, US, pp. 24:1-24:27.

[3] Holtrop, J. (1984), "A Statistical Re-analysis of Resistance and Propulsion", *International Shipbuilding Progress,* vol. 31, no. Part 363, pp. 272-276.

[4] United Kingdom Meteorological Office (UKMO) (2011), *Official World Weather Forecasts*, available at: http://www.worldweather.org/ (accessed 3 November 2009).

[5] Dimopoulos, G. G. et al (2008), "Thermoeconomic Simulation of Marine Energy Systems for a Liquefied Natural Gas Carrier", *Int. J. of Thermodynamics,* vol. 11, no. 4, pp. 195-201.

[6] King, J. (2002), "Marine Propulsion - The Transport Technology for the 21st Century?", *Royal Academy of Engineering,* [Online], vol. ISSN 1472-9768, no. 12, pp. 27 May 2011 available at: www.raeng.org.uk/news/publications/ingenia/issue12/King.pdf.

[7] Sariyanidis, C. (2008), "Alternative Energy Systems for LNG Carriers", *CS & Associates LTD - Shipping Calendar,* vol. 3, no. 1.

[8] Hinks, A. R. (1999), "Aero-Derivative Gas Turbines in the Marine Environment", *Gas Turbine Operation and Technology for Land, Sea and Air Propulsion and Power Systems,* Vol. 34, 18-21 October, Ottawa, Research and Technology Organization (RTO), France, pp. 11-1.

[9] Woodyard, D. (2004), *Pounder's Marine Diesel Engines,* Elsevier Butterworth-Heinemann.

[10] Schamp, A., et al (1999), "Experience with Aero-Derivative Gas Turbines as Marine Propulsion Machinery", *Gas Turbine Operation and Technology for Land, Sea and air Propulsion and Power Systems,* Vol. 34, 18-21 October, Ottawa, RTO, France, pp. 9-1.

[11] GE- Marine, (2006), *LM2500 Gas Turbine*, General Electric, New York.

[12] Watson, B., (2006), *LNG Shipping Operations*, Rolls-Royce, UK.

[13] Shepherd, S. B. and Bowen, T. L. and Chiprich, J. M. "Design and Development of the WR-21 Intercooled Recuperated (ICR) Marine Gas Turbine", *Journal of Engineering for Gas Turbines and Power,* vol. 117, pp. 557-562.

[14] Parker, M. L. et al (1998), "Advances in a Gas Turbine System for Ship Propulsion", *RTO AVT Symposium on "Gas Turbine Engine Combustion, Emissions and Alternative Fuels",* Vol. MP-14, 12 - 16 October 1998, Lisbon, Portugal, NATO, US, pp. 2-1.

[15] Jane's (2007), *Jane's Marine Propulsion: Gas Turbines*, available at: http://jmp.janes.com (accessed 31 May 2011).

[16] GE-Energy (2011), *www.ge-energy.com (LM2500 Gas Turbines for Offshore Applications - Fact Sheet)* (accessed 05).

[17] Chase, J., et al (2004), *Queen Mary 2 - Technical Information*, available at: www.cunardline.com (accessed 28/05).

[18] Flounders, E. (2011), *Queen Mary 2 - Technical Information*, available at: www.cunard.co.uk (accessed 28/05).

[19] MT30 Factsheet, (2009), *The MT3O Marine Gas Turbine*, Rolls-Royce, UK.

[20] Rolls-Royce Plc (2009), *MT30 Brochure*, available at: www.rolls-royce.com (accessed 04 May).

[21] Groghan, D. A. (1992), "Gas turbines", in Harrington, R. L. (ed.) *Marine Engineering,* The Society of Naval Architects and Marine Engineers, USA, pp. 146-183.

[22] Wiens, B. (1996), "Turbo Expo Shows Off Latest in Gas Turbines", September, pp. 38.

[23] Palmer, J. A. (1992), "Basic Concepts", in Harrington, R. L. (ed.) *Marine Engineering,* SNAME, USA, pp. 1-45.

[24] Saravanamuttoo, H. I. H. (1999), "Canadian experience with Aero-derivative Gas Turbines", *Gas Turbine operation and Technology for Land, Sea and Air Propulksion and Power Systems,* Vol. 34, 18-21, October, Ottawa, Research and Technology Organizaton (RTO), France, pp. 17-1.

[25] Beverly, J. A. (1992), "Electric Propulsion Drives", in Harrington, R. L. (ed.) *Marine Engineering,* The Society of Naval Architects and Marine Engineers, ASME, USA, pp. 304-321.

[26] Buetzow, M. R. et al (2003), "Ship Mission and Owner's Requirements", in Lamb, T. (ed.) *Ship Design and Construction, Vol 1,* Society of Naval Architects and Marine Engineers, Jersy, USA, pp. 7-1-7-23.

[27] Forecast International, (2010), *A Special Focused Market Segment Analysis: The Market for Gas Turbine Marine Engines 2010 - 2019*, Forecast International, USA.

[28] General Electric 7LM2500PC101/102/103 and 104 Gas Turbine Performance Data, GE MID-TD-2500-5.

[29] Brooks, F. J. (2000), *GE Gas Turbine Performance Characteristics*, GER 3657H, Germany.

[30] Moody, R. D. (2009), *Preliminary Power Prediction during Early Design Stages of a Ship*, available at: http://dk.cput.ac.za/td_ctech/175 (accessed 25 May).

[31] Doyle, T. J. (1989), "Surface Ship Machinery - Assessing Weight Reduction Potential", *Naval Engineers Journal,* vol. 101, no. 6, pp. 42-52.

[32] Parsons, M. G. (2003), "Parametric Design of Ships", in *Ship Design and Construction, Vol 1,* SNAME, New Jersy, pp. 11:1-11:48.

[33] Harvald, S. A. (2008), *Resistance and Propulsion of Ships*, available at: www.dieselduck.net (accessed May, 27).

[34] Specialist Committee on Powering Performance of the 24th ITTC (2005), Testing and Extrapolation Methods, Propulsion, Performance, Predicting Powering Margins, 7.5 - 02 03 - 01.5, International Towing Tank Conference.

[35] Moon, K., et al (2009), "Fire Risk Assessment of Gas Turbine Propulsion System for LNG Carriers", *Journal of Loss Prevention in the Process Industries,* vol. 11, no. 8, pp. 1-7.

[36] Haglind, F. (2008), "A review on the use of gas and steam turbine combined cycles as prime movers for large ships. Part II: Previous work and implications", *Energy Conversion and Management,* vol. 49, no. 12, pp. 3468-3475.

[37] Gupta, B. and Prasad, K., (2011), *The Future of LNG Transportation - Various Propulsion Alternatives*, Marine Engineering and Research Institute, Kolkata, India.

[38] Chang, D. (2008), "Economic Evaluation of Propulsion Systems for LNG Carriers: A comparative Life Cycle Cost Approach", 2008, GASTECH, .

[39] Curt, B. (2004), "Marine Transportation of LNG", *Intertank Conference,* March, 29, Qatar, Qatar Gas, Qatar, .

[40] Jarlsby, E., et al (2008), Developing LNG as a clean fuel for Ships in the Baltic and North Sea, D1.6, Maritime Gas Fuel Logistics (MAGALOG) Project, Norway.

[41] Anderson, H. (2010), Potential and Conditions for Short Sea Shipping in East Asia, X-10/245, Department of Shipping and Marine Technology, Chalmers University of Technology, Goteborg, Sweden.

[42] MacMillan, W. L. (1974), *Development of a Modular Type Program for the Calculation for the calculation of Gas Turbine Off-Design Performance* (unpublished PhD thesis), Cranfield University (formerly C. I. T.), UK.

[43] Van Den Hout, F. (1991), *Gas Turbine Performance Simulation Improvemments to the TURBOMATCH scheme* (unpublished MSc thesis), Cranfield University (formerly C.I.T.), UK.

[44] Isensee, J. and Bertram, V. (2004), "Quantifying External Costs of Emissions due to Ship Operation", *Journal of Engineering for the Maritime Environment,* vol. 218, no. M, pp. 41-51.

[45] Lefebvre, A. H. (1984), "Fuel effects on Gas Turbine Combustion - Liner Temperature, Pattern Factor and Pollutant Emissions", *Journal of Aircraft,* vol. 21, no. 11, pp. 887-898.

[46] Razak, A. M. Y. (2007), *Industrial Gas Turbines,* First ed, Woodhead Publishing Limited, England.

[47] M. I. Wood (2000), "Gas turbine hot section components: The challenge of 'residual life' assessment", *Proceedings of the Institute of Mechanical Engineers,* vol. 214, no. A03099, pp. 193-201.

[48] Torres, G. O. (1987), *Gas Turbine Hot Section Life Usage Considerations* (unpublished MSc thesis), Cranfield University, United Kingdom.

[49] Morris, A. and Wojnarowski, A. (2009), *Port Distance Calculator*, available at: http://www.searates.com/reference/portdistance/ (accessed 11/29).

[50] The LNG Industry (2008), World Energy Situation, , International Group of Liquied Natural Gas Importers, France.

[51] Foss, M. M. et al (2011), *An overview on liquefied natural gas (LNG), its properties, organization of the LNG industry and safety considerations*, available at:

http://www.beg.utexas.edu/energyecon/lng/documents/CEE_INTRODUCTION_TO_LNG_FINAL.pdf (accessed June 12).

[52] Van, S. H. et al (2006), "Flow measurement around a model ship with propeller and rudder", *Experiments in Fluids,* vol. 40, no. DOI 10.1007/S00348 - 005 - 0093 - 6, pp. 533-545.

[53] Rawson, K. J. et al (2001), *Basic Ship Theory,* Fifth ed, Butterworh Henemann, United Kingdom.

[54] United Kingdom Hydrographic Office (UKHO) (2009), *Online Tidal Predictions*, available at: http://easytide.ukho.gov.uk/EasyTide/EasyTide/SelectPort.aspx (accessed 03/11).

[55] UK Meteorological Office (UKMO) (2007), *Beaufort Wind Force Scale*, available at: www.metoffice.gov.uk/weather/marine/guide/beaufortscale.html (accessed 09/2007).

[56] HydroComp (2003), Apllicability Range of Holtrop - 1984 Method, 128, HydroComp, US.

[57] Schneekluth, H. and Bertram, V. (1998), ***Ship Design for Efficiency and Economy***, 2nd ed, Butterworth Heinmann, Oxford.

[58] Watson, D. G. M. (1998), *Practical Ship Design,* Elsevier Science Ltd, Oxford.

[59] Watson, D. G. M. and Gilfillan, A. W. (1977), "Some Ship Design Methods", *Transactions of RINA,* vol. 119.

[60] Global Security.org (2011), *Container Ship Types*, available at: http://www.globalsecurity.org/military/systems/ship/container-types.htm (accessed 19th January).

[61] Kai, L. (2004), "Passenger Ships", in *Ship Design and Construction Vol. 2,* Society of Naval Archtects and Marine Engineers, New Jersey, pp. 37-1-37-39.

[62] Briney, A. (2011), *A history and Overview of the Suez Canal in Egypt*, available at: http://geography.about.com/od/specificplacesofinterest/a/suezcanal (accessed 02/21).

[63] Knox, J. (2004), "Ferries", in Lamb, T. (ed.) *Ship Design and Construction, Vol. 2,* The Society of Naval Architects and Marine Engineers, USA, pp. 38-1-38-31.

[64] Journee, J. M. J. et al (2011), *Ship Routeing for Optimum Performance Prediction of Speed and Power of a Ship in a Seaway*, available at: www.shipmotions.nl. (accessed 4th May).

[65] Woodward, J. B. (1975), *Marine Gas Turbines,* Wiley, United States of America.

[66] Walsh, P. P. and Fletcher, P. (2000), *Gas Turbine Performance,* Blackwell Science, United Kingdom.

[67] Wayne, W.S., Cooke, J.D., Tooke, R.W. and Morley, J., (2005), *A natural evolution of the modern LNG carrier - The application of gas turbines for LNG carrier propulsion systems*, Bilbao ed.

[68] Saravanamuttoo, H. I. H. and et al (2008), *Gas Turbine Theory,* 6th ed, Pearson Education Limited, England.

[69] Lipfert, F. W. (1972), "Correlation of gas turbine emissions data", *American Society of Mechanical Engineers (Paper),* vol. 72-GT-60.

[70] CSGNetwork.com (2011), *Specific Gravity of Liquids Table*, available at: http://www.csgnetwork.com/specificgravliqtable.html (accessed June 16).

[71] Anderson, R., et al (2004), Natural Gas Facts - Liquefied Natural Gas, 06, US Department of Energy, US.

[72] Wenninger, M. and Tolgos, S. (2008), LNG Carrrier Power: Total Fuel Flexibility & Maintainability with 51/60DF Electric Propulsion, D2366314-N2, MAN Diesel, Ausburg, Germany.

[73] Shanghi, V., et al (1998), "Preliminary Estimation of Engine Gas-Flow Path Size and weight", *Journal of Propulsion and Power,* vol. 14, no. 2, pp. 208-214.

APPENDICES

Appendix A **Gas Turbine Modelling and Simulation**

A.1 25MW Simple Cycle Model

```
!TURBOMATCH PROGRAM: SIMULATION OF
!25MW SIMPLE CYCLE, SINGLE SPOOL MARINE GAS TURBINE
////
OD SI KE CT FP
-1
-1
INTAKE  S1-2     D1-4          R100
COMPRE  S2-3     D5-10         R101     V5  V6
PREMAS  S3,13,4  D11-14
BURNER  S4-5     D15-17        R102
DUCTER  S5-6     D18-21
MIXEES  S6,13,7
TURBIN  S7-8     D22-29,101            V23
TURBIN  S8-9     D30-38                V30 V31
DUCTER  S9-10    D39-42
NOZCON  S10-11,1 D43           R107
PERFOR  S1,0,0   D30,44-46,107,100,102,0,0,0,0,0,0
CODEND
DATA ITEMS////
!INTAKE
1 0.0          ! INTAKE ALTITUDE
2 0.0          ! ISA DEVIATION
3 0.0          ! MACH NO
4 0.9951       ! PRESSURE RECOVERY
!COMPRESSOR
5 0.85         ! Z PARAMETER
6 0.999        ! ROTATIONAL SPEED N
7 19.25        ! PRESSURE RATIO
8 0.95         ! ISENTROPIC EFFICIENCY
9 0.0          ! ERROR SELECTION
10 4.0         ! MAP NUMBER
!PREMAS
11 0.1         ! BLEED AIR
12 0.2         ! FLOW LOSS
13 1.0         ! PRESSURE RECOVERY
14 0.00        ! PRESSURE DROP
!BURNER
15 0.07        ! FRACTIONAL PRESSURE LOSS DP/P
16 0.998       ! COMBUSTION EFFICIENCY
17 -1.0        ! FUEL FLOW
!DUCTER
18 0.0         !NO INTERCOOLING
19 0.02        !PRESSURE LOSS
```

```
20 0.0          !PRESSURE RECOVERY
21 0.0          !LIMITING VALUE OF FUEL FLOW
!HP TURBINE
22 0.0        ! AUXILIARY WORK
23 0.81       ! NDMF
24 0.68       ! NDSPEED CN
25 0.87       ! ISENTROPIC EFFICIENCY
26 -1.0       ! PCN
27 1.0        ! COMPRESSOR NUMBER
28 2.0        ! TURBINE MAP NUMBER
29 -1.0       ! POWER LOW INDEX
!POWER TURBINE
30 25000000.00 ! AUXILIARY WORK
31 0.89        ! NDMF
32 0.68        ! NDSPEED CN
33 0.89        ! ISENTROPIC EFFICIENCY
34 1.0         ! PCN
35 0.0         ! COMPRESSOR NUMBER
36 5.0         ! MAP NUMBER
37 3.0         ! POWER LOW INDEX
38 -1.0        ! COMWORK
!DUCTER
39 0.0          !NO INTERCOOLING
40 0.026       !PRESSURE LOSS
41 0.0          !PRESSURE RECOVERY
42 0.0          !LIMITING VALUE OF FUEL FLOW
!NOZCON
43 -1.0         ! THROAT AREA
!PERFOR
44 1.0          ! PROPELLER EFFICIENCY
45 0.0          ! SCALING INDEX
46 0.0          ! REQUIRED THRUST
-1
1 2 72.5        ! INLET MASS FLOW
5 6 1500.0    ! COMBUSTION OUTLET TEMPERATURE
-1
-3
```

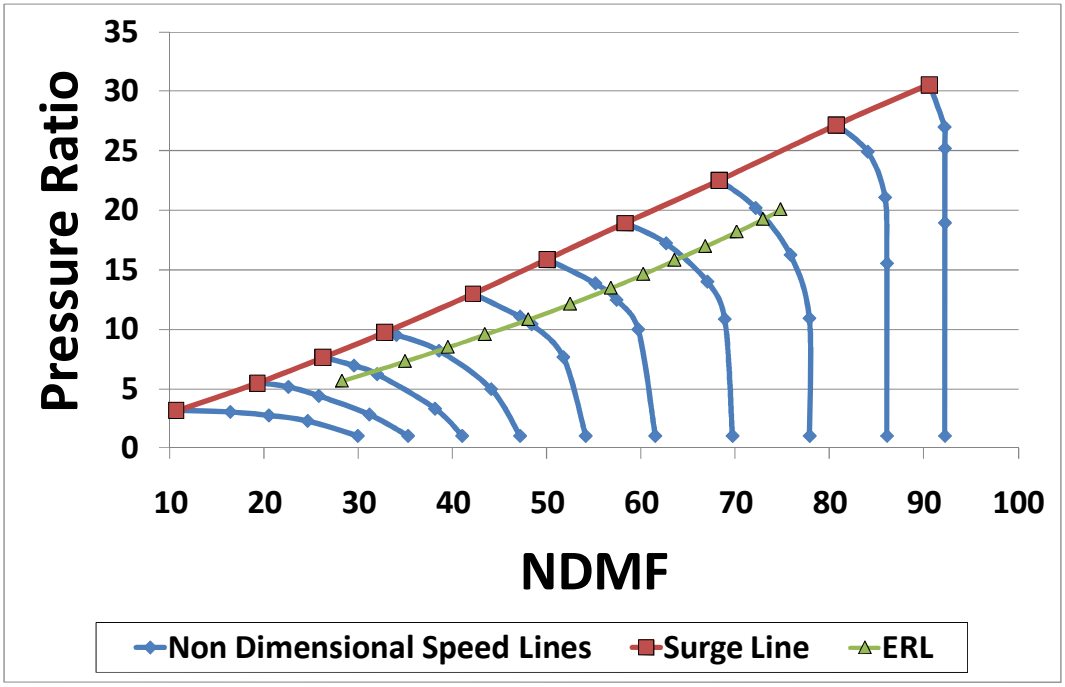

Fig. A: 1 Compressor map of the SC marine GT model, showing the Equilibrium Running Line (ERL)

A.2 25MW Intercooled Recuperated Model

```
!TURBOMATCH PROGRAM: SIMULATION OF
!25MW INTERCOOLED RECUPERATED MARINE GAS TURBINE
////
 OD SI KE CT FP
 -1
 -1
 INTAKE  S1-2      D1-4            R300
 COMPRE  S2-3      D5-11           R301   V5  V6
 DUCTER  S3-4      D12-15          R305
 NOZCON  S4,5,1    D16             R307
 COMPRE  S5-6      D17-23          R302   V17 V18
 PREMAS  S6,7,20   D24-27
 PREMAS  S20,21,22 D28-31
 HETCOL  S7-8      D32-35
 DUCTER  S8-9      D36-39
 BURNER  S9-10     D40-42          R303
 MIXEES  S10,21,11
 TURBIN  S11-12    D43-50,302,51          V44
 MIXEES  S12,22,13
 DUCTER  S13-14    D52-55
 TURBIN  S14-15    D56-63,301,64          V57
 DUCTER  S15-16    D65-68
 TURBIN  S16-17    D69-78                 V69 V70
```

```
HETHOT  S7,17,18  D79-82
DUCTER  S18-19    D83-86        R306
NOZCON  S19-20,1  D87           R304
PERFOR  S1,0,0    D69,88-90,304,300,303,0,0,305,0,0,0
CODEND

DATA ITEMS////
1 0.0          !INTAKE ALTITUDE
2 0.0          !ISA DEVIATION
3 0.0          !MACH NUMBER
4 0.9951       !PRESSURE RECOVERY
!LP COMPRESSOR
5 -1.0         !Z PARAMETER
6 -1.0         !ROTATIONAL SPEED N
7 3.25         !PRESSURE RATIO
8 0.91         !ISENTROPIC EFFICIENCY
9 0.0          !ERROR SELECTION
10 4.0         !MAP NUMBER
11 0.0         !ANGLE
!INTERCOOLER
12 2.0         !INTERCOOLER
13 0.03        !PRESSURE LOSS
14 0.90        !INTERCOOLER EFFECTIVENESS
15 100000.00   !LIMITING VALUE OF FUEL FLOW
!NOZCON (No effect on the performance of the cycle)
16 -1.0        !AIR FIXED
!HP COMPRESSOR
17 -1.0        !SURGE MARGIN
18 -1.0        !SPOOL SPEED
19 6.5         !PRESSURE RATIO
20 0.91        !EFFICIENCY
21 0.0         !ERROR SELECTOR
22 5.0         !COMPRESSOR MAP NUMBER
23 0.0         !ANGLE
!HP TURBINE COOLING
24 0.90        !BLEED AIR
25 0.0         !FLOW LOSS
26 1.0         !PRESSURE RECOVERY
27 0.0         !PRESSURE LOSS
!IP TURBINE COOLING
28 0.70        !BLEED AIR
29 0.0         !FLOW LOSS
30 1.0         !PRESSURE RECOVERY
31 0.0         !PRESSURE LOSS
!HEAT EXCHANGER, COLD SIDE
32 0.1         !COLD SIDE PRESSURE LOSS
33 0.73        !EFFECTIVENESS
34 1.0         !TYPE RECUPERATOR
```

```
35 0.02        !MASS FLOW LEAKAGE
!DUCTER
36 0.0         !NO INTERCOOLING
37 0.0         !PRESSURE LOSS
38 0.0         !EFFICIENCY
39 0.0         !LIMITING VALE OF FUEL FLOW
!BURNER
40 0.065       !PRESSURE LOSS
41 0.998       !EFFICIENCY
42 -1.0        !FUEL FLOW
!HP TURBINE
43 0.0         !AUXILIARY POWER REQUIRED
44 0.8         !NON-DIMENSIONAL MASSFLOW (DEFAULT=0.8)
45 0.6         !NON-DIMENSIONAL SPEED (DEFAULT=0.6)
46 0.87        !EFFICIENCY
47 -1.0        !COMPRESSOR TURBINE
48 2.0         !COMPRESSOR NUMBER
49 3.0         !TURBINE MAP NUMBER
50 3.0         !POWER LOW INDEX
51 0.0         !ANGLE
!DUCTER
52 0.0         NO INTERCOOLING
53 0.0         !PRESSURE LOSS
54 0.0         !EFFICIENCY
55 100000.0    !LIMITING VALUE OF FUEL FLOW
!IP TURBINE
56 0.0         !AUXILIARY POWER REQUIRED
57 0.8         !NON-DIMENSIONAL MASS FLOW (DEFAULT=0.8)
58 0.5         !NON-DIMENSIONAL SPEED
59 0.87       !EFFICIENCY
60 -1.0        !COMPRESSOR TURBINE
61 1.0         !COMPRESSOR NUMBER
62 1.0         !TURBINE MAP NUMBER
63 3.0         !POWER LOW INDEX
64 0.0         !ANGLE
!DUCTER
65 0.0         !NO INTERCOOLING
66 0.0         !PRESSURE LOSS
67 0.0         !EFFICIENCY
68 100000.0 !LIMITING VALUE OF FUEL FLOW
!POWER TURBINE
69 25000000.00 !POWER REQUIRED
70 -1.0        !NON-DIMENSIONAL MASS FLOW
71 -1.0        !NON-DIMENSIONAL SPEED
72 0.90        !EFFICIENCY
73 1.0         !RELATIVE ROTATIONAL
74 0.0         !COMPRESSOR NUMBER
75 5.0         !TURBINE MAP NUMBER
```

```
 76 3.0          !POWER LAW INDEX
 77 -1.0         !AUXILIARY WORK CONSTANT
 78 0.0          !ANGLE
!HOT HEAT EXCHANGER
 79 0.1          !HOTSIDE PRESSURE LOSS
 80 0.73         !EFFECTIVENESS
 81 1.0          !TYPE RECUPERATOR
 82 0.02         !MASS FLOW LEAKAGE
!DUCTER
 83 0.0          !NO INTERCOOLING
 84 0.02         !PRESSURE LOSS
 85 0.0          !EFFICIENCY
 86 100000.0 !LIMITING VALUE OF FUEL FLOW
!CONVERGENT NOZZLE
 87 -1.0         !AIR FIXED
!PERFORMANCE
 88 1.0          !PROPELLER EFFICIENCY
 89 0.0          !SCALING INDEX (0=NO SCALING)
 90 0.0          !REQUIRED THRUST
-1
1 2  72.0        !INLET MASS FLOW
4 6  320.00      !INTERCOOLER OUTPUT TEMPERATURE
10 6 1451.00 !COMBUSTION OUTLET TEMPERATURE
-1
-3
```

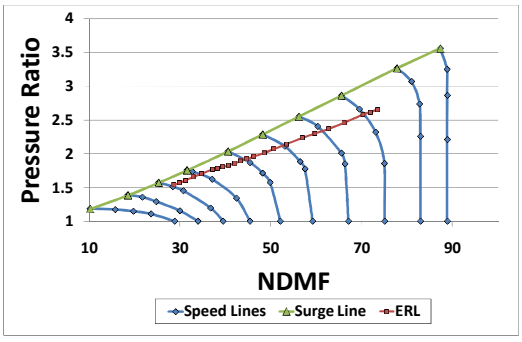

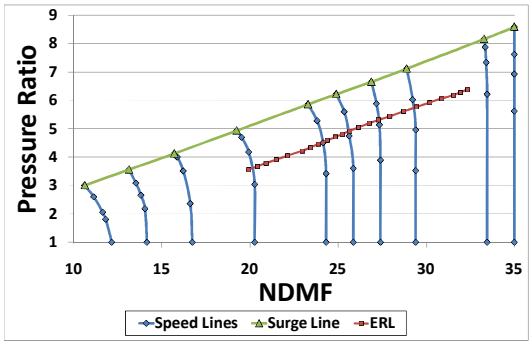

Fig. A: 2 LPC and HPC performance maps of the ICR marine GT model

A.3 36MW Dual Spool, Simple Cycle Model

```
!TURBOMATCH PROGRAM: SIMULATION OF
!36MW DUAL SPOOL, SIMPLE CYCLE MARINE GAS TURBINE MODEL
////
OD SI KE VA FP
-1
-1
INTAKE  S1-2      D1-4           R300
COMPRE  S2-3      D5-11          R301   V5  V6
DUCTER  S3-4      D12-15         R305
COMPRE  S3-4      D16-22         R302   V16 V17
PREMAS  S4,5,13   D23-26
PREMAS  S13,14,15 D27-30
BURNER  S5-6      D31-33         R303
MIXEES  S6,14,7
TURBIN  S7-8      D34-41,302,42          V35
MIXEES  S8,15,9
TURBIN  S9-10     D43-50,301,51          V44
TURBIN  S10-11    D52-60                 V52 V53
DUCTER  S11-12    D61-65
NOZCON  S11-12,1  D66                    R304
PERFOR  S1,0,0    D52,67-69,304,300,303,0,0,0,0,0,0
CODEND
DATA ITEMS////
1 0.0            !INTAKE ALTITUDE
2 0.0            !ISA DEVIATION
3 0.0            !MACH NUMBER
4 0.9951         !PRESSURE RECOVERY
!LP COMPRESSOR
5 -1.0           !Z PARAMETER
6 -1.0           !ROTATIONAL SPEED N
7 3.0            !PRESSURE RATIO
8 0.89           !ISENTROPIC EFFICIENCY
9 0.0            !ERROR SELECTION
10 2.0           !MAP NUMBER
11 0.0           !ANGLE
!DUCTER
12 0.0           !NO INTERCOOLING
13 0.01          !PRESSURE LOSS
14 0.0           !PRESSURE RECOVERY
15 0.0           !LIMITING VALUE OF FUEL FLOW
!HP COMPRESSOR
16 -1.0          !SURGE MARGIN
17 -1.0          !SPOOL SPEED
18 8.0           !PRESSURE RATIO
19 0.89          !EFFICIENCY
20 1.0           !ERROR SELECTOR
```

```
21 5.0          !COMPRESSOR MAP NUMBER
22 0.0          !ANGLE
!PREMAS 1
23 0.85         !BYPASS RATIO
24 2.25         !MASS FLOW LOSS
25 1.0          !PRESSURE FACTOR
26 0.0          !PRESSURE LOSS
!PREMAS 2
27 0.725        !BYPASS RATIO
28 0.0          !MASS FLOW LOSS
29 1.0          !PRESSURE FACTOR
30 0.0          !PRESSURE LOSS
!BURNER
31 0.065        !PRESSURE LOSS
32 0.998        !EFFICIENC
33 -1.0         !FUEL FLOW
!HP TURBINE
34 0.0          !AUXILIARY POWER REQUIRED
35 0.8          !NON-DIMENSIONAL MASSFLOW (DEFAULT=0.8)
36 0.6          !NON-DIMENSIONAL SPEED (DEFAULT=0.6)
37 0.87         !EFFICIENCY
38 -1.0         !COMPRESSOR TURBINE
39 2.0          !COMPRESSOR NUMBER
40 1.0          !TURBINE MAP NUMBER
41 -1.0         !POWER LOW INDEX
42 0.0          !ANGLE
!IP TURBINE
43 0.0          !AUXILIARY POWER REQUIRED
44 0.8          !NON-DIMENSIONAL MASS FLOW (DEFAULT=0.8)
45 0.6          !NON-DIMENSIONAL SPEED
46 0.87         !EFFICIENCY
47 -1.0         !COMPRESSOR TURBINE
48 1.0          !COMPRESSOR NUMBER
49 3.0          !TURBINE MAP NUMBER
50 -1.0         !POWER LOW INDEX
51 0.0          !ANGLE
!POWER TURBINE
52 36000000.00 !POWER REQUIRED
53 -1.0         !NON-DIMENSIONAL MASS FLOW
54 -1.0         !NON-DIMENSIONAL SPEED
55 0.89         !EFFICIENCY
56 1.0          !RELATIVE ROTATIONAL
57 0.0          !COMPRESSOR NUMBER
58 5.0          !TURBINE MAP NUMBER
59 3.0          !POWER LAW INDEX
60 -1.0         !AUXILIARY WORK CONSTANT
61 0.0          !ANGLE
!DUCTER
```

```
62 0.0          !NO INTERCOOLING
63 0.005       !PRESSURE LOSS
64 0.0          !PRESSURE RECOVERY
65 0.0          !LIMITING VALUE OF FUEL FLOW
!CONVERGENT NOZZLE
66 -1.0         !AIR FIXED
!PERFORMANCE
67 1.00         !PROPELLER EFFICIENCY
68 0.0          !SCALING INDEX (0=NO SCALING)
69 0.0          !REQUIRED THRUST
-1
1 2 105.00     !INLET MASS FLOW
6 6 1550.00   !COMBUSTION OUTLET TEMPERATURE
-1
-3
```

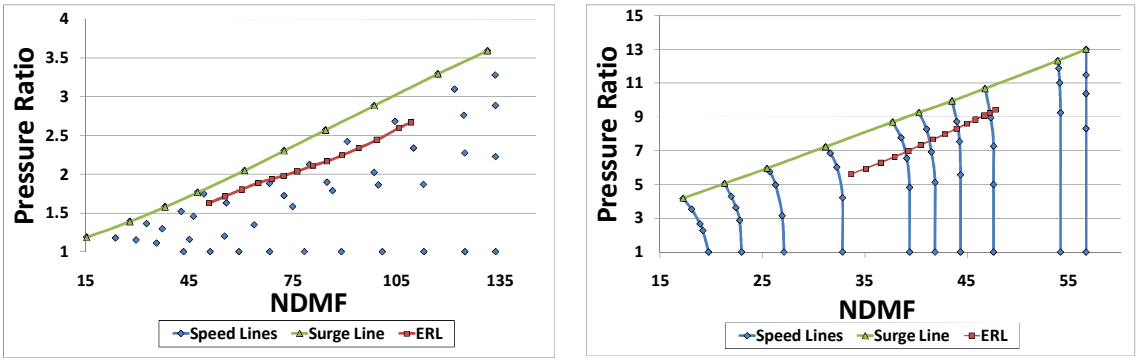

Fig. A: 3 LPC and HPC performance maps of the 36MW marine GT model

A.4 19MW Dual Spool, Simple Cycle Model

```
!TURBOMATCH PROGRAM: SIMULATION OF
!19MW DUAL SPOOL, SIMPLE CYCLE MARINE GAS TURBINE MODEL
////
OD SI KE VA FP
-1
-1
INTAKE  S1-2        D1-4          R300
COMPRE  S2-3     D5-11          R301   V5  V6
DUCTER  S3-4       D12-15         R305
COMPRE  S3-4       D16-22         R302   V16 V17
PREMAS  S4,5,13   D23-26
PREMAS  S13,14,15 D27-30
BURNER  S5-6       D31-33         R303
MIXEES  S6,14,7
TURBIN  S7-8        D34-41,302,42         V35
MIXEES  S8,15,9
TURBIN  S9-10       D43-50,301,51         V44
TURBIN  S10-11     D52-60              V52 V53
DUCTER  S11-12    D61-65
NOZCON  S11-12,1 D66                 R304
PERFOR  S1,0,0    D52,67-69,304,300,303,0,0,0,0,0,0
CODEND
DATA ITEMS////
1 0.0           !INTAKE ALTITUDE
2 0.0           !ISA DEVIATION
3 0.0           !MACH NUMBER
4 0.9951      !PRESSURE RECOVERY
!LP COMPRESSOR
5 -1.0          !Z PARAMETER
6 -1.0          !ROTATIONAL SPEED N
7 3.0           !PRESSURE RATIO
8 0.890        !ISENTROPIC EFFICIENCY
9 0.0           !ERROR SELECTION
10 2.0          !MAP NUMBER
11 0.0          !ANGLE
!DUCTER
12 0.0        !NO INTERCOOLING
13 0.01      !PRESSURE LOSS
14 0.0        !PRESSURE RECOVERY
15 0.0        !LIMITING VALUE OF FUEL FLOW
!HP COMPRESSOR
16 -1.0       !SURGE MARGIN
17 -1.0       !SPOOL SPEED
18 8.05      !PRESSURE RATIO
19 0.890     !EFFICIENCY
20 1.0        !ERROR SELECTOR
```

```
21 5.0        !COMPRESSOR MAP NUMBER
22 0.0        !ANGLE
!PREMAS 1
23 0.85       !BYPASS RATIO
24 2.35       !MASS FLOW LOSS
25 1.0        !PRESSURE FACTOR
26 0.0        !PRESSURE LOSS
!PREMAS 2
27 0.725      !BYPASS RATIO
28 0.0        !MASS FLOW LOSS
29 1.0        !PRESSURE FACTOR
30 0.0        !PRESSURE LOSS
!BURNER
31 0.065      !PRESSURE LOSS
32 0.998      !EFFICIENC
33 -1.0       !FUEL FLOW
!HP TURBINE
34 0.0        !AUXILIARY POWER REQUIRED
35 0.8        !NON-DIMENSIONAL MASSFLOW (DEFAULT=0.8)
36 0.6        !NON-DIMENSIONAL SPEED (DEFAULT=0.6)
37 0.88       !EFFICIENCY
38 -1.0       !COMPRESSOR TURBINE
39 2.0        !COMPRESSOR NUMBER
40 1.0        !TURBINE MAP NUMBER
41 -1.0       !POWER LOW INDEX
42 0.0        !ANGLE
!IP TURBINE
43 0.0        !AUXILIARY POWER REQUIRED
44 0.8        !NON-DIMENSIONAL MASS FLOW (DEFAULT=0.8)
45 0.6        !NON-DIMENSIONAL SPEED
46 0.87       !EFFICIENCY
47 -1.0       !COMPRESSOR TURBINE
48 1.0        !COMPRESSOR NUMBER
49 3.0        !TURBINE MAP NUMBER
50 -1.0       !POWER LOW INDEX
51 0.0        !ANGLE
!POWER TURBINE
52 19020000.00 !POWER REQUIRED
53 -1.0       !NON-DIMENSIONAL MASS FLOW
54 -1.0       !NON-DIMENSIONAL SPEED
55 0.89       !EFFICIENCY
56 1.0        !RELATIVE ROTATIONAL
57 0.0        !COMPRESSOR NUMBER
58 5.0        !TURBINE MAP NUMBER
59 3.0        !POWER LAW INDEX
60 -1.0       !AUXILIARY WORK CONSTANT
61 0.0        !ANGLE
!DUCTER
```

```
62 0.0          !NO INTERCOOLING
63 0.005        !PRESSURE LOSS
64 0.0          !PRESSURE RECOVERY
65 0.0          !LIMITING VALUE OF FUEL FLOW
!CONVERGENT NOZZLE
66 -1.0         !AIR FIXED
!PERFORMANCE
67 1.00         !PROPELLER EFFICIENCY
68 0.0          !SCALING INDEX (0=NO SCALING)
69 0.0          !REQUIRED THRUST
-1
1 2 61.00       !INLET MASS FLOW
6 6 1480.00  !COMBUSTION OUTLET TEMPERATURE
-1
-3
```

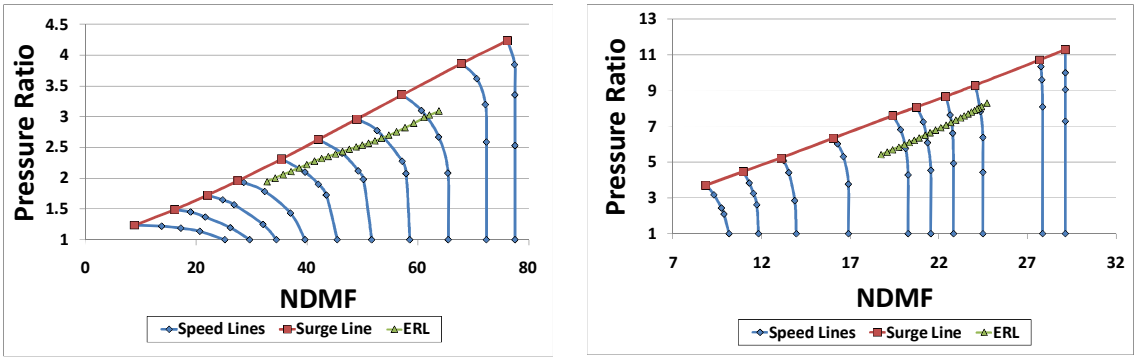

Fig. A: 4 LPC and HPC performance characteristics of the 19MW marine GT model

Appendix B **Cargo ship Voyage Analysis**

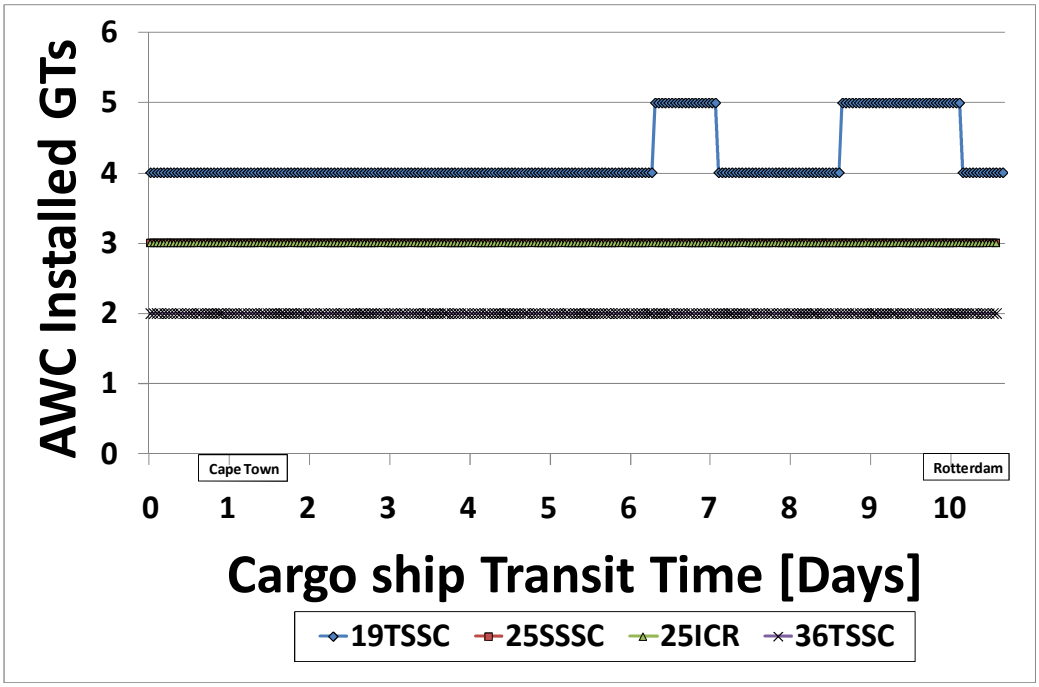

Fig B: 1 Profile of operating number of engines for each of the GT models

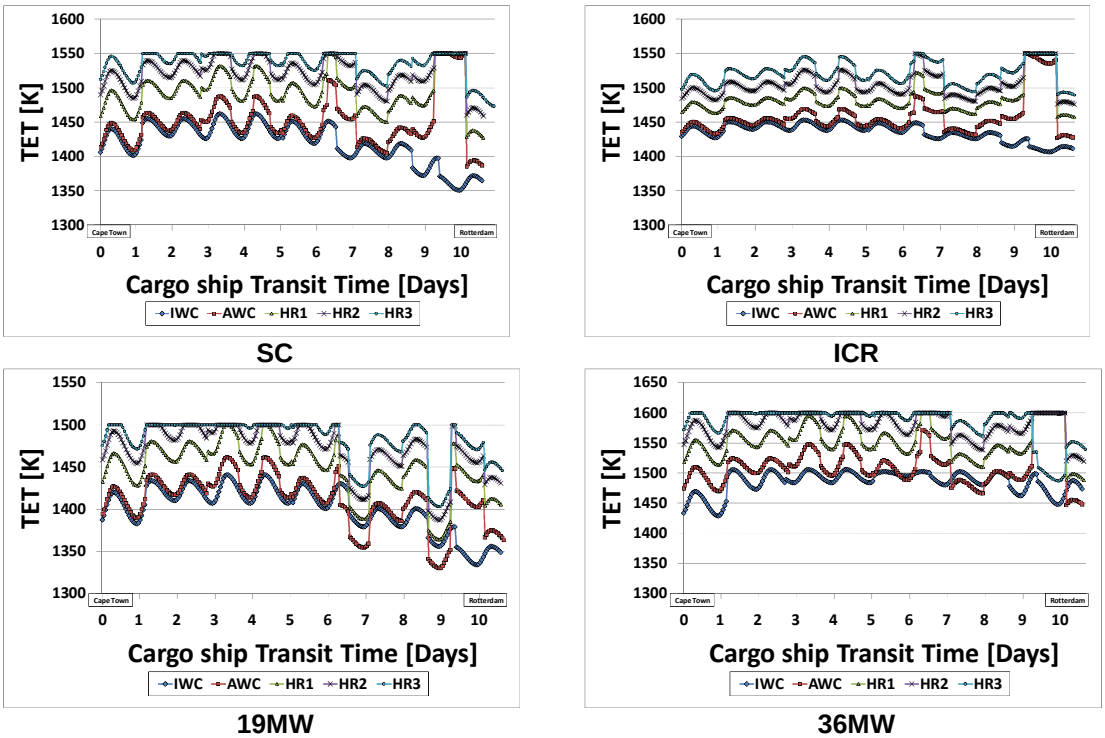

Fig B: 2 Variation of the TET for the variety of GT models when operated as the propulsion prime mover for the cargo ship

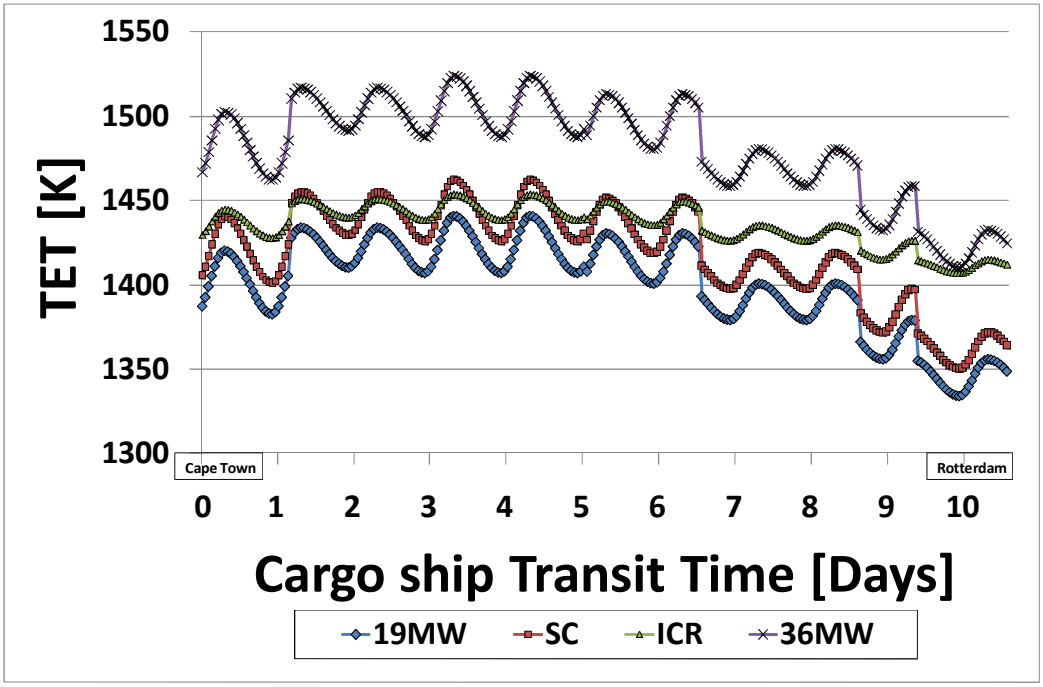

Fig B: 3 Variation of TET for the various engine models under IWC in winter

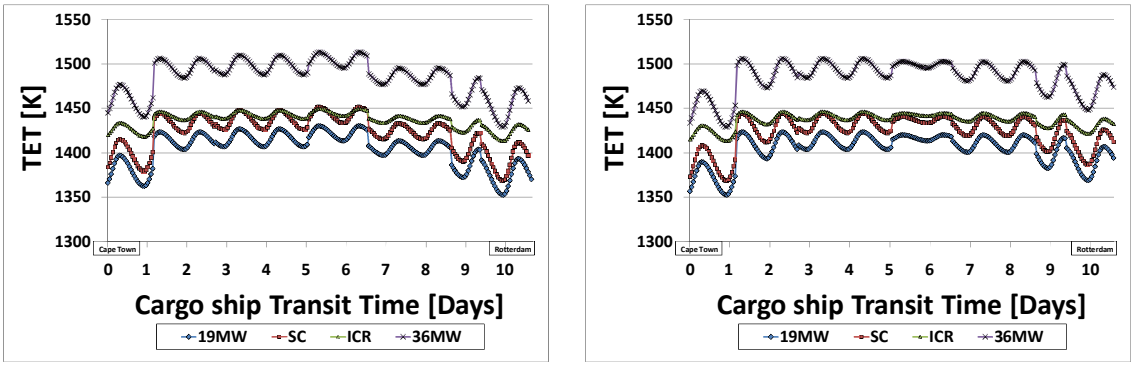

Fig B: 4 Variation of TET for the various engine models under IWC in spring and summer

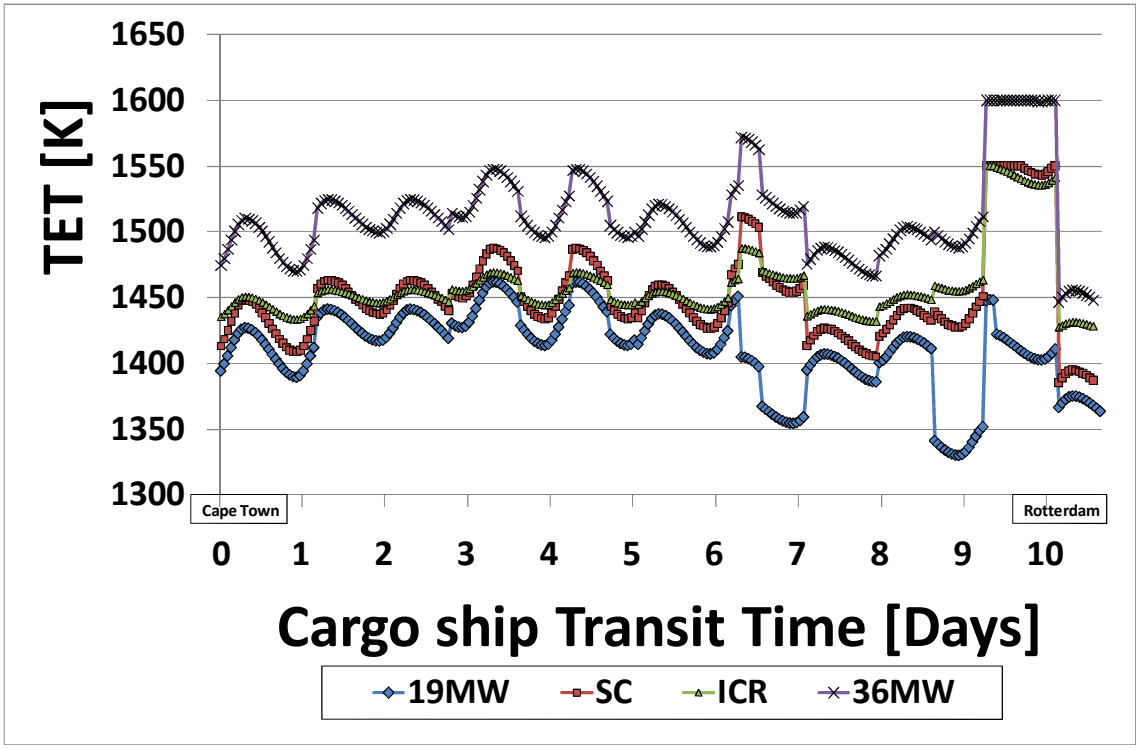

Fig B: 5 Variation of TET for the various engine models under AWC in winter

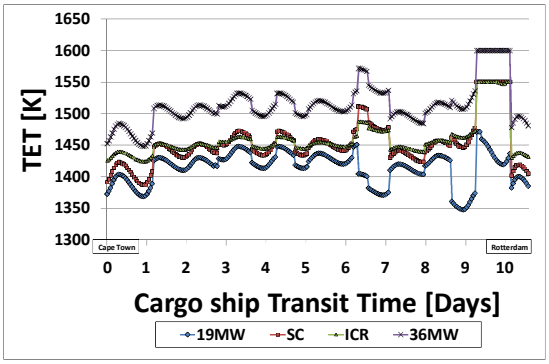

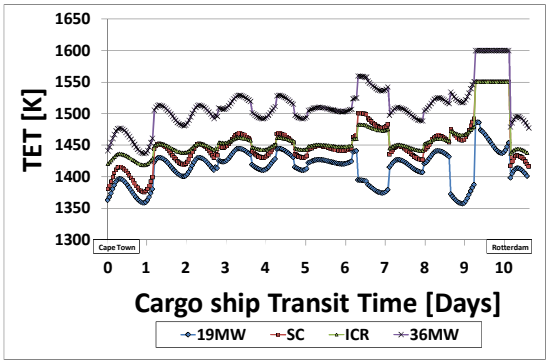

Fig B: 6 Variation of TET for the various engine models under AWC in spring and summer

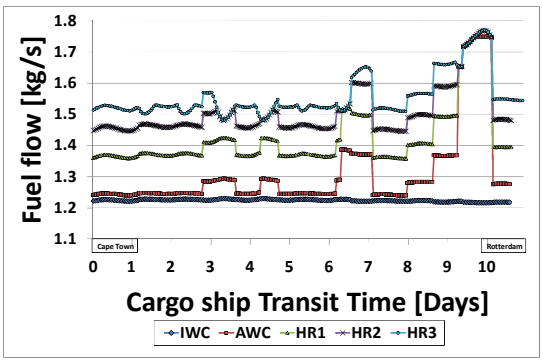

SC

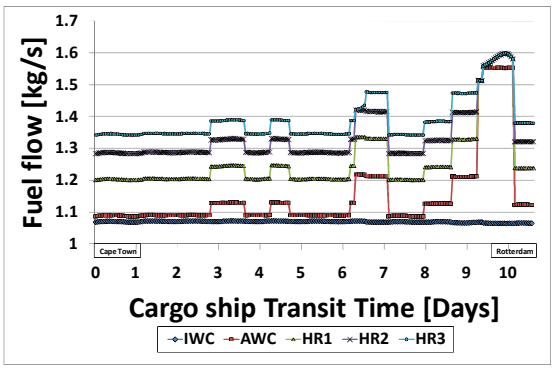

ICR

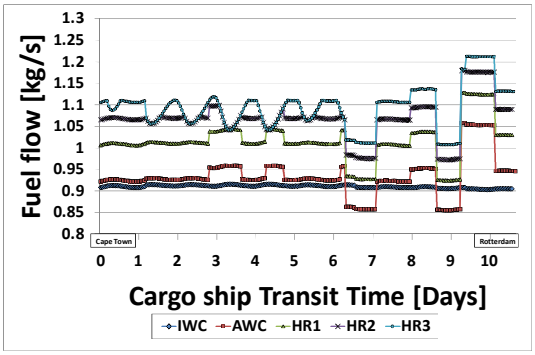

19MW

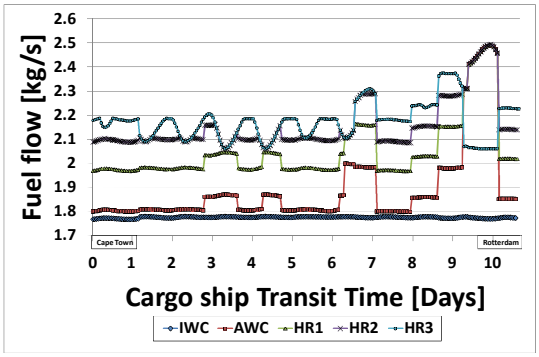

36MW

Fig B: 7 Fuel flow profiles of the GT models under the variety of investigated scenarios

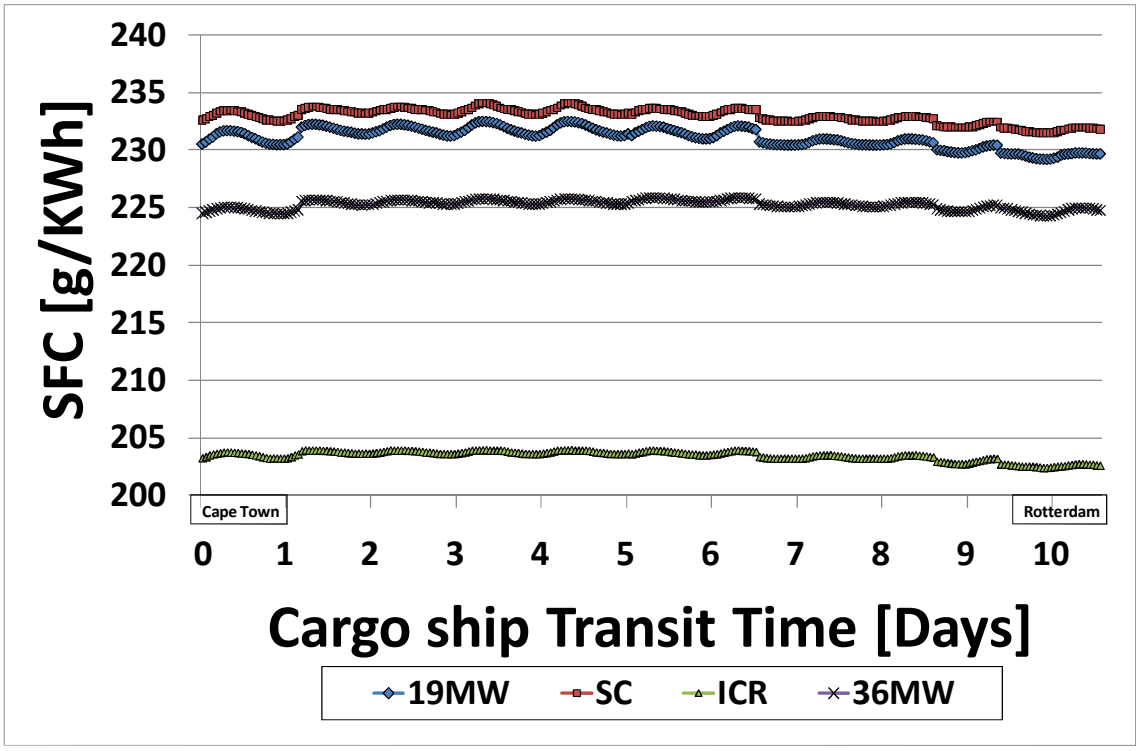

Fig B: 8 Variation of SFC for each of the GT models under IWC

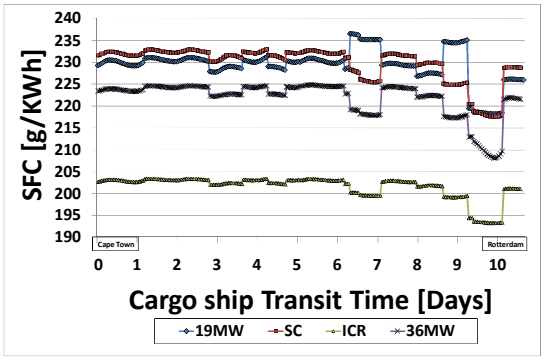

AWC

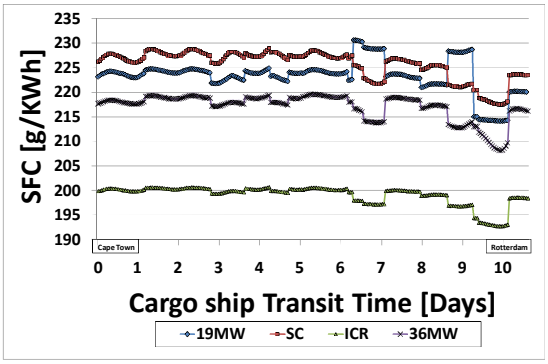

HR1

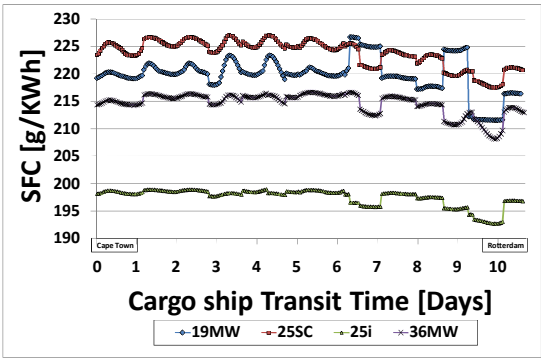

HR2

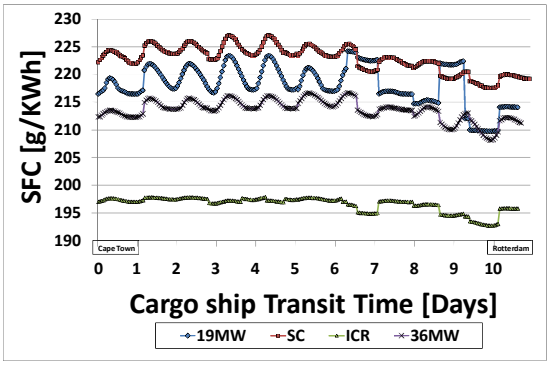

HR3

Fig B: 9 Variation of SFC according to the various investigated scenarios

Table B: 1 Voyage analysis of the cargo ship with the SC model as propulsion prime mover in winter

	IWC	AWC	F1	F2	F3
FB [kg]	1118806.113	1199322.842	1308616	1382854.68	1433706.661
FB [tons]	3356.418339	3597.968526	3925.847	4148.56404	4301.119983
LC [%]	0.006687	0.196551352	0.470037	1.170149358	2.028586992
CO [kg]	1699.227	1565.701641	1416.072	1328.167996	1289.108519
UHC [kg]	3377.154	2934.619758	2428.25	2148.93858	2014.601771
NOx [kg]	32.489964	37.2098322	43.91726	49.05976553	52.41117802
NOx [tons]	32489.964	37209.8322	43917.26	49059.76553	52411.17802
CO_2 [kg]	10532217.14	11290177.24	12318991	13017787.7	13496282.14
CO_2 [tons]	10532.21714	11290.17724	12318.99	13017.7877	13496.28214
Transit time [hrs]	254	254	255	255	256

Table B: 2 Voyage analysis of the cargo ship with the SC model as propulsion prime mover in spring

	IWC	AWC	F1	F2	F3
FB [kg]	1119064.128	1193537.221	1302157	1382392.288	1378946.219
FB [tons]	3357.192384	3580.611662	3906.47	4147.176865	4136.838656
LC [%]	0.005576186	0.256432424	0.524868	1.284869953	1.313193674
CO [kg]	1677.773372	1552.824518	1404.848	1327.172465	1329.378233
UHC [kg]	3328.708395	2915.884141	2414.086	2153.382698	2160.714419
NOx [kg]	32688.1047	37250.08014	43945.96	49330.93805	49196.36242
NOx [tons]	32.6881047	37.25008014	43.94596	49.33093805	49.19636242
CO_2 [kg]	10534682.14	11235703.98	12258116	13013430.44	12980996.1
CO_2 [tons]	10534.68214	11235.70398	12258.12	13013.43044	12980.9961
Transit time [hrs]	254	254	255	256	256

Table B: 3 Voyage analysis of the cargo ship with the SC model as propulsion prime mover in summer

	IWC	AWC	F1	F2	F3
FB [kg]	1119212.937	1194893.225	1298700	1378946.219	1435492.323
FB [tons]*	3357.638811	3584.679676	3896.1	4136.838656	4306.476969
LC [%]	0.005223	0.280539844	0.537875	1.313193674	1.313193674
CO [kg]	1671.987	1563.964805	1410.283	1329.378233	1291.056
UHC [kg]	3316.602	2944.353516	2430.349	2160.714419	2023.872
NOx [kg]	32761.521	37265.83945	43791.84	49196.36242	52927.062
NOx [tons]	32.761521	37.26583945	43.79184	49.19636242	52.927062
CO_2 [kg]	10536082.23	11248457.13	12225629	12980996.1	13513060.07
CO_2 [tons]	10536.08223	11248.45713	12225.63	12980.9961	13513.06007
Transit time [hrs]	254	255	255	256	257

Table B: 4 Voyage analysis of the cargo ship with the ICR model as propulsion prime mover in winter

	IWC	AWC	HR1	HR1	HR1
FB [kg]	2653618.626	3161368.884	3471661	3680770.139	3826568.164
FB [tons]	2653.618626	3161.368884	3471.661	3680.770139	3826.568164
LC [%]	8.06824E-05	0.005199529	0.009465	0.015657198	0.025268721
CO [kg]	1543.504212	1331.196071	1237.272	1160.257938	1102.406512
UHC [kg]	2035.119718	1632.386282	1459.452	1327.888191	1238.41936
NOx [kg]	22006.82894	27714.60638	31275.07	33841.06091	35885.2664
NOx [tons]	22.00682894	27.71460638	31.27507	33.84106091	35.8852664
CO2 [kg]	8327230.103	9920517.881	10894064	11550097.75	12007477.92
CO2 [tons]	8327.230103	9920.517881	10894.06	11550.09775	12007.47792
Transit time [hrs]	254	254	255	255	255

Table B: 5 Voyage analysis of the cargo ship with the ICR model as propulsion prime mover in spring

	IWC	AWC	HR1	HR1	HR1
FB [kg]	2932245.477	3149420.127	3455496	3668697.427	3810146.422
FB [tons]	2932.245477	3149.420127	3455.496	3668.697427	3810.146422
LC [%]	0.000411	0.006169837	0.009156	0.015874494	0.025950234
CO [kg]	1414.452	1327.71707	1234.722	1157.39142	1098.03498
UHC [kg]	1785.942	1632.206953	1459.076	1326.515953	1236.446191
NOx [kg]	25130.865	27711.22574	31229.58	33841.76043	35896.64484
NOx [tons]	25.130865	27.71122574	31.22958	33.84176043	35.89664484
CO2 [kg]	9201489.789	9882971.48	10843328	11512240.78	11955960.04
CO2 [tons]	9201.489789	9882.97148	10843.33	11512.24078	11955.96004
Transit time [hrs]	254	254	255	255	255

Table B: 6 Voyage analysis of the cargo ship with the SC model as propulsion prime mover in summer

	IWC	AWC	HR1	HR1	HR1
FB [kg]	2932350.435	3145750.671	3449399	3658950.828	3820279.35
FB [tons]	2932.350435	3145.750671	3449.399	3658.950828	3820.27935
LC [%]	0.000408	0.006129	0.008955	0.015732	0.025536
CO [kg]	1413.318	1326.696	1235.07	1156.854	1105.818
UHC [kg]	1785.267	1631.526	1460.175	1327.407	1245.21
NOx [kg]	25142.661	27713.655	31199.69	33816.207	35957.988
NOx [tons]	25.142661	27.713655	31.19969	33.816207	35.957988
CO2 [kg]	9201855.153	9871395.582	10824275	11481679.49	11987685.06
CO2 [tons]	9201.855153	9871.395582	10824.28	11481.67949	11987.68506
Transit time [hrs]	254	254	255	255	256

Table B: 7 Voyage analysis of the cargo ship with the 19MW model as propulsion prime mover in winter

	IWC	AWC	HR1	HR2	HR3
FB [kg]	832408.885	854201.2846	928340.6396	975702.6	1008301.826
FB [tons]	832.408885	854.2012846	928.3406396	975.7026	1008.301826
FB [tons]*	3509.881556	3601.769981	3914.381198	4114.085	4251.540373
LC [%]	0.000222	0.000413742	0.002735231	0.00731	0.011234769
CO [kg]	387.011	380.538	345.2099059	327.1342	319.761098
UHC [kg]	1200.156	1001.105	519.595349	646.2847	757.0863451
NOx [kg]	16641.686	17663.561	20825.71798	23079.9	24503.69277
NOx [tons]	16.641686	17.663561	20.82571798	23.0799	24.50369277
NOx [tons]*	70.17025863	74.47903078	87.81237774	97.31722	103.3206887
CO2 [kg]	2612071.357	2701561.969	2913088.394	3061682	3163920.783
CO2 [tons]	2612.071357	2701.561969	2913.088394	3061.682	3163.920783
CO2 [tons]*	11013.89142	11391.23176	12283.14042	12909.69	13340.78408
Transit time [hrs]	254	254	254	254	255

Table B: 8 Voyage analysis of the cargo ship with the 19MW model as propulsion prime mover in spring

	IWC	AWC	HR1	HR2	HR3
FB [kg]	832664.707	853392.9592	927307.1945	976805.7	1005056.085
FB [tons]	832.664707	853.3929592	927.3071945	976.8057	1005.056085
FB [tons]*	3510.960238	3598.361648	3910.02364	4118.736	4237.854592
LC [%]	0.000188516	0.000412243	0.002563813	0.007986	0.012339222
CO [kg]	381.9564688	373.2534942	341.1140625	322.072	313.7462451
UHC [kg]	1211.510547	951.2853463	469.2997266	626.6587	730.4212062
NOx [kg]	16773.62918	17649.06152	20968.70509	23381.04	24689.38477
NOx [tons]	16.77362918	17.64906152	20.96870509	23.38104	24.68938477
NOx [tons]*	70.72660173	74.41789319	88.41528792	98.58696	104.1036656
CO2 [kg]	2612877.75	2677195.223	2909870.931	3065157	3153712.873
CO2 [tons]	2612.87775	2677.195223	2909.870931	3065.157	3153.712873
CO2 [tons]*	11017.29161	11288.48851	12269.57388	12924.34	13297.74207
Transit time [hrs]	254	254	254	254	255

Table B: 9 Voyage analysis of the cargo ship with the 19MW model as propulsion prime mover in summer

	IWC	AWC	HR1	HR2	HR3
FB [kg]	832692.775	853248.987	928338.8677	976448.9	1000705.128
FB [tons]	832.692775	853.248987	928.3388677	976.4489	1000.705128
FB [tons]*	3511.078588	3597.754584	3914.373727	4117.231	4219.508628
LC [%]	0.000177	0.000502047	0.002720864	0.008065	0.012394607
CO [kg]	380.712	372.3679688	339.951821	321.7429	312.0414708
UHC [kg]	1221.621	961.1310391	469.5155409	616.5153	710.5141012
NOx [kg]	16799.724	17695.36145	21044.3655	23391.77	24608.01614
NOx [tons]	16.799724	17.69536145	21.0443655	23.39177	24.60801614
NOx [tons]*	70.83663146	74.61311848	88.73431274	98.63221	103.7605719
CO2 [kg]	2612991.938	2677474.526	2913100.829	3064032	3140058.229
CO2 [tons]	2612.991938	2677.474526	2913.100829	3064.032	3140.058229
CO2 [tons]*	11017.77308	11289.6662	12283.19286	12919.6	13240.16678
Transit time [hrs]	254	254	254	254	255

Table B: 10 Voyage analysis of the cargo ship with the 36MW model as propulsion prime mover in winter

	IWC	AWC	HR1	HR2	HR3
FB [kg]	1622384.893	1731808.73	1881305.009	1976034.028	1993713.932
FB [tons]	3244.769786	3463.617459	3762.610017	3952.068056	3987.427864
LC [%]	0.016918	0.088437287	0.261788885	0.573397529	0.756533203
CO [kg]	562.726	520.6330543	474.3480577	444.1725869	438.3350391
UHC [kg]	640.876	559.6259922	468.8282885	416.361834	406.8505078
NOx [kg]	26462.809	30244.25059	35650.26323	39434.51931	40268.35986
NOx [tons]	52.925618	60.48850118	71.30052646	78.86903861	80.53671973
CO_2 [kg]	5090988.81	5434278.944	5903354.075	6200525.222	6255921.627
CO_2 [tons]	10181.97762	10868.55789	11806.70815	12401.05044	12511.84325
Transit time [hrs]	254	254	255	255	255

Table B: 11 Voyage analysis of the cargo ship with the 36MW model as propulsion prime mover in spring

	IWC	AWC	HR1	HR2	HR3
FB [kg]	1622754.513	1738419.844	1874395.623	1978000.681	2030009.706
FB [tons]	3245.509026	3476.839688	3748.791246	3956.001361	4060.019412
LC [%]	0.014504	0.099769	0.26383834	0.599311876	0.849422
CO [kg]	553.151	519.256	468.4897852	441.7230388	429.158
UHC [kg]	627.482	558.582	463.1706445	414.3866047	392.242
NOx [kg]	26674.709	30577.331	35820.07014	39775.10698	41769.609
NOx [tons]	53.349418	61.154662	71.64014027	79.55021395	83.539218
CO_2 [kg]	5092119.108	5455025.515	5881662.974	6206688.246	6369728.616
CO_2 [tons]	10184.23822	10910.05103	11763.32595	12413.37649	12739.45723
Transit time [hrs]	254	255	255	256	257

Table B: 12 Voyage analysis of the cargo ship with the 36MW model as propulsion prime mover in summer

	IWC	AWC	HR1	HR2	HR3
FB [kg]	1622786.724	1724487.668	1867569.158	1970135.138	2022580.212
FB [tons]	3245.573448	3448.975336	3735.138316	3940.270275	4045.160424
LC [%]	0.0135	0.104527	0.270481576	0.592911938	0.827745402
CO [kg]	551.69	519.352	470.5305642	443.4139144	431.3759884
UHC [kg]	625.304	560.826	466.9248444	417.3796109	395.6162741
NOx [kg]	26697.308	30276.607	35618.35535	39542.18235	41508.31708
NOx [tons]	53.394616	60.553214	71.2367107	79.0843647	83.01663415
CO_2 [kg]	5092208.799	5411303.185	5860257.152	6182032.443	6346449.996
CO_2 [tons]	10184.4176	10822.60637	11720.5143	12364.06489	12692.89999
Transit time [hrs]	254	255	255	256	257

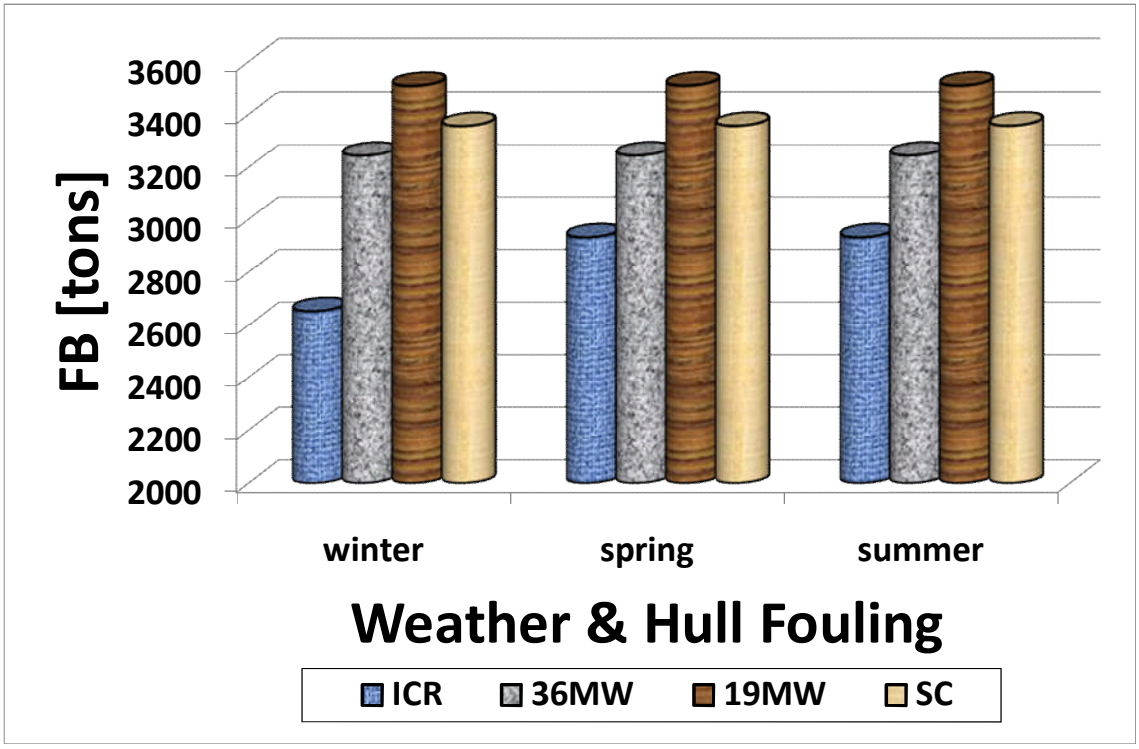

Fig B: 10 Quantities of FB per voyage under IWC

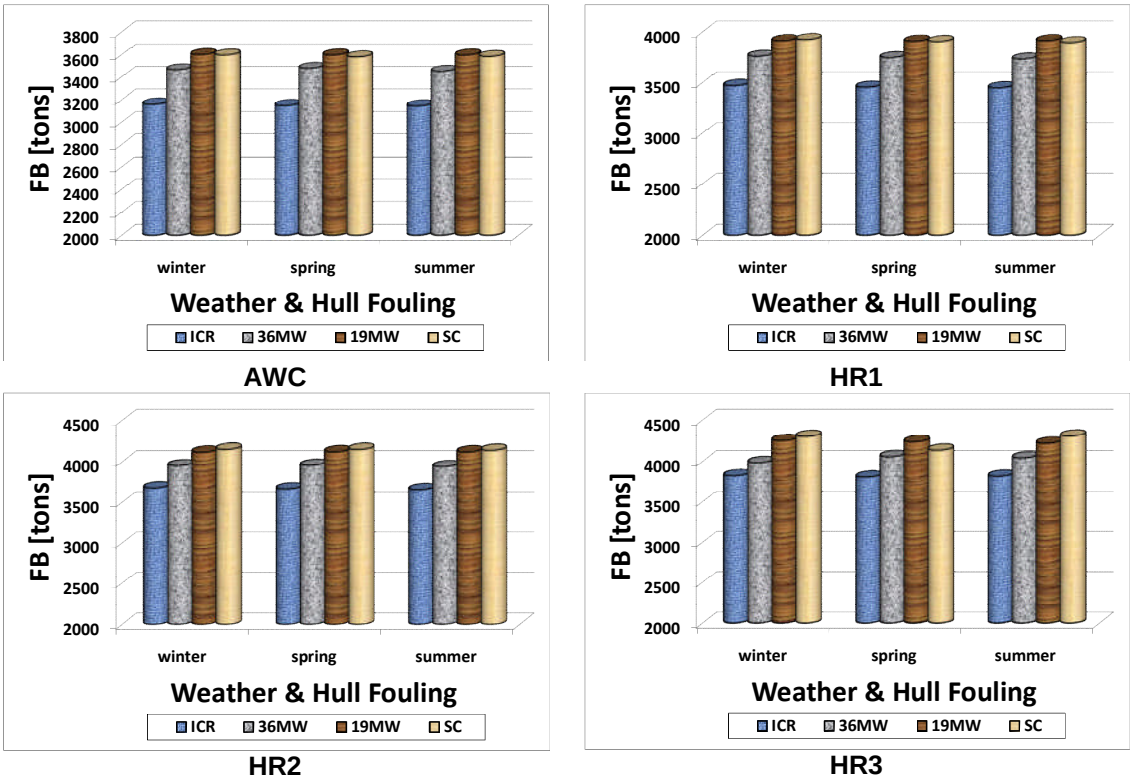

Fig B: 11 Quantities of FB under the variety of investigated scenarios

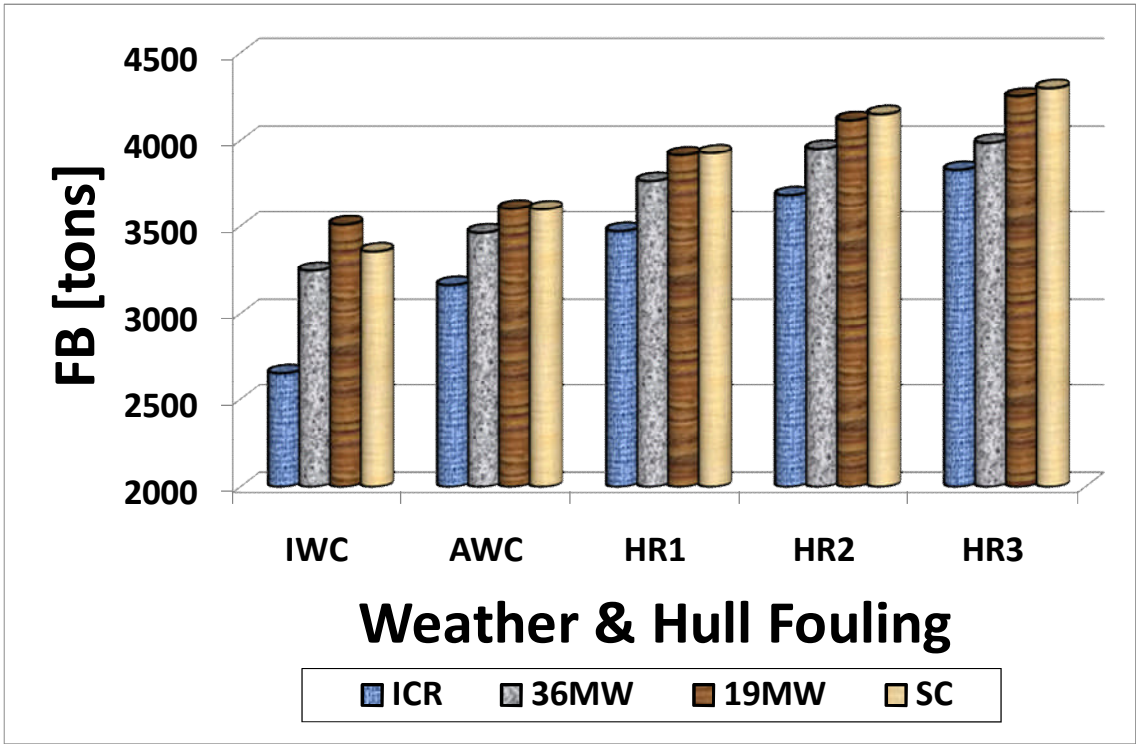

Fig B: 12 Pattern of FB under the variety of investigated scenarios in winter

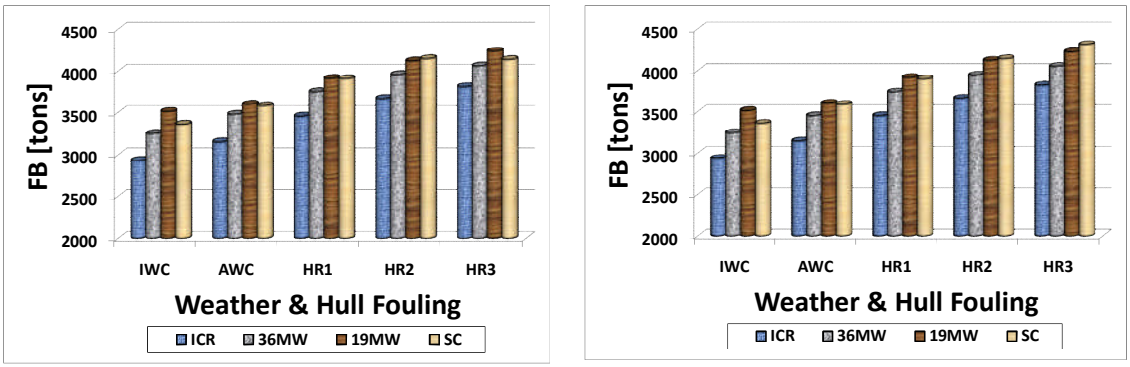

Fig B: 13 Pattern of FB under the variety of investigated scenarios in spring and summer seasons

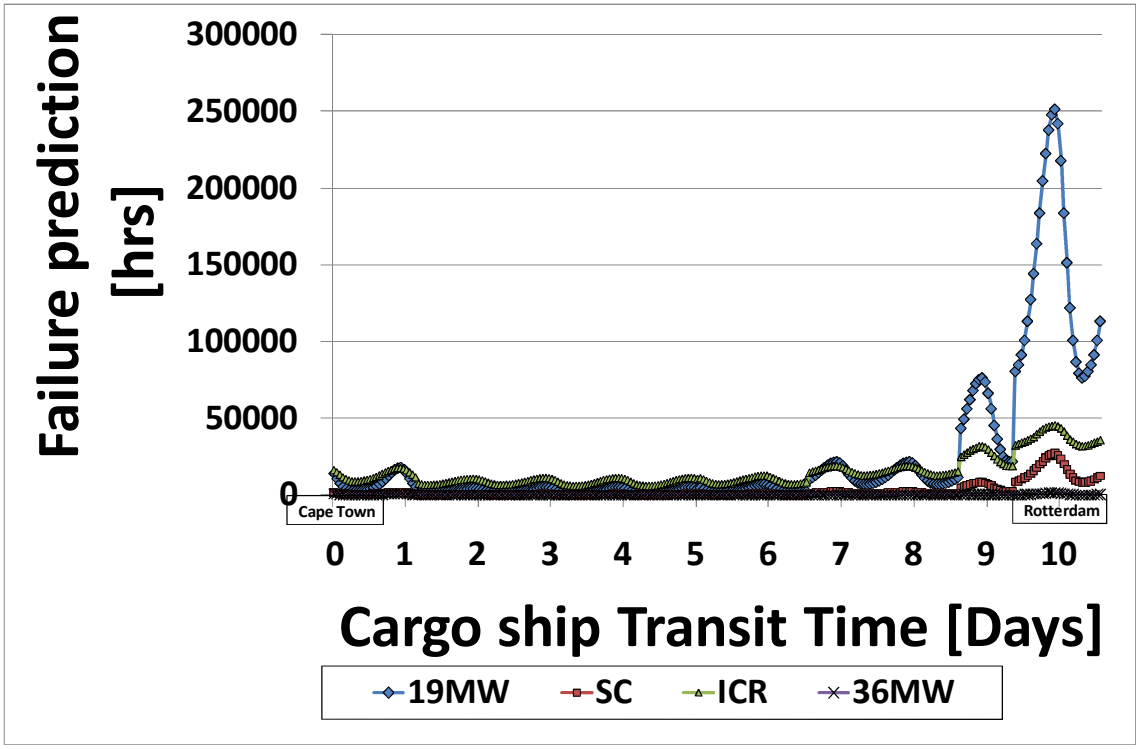

Fig B: 14 Variation of the engine time-to-failure for each of the models when operating under IWC

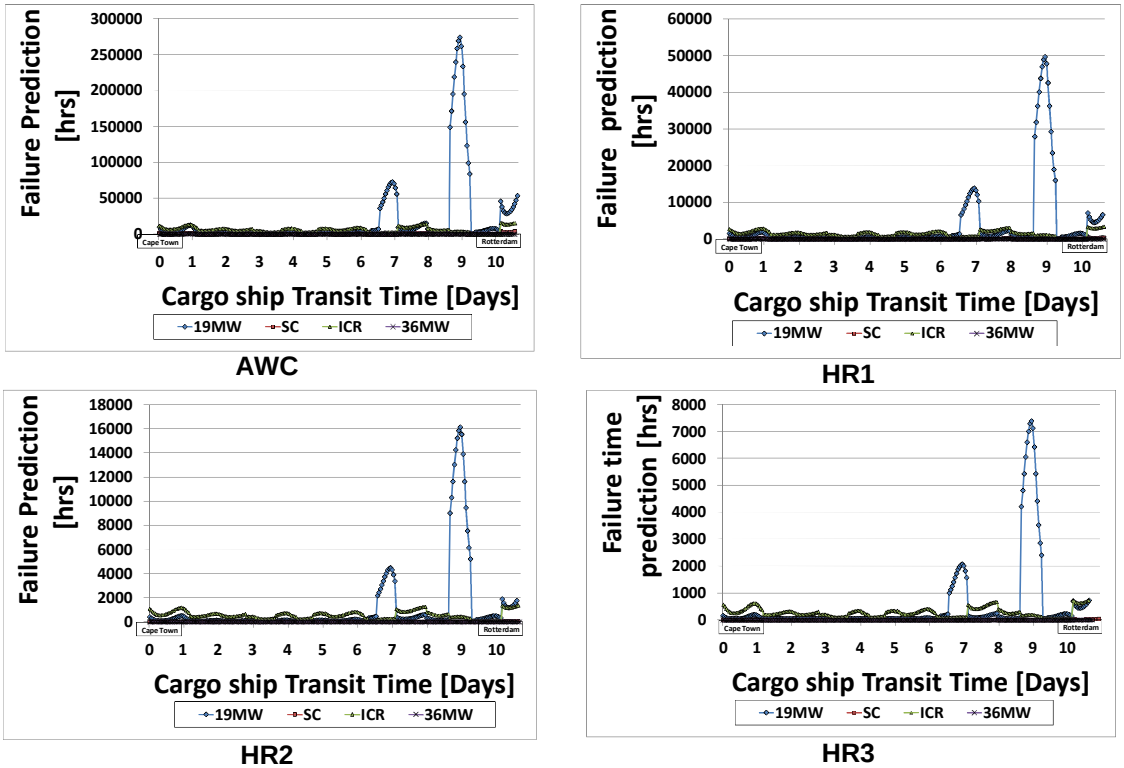

Fig B: 15 Variation of the engine time-to-failure for each of the models according to the selected scenarios

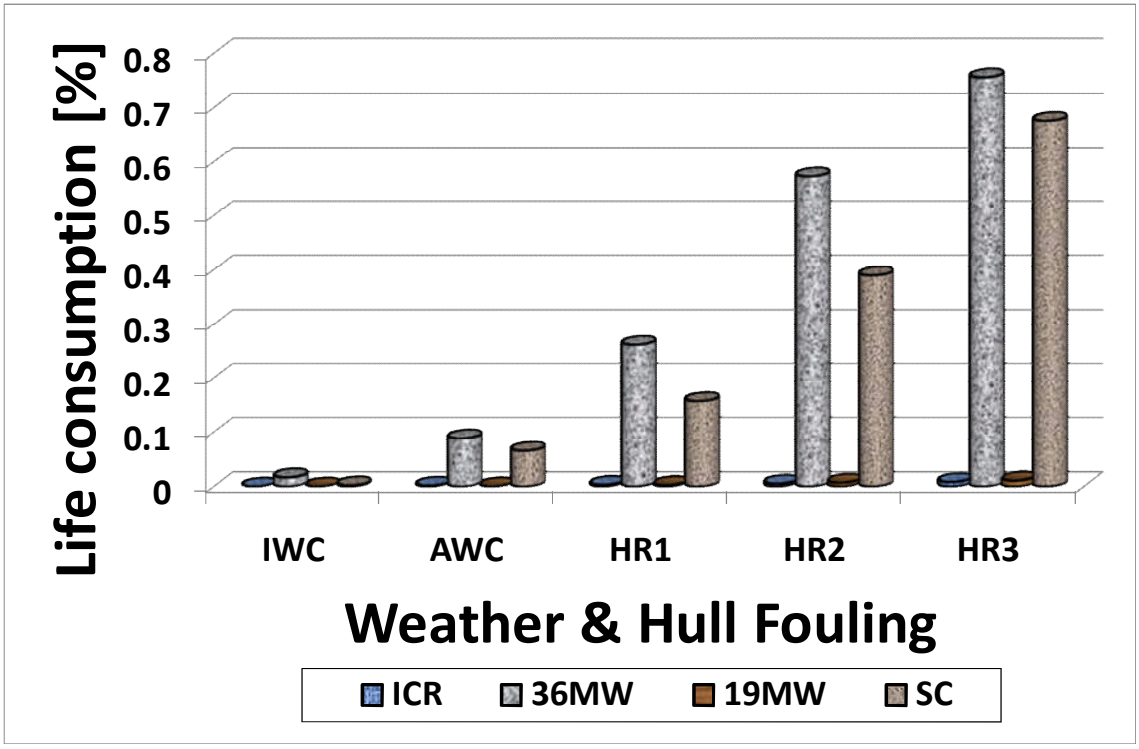

Fig B: 16 HPT Life consumption patterns in winter

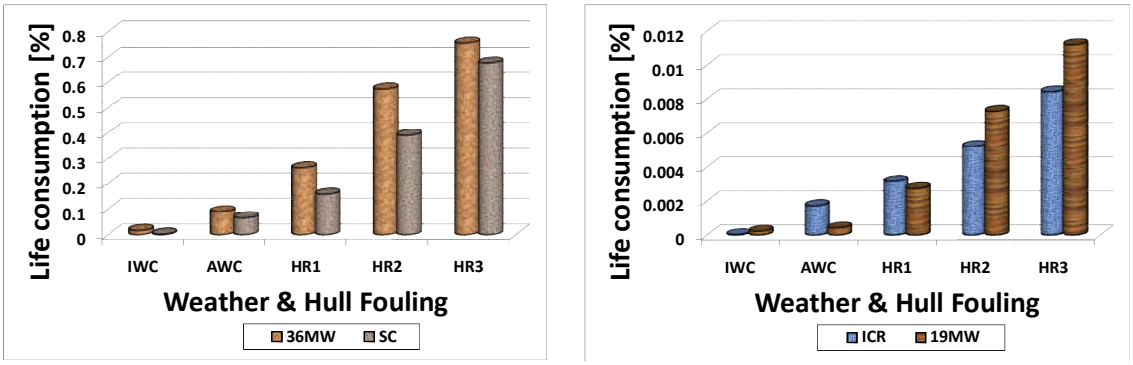

Fig B: 17 Comparison of the HPT life consumption between the (a) SC model and (b) 36MW

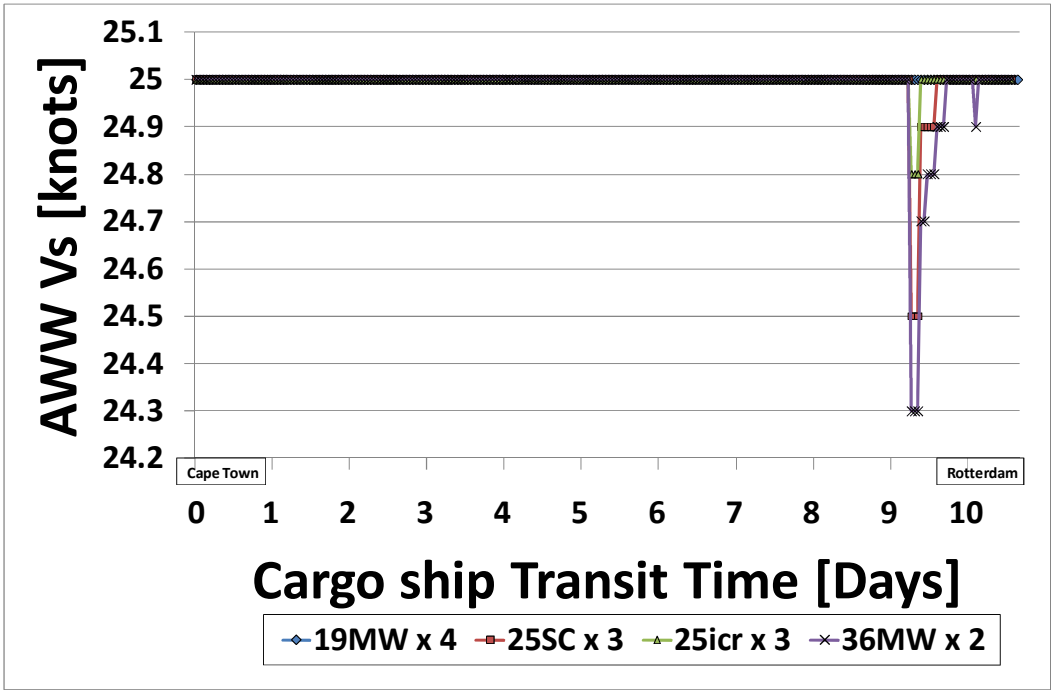

Fig B: 18 Variation of ship speed under AWC during winter

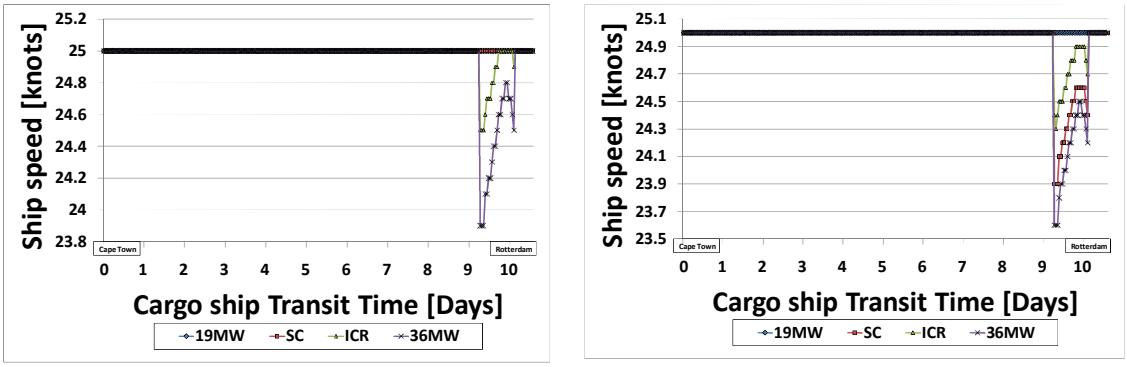

Fig B: 19 Variation of ship speed under AWC during spring and summer

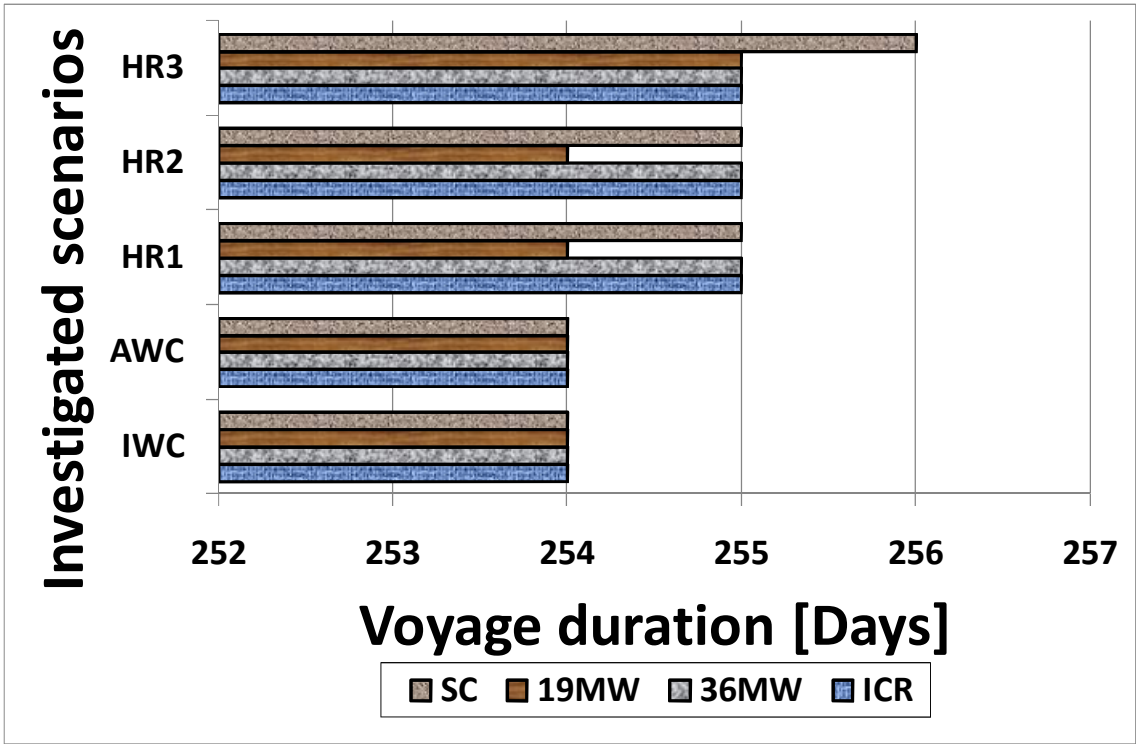

Fig B: 20 Profiles of the transit times for each of the GT models in winter

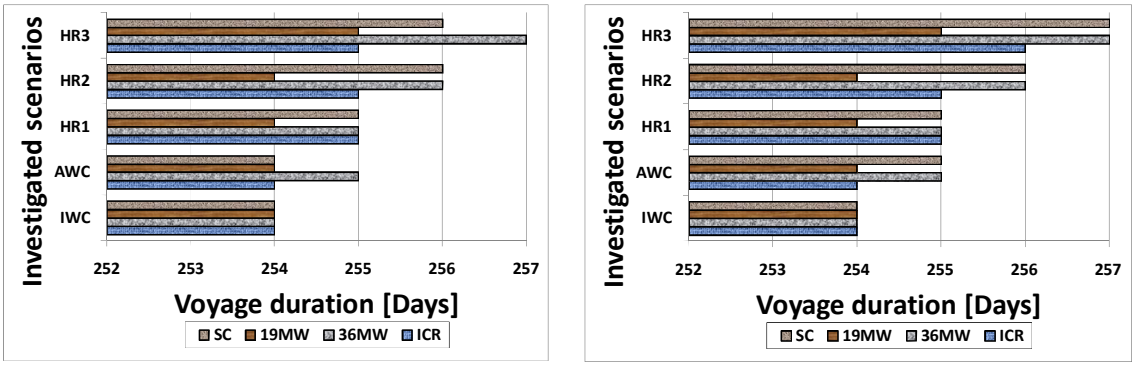

Fig B: 21 Profiles of the transit times for each of the GT models in spring and summer seasons

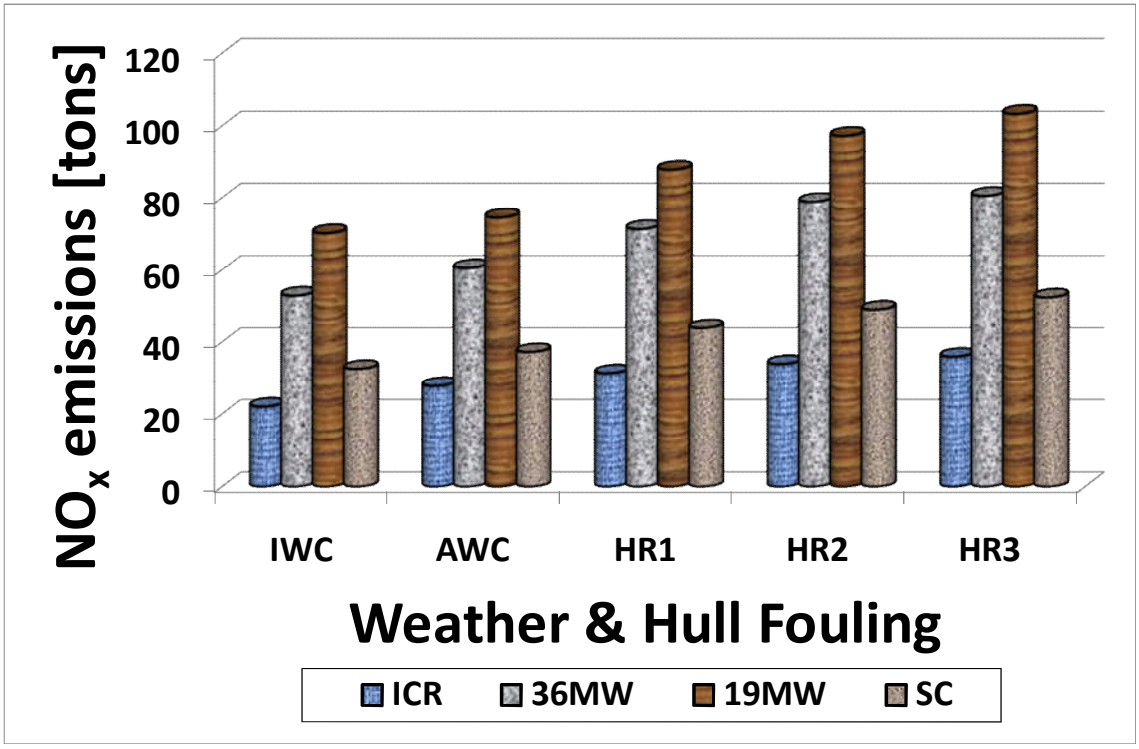

Fig B: 22 NOx emissions quantities in winter season under IWC

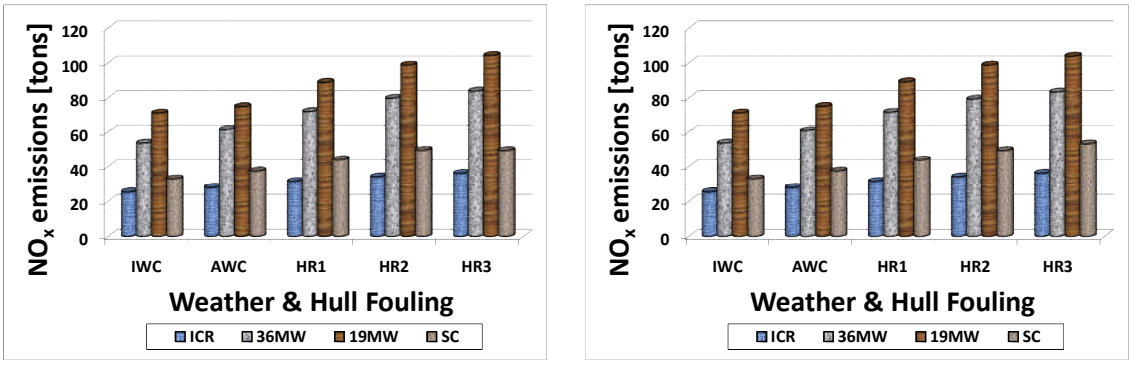

Fig B: 23 NOx emissions quantities in spring and summer seasons under IWC

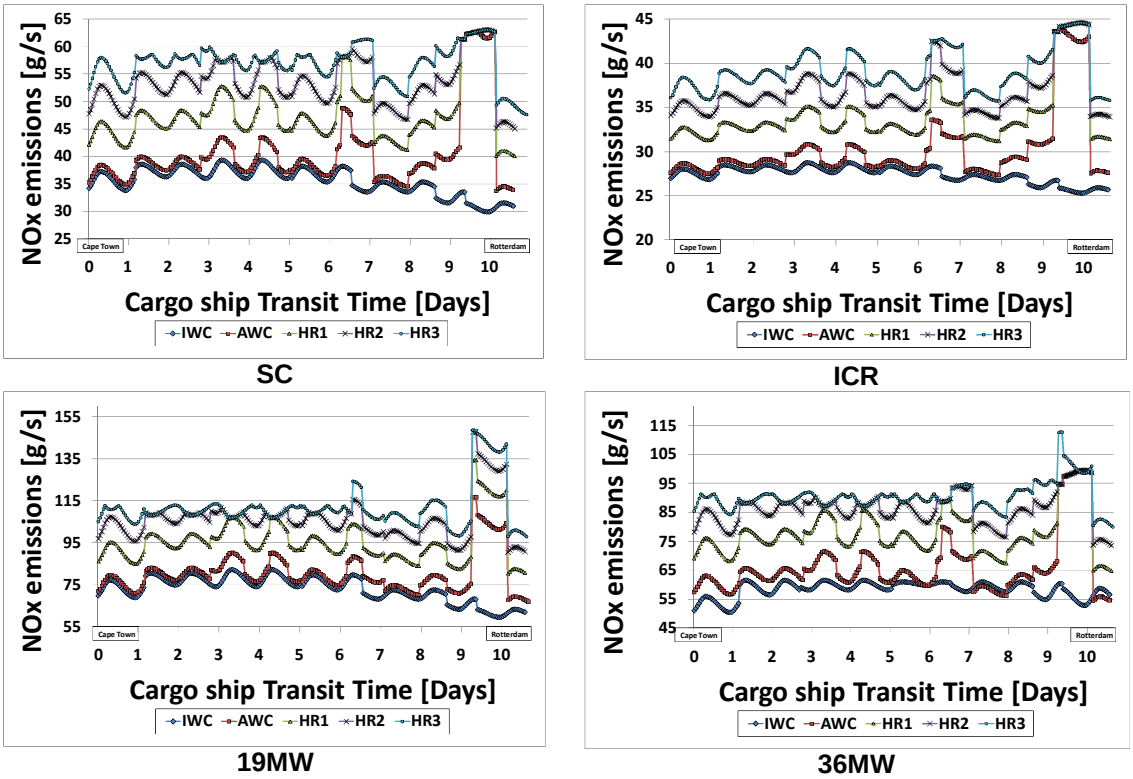

Fig B: 24 Variation of NOx emissions for the variety of GT models in winter season

Appendix C **Cruise Liner Voyage analysis**

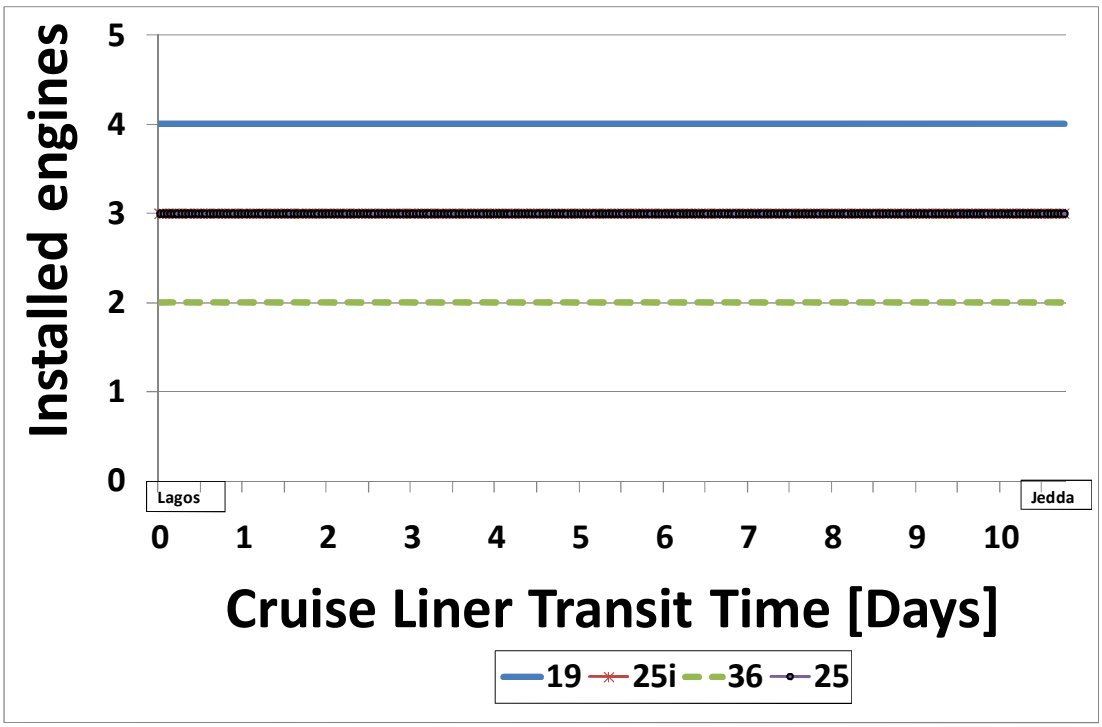

Fig C: 1 Number of operating Gas Turbines required as the voyage progresses

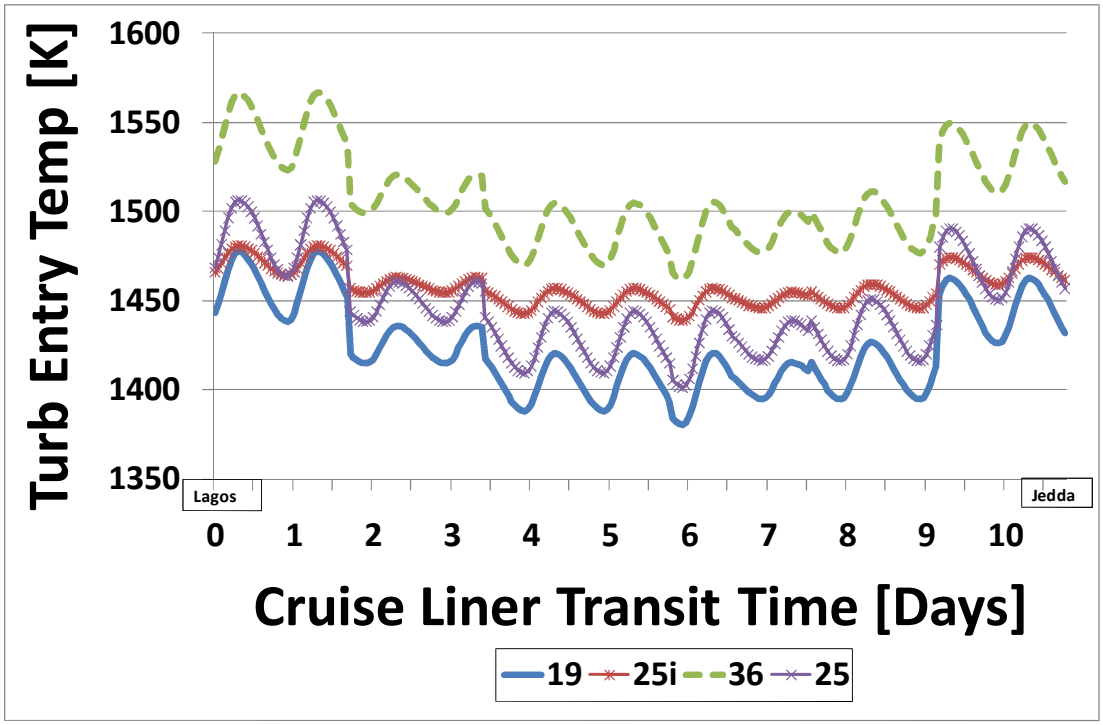

Fig C: 2 Variation of TET in winter season under IWC

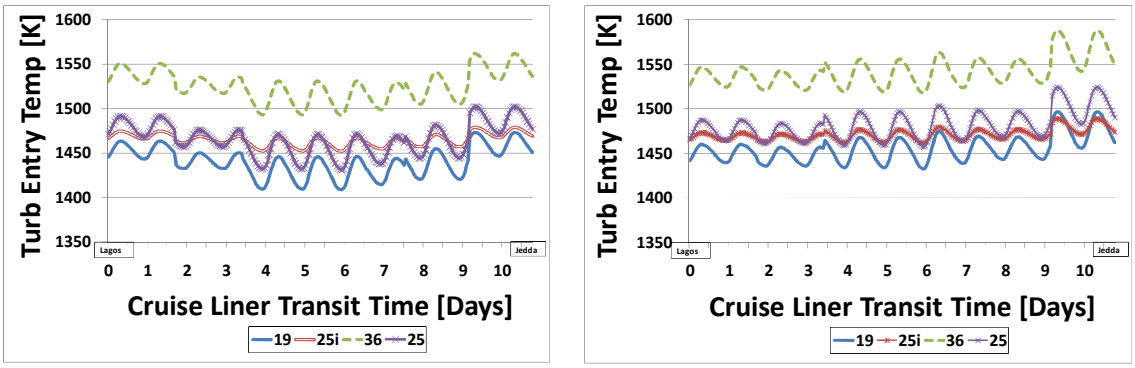

Fig C: 3 Variation of TET in spring and summer seasons under IWC

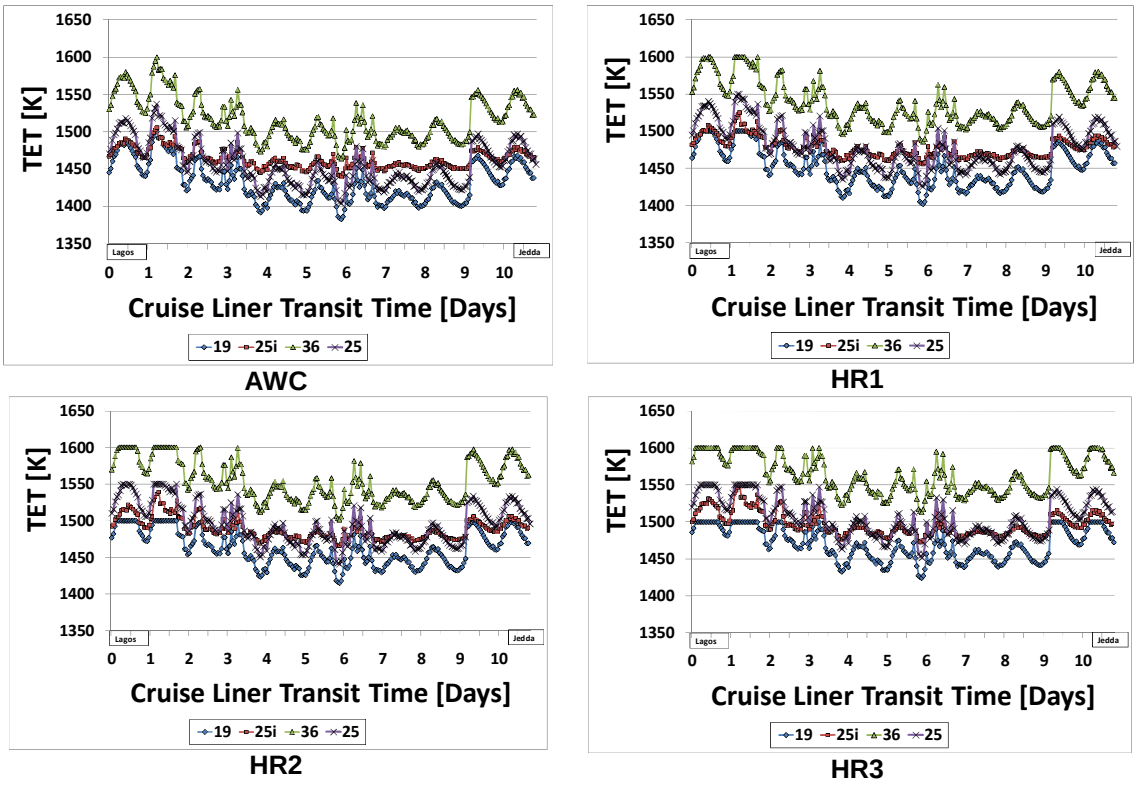

Fig C: 4 Variation of the TET according to the variety of scenarios in winter season

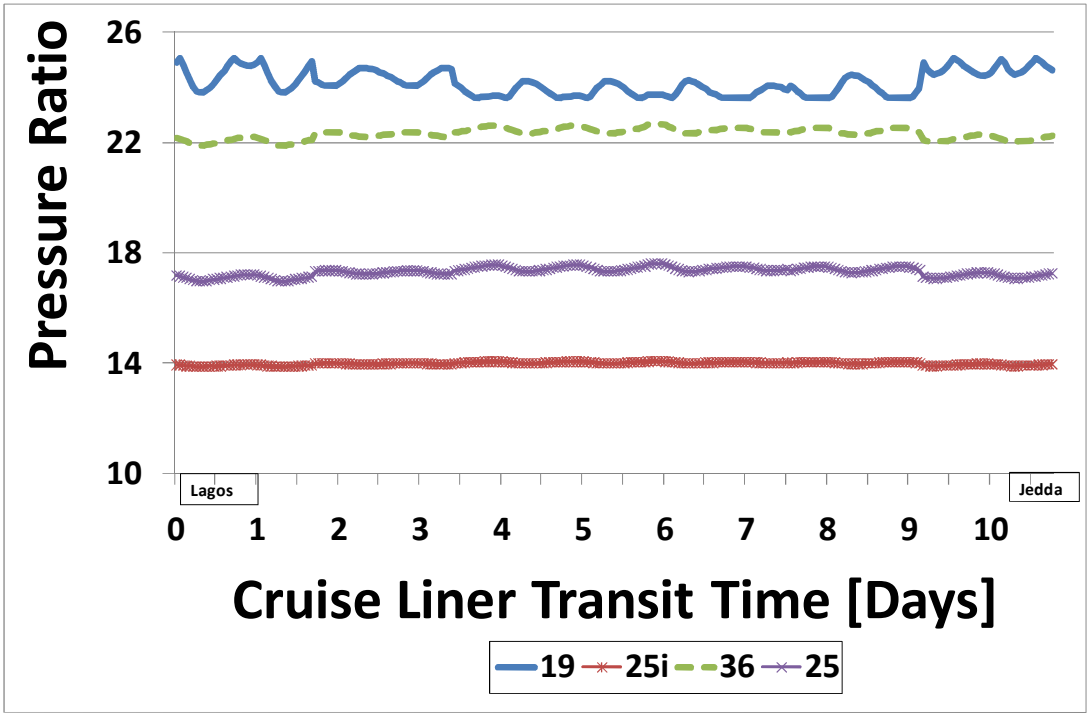

Fig C: 5 Variation of the Pressure Ratio according to the variety of models

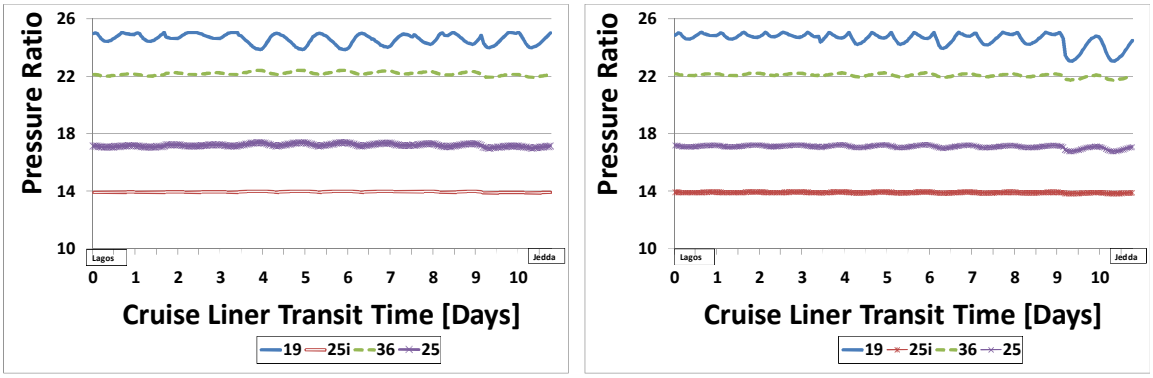

Fig C: 6 Variation of the Pressure Ratio according to the variety of models in spring and summer seasons

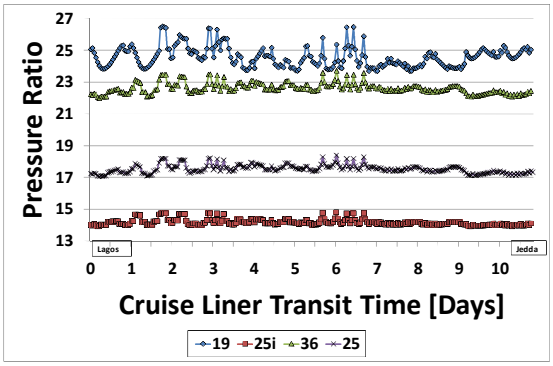

AWC

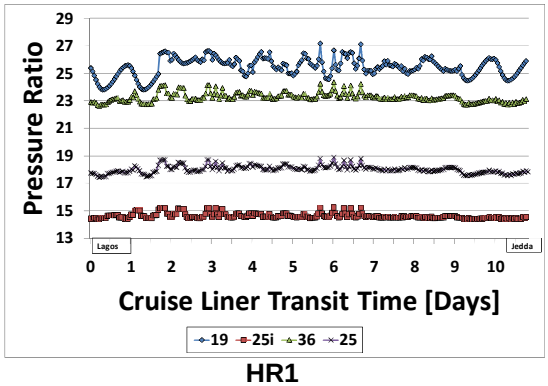

HR1

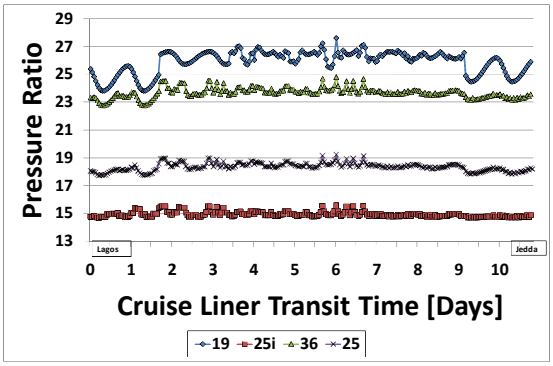

HR2

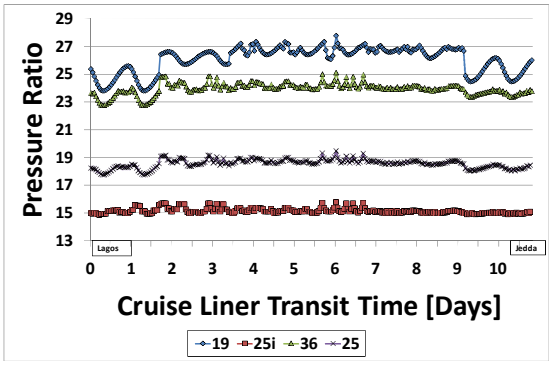

HR3

Fig C: 7 Variation of the Pressure Ratio according to the variety of scenarios in winter

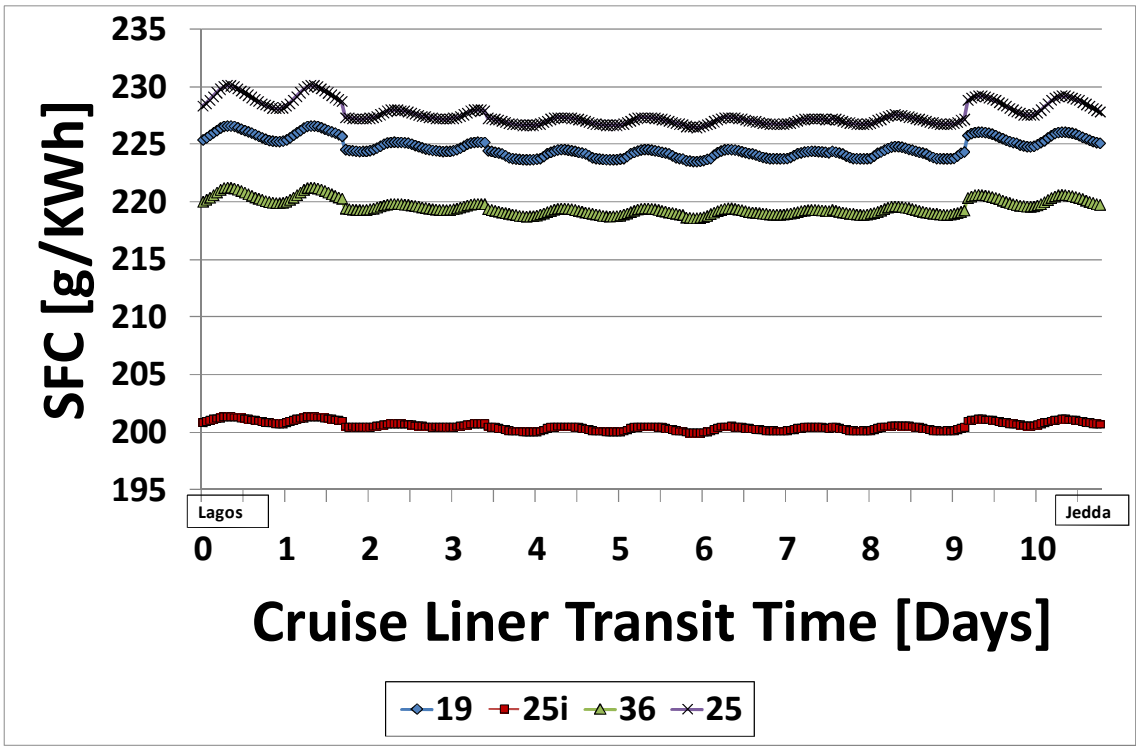

Fig C: 8 Variation of SFC in winter under IWC

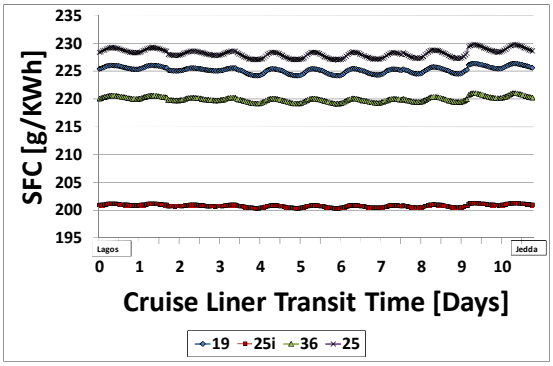

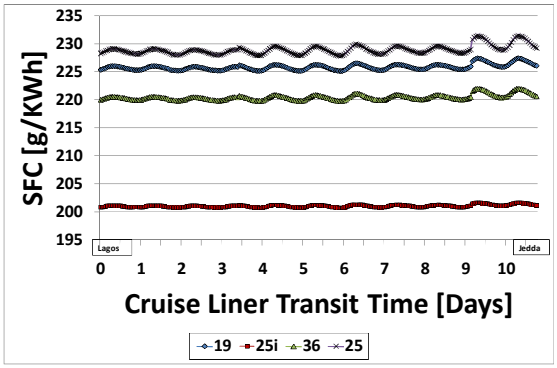

Fig C: 9 Variation of the SFC under IWC in spring and summer

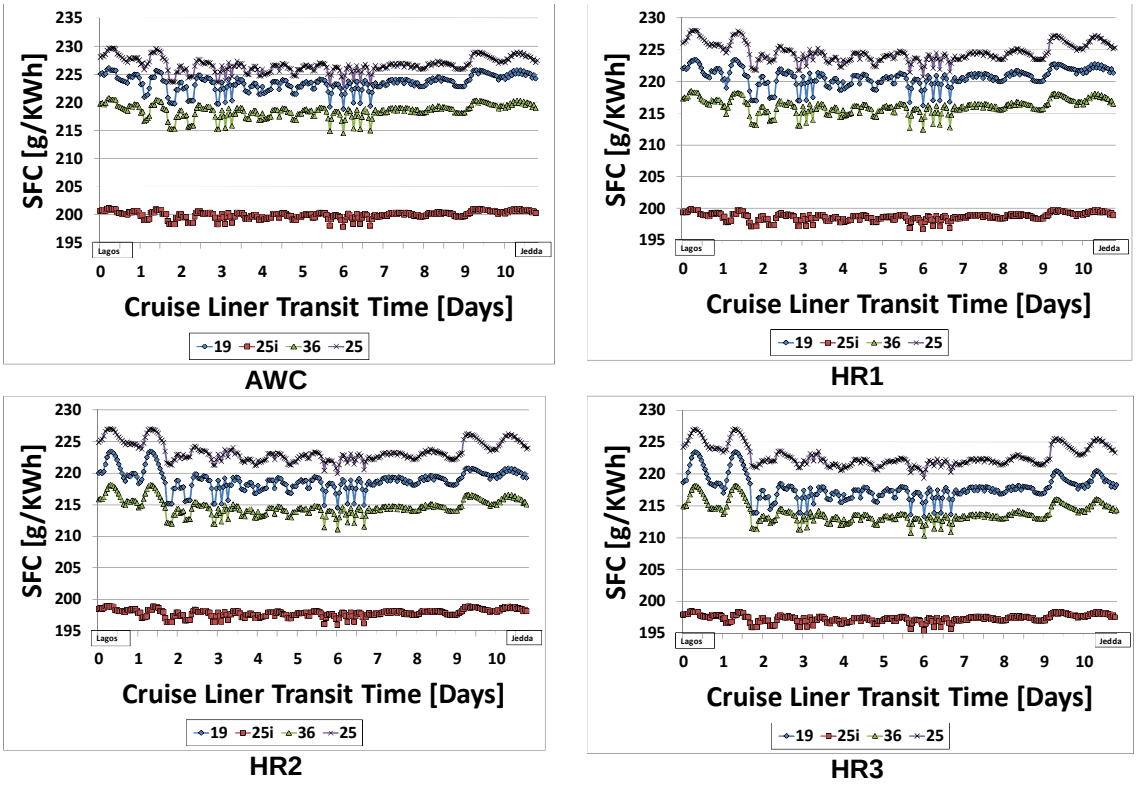

Fig C: 10 Variation of the SFC under the variety of scenarios

Table B: 13 Voyage analysis of the cruise liner with the 19MW GT model as the propulsion prime mover in winter season

	IWC	AWC	HR1	HR2	HR3
FB [kg]	918311.867	935615.352	974670.9283	1000579.507	1021332.124
FB [tons]	3673.247468	3742.461408	3898.683713	4002.318028	4085.328496
LC [%]	0.000758	0.001341	0.003090206	0.00491408	0.006468244
CO [kg]	377.777	370.486	354.6273473	344.2910725	339.0330534
UHC [kg]	874.911	757.494	514.8010534	445.2526336	458.1150382
NOx [kg]	19223.463	19993.243	21773.50524	23001.80483	23914.46855
NOx [tons]	76.893852	79.972972	87.09402095	92.00721931	95.6578742
CO_2 [kg]	2881656.063	2935926.428	3058470.341	3139741.471	3204862.448
CO_2 [tons]	11526.62425	11743.70571	12233.88136	12558.96588	12819.44979
Transit time [hrs]	259	259	259	259	260

Table B: 14 Voyage analysis of the cruise liner with the 19MW GT model as the propulsion prime mover in spring season

	IWC	AWC	HR1	HR2	HR3
FB [kg]	920685.864	938026.706	977881.417	1003153.024	1022132.676
FB [tons]	3682.743456	3752.106824	3911.525668	4012.612096	4088.530706
LC [%]	0.001105	0.001804	0.004766	0.008084359	0.010708812
CO [kg]	356.023	349.19	333.873	324.3925573	320.0819157
UHC [kg]	428.904	368.385	393.957	544.0265344	668.4739464
NOx [kg]	20223.425	21030.377	22943.145	24212.51417	25076.48
NOx [tons]	80.8937	84.121508	91.77258	96.85005667	100.30592
CO_2 [kg]	2889086.336	2943487.681	3068549.703	3147833.86	3207337.435
CO_2 [tons]	11556.34534	11773.95072	12274.19881	12591.33544	12829.34974
Transit time [hrs]	259	259	259	259	260

Table B: 15 Voyage analysis of the cruise liner with the 19MW GT model as the propulsion prime mover in summer season

	IWC	AWC	HR1	HR2	HR3
FB [kg]	922848.489	940023.725	980589.521	1006175.447	1020255.906
FB [tons]	3691.393956	3760.0949	3922.358084	4024.701788	4081.023624
LC [%]	0.002317	0.003466	0.007731	0.012096	0.014754
CO [kg]	338.071	331.625	319.576	312.478	309.628
UHC [kg]	259.581	303.005	576.94	776.474	872.648
NOx [kg]	21155.171	21983.719	23908.438	25120.418	25748.779
NOx [tons]	84.620684	87.934876	95.633752	100.481672	102.995116
CO_2 [kg]	2895861.62	2949761.286	3077030.225	3157253.017	3201377.662
CO_2 [tons]	11583.44648	11799.04514	12308.1209	12629.01207	12805.51065
Transit time [hrs]	259	259	259	260	262

Table B: 16 Voyage analysis of the cruise liner with the 19MW GT model as the propulsion prime mover in winter season

	IWC	AWC	HR1	HR2	HR3
FB [kg]	1240449	1265632	1324778	1367227	1396428.083
FB [tons]	3721.348	3796.896	3974.333	4101.682	4189.284249
LC [%]	0.014232	0.03138	0.099065	0.19475	0.28603
CO [kg]	544.504	531.5865	502.6254	483.8399	471.322
UHC [kg]	1002.134	959.7693	866.3181	808.0182	770.071
NOx [kg]	12589.97	13109.19	14358.59	15298.12	15959.678
NOx [tons]	37.76991	39.32758	43.07576	45.89437	47.879034
CO_2 [kg]	3892479	3971477	4157047	4290238	4381837.175
CO_2 [tons]	11677.44	11914.43	12471.14	12870.72	13145.51153
Transit time [hrs]	259	259	259	259	259

Table B: 17 Voyage analysis of the cruise liner with the 19MW GT model as the propulsion prime mover in spring season

	IWC	AWC	HR1	HR2	HR3
FB [kg]	1243613	1269193	1329798	1373507	1403446.089
FB [tons]	3730.839	3807.58	3989.395	4120.522	4210.338267
LC [%]	0.020326	0.041817	0.138482	0.291976	0.457259
CO [kg]	509.379	496.9931	471.024	454.609	443.995
UHC [kg]	926.134	885.7641	801.714	749.127	715.441
NOx [kg]	13158.89	13708.3	15054.09	16077.24	16798.363
NOx [tons]	39.47666	41.1249	45.16227	48.23171	50.395089
CO_2 [kg]	3902371	3982655	4172818	4309969	4403875.638
CO_2 [tons]	11707.11	11947.96	12518.45	12929.91	13211.62691
Transit time [hrs]	259	259	259	259	259

Table B: 18 Voyage analysis of the cruise liner with the 19MW GT model as the propulsion prime mover in summer season

	IWC	AWC	HR1	HR2	HR3
FB [kg]	922848.489	940023.725	980589.521	1006175.447	1020255.906
FB [tons]	3691.393956	3760.0949	3922.358084	4024.701788	4081.023624
LC [%]	0.002317	0.003466	0.007731	0.012096	0.014754
CO [kg]	338.071	331.625	319.576	312.478	309.628
UHC [kg]	259.581	303.005	576.94	776.474	872.648
NOx [kg]	21155.171	21983.719	23908.438	25120.418	25748.779
NOx [tons]	84.620684	87.934876	95.633752	100.481672	102.995116
CO_2 [kg]	2895861.62	2949761.286	3077030.225	3157253.017	3201377.662
CO_2 [tons]	11583.44648	11799.04514	12308.1209	12629.01207	12805.51065
Transit time [hrs]	259	259	259	260	262

Table B: 19 Voyage analysis of the cruise liner with the ICR GT model as the propulsion prime mover in winter season

	IWC	AWC	HR1	HR2	HR3
FB [kg]	1092704	1116550	1172042	1211663	1239807
FB [tons]	3278.111	3349.65	3516.127	3634.989	3719.421
LC [%]	0.000449	0.000653	0.001327	0.002209	0.003193
CO [kg]	456.162	448.612	431.553	417.83	407.329
UHC [kg]	550.942	537.338	506.942	483.534	466.231
NOx [kg]	9488.912	9754.88	10373.05	10833.07	11174.93
NOx [tons]	28.46674	29.26464	31.11916	32.4992	33.52478
CO_2 [kg]	3428943	3503810	3677897	3802222	3890516
CO_2 [tons]	10286.83	10511.43	11033.69	11406.67	11671.55
Transit time [hrs]	259	259	259	259	259

Table B: 20 7 Voyage analysis of the cruise liner with the ICR GT model as the propulsion prime mover in spring season

	IWC	AWC	HR1	HR2	HR3
FB [kg]	1094085	1117947	1173525	1213226	1241441
FB [tons]	3282.255	3353.841	3520.575	3639.679	3724.322
LC [%]	0.000568	0.000812	0.001664	0.002805	0.00409
CO [kg]	443.749	436.481	417.637	402.587	391.51
UHC [kg]	538.229	524.973	491.528	466.036	448.194
NOx [kg]	9661.819	9934.379	10581.16	11069.03	11440.9
NOx [tons]	28.98546	29.80314	31.74349	33.20709	34.32269
CO_2 [kg]	3433258	3508149	3682567	3807085	3895623
CO_2 [tons]	10299.77	10524.45	11047.7	11421.25	11686.87
Transit time [hrs]	259	259	259	259	259

Table B: 21 7 Voyage analysis of the cruise liner with the ICR GT model as the propulsion prime mover in summer season

	IWC	AWC	HR1	HR2	HR3
FB [kg]	1095304	1119217	1174936	1214709	1242973
FB [tons]	3285.911	3357.652	3524.809	3644.126	3728.918
LC [%]	0.000736	0.001041	0.002183	0.003722	0.005474
CO [kg]	432.865	424.858	404.178	388.483	377.409
UHC [kg]	526.638	512.17	475.839	449.718	432.524
NOx [kg]	9830.274	10112.75	10793.24	11317.42	11724.5
NOx [tons]	29.49082	30.33826	32.37971	33.95227	35.17351
CO_2 [kg]	3437108	3512158	3686934	3811718	3900395
CO_2 [tons]	10311.32	10536.47	11060.8	11435.15	11701.19
Transit time [hrs]	259	259	259	259	259

Table B: 22 Voyage analysis of the cruise liner with the SC GT model as the propulsion prime mover in winter season

	IWC	AWC	HR1	HR2	HR3
FB [kg]	1240449	1265632	1324778	1367227	1396428.083
FB [tons]	3721.348	3796.896	3974.333	4101.682	4189.284249
LC [%]	0.014232	0.03138	0.099065	0.19475	0.28603
CO [kg]	544.504	531.5865	502.6254	483.8399	471.322
UHC [kg]	1002.134	959.7693	866.3181	808.0182	770.071
NOx [kg]	12589.97	13109.19	14358.59	15298.12	15959.678
NOx [tons]	37.76991	39.32758	43.07576	45.89437	47.879034
CO_2 [kg]	3892479	3971477	4157047	4290238	4381837.175
CO_2 [tons]	11677.44	11914.43	12471.14	12870.72	13145.51153
Transit time [hrs]	259	259	259	259	259

Table B: 23 Voyage analysis of the cruise liner with the SC GT model as the propulsion prime mover in spring season

	IWC	AWC	HR1	HR2	HR3
FB [kg]	1243613	1269193	1329798	1373507	1403446.089
FB [tons]	3730.839	3807.58	3989.395	4120.522	4210.338267
LC [%]	0.020326	0.041817	0.138482	0.291976	0.457259
CO [kg]	509.379	496.9931	471.024	454.609	443.995
UHC [kg]	926.134	885.7641	801.714	749.127	715.441
NOx [kg]	13158.89	13708.3	15054.09	16077.24	16798.363
NOx [tons]	39.47666	41.1249	45.16227	48.23171	50.395089
CO_2 [kg]	3902371	3982655	4172818	4309969	4403875.638
CO_2 [tons]	11707.11	11947.96	12518.45	12929.91	13211.62691
Transit time [hrs]	259	259	259	259	259

Table B: 24 Voyage analysis of the cruise liner with the SC GT model as the propulsion prime mover in summer season

	IWC	AWC	HR1	HR2	HR3
FB [kg]	1247472	1273497	1334842	1376255	1402560.347
FB [tons]	3742.417	3820.491	4004.526	4128.766	4207.681041
LC [%]	0.044081	0.079363	0.248999	0.464524	0.672088065
CO [kg]	482.486	470.734	446.901	433.4495	424.7709577
UHC [kg]	868.53	830.069	751.723	707.5312	679.4366923
NOx [kg]	13723.55	14301.43	15725.31	16732.71	17387.93013
NOx [tons]	41.17066	42.9043	47.17592	50.19812	52.1637904
CO_2 [kg]	3914475	3996146	4188656	4318541	4401051.13
CO_2 [tons]	11743.43	11988.44	12565.97	12955.62	13203.15339
Transit time [hrs]	259	259	259	259	259

Table B: 25 Voyage analysis of the cruise liner with the 36MW GT model as the propulsion prime mover in winter season

	IWC	AWC	HR1	HR2	HR3
FB [kg]	1794890	1829940	1910608	1965192	2008999
FB [tons]	3589.78	3659.88	3821.216	3930.383	4017.998
LC [%]	0.054626	0.091716	0.204317	0.312615	0.401177
CO [kg]	541.775	529.563	502.122	484.1656	473.9043
UHC [kg]	571.979	548.838	497.969	466.2269	447.3923
NOx [kg]	30840.83	32120.08	35131.06	37255.11	38839.57
NOx [tons]	61.68166	64.24017	70.26211	74.51022	77.67913
CO_2 [kg]	5632271	5742253	5995337	6166545	6303989
CO_2 [tons]	11264.54	11484.51	11990.67	12333.09	12607.98
Transit time [hrs]	259	259	259	259	260

Table B: 26 Voyage analysis of the cruise liner with the 36MW GT model as the propulsion prime mover in spring season

	IWC	AWC	HR1	HR2	HR3
FB [kg]	1798234	1847510	1915885	1971475	2012209
FB [tons]	3596.469	3695.019	3831.77	3942.95	4024.417
LC [%]	0.078251	0.12313	0.295453	0.496487	0.642808
CO [kg]	508.859	501.17	471.533	454.489	445.9208
UHC [kg]	530.918	513.155	461.745	432.003	416.4366
NOx [kg]	32365.56	33968.13	36913.39	39139.44	40647.09
NOx [tons]	64.73112	67.93626	73.82678	78.27888	81.29417
CO_2 [kg]	5642765	5797368	6011895	6186274	6314019
CO_2 [tons]	11285.53	11594.74	12023.79	12372.55	12628.04
Transit time [hrs]	259	259	259	259	260

Table B: 27 Voyage analysis of the cruise liner with the 36MW GT model as the propulsion prime mover in summer season

FB [kg]	1801888	1851468	1916764	1980547	2004948
FB [tons]	3603.776	3702.936	3833.529	3961.095	4009.897
LC [%]	0.166982	0.243795	0.518801	0.785006	0.94698
CO [kg]	482.506	474.648	447.0648	436.133	428.6457
UHC [kg]	498.748	481.036	434.1108	412.688	400.0204
NOx [kg]	33786.52	35442.6	38335.92	40630.44	41641.51
NOx [tons]	67.57304	70.8852	76.67185	81.26088	83.28301
CO_2 [kg]	5654214	5809782	6014617	6214693	6291153
CO_2 [tons]	11308.43	11619.56	12029.23	12429.39	12582.31
Transit time [hrs]	259	259	259	260	261

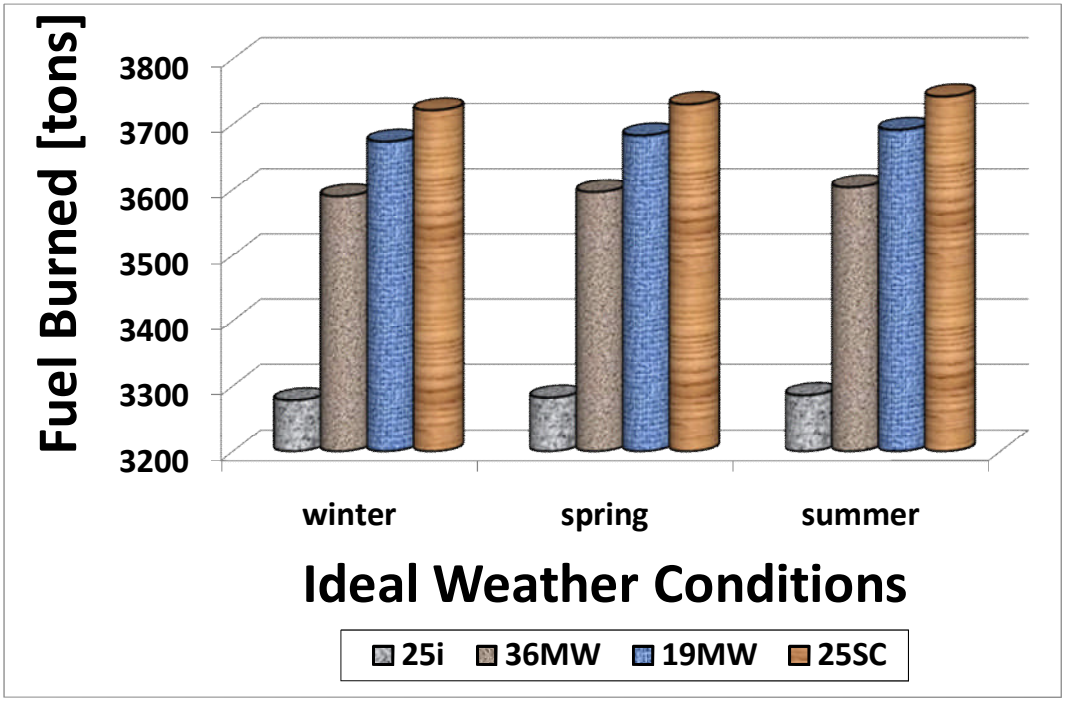

Fig C: 11 Quantity of fuel burned per voyage under IWC

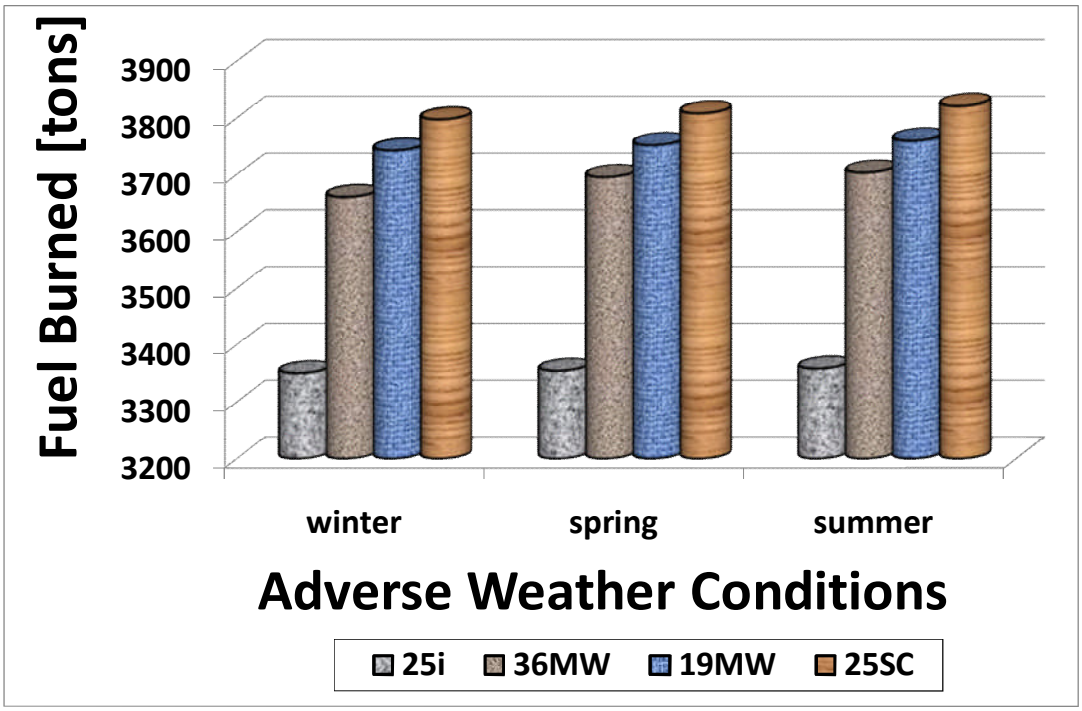

Fig C: 12 Quantity of fuel burned per voyage under AWC

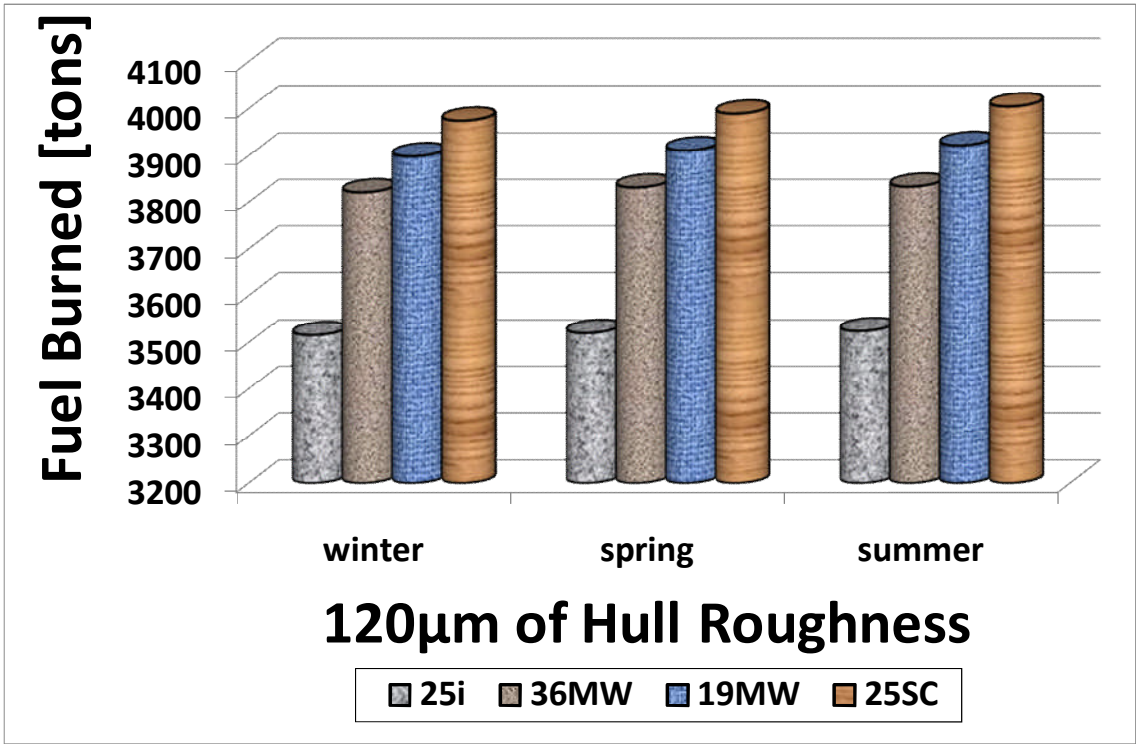

Fig C: 13 Quantity of fuel burned per voyage under HR1

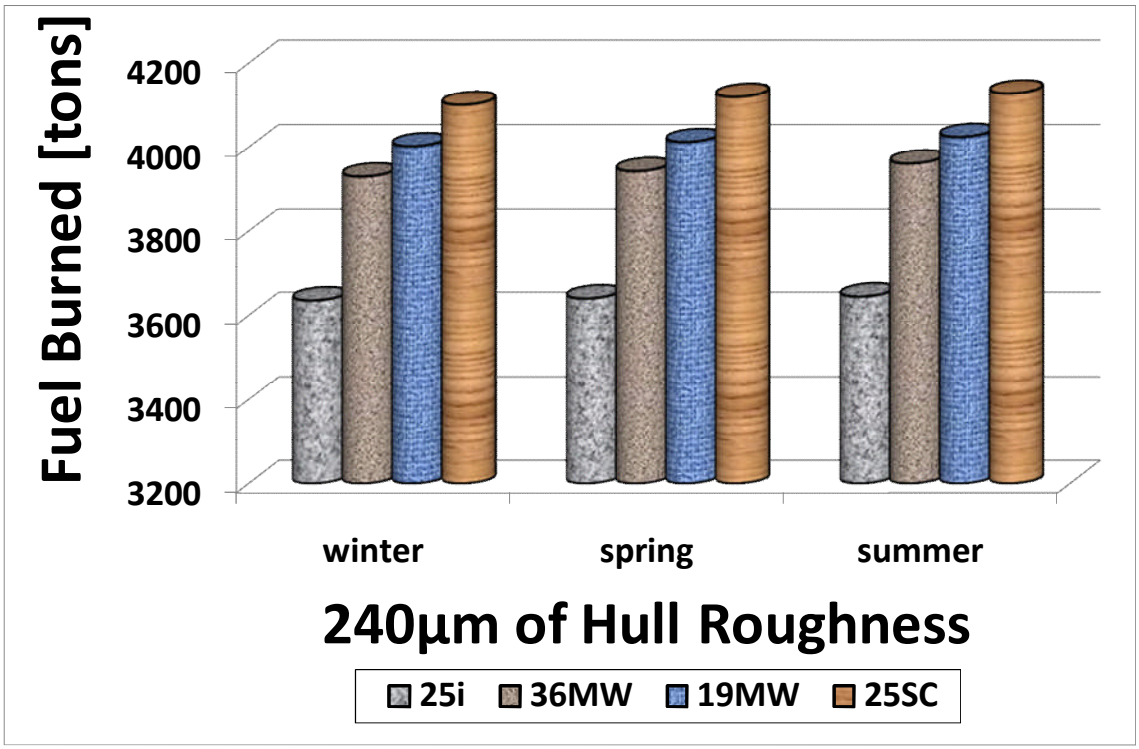

Fig C: 14 Quantity of fuel burned per voyage under HR2

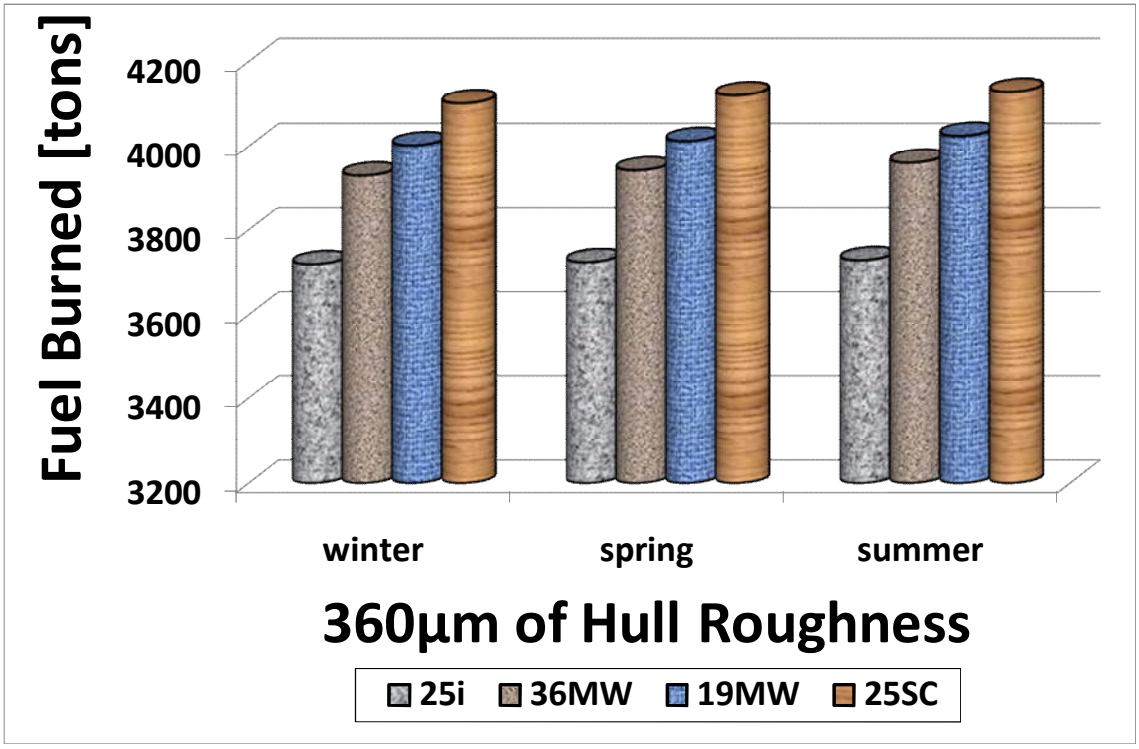

Fig C: 15 Quantity of fuel burned per voyage under HR3

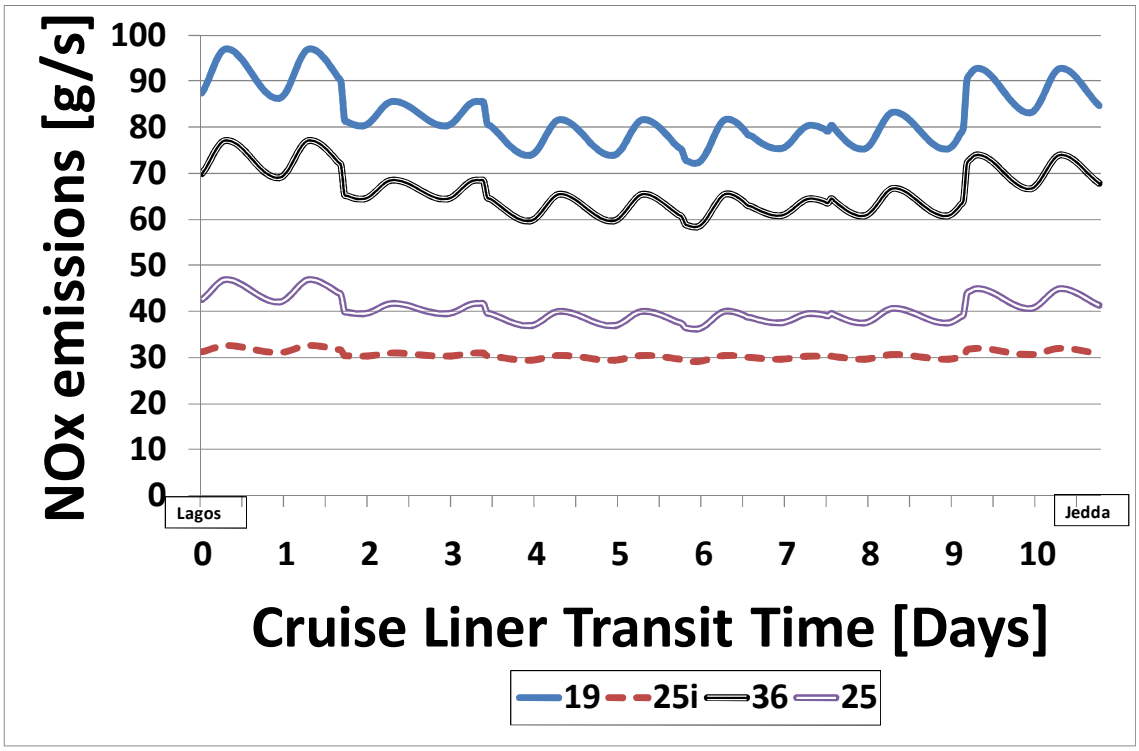

Fig C: 16 Variation of NO_x emissions in winter under IWC

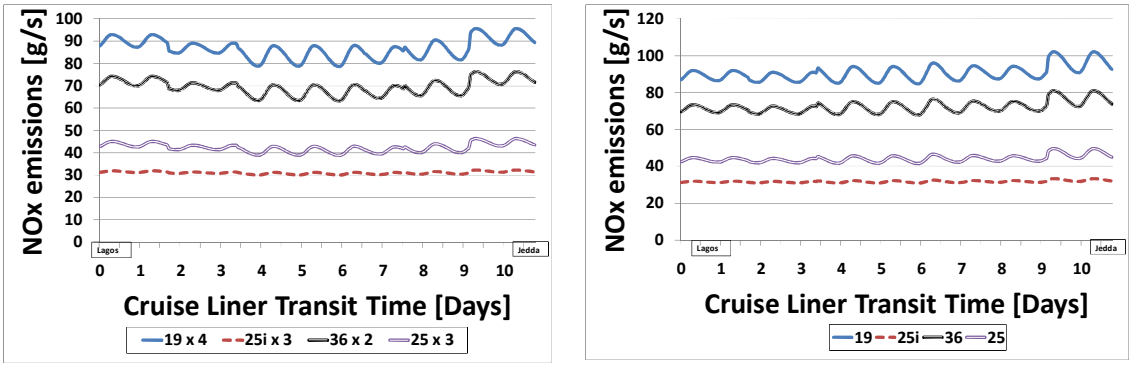

Fig C: 17 Variation of NOx emissions under IWC in spring and summer weather

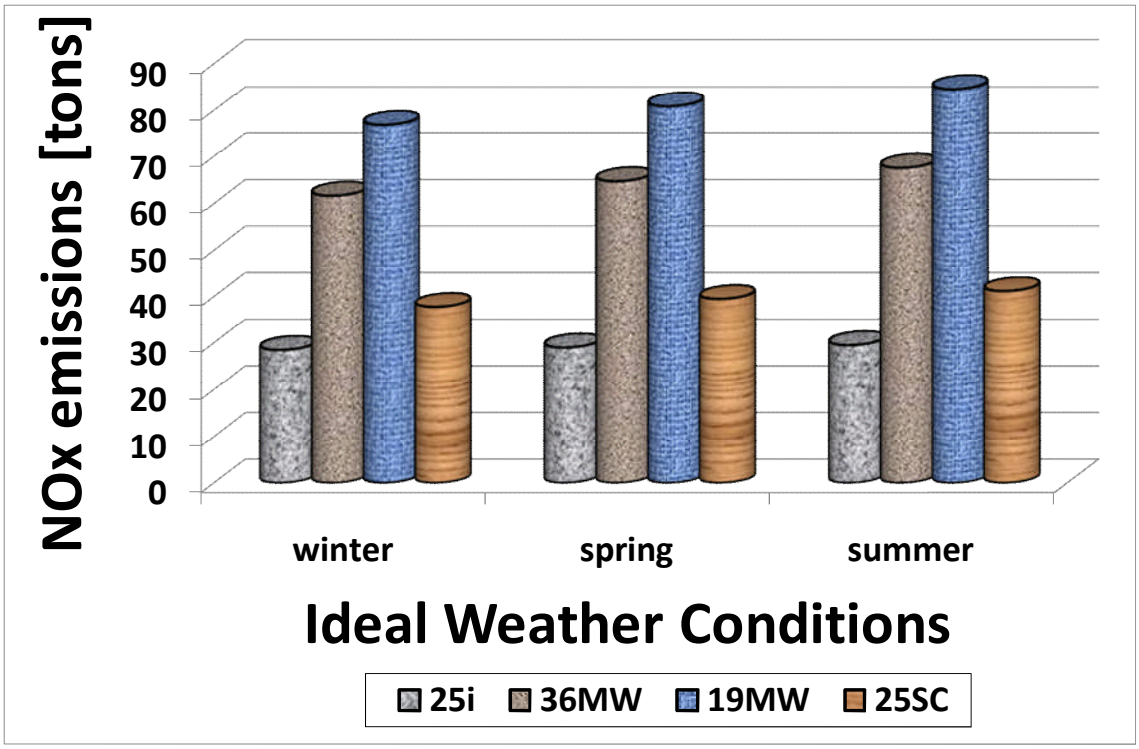

Fig C: 18 Quantities of NO_x emissions under IWC

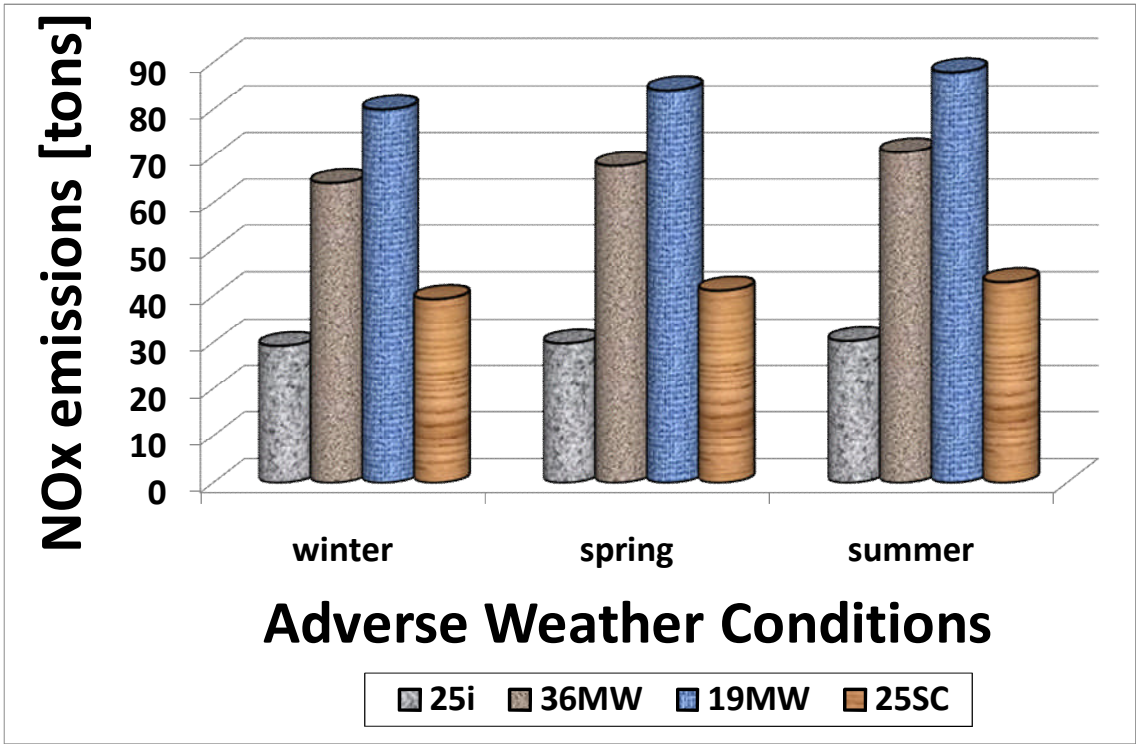

Fig C: 19 Quantities of NO_x emissions under AWC

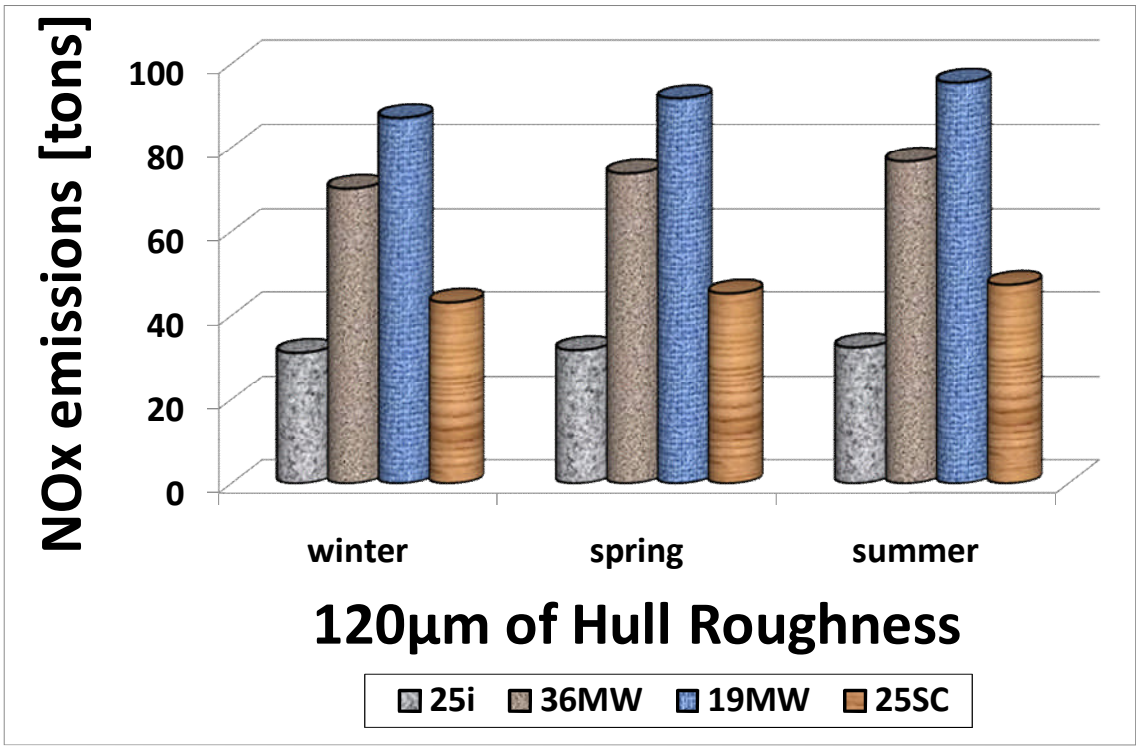

Fig C: 20 Quantities of NO_x emissions under HR1

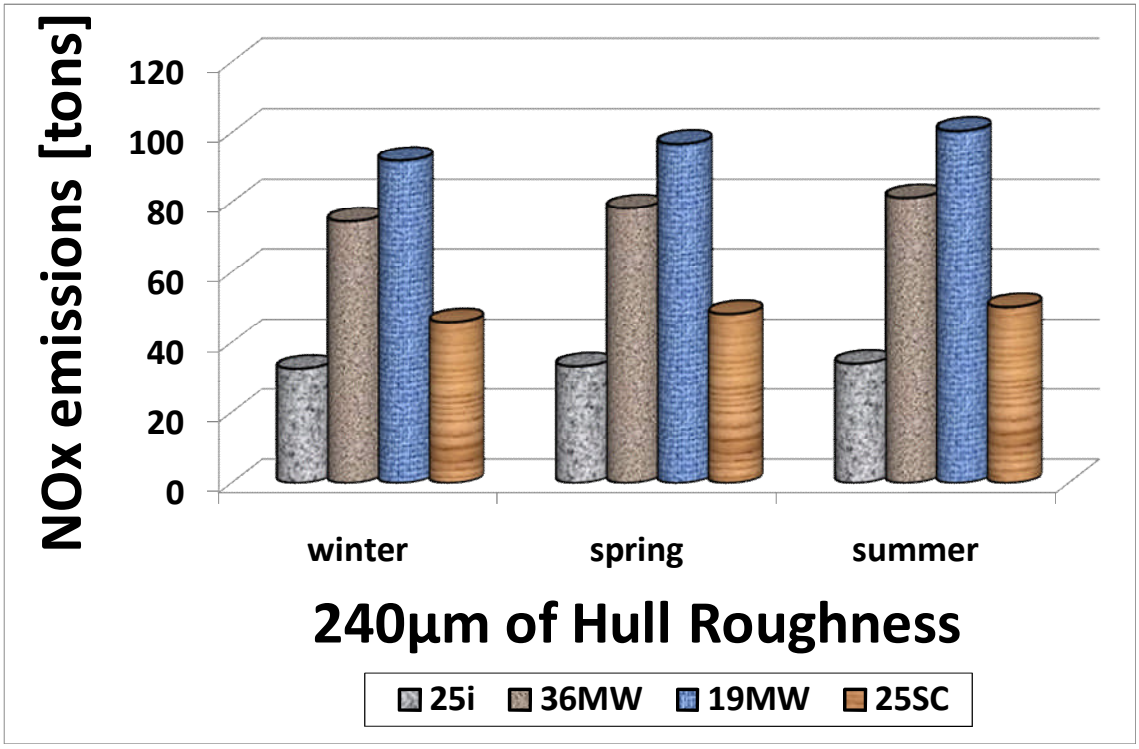

Fig C: 21 Quantities of NO_x emissions under HR2

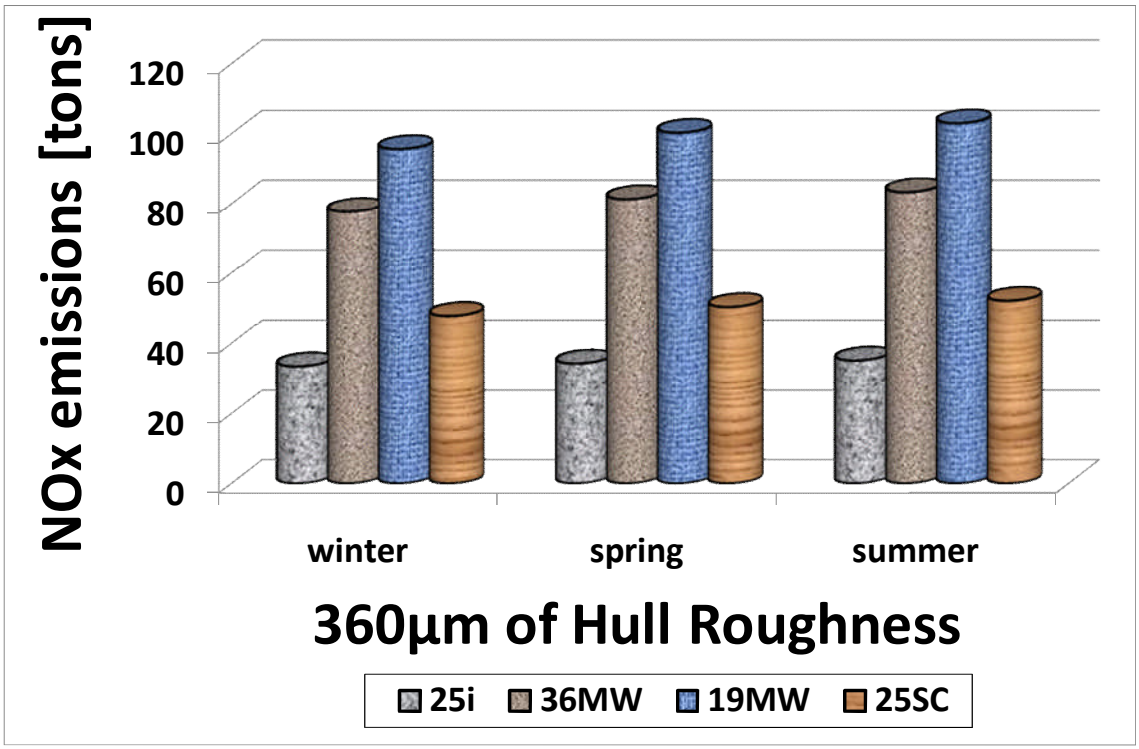

Fig C: 22 Quantities of NO_x emissions under HR3

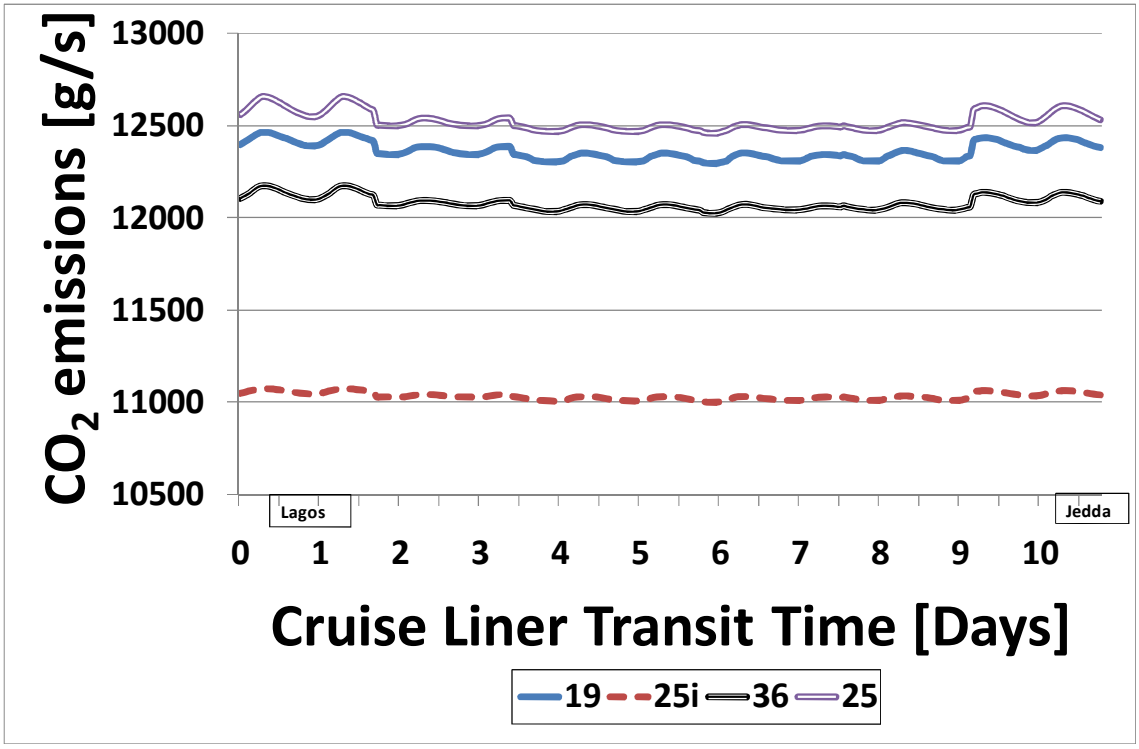

Fig C: 23 Variation of CO_2 emissions in winter under IWC

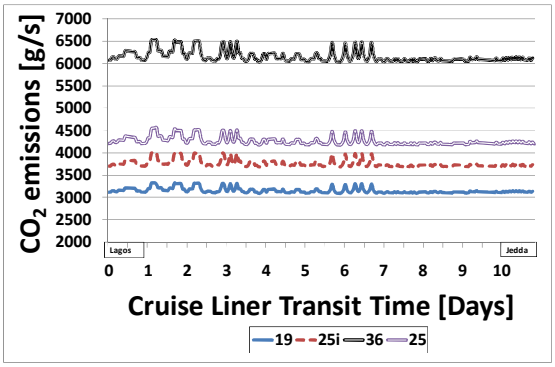

AWC

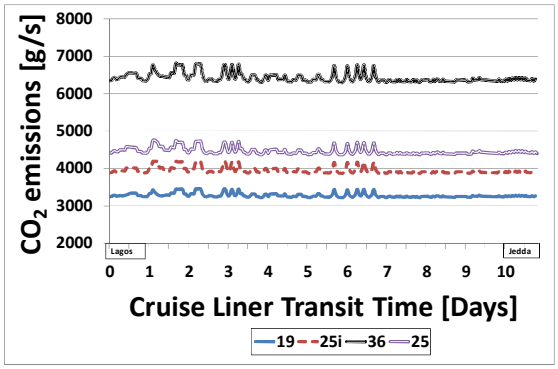

HR1

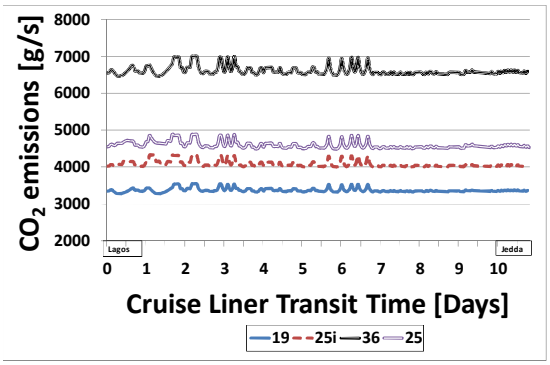

HR2

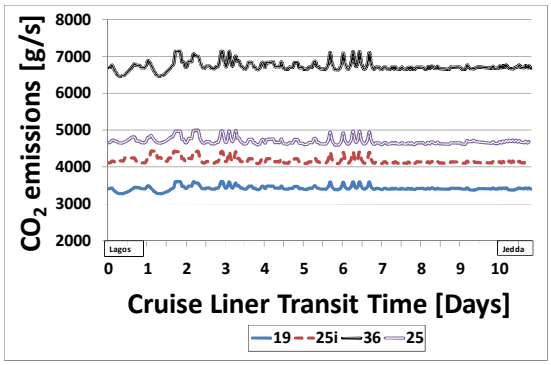

HR3

Fig C: 24 Variation of CO_2 emissions in winter under a variety of adverse scenarios

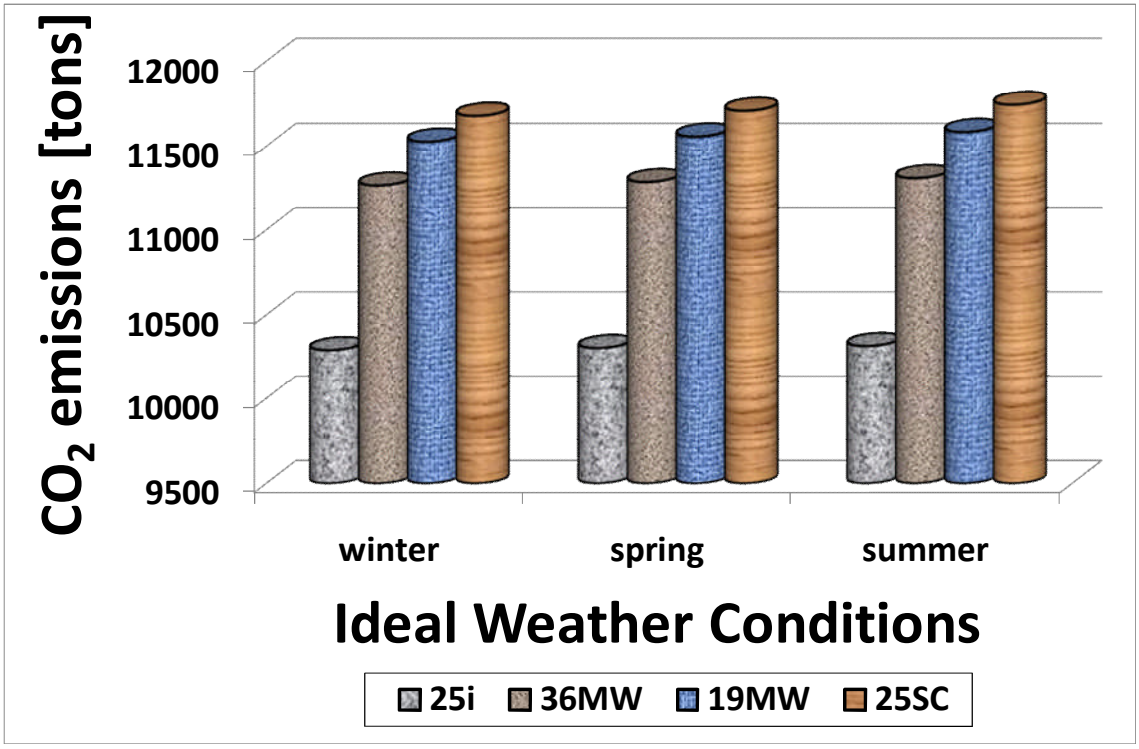

Fig C: 25 Quantities of CO2 emissions per voyage under IWC

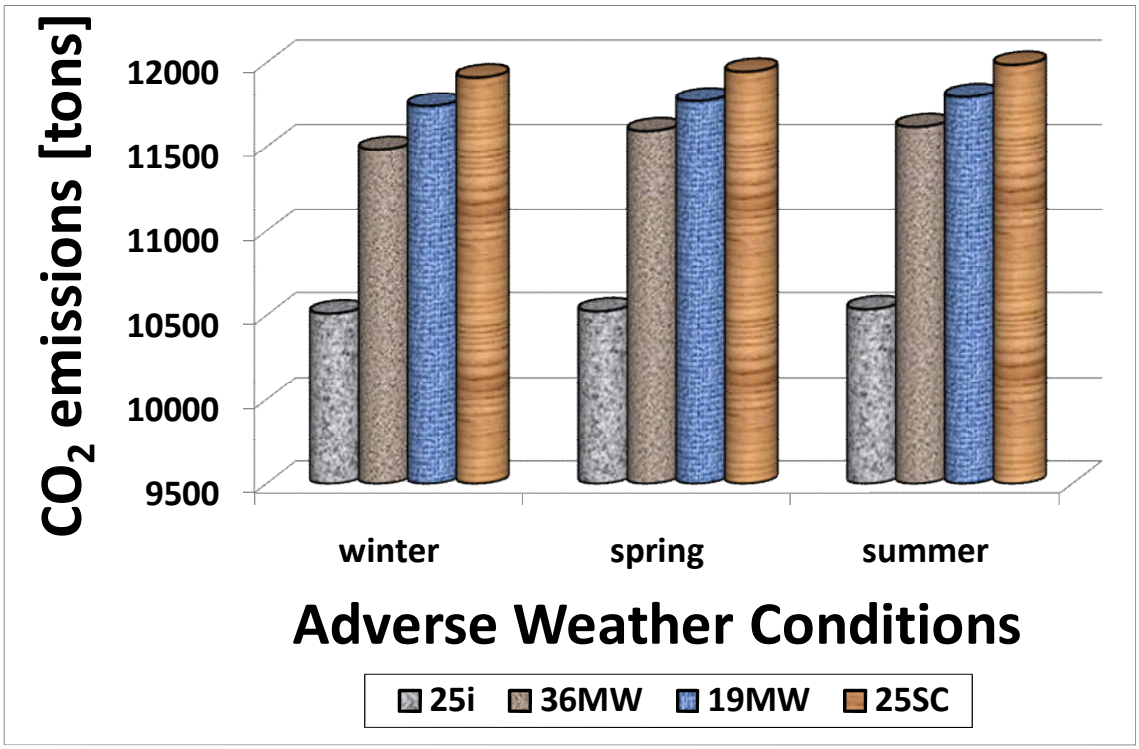

Fig C: 26 Quantities of CO2 emissions per voyage under AWC

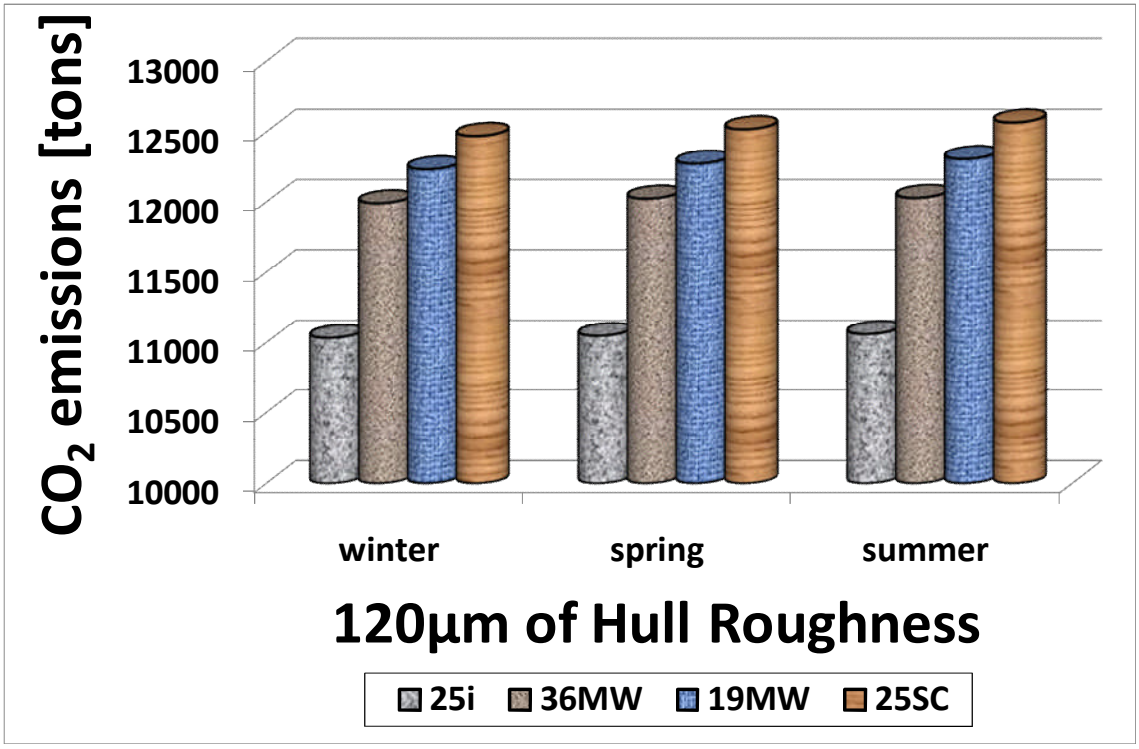

Fig C: 27 Quantities of CO2 emissions per voyage under HR1

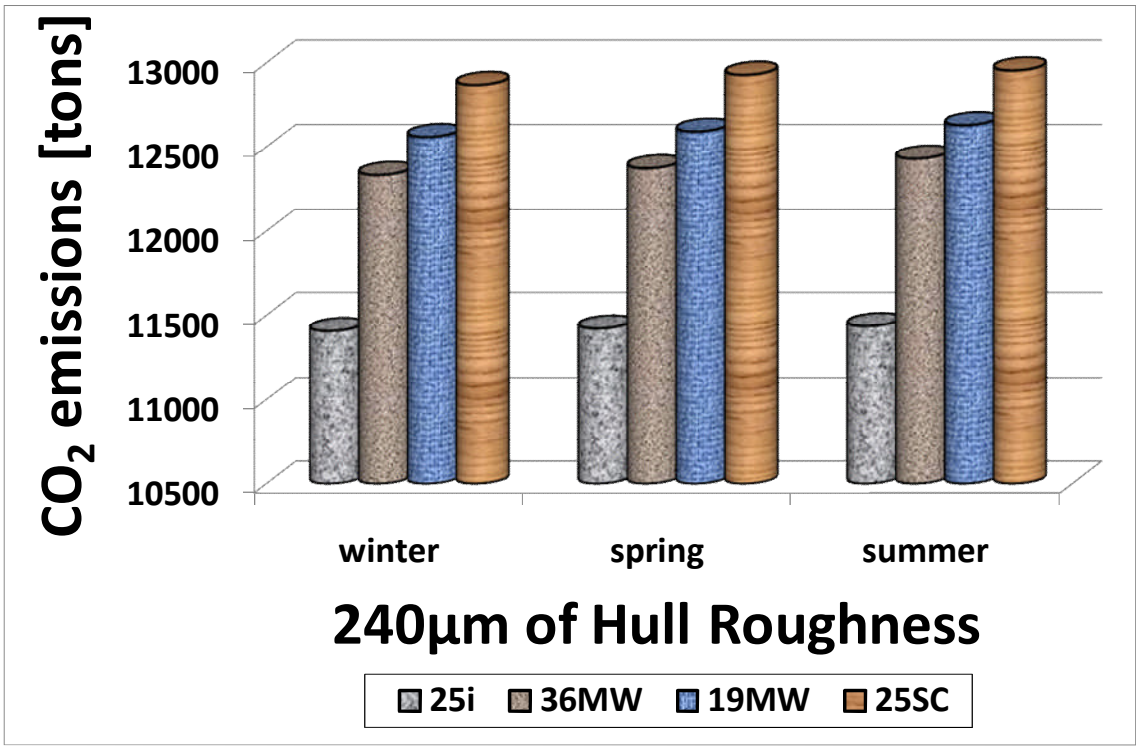

Fig C: 28 Quantities of CO2 emissions per voyage under HR2

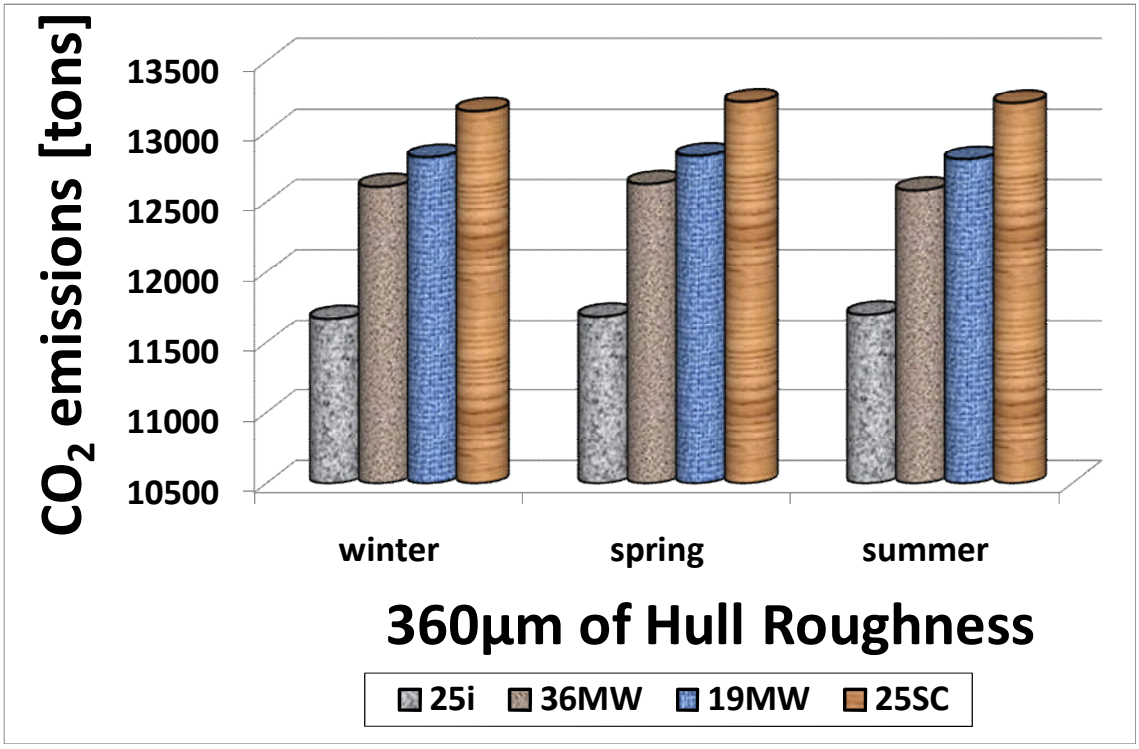

Fig C: 29 Quantities of CO2 emissions per voyage under HR3

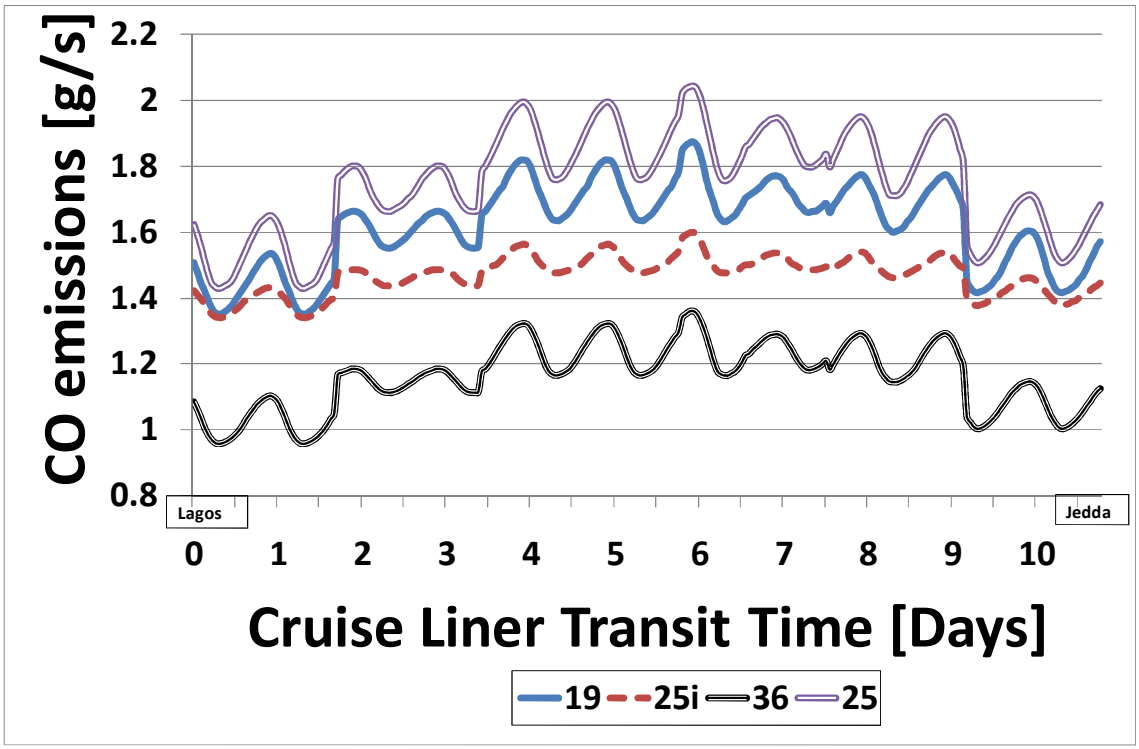

Fig C: 30 Variation of CO emissions under IWC in winter

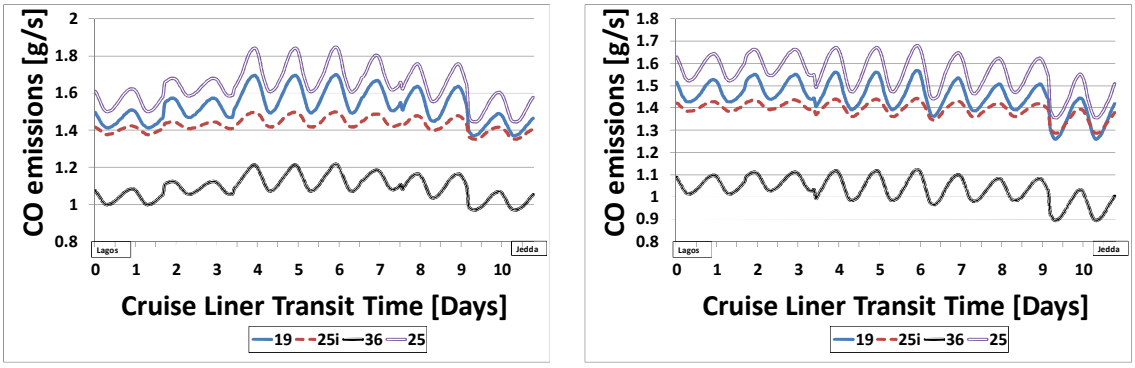

Fig C: 31 Variation of CO emissions under IWC in spring and summer

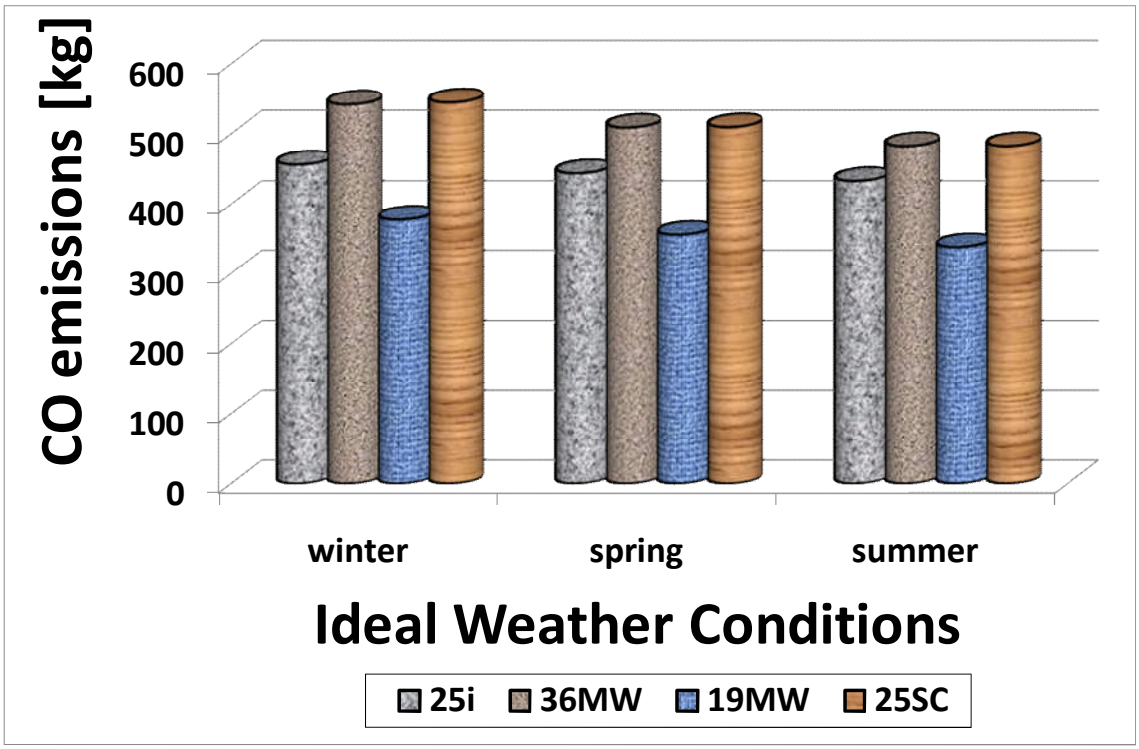

Fig C: 32 Quantities of CO emissions per voyage under IWC

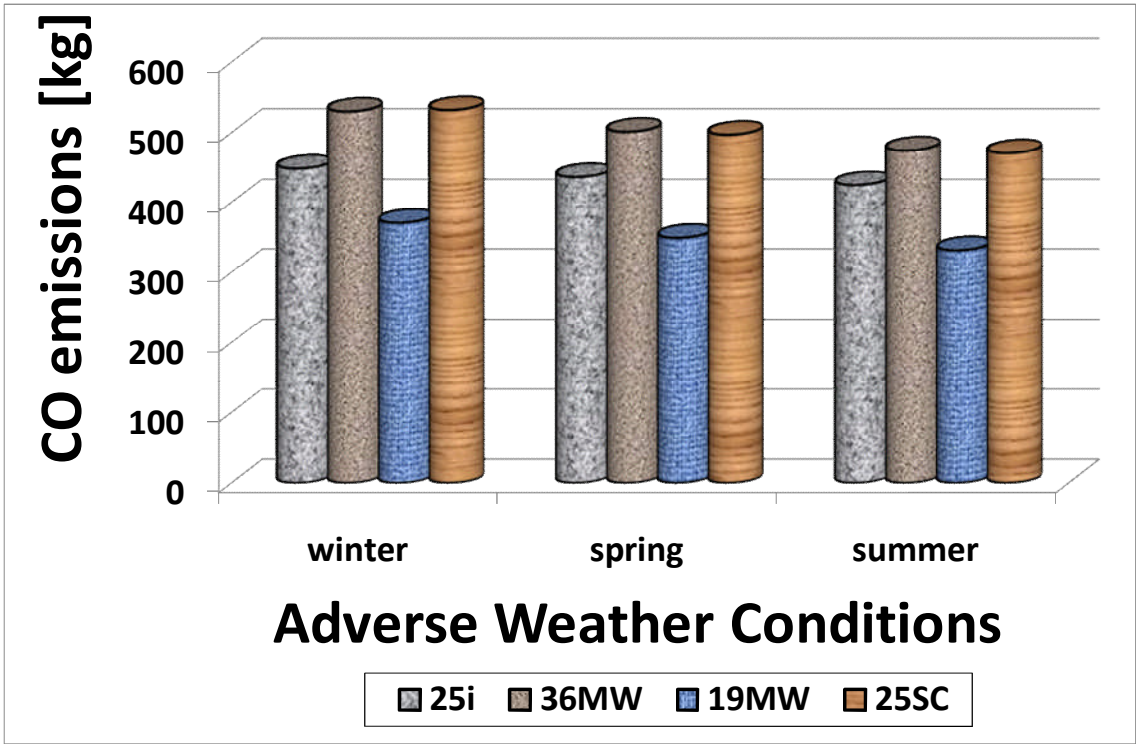

Fig C: 33 Quantities of CO emissions per voyage under AWC

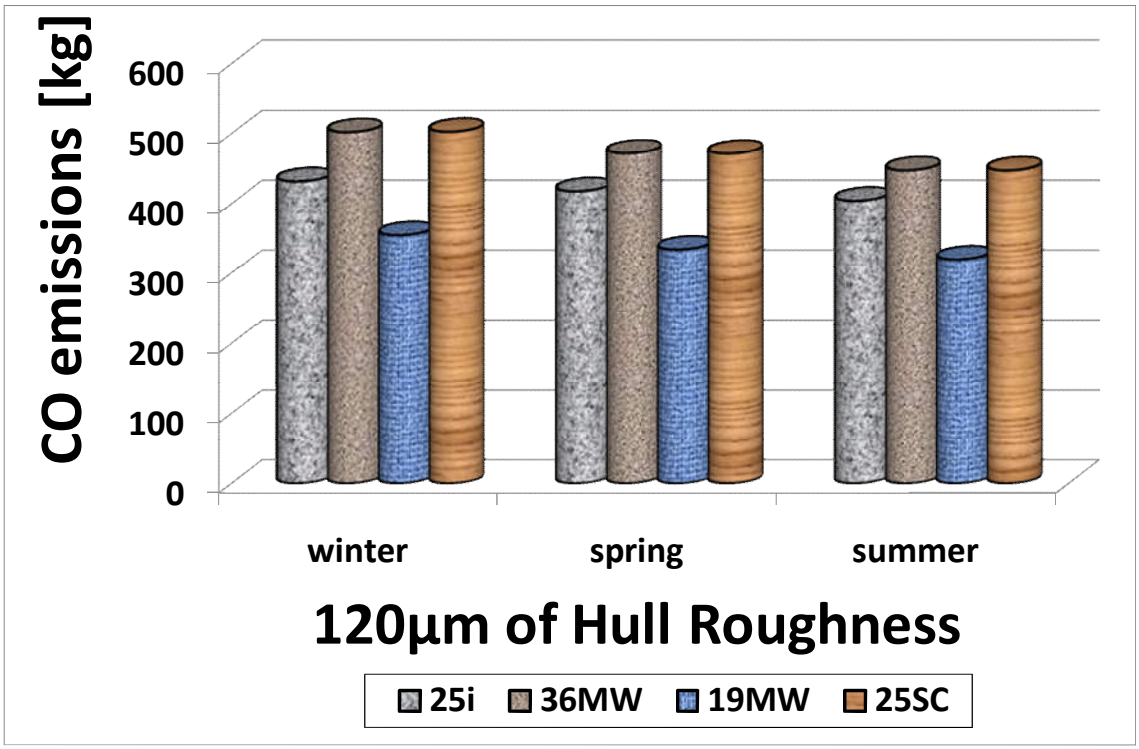

Fig C: 34 Quantities of CO emissions per voyage under HR1

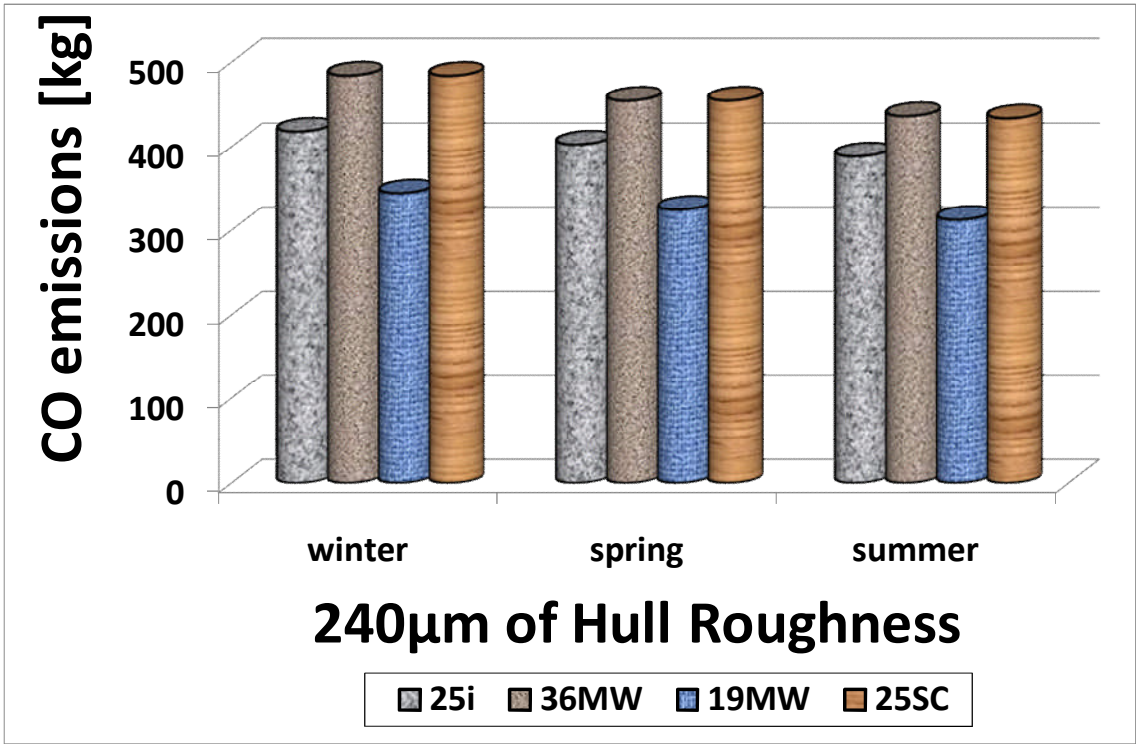

Fig C: 35 Quantities of CO emissions per voyage under HR2

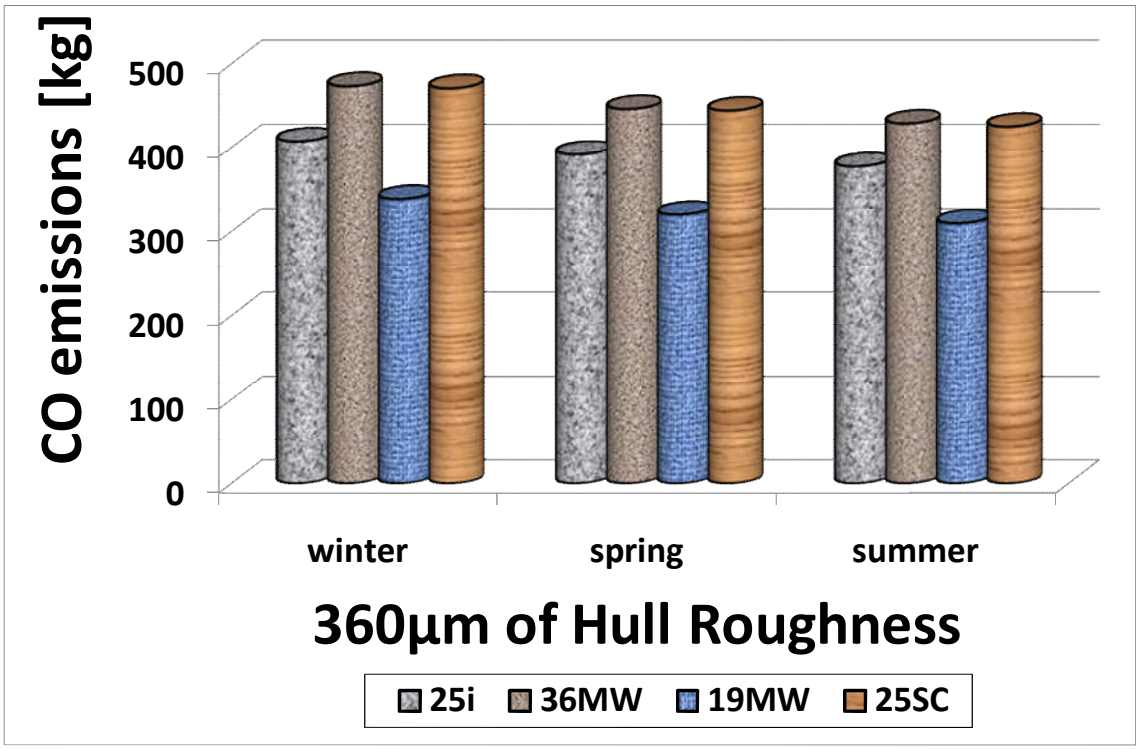

Fig C: 36 Quantities of CO emissions per voyage under HR3

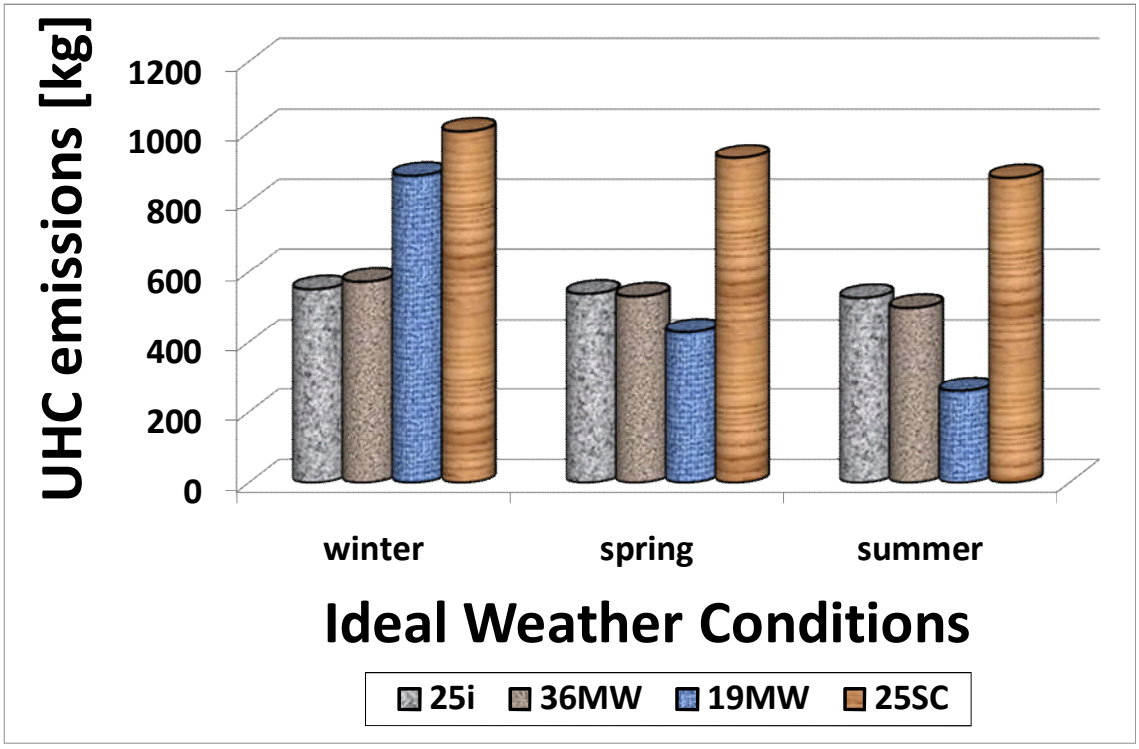

Fig C: 37 Quantities of UHC emissions per voyage under IWC

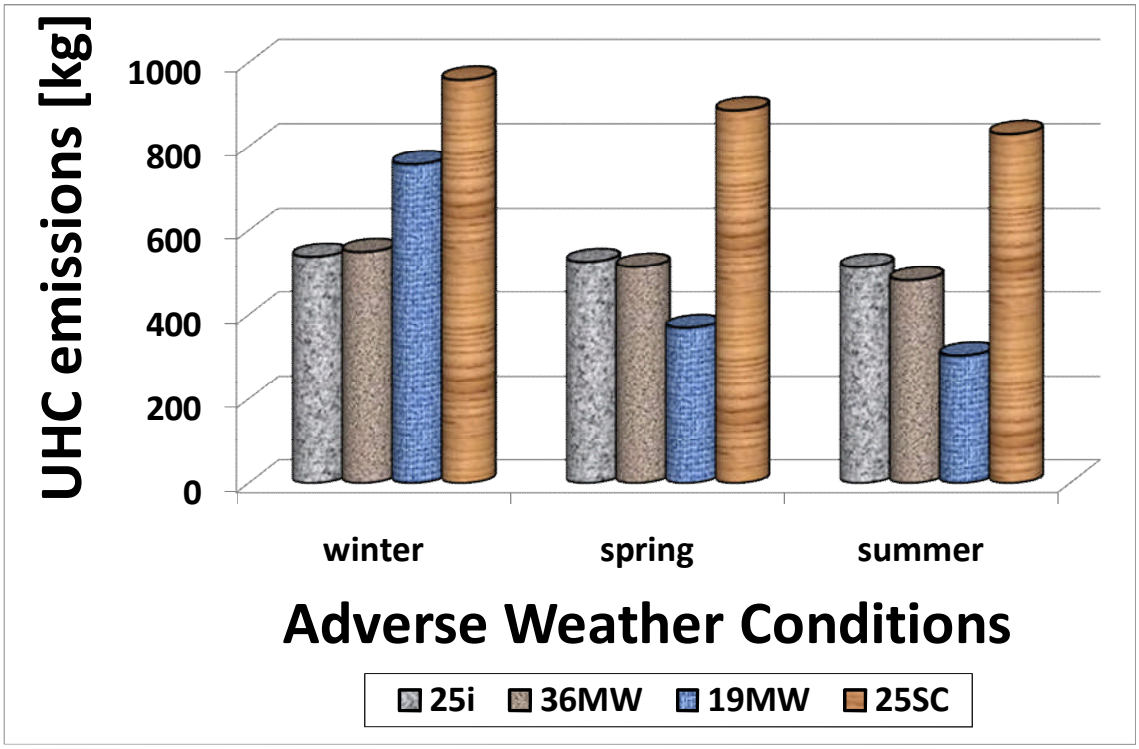

Fig C: 38 Quantities of UHC emissions per voyage under AWC

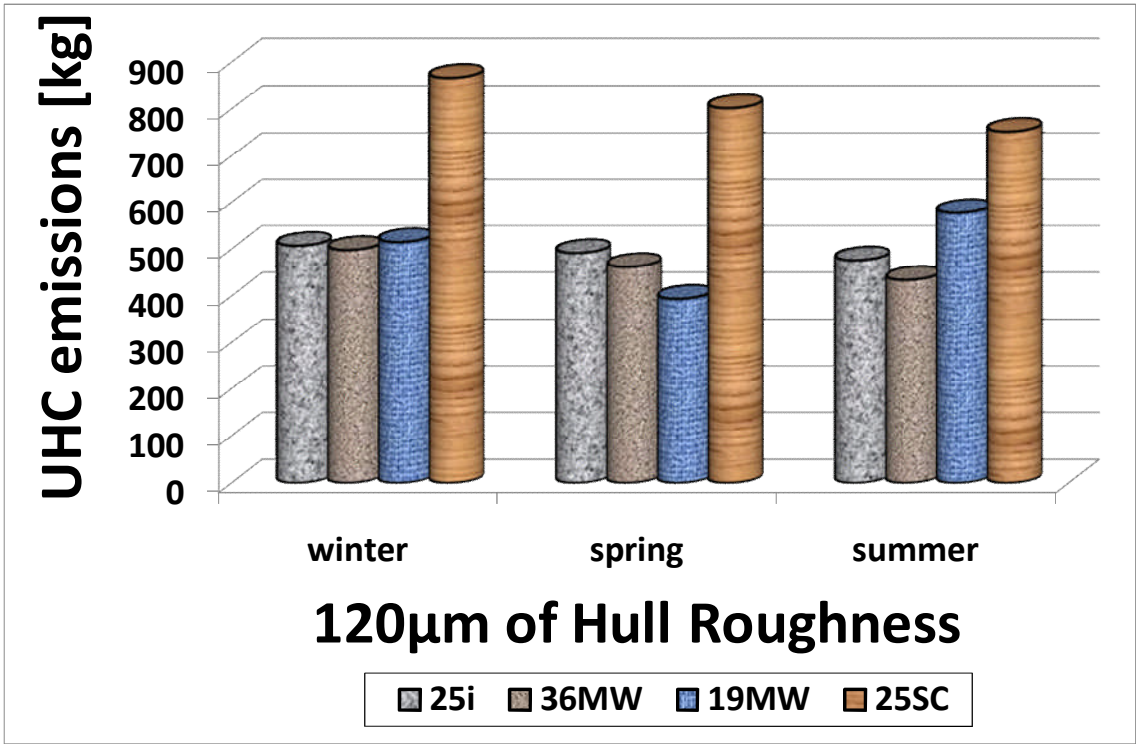

Fig C: 39 Quantities of CO emissions per voyage under HR1

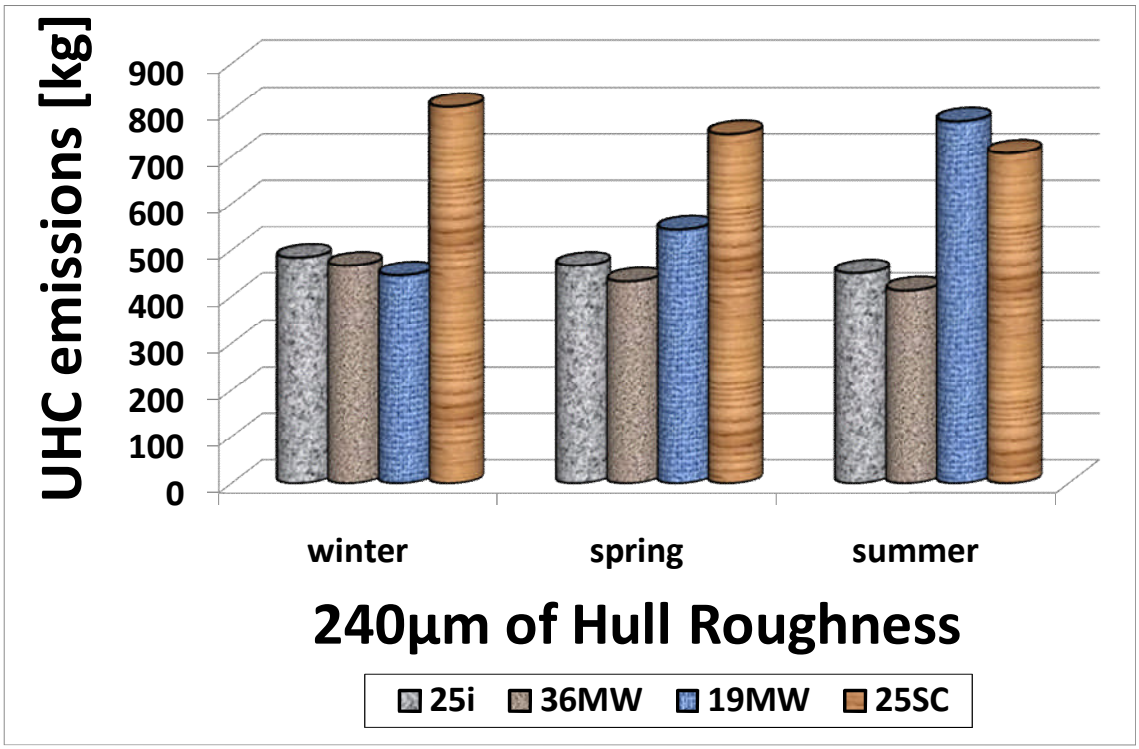

Fig C: 40 Quantities of CO emissions per voyage under HR2

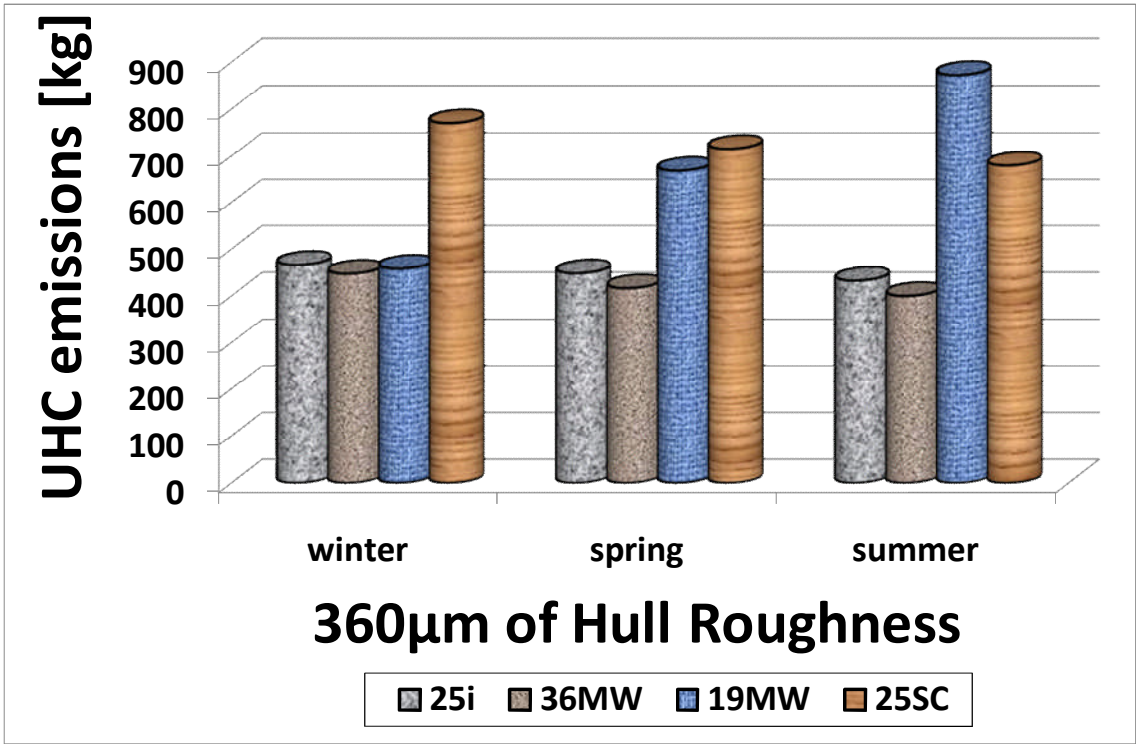

Fig C: 41 Quantities of CO emissions per voyage under HR3

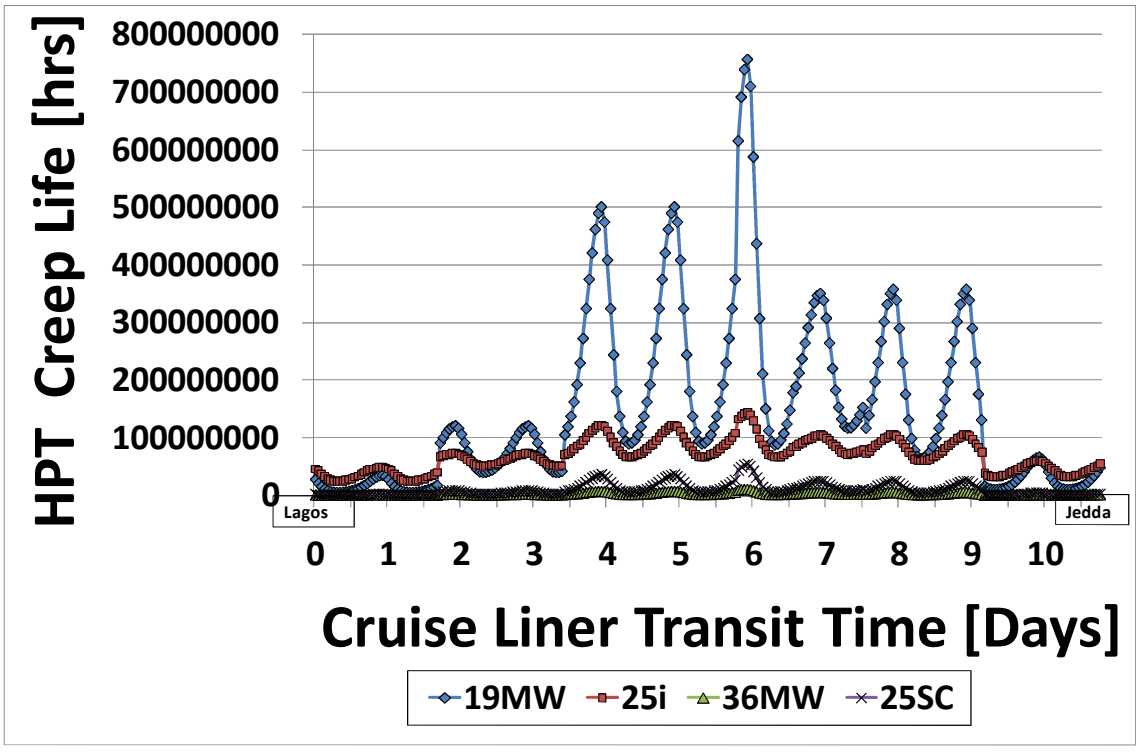

Fig C: 42 Variation of the HPT creep life in ideal winter weather

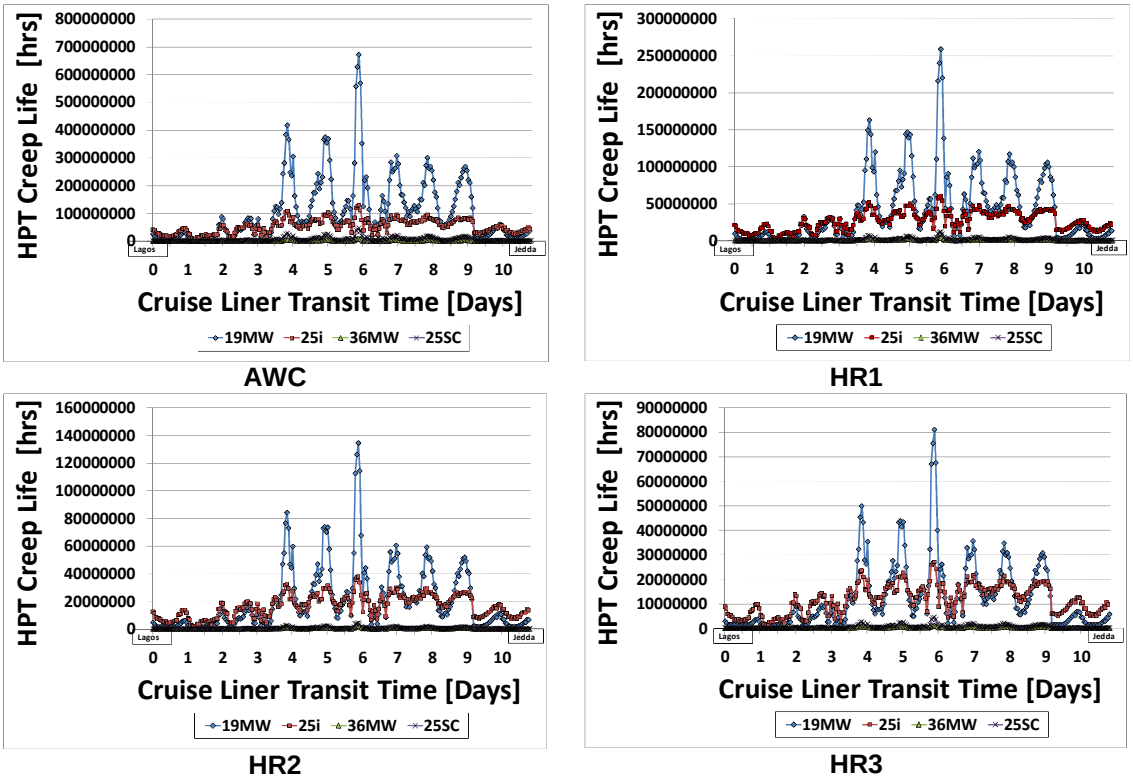

Fig C: 43 Variation of the HPT creep life under the various investigating scenarios

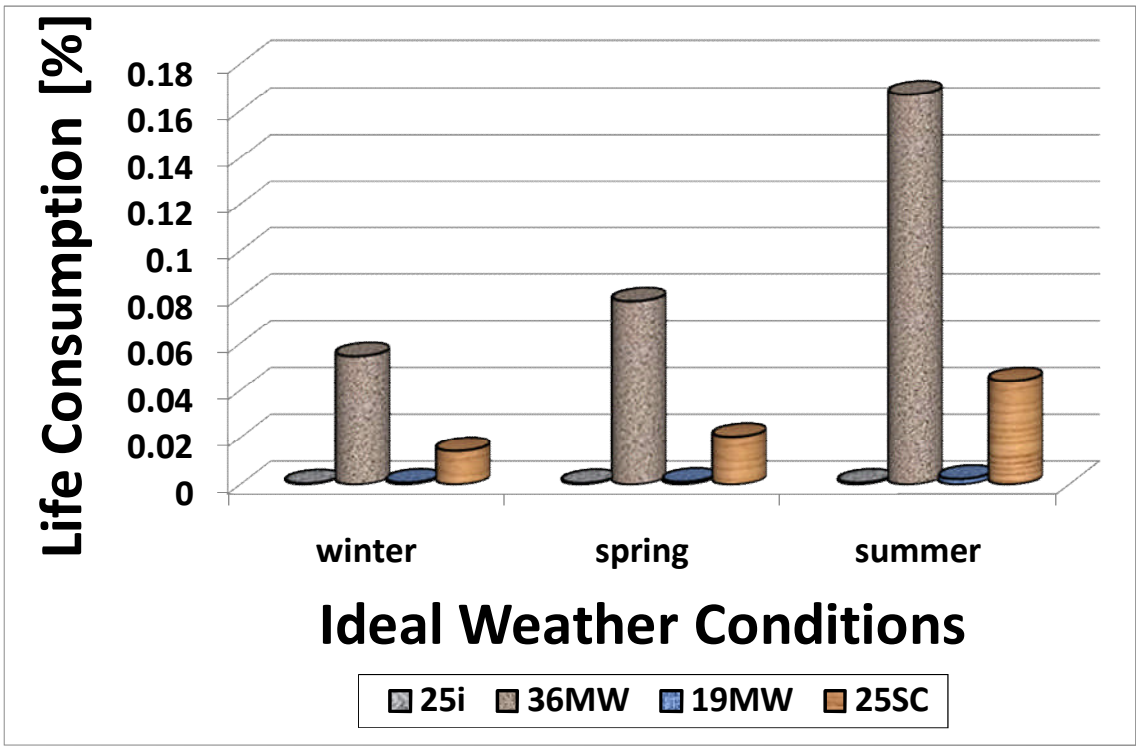

Fig C: 44 Percentage of HPT life consumption for the variety of investigated scenarios

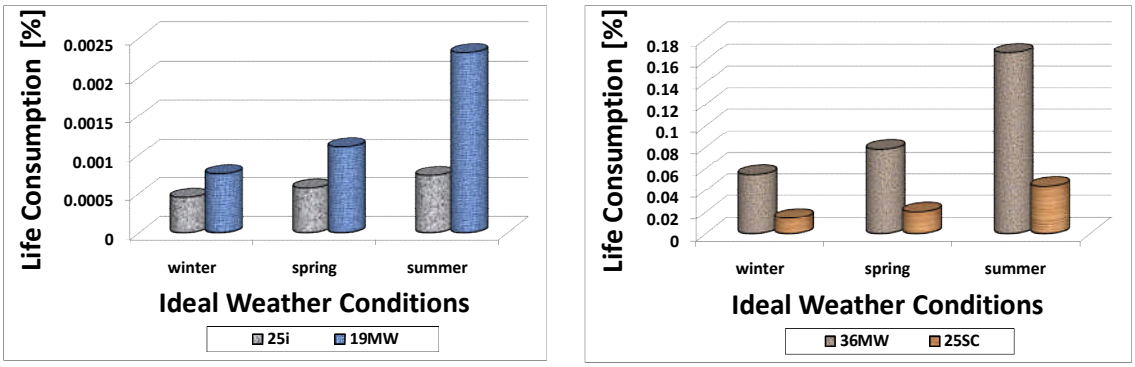

Fig C: 45 Comparative illustration of the life consumption profiles under IWC between (a) The ICR and 19MW models (b) The 36MW and the 25SC models

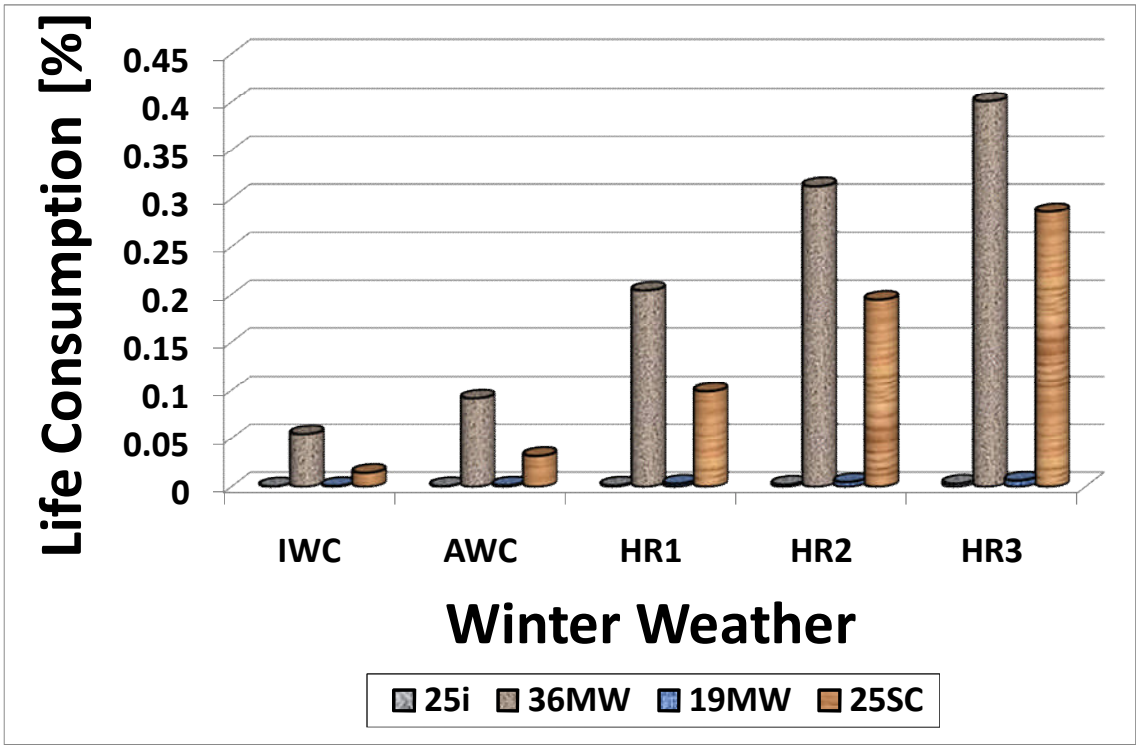

Fig C: 46 HPT blade life consumed per winter voyage

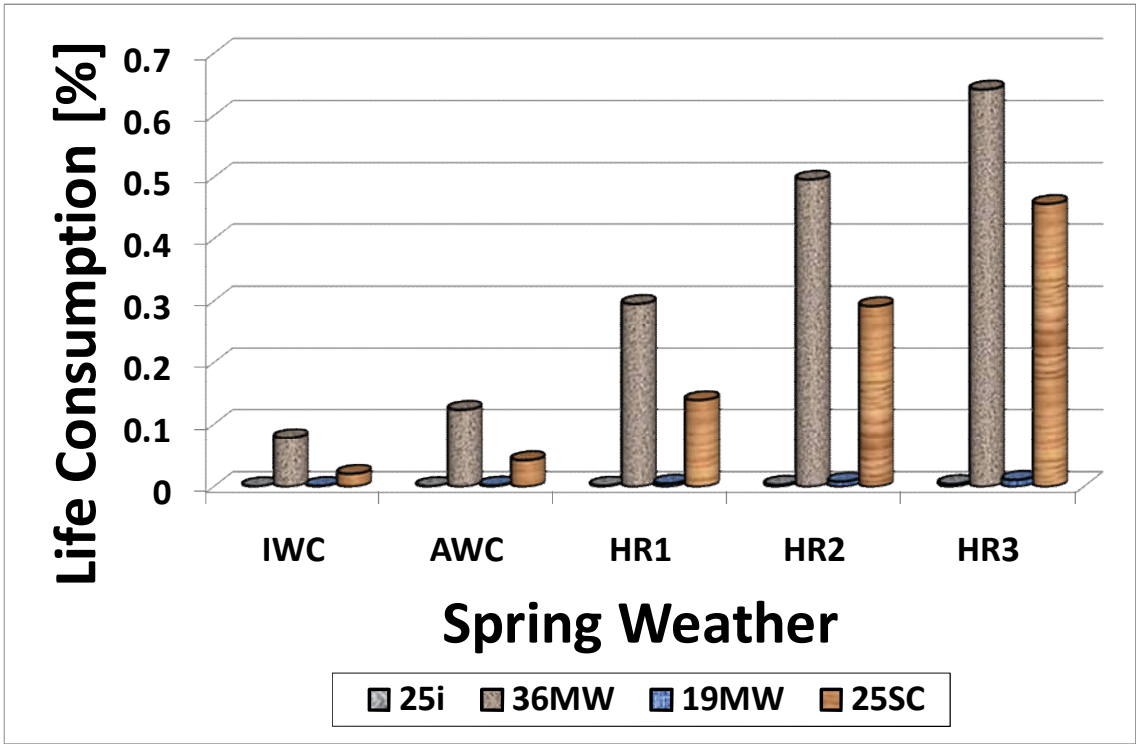

Fig C: 47 HPT blade life consumed during a spring voyage

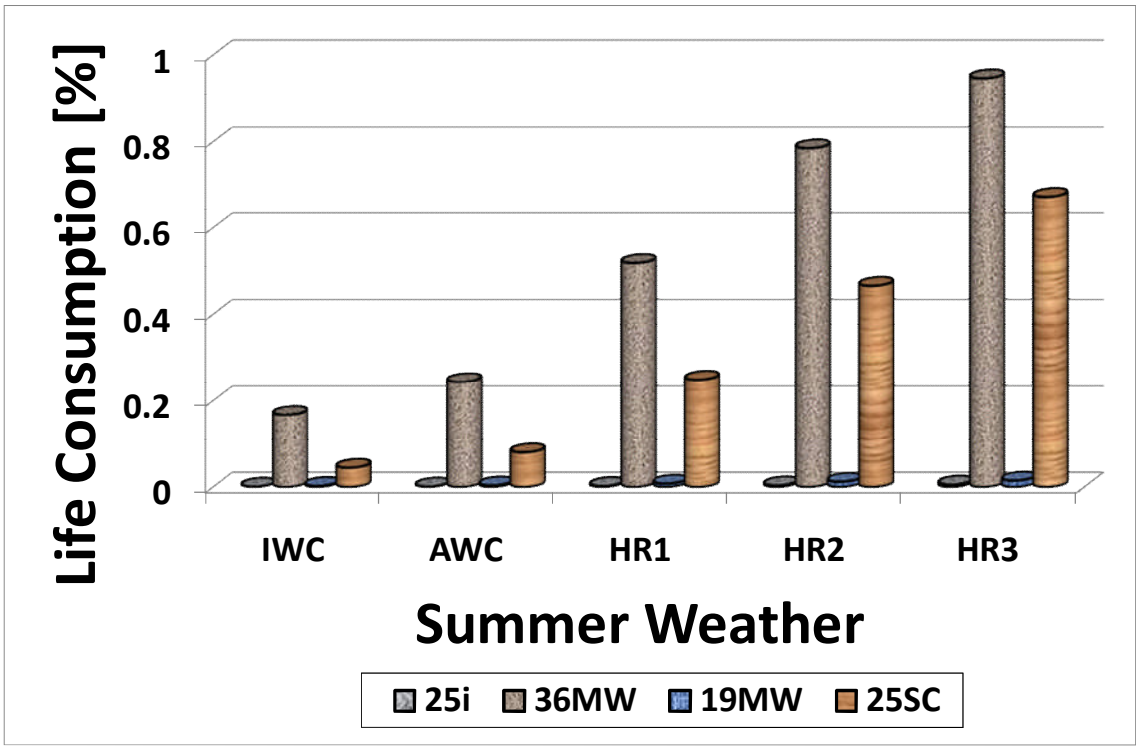

Fig C: 48 HPT blade life consumed during a summer voyage

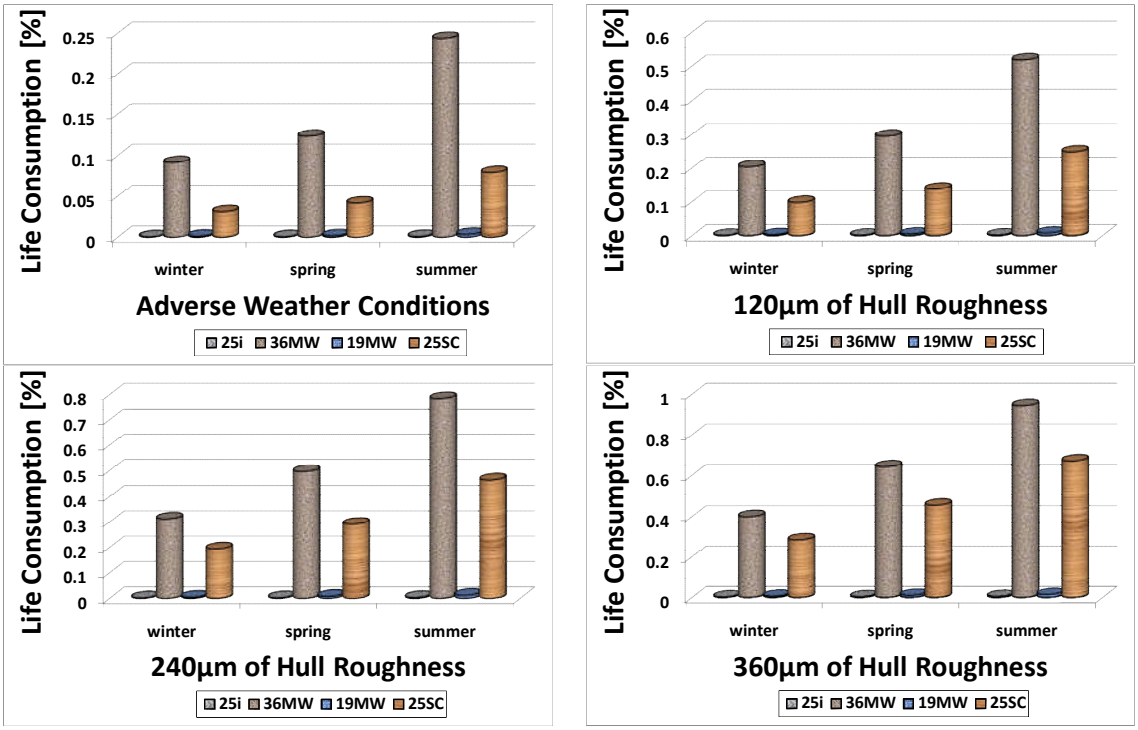

Fig C: 49 Percentages of life consumption under the various investigating scenarios

Appendix D **Voyage analysis of the Fast Speed Ferry**

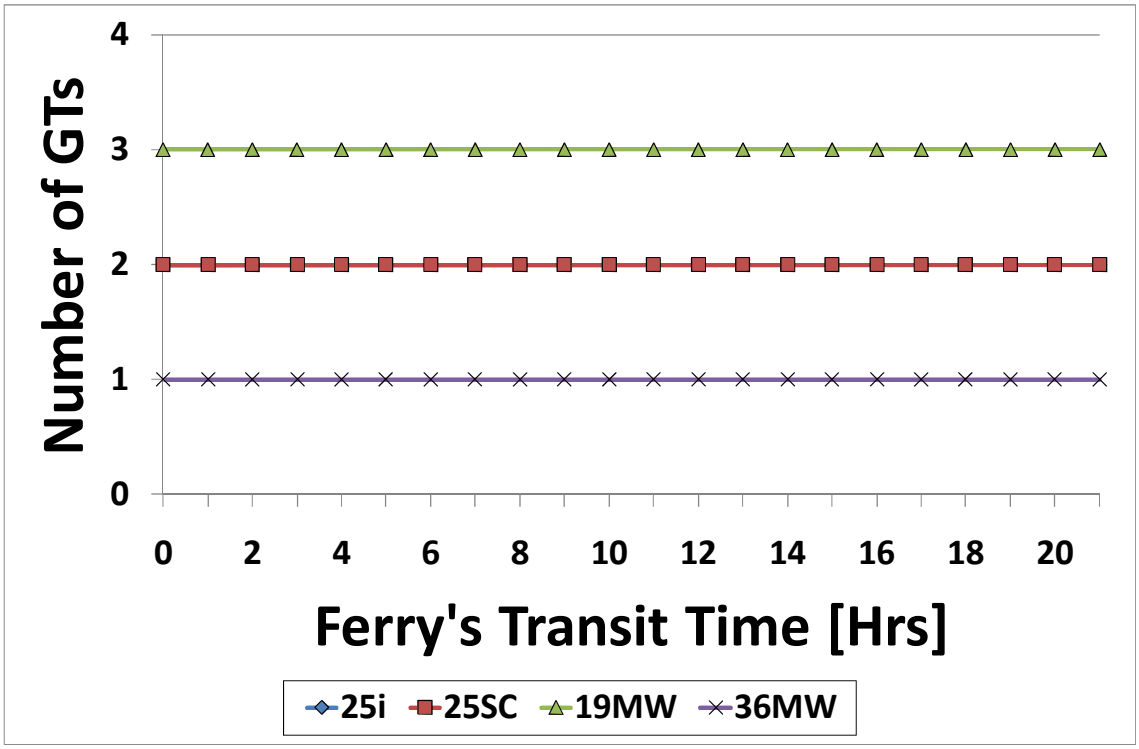

Fig D: 1 Number of GTs constituting the Ferry's power plant for each of the models

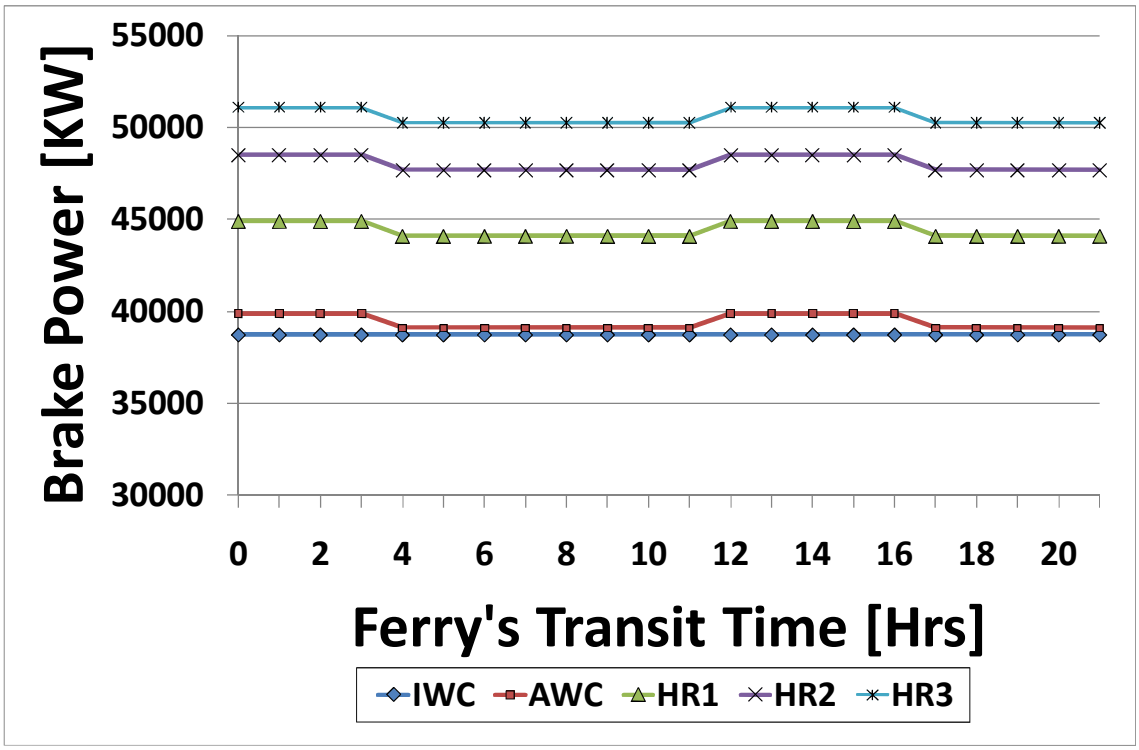

Fig D: 2 Variation of the brake power for the variety of investigated scenarios

Table D: 1 Voyage analysis of the cruise liner with the 19MW GT model as the propulsion prime mover in winter season

	IWC	AWC	HR1	HR2	HR3
FB [kg]	200709.762	203372.584	223338.948	238258.852	249707.15
FB [tons]	200.709762	203.372584	223.338948	238.258852	249.70715
LC [%]	0.000039	0.000053	0.000843	0.00543	0.016284
CO [kg]	108.596	106.846	94.95	86.77	81.518
UHC [kg]	212.808	206.598	167.028	142.626	128.126
NOx [kg]	1817.28	1863.766	2236.684	2544.132	2798.724
NOx [tons]	1.81728	1.863766	2.236684	2.544132	2.798724
CO_2 [kg]	629809.942	638175.106	700815.228	747626.296	783552.316
CO_2 [tons]	629.809942	638.175106	700.815228	747.626296	783.552316
Transit time [hrs]	22	22	22	22	22

Table D: 2 Voyage analysis of the cruise liner with the 19MW GT model as the propulsion prime mover in spring season

	IWC	AWC	HR1	HR2	HR3
FB [kg]	201206.548	203057.97	223565.754	237569.456	251137.524
FB [tons]	201.206548	203.05797	223.565754	237.569456	251.137524
LC [%]	0.000126	0.000228	0.003991	0.020888	0.0494
CO [kg]	98.642	95.234	84.438	78.898	75.288
UHC [kg]	190.41	181.37	145.984	128.734	116.224
NOx [kg]	1939.408	2002.678	2420.344	2741.436	3021.04
NOx [tons]	1.939408	2.002678	2.420344	2.741436	3.02104
CO_2 [kg]	631369.396	637191.728	701529.592	745470.118	788035.618
CO_2 [tons]	631.369396	637.191728	701.529592	745.470118	788.035618
Transit time [hrs]	22	22	22	22	22

Table D: 3 Voyage analysis of the cruise liner with the 19MW GT model as the propulsion prime mover in summer season

	IWC	AWC	HR1	HR2	HR3
FB [kg]	202010.882	203787.098	224911.29	240060.018	245582.394
FB [tons]	202.010882	203.787098	224.91129	240.060018	245.582394
LC [%]	0.00068	0.000866	0.013257	0.05873	0.087057
CO [kg]	88.248	87.344	77.808	72.576	70.642
UHC [kg]	166.914	163.84	132.346	115.448	109.422
NOx [kg]	2097.296	2133.498	2596.482	2965.31	3103.902
NOx [tons]	2.097296	2.133498	2.596482	2.96531	3.103902
CO_2 [kg]	633893.85	639469.46	705759.242	753277.044	770580.888
CO_2 [tons]	633.89385	639.46946	705.759242	753.277044	770.580888
Transit time [hrs]	22	22	22	22	22

Table D: 4 Voyage analysis of the cruise liner with the ICR GT model as the propulsion prime mover in winter season

	IWC	AWC	HR1	HR2	HR3
FB [kg]	176234.614	178838.794	198223.346	212101.12	221989.608
FB [tons]	176.234614	178.838794	198.223346	212.10112	221.989608
LC [%]	0.00001	0.000012	0.000057	0.00015	0.000311
CO [kg]	85.856	84.596	77.414	72.83	68.89
UHC [kg]	105.848	103.55	90.578	82.79	76.484
NOx [kg]	1459.878	1489.35	1700.054	1846.542	1962.208
NOx [tons]	1.459878	1.48935	1.700054	1.846542	1.962208
CO_2 [kg]	553025.678	561194.442	622040.702	665586.784	696592.308
CO_2 [tons]	553.025678	561.194442	622.040702	665.586784	696.592308
Transit time [hrs]	22	22	22	22	22

Table D: 5 Voyage analysis of the cruise liner with the ICR GT model as the propulsion prime mover in spring season

	IWC	AWC	HR1	HR2	HR3
FB [kg]	176596.168	178259.846	198589.796	212505.748	222448.448
FB [tons]	176.596168	178.259846	198.589796	212.505748	222.448448
LC [%]	0.000016	0.000019	0.000087	0.000239	0.000534
CO [kg]	81.154	80.418	74.106	68.988	64.882
UHC [kg]	100.168	98.788	87.192	78.498	72.35
NOx [kg]	1505.43	1524.286	1746.764	1904.954	2045.55
NOx [tons]	1.50543	1.524286	1.746764	1.904954	2.04555
CO_2 [kg]	554160.824	559384.602	623175.426	666835.356	698019.49
CO_2 [tons]	554.160824	559.384602	623.175426	666.835356	698.01949
Transit time [hrs]	22	22	22	22	22

Table D: 6 Voyage analysis of the cruise liner with the ICR GT model as the propulsion prime mover in summer season

	IWC	AWC	HR1	HR2	HR3
FB [kg]	176968.904	178637.362	198088.092	212043.546	221997.778
FB [tons]	176.968904	178.637362	198.088092	212.043546	221.997778
LC [%]	0.000028	0.000032	0.000144	0.000432	0.000961
CO [kg]	76.744	76.232	69.956	64.56	60.324
UHC [kg]	94.986	94.02	82.616	73.754	67.552
NOx [kg]	1556.244	1575.474	1803.316	1989.098	2141.988
NOx [tons]	1.556244	1.575474	1.803316	1.989098	2.141988
CO_2 [kg]	555342.566	560579.276	621602.382	665379.548	696617.776
CO_2 [tons]	555.342566	560.579276	621.602382	665.379548	696.617776
Transit time [hrs]	22	22	22	22	22

Table D: 7 Voyage analysis of the cruise liner with the SC GT model as the propulsion prime mover in winter season

	IWC	AWC	HR1	HR2	HR3
FB [kg]	204759.939	207272.382	225980.463	239432.496	248986.326
FB [tons]	204.759939	207.272382	225.980463	239.432496	248.986326
LC [%]	0	0.000001	0.000004	0.000015	0.000038
CO [kg]	121.38	119.814	109.197	102.849	98.556
UHC [kg]	490.014	478.296	401.526	298.146	190.365
NOx [kg]	3460.38	3543.351	4207.695	4737.942	5141.622
NOx [tons]	3.46038	3.543351	4.207695	4.737942	5.141622
CO_2 [kg]	642524.061	650422.935	709123.401	751333.218	781296.885
CO_2 [tons]	642.524061	650.422935	709.123401	751.333218	781.296885
Transit time [hrs]	22	22	22	22	22

Table D: 8 Voyage analysis of the cruise liner with the SC GT model as the propulsion prime mover in spring season

FB [kg]	205242.711	207413.217	226327.017	239925.375	249486.453
FB [tons]	205.242711	207.413217	226.327017	239.925375	249.486453
LC [%]	0.000002	0.000002	0.000014	0.000051	0.000129
CO [kg]	111.34487	110.058	100.182	94.425	90.336
UHC [kg]	442.156957	433.161	317.877	141.363	53.229
NOx [kg]	3716.99948	3802.632	4532.991	5112.681	5547.297
NOx [tons]	3.71699948	3.802632	4.532991	5.112681	5.547297
CO_2 [kg]	644047.697	650864.628	710209.35	752882.598	782873.814
CO_2 [tons]	644.047697	650.864628	710.20935	752.882598	782.873814
Transit time [hrs]	22	22	22	22	22

Table D: 9 Voyage analysis of the cruise liner with the SC GT model as the propulsion prime mover in summer season

	IWC	AWC	HR1	HR2	HR3
FB [kg]	205973.331	207622.983	226839.63	240414.396	249936.6
FB [tons]	205.973331	207.622983	226.83963	240.414396	249.9366
LC [%]	0.000008	0.00001	0.000066	0.000232	0.000598
CO [kg]	100.746	99.876	90.948	85.584	82.02
UHC [kg]	379.92	367.128	121.839	78.138	133.905
NOx [kg]	4063.557	4128.798	4940.835	5571.945	6044.529
NOx [tons]	4.063557	4.128798	4.940835	5.571945	6.044529
CO_2 [kg]	646339.269	651516.897	711818.958	754413.897	784299.24
CO_2 [tons]	646.339269	651.516897	711.818958	754.413897	784.29924
Transit time [hrs]	22	22	22	22	22

Table D: 10 Voyage analysis of the cruise liner with the 36MW GT model as the propulsion prime mover in winter season

	IWC	AWC	HR1	HR2	HR3
FB [kg]	183219.915	185181.543	189201.046	198115.592	198115.592
FB [tons]	183.219915	185.181543	189.201046	198.115592	198.115592
LC [%]	0.035334	0.042521	0.058217	0.060428	0.060428
CO [kg]	39.511	38.871	37.519	39.253	39.253
UHC [kg]	35.011	34.069	32.108	33.55	33.55
NOx [kg]	3584.401	3665.883	3834.537	4013.038	4013.038
NOx [tons]	3.584401	3.665883	3.834537	4.013038	4.013038
CO_2 [kg]	574919.632	581064.815	593663.692	621635.219	621635.219
CO_2 [tons]	574.919632	581.064815	593.663692	621.635219	621.635219
Transit time [hrs]	22	22	22	23	23

Table D: 11 Voyage analysis of the cruise liner with the 36MW GT model as the propulsion prime mover in spring season

	IWC	AWC	HR1	HR2	HR3
FB [kg]	180963.836	183841.975	187776.214	189594.453	189594.453
FB [tons]	180.963836	183.841975	187.776214	189.594453	189.594453
LC [%]	0.068758	0.054808	0.076641	0.073243	0.073243
CO [kg]	36.812	39.579	38.224	38.42	38.42
UHC [kg]	32.545	36.026	33.988	33.899	33.899
NOx [kg]	3718.936	3710.457	3876.102	3899.889	3899.889
NOx [tons]	3.718936	3.710457	3.876102	3.899889	3.899889
CO_2 [kg]	567819.986	576863.943	589192.937	594898.1	594898.1
CO_2 [tons]	567.819986	576.863943	589.192937	594.8981	594.8981
Transit time [hrs]	22	23	23	23	23

Table D: 12 Voyage analysis of the cruise liner with the 36MW GT model as the propulsion prime mover in summer season

	IWC	AWC	HR1	HR2	HR3
FB [kg]	172010.177	180119.367	180136.641	180136.641	188228.742
FB [tons]	172.010177	180.119367	180.136641	180.136641	188.228742
LC [%]	0.088219	0.091435	0.091591	0.091591	0.094993
CO [kg]	35.795	37.46	37.454	37.454	39.111
UHC [kg]	32.839	34.326	34.316	34.316	35.794
NOx [kg]	3596.258	3763.559	3764.294	3764.294	3931.881
NOx [tons]	3.596258	3.763559	3.764294	3.764294	3.931881
CO_2 [kg]	539723.213	565168.056	565221.943	565221.943	590612.854
CO_2 [tons]	539.723213	565.168056	565.221943	565.221943	590.612854
Transit time [hrs]	22	23	23	23	24

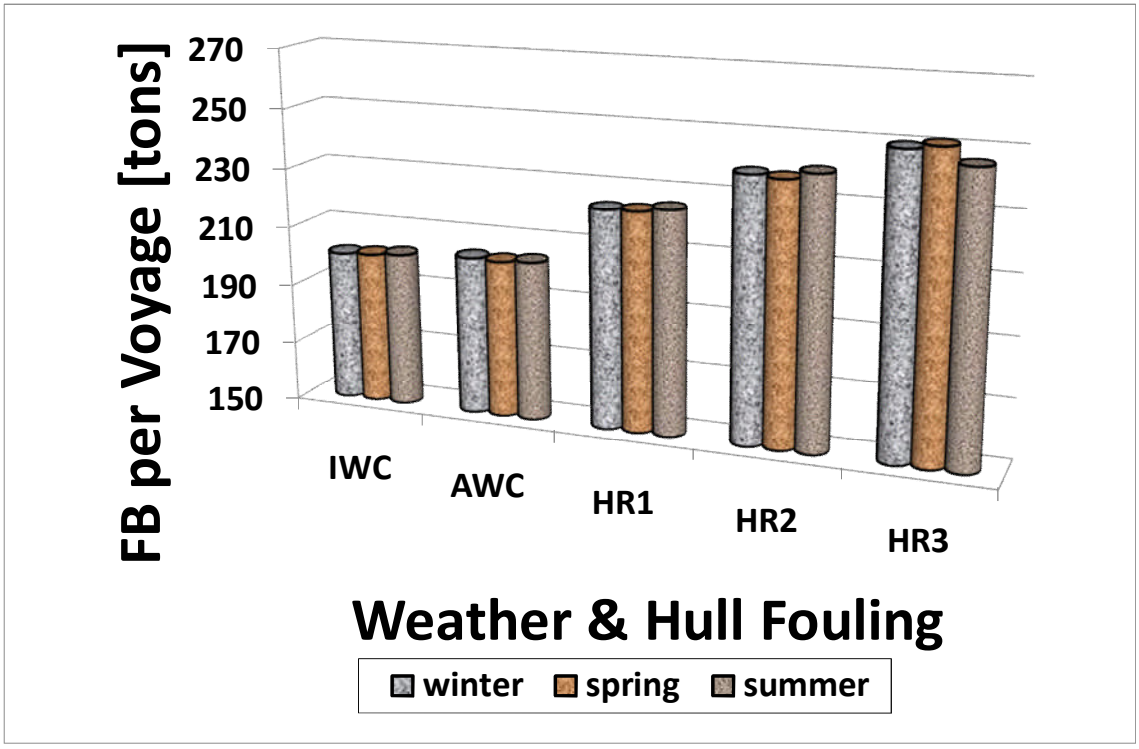

Fig D: 3 Quantities of the FB per voyage when operating the SC model

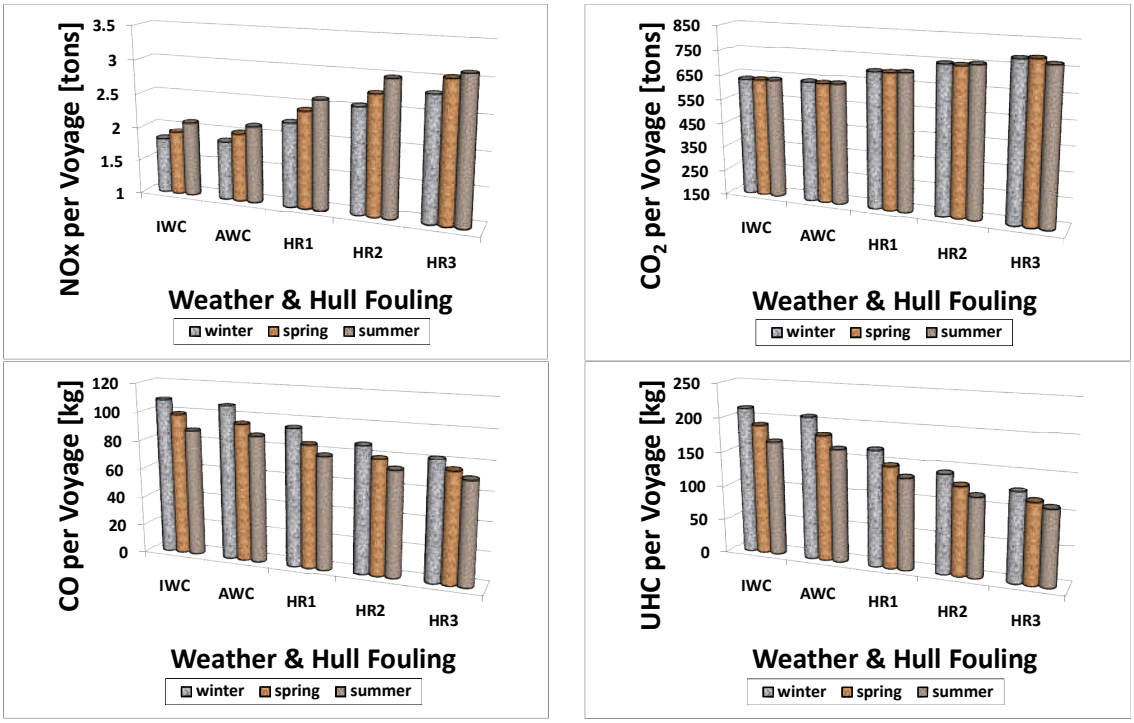

Fig D: 4 Emissions quantities per voyage when operating the SC model

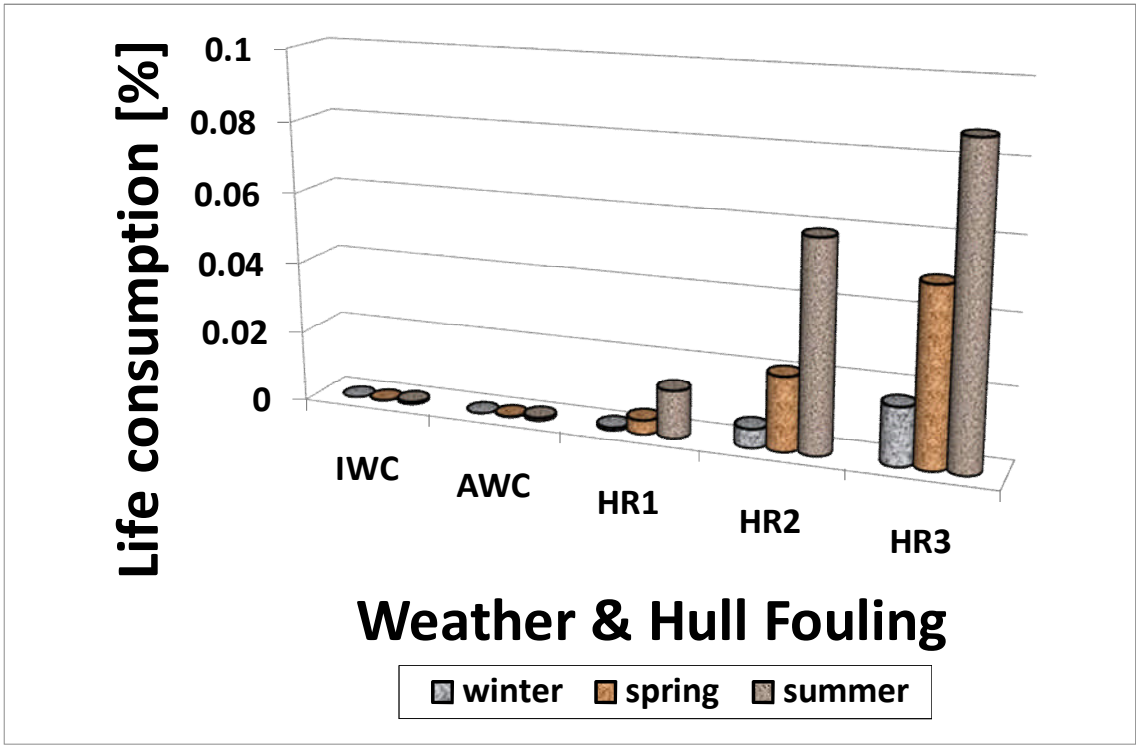

Fig D: 5 Percentage of HPT life consumed per voyage when operating the SC model

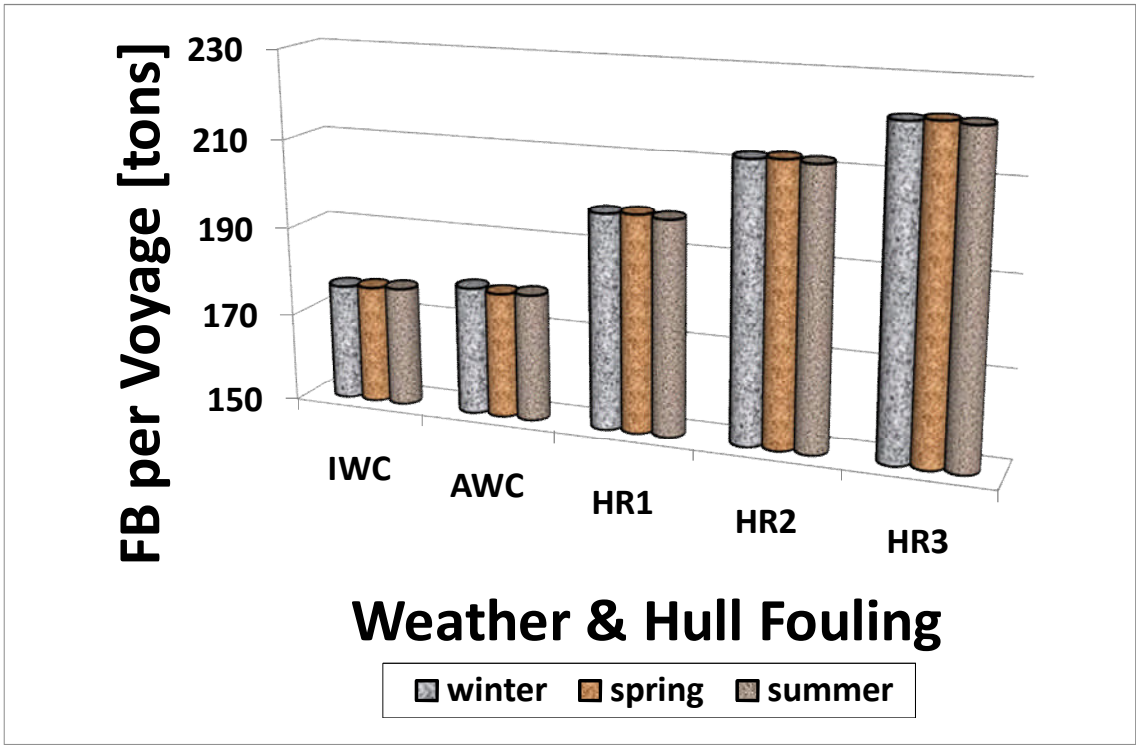

Fig D: 6 Quantities of FB per voyage when operating the ICR model

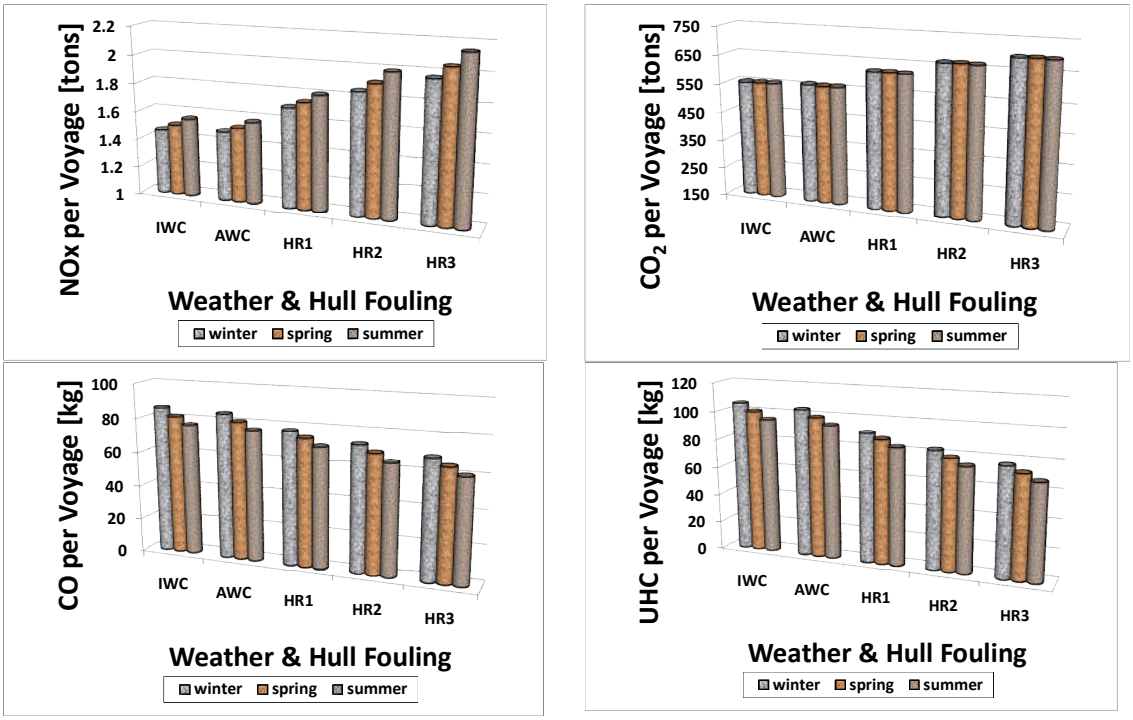

Fig D: 7 NOx Emission quantities per voyage when operating the ICR model

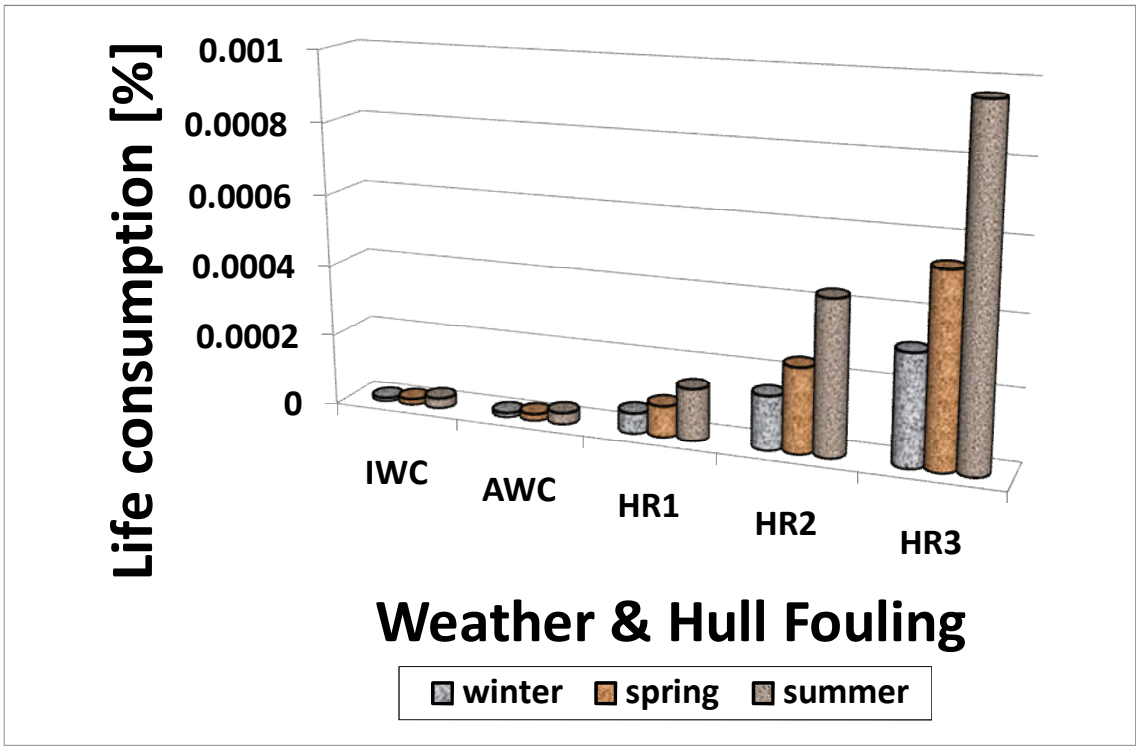

Fig D: 8 Percentage of HPT life consumed per voyage when operating the ICR model

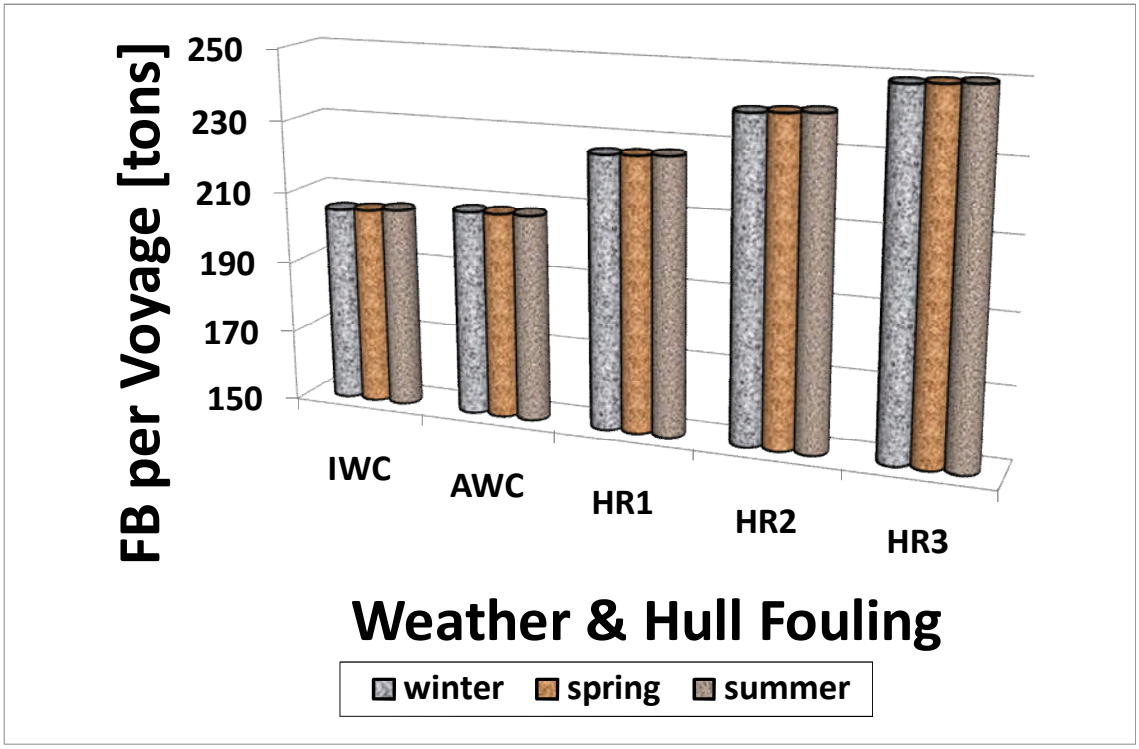

Fig D: 9 Quantities of FB per voyage when operating the 19MW model

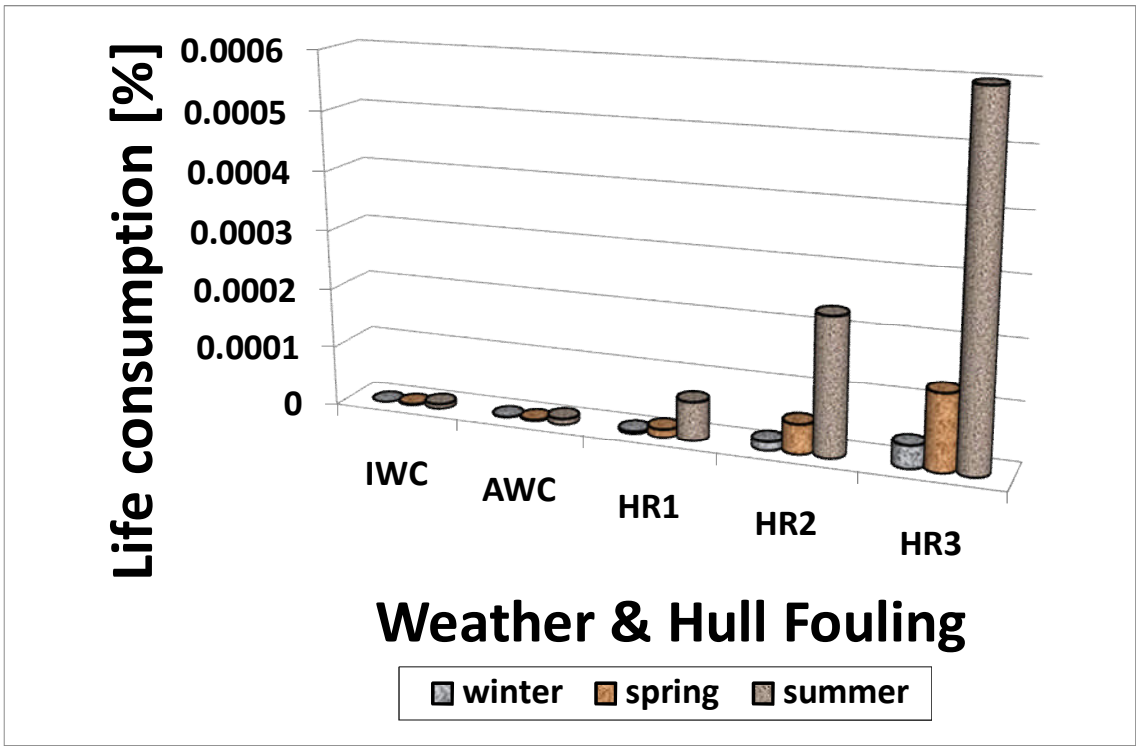

Fig D: 10 Percentage of HPT life consumed per voyage when operating the 19MW model

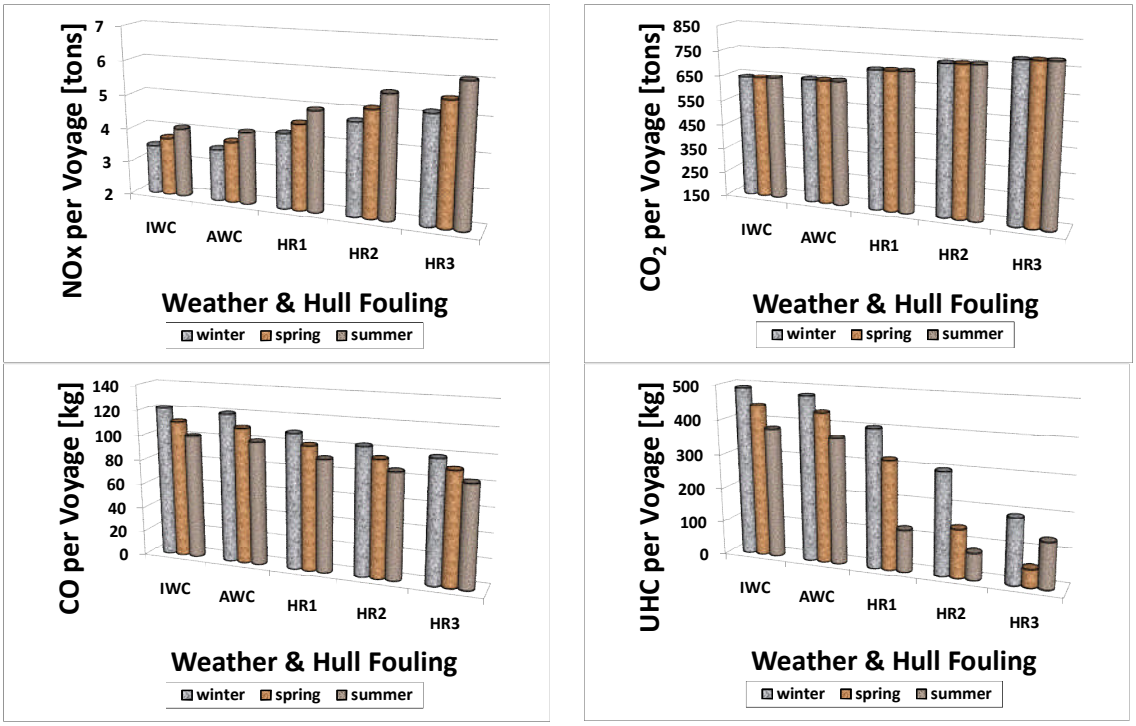

Fig D: 11 CO emission quantities per voyage when operating the 19MW model

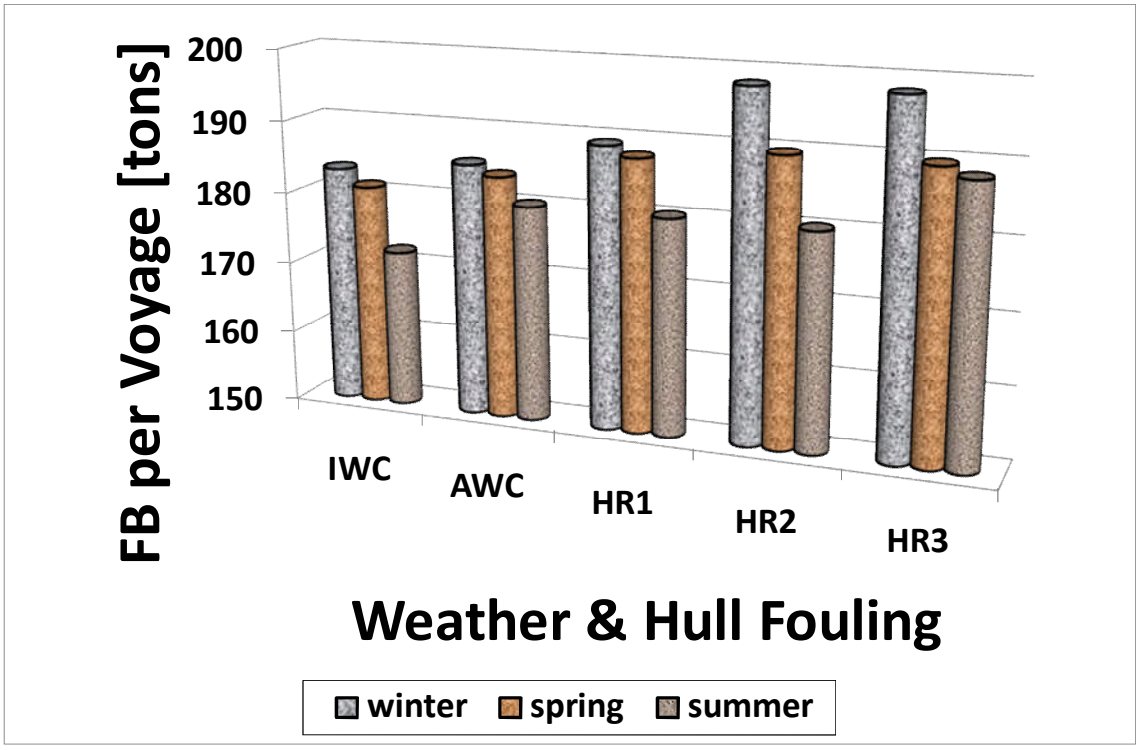

Fig D: 12 Quantities of FB per voyage when operating the 36MW model

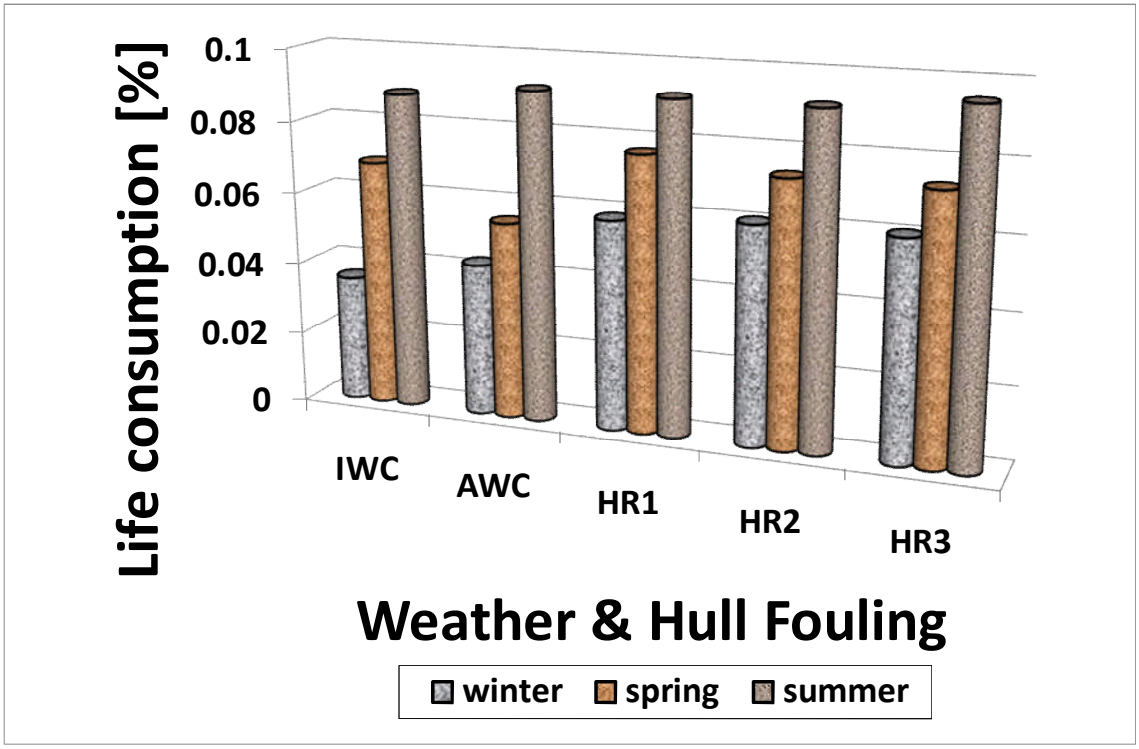

Fig D: 13 Percentage of HPT life consumed per voyage when operating the 36MW model

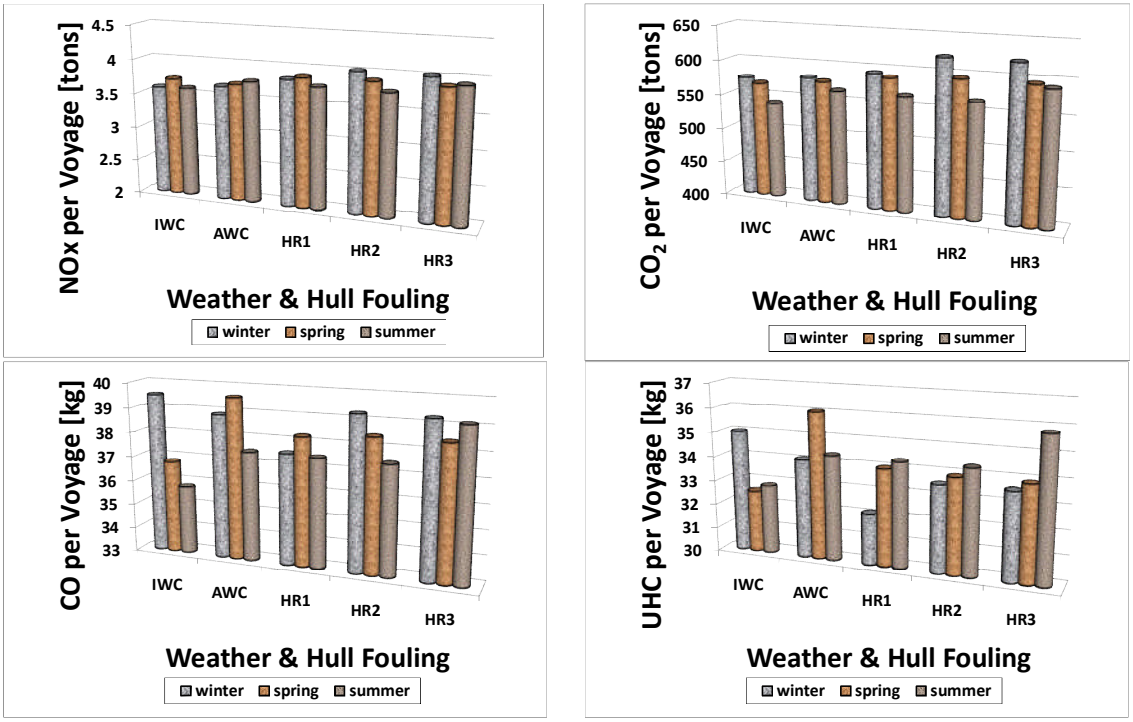

Fig D: 14 CO emission quantities per voyage when operating the 36MW model

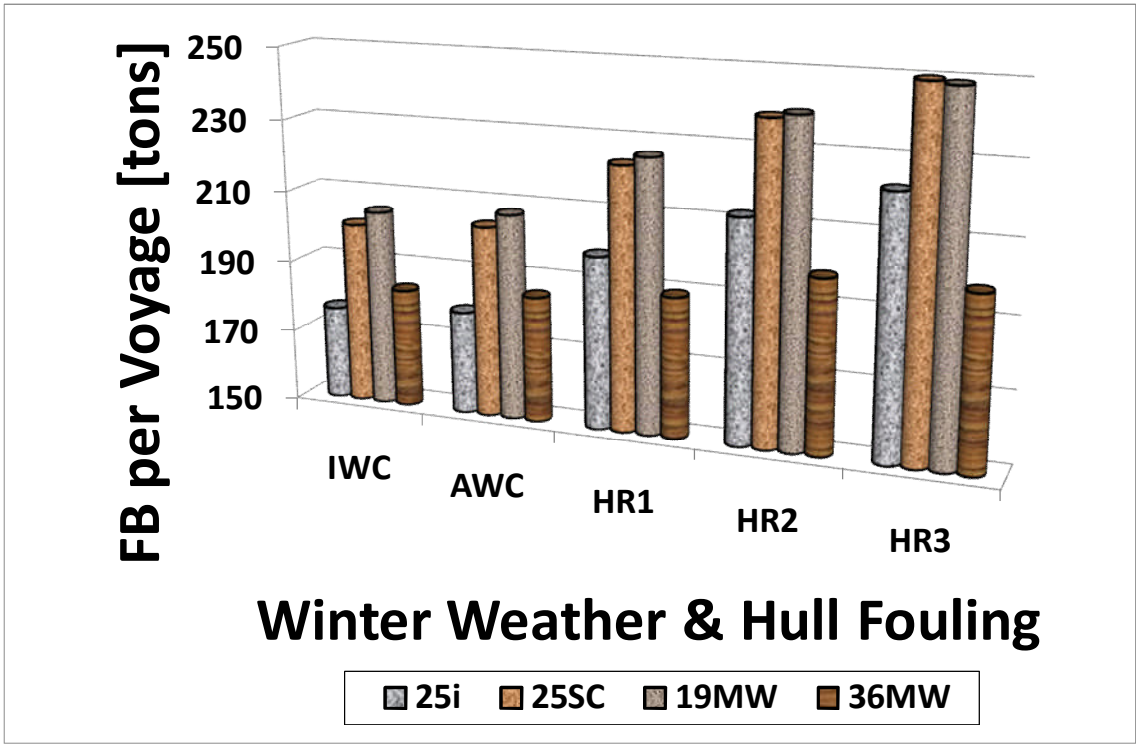

Fig D: 15 FB for the variety of GT models when operating in winter weather

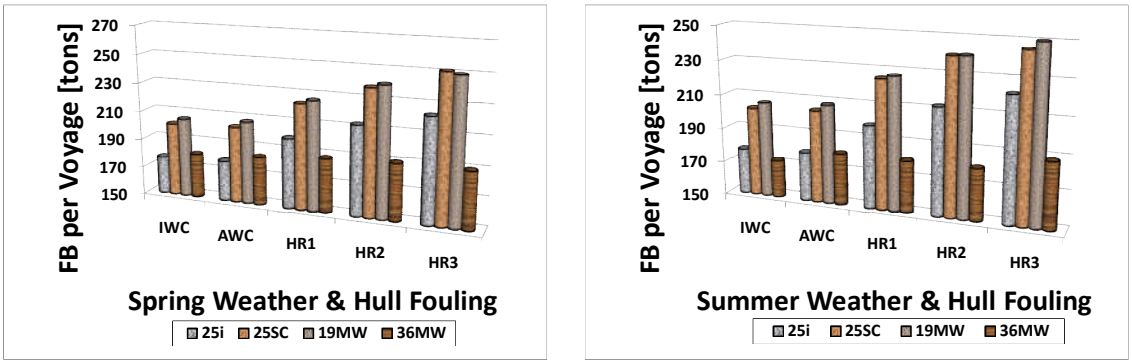

Fig D: 16 FB for the variety of GT models when operating in spring and summer weather respectively

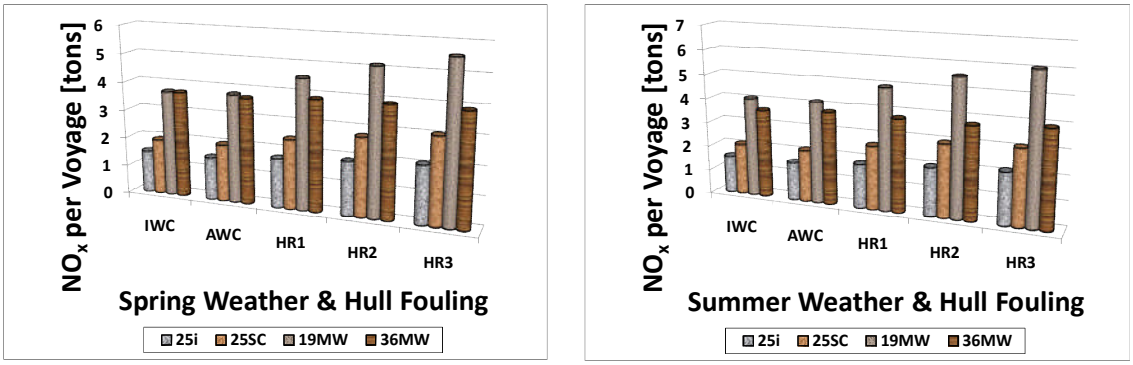

Fig D: 17 NOx emissions when operating in spring and summer weather

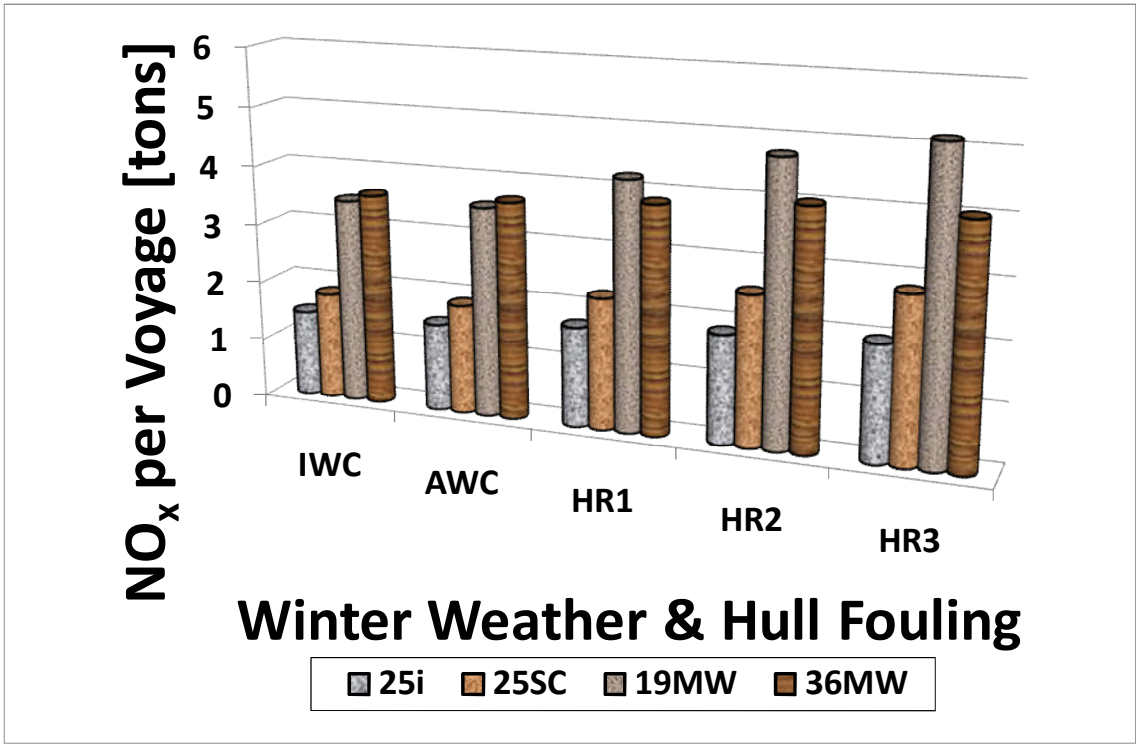

Fig D: 18 NOx emissions when operating in winter weather

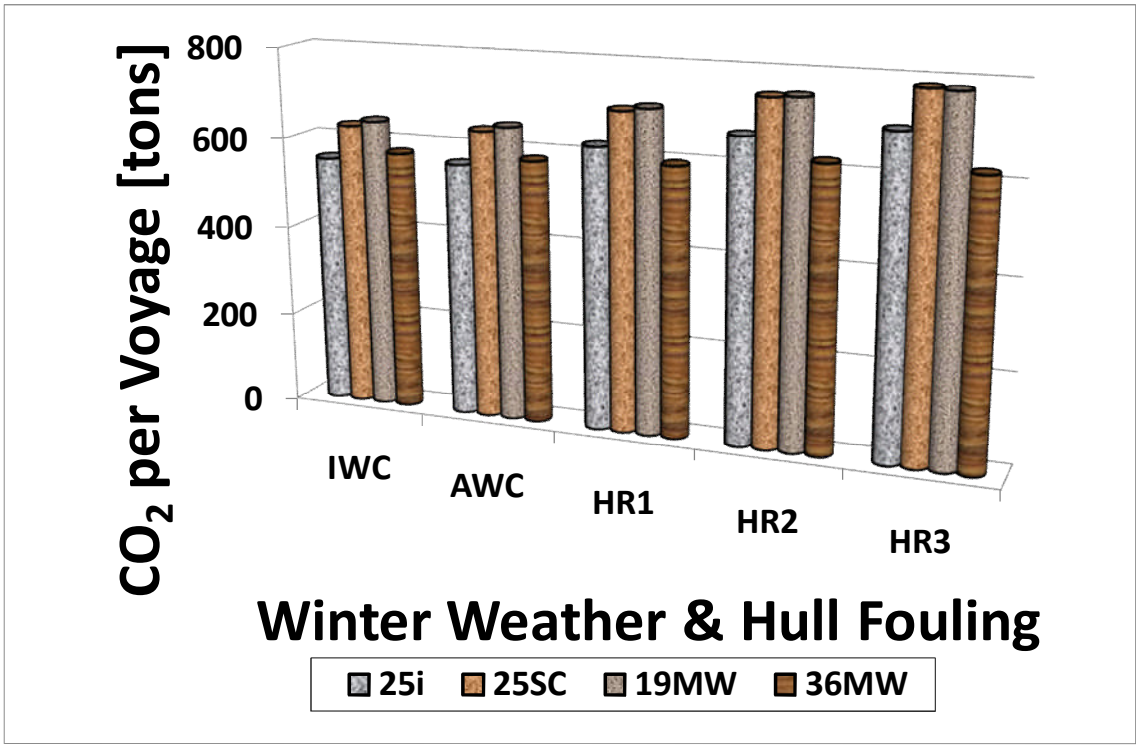

Fig D: 19 CO_2 emissions when operating in winter weather

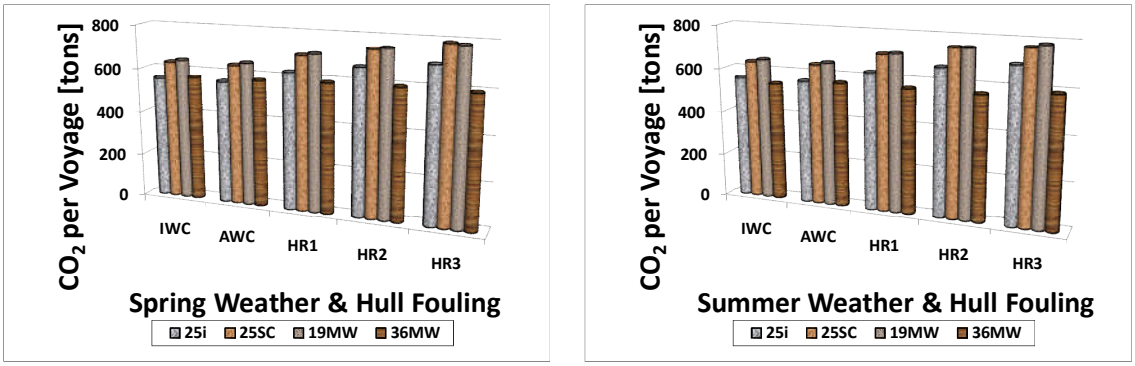

Fig D: 20 CO_2 emissions when operating in winter weather

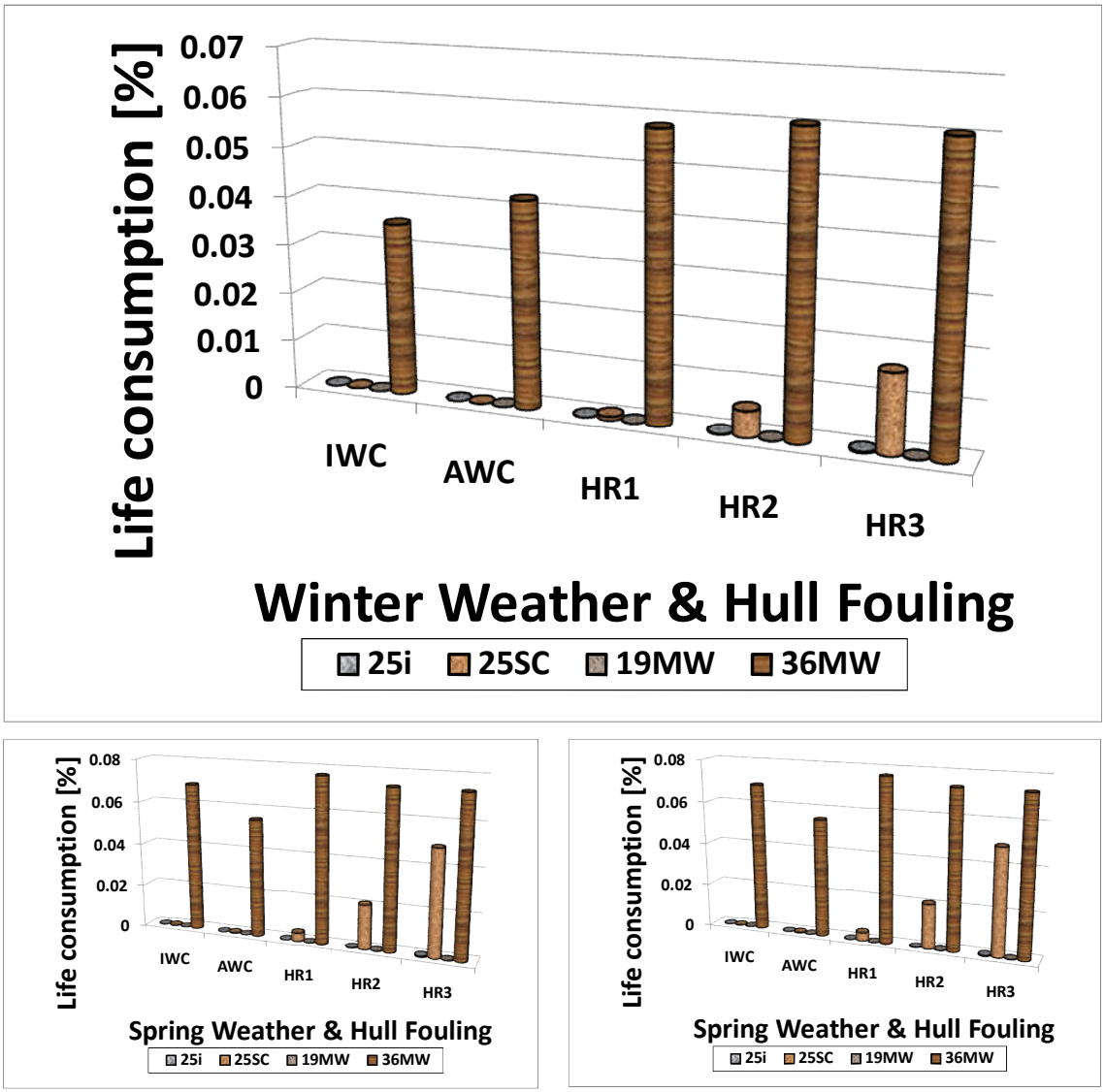

Fig D: 21 Fraction of life consumption for the variety of models in winter, spring and summer

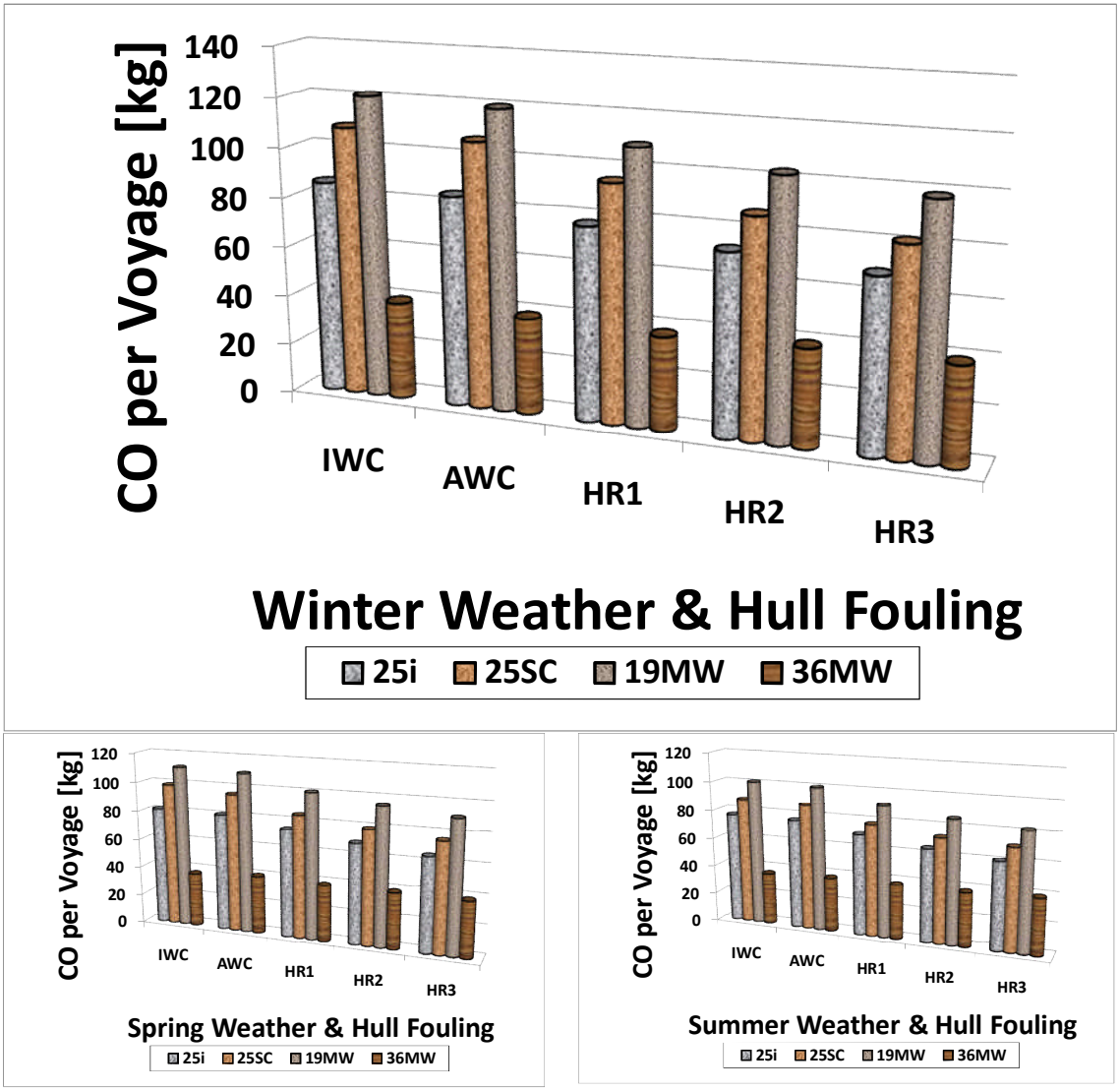

Fig D: 22 CO emissions quantities for the variety of investigated scenarios

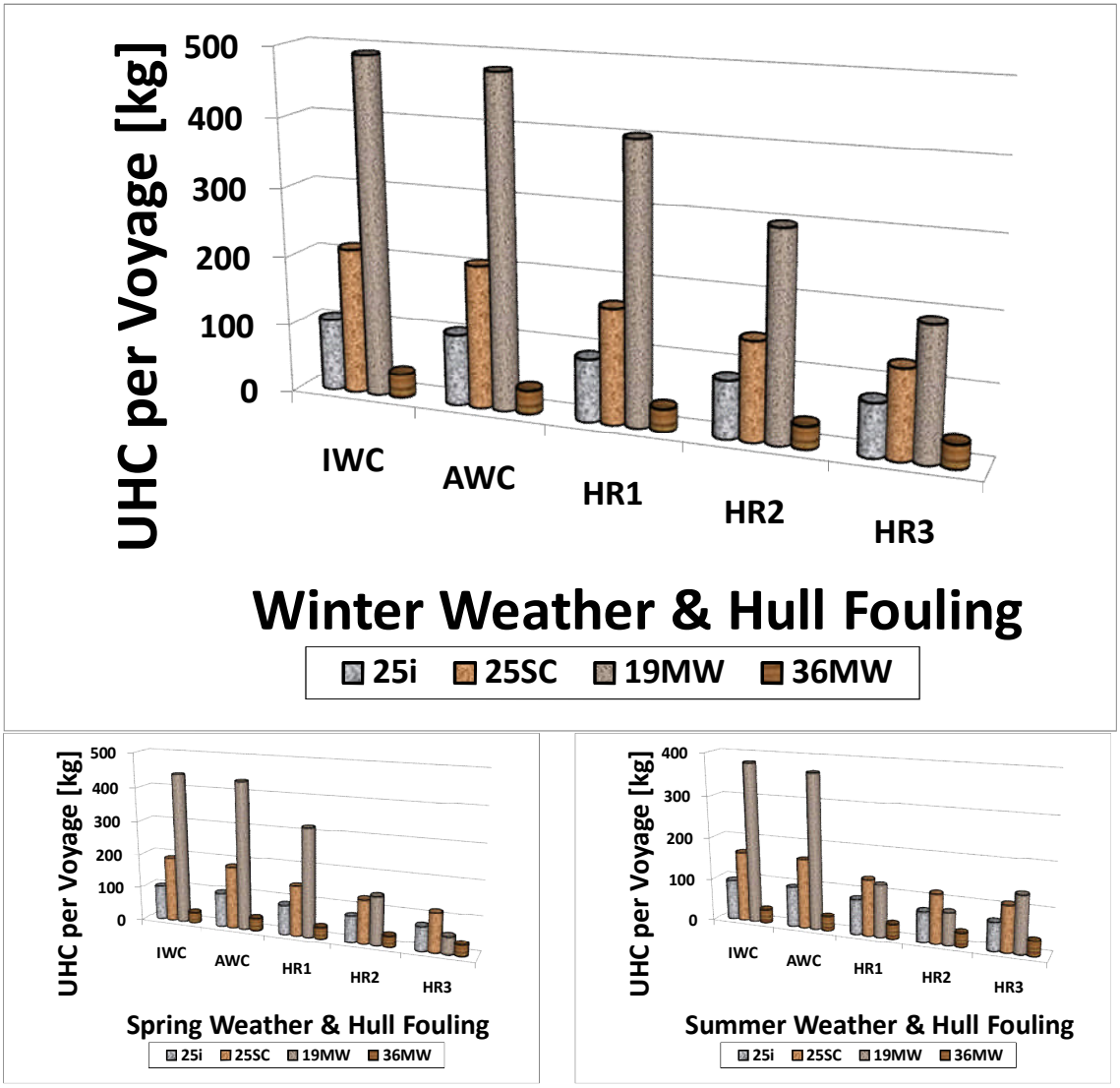

Fig D: 23 UHC emissions quantities for the variety of investigated scenarios.